Assessment by kriging of the reliability of structures subjected to fatigue stress

Benjamin Echard

N° d'ordre : D.U. : 2269
EDSPIC : 571

Université BLAISE PASCAL - Clermont II
École Doctorale
Sciences Pour l'Ingénieur de Clermont-Ferrand

Thèse

présentée par

Benjamin ECHARD
Ingénieur IFMA

en vue d'obtenir le grade de :

Docteur d'Université
Spécialité : Génie Mécanique

Évaluation par krigeage de la fiabilité des structures sollicitées en fatigue

soutenue publiquement le 25 septembre 2012 devant un jury composé de :

Dr. Mansour AFZALI	CETIM, Senlis	Invité
Dr. André BIGNONNET	AB Consulting, Beaulieu-sur-Layon	Examinateur
Pr. Pierre-Alain BOUCARD	ENS, Cachan	Président du jury
Pr. Alaa CHATEAUNEUF	Polytech', Clermont-Ferrand	Examinateur
Dr. Nicolas GAYTON	IFMA, Clermont-Ferrand	Co-encadrant
Pr. Maurice LEMAIRE	IFMA, Clermont-Ferrand	Directeur de thèse
Pr. Bruno SUDRET	ETH Zurich, Suisse	Rapporteur
Pr. Pierre VILLON	UTC, Compiègne	Rapporteur

Institut Pascal - Axe Mécanique Matériaux et Structures
Université Blaise Pascal et Institut Français de Mécanique Avancée

Kriging-based reliability assessment of structures submitted to fatigue

by

Benjamin ECHARD

A thesis submitted in partial fulfillment
of the requirements for the degree of
Doctor of Philosophy
(Mechanical Engineering)

2012

Blaise Pascal University - Clermont II

Clermont-Ferrand, France

defended publicly on 25th September 2012 before the following jury:

Dr. Mansour AFZALI	CETIM, Senlis	Guest member
Dr. André BIGNONNET	AB Consulting, Beaulieu-sur-Layon	Examiner
Pr. Pierre-Alain BOUCARD	ENS, Cachan	President of the jury
Pr. Alaa CHATEAUNEUF	Polytech', Clermont-Ferrand	Examiner
Dr. Nicolas GAYTON	IFMA, Clermont-Ferrand	Co-supervisor
Pr. Maurice LEMAIRE	IFMA, Clermont-Ferrand	Supervisor
Pr. Bruno SUDRET	ETH Zurich, Switzerland	Reviewer
Pr. Pierre VILLON	UTC, Compiègne	Reviewer

A mes parents, Martine et Jean-Claude, pour leur soutien.

A Georgina pour sa patience et son amour.

Remerciements

Je souhaite remercier toutes les personnes avec qui j'ai eu l'opportunité de travailler au cours de ces trois ans, et notamment :

- Maurice Lemaire pour m'avoir fait l'honneur d'être mon directeur de thèse. Etant votre dernier thésard, j'espère avoir été à la hauteur.
- Nicolas Gayton pour m'avoir fait confiance et parfaitement encadré. Ce fut un vrai plaisir de travailler avec toi ;
- les membres de mon jury : Pierre-Alain Boucard qui a su me mettre en confiance dès le début de la présentation, Bruno Sudret et Pierre Villon qui ont pris le temps de rapporter ma thèse, Mansour Afzali, André Bignonnet et Alaa Chateauneuf qui ont accepté d'examiner mon travail ;
- Gilles Defaux pour ton aide, ta bonne humeur et les Copils APPRoFi ;
- toutes les autres personnes qui ont participé de près ou de loin au projet APPRoFi ;
- Olivier Rochat pour notre belle collaboration et ta venue à ma soutenance ;
- les enseignants et le personnel administratif de l'IFMA ;
- mes collègues thésards et particulièrement ceux de l'open-space au fond du couloir : Polo, Ju, Hanh, Guillaume, Pierrot, Ricardo, Moncef, Bob et Simon. Je remercie aussi Cécile pour ses conseils pendant cette difficile année d'ATER et Vincent pour son aide et les bons moments passés lors des conférences à Munich et Zurich.

Enfin, je remercie mes parents et Georgina pour m'avoir toujours soutenu dans cette belle aventure.

Benjamin Echard, le 16 novembre 2012.

Résumé

Les méthodes traditionnelles de dimensionnement à la fatigue s'appuient sur l'utilisation de coefficients dits de "sécurité" dans le but d'assurer l'intégrité de la structure en couvrant les incertitudes inhérentes à la fatigue. Ces méthodes de l'ingénieur ont le mérite d'être simples d'application et de donner des solutions heureusement satisfaisantes du point de vue de la sécurité. Toutefois, elles ne permettent pas au concepteur de connaître la véritable marge de sécurité de la structure et l'influence des différents paramètres de conception sur la fiabilité. Les approches probabilistes sont envisagées dans cette thèse afin d'acquérir ces informations essentielles pour un dimensionnement optimal de la structure vis-à-vis de la fatigue.

Une approche générale pour l'analyse probabiliste en fatigue est proposée dans ce manuscrit. Elle s'appuie sur la modélisation des incertitudes (chargement, propriétés du matériau, géométrie, courbe de fatigue) et vise à quantifier le niveau de fiabilité de la structure étudiée pour un scénario de défaillance en fatigue. Les méthodes classiques de fiabilité nécessitent un nombre important d'évaluations du modèle mécanique de la structure et ne sont donc pas envisageables lorsque le calcul du modèle est coûteux en temps. Une famille de méthodes appelée AK-RM (Active learning and Kriging-based Reliability Methods) est précisément proposée dans ces travaux de thèse afin de résoudre le problème de fiabilité avec un minimum d'évaluations du modèle mécanique. L'approche générale est appliquée à deux cas-tests fournis par SNECMA dans le cadre du projet ANR APPRoFi.

Mots-clés : dimensionnement en fatigue, analyse probabiliste en fatigue, analyse de fiabilité, métamodèle, krigeage, classification

Abstract

Traditional procedures for designing structures against fatigue are grounded upon the use of so-called safety factors in an attempt to ensure structural integrity while masking the uncertainties inherent to fatigue. These engineering methods are simple to use and fortunately, they give satisfactory solutions with regard to safety. However, they do not provide the designer with the structure's safety margin as well as the influence of each design parameter on reliability. Probabilistic approaches are considered in this thesis in order to acquire this information, which is essential for an optimal design against fatigue.

A general approach for probabilistic analysis in fatigue is proposed in this manuscript. It relies on the modelling of the uncertainties (load, material properties, geometry, and fatigue curve), and aims at assessing the reliability level of the studied structure in the case of a fatigue failure scenario. Classical reliability methods require a large number of calls to the mechanical model of the structure and are thus not applicable when the model evaluation is time-demanding. A family of methods named AK-RM (Active learning and Kriging-based Reliability methods) is proposed in this research work in order to solve the reliability problem with a minimum number of mechanical model evaluations. The general approach is applied to two case studies submitted by SNECMA in the frame of the ANR project APPRoFi.

Keywords: fatigue design, probabilistic analysis in fatigue, reliability analysis, metamodel, Kriging, classification

Résumé étendu

Contexte

Le phénomène de fatigue se traduit par une lente dégradation des propriétés mécaniques d'un matériau sous l'application d'un chargement variable dans le temps. Cette dégradation progressive appelée endommagement par fatigue peut entrainer la formation de fissures au sein d'une structure constituée de ce matériau et éventuellement conduire à sa rupture brutale. Bien que le phénomène de fatigue soit affecté par de nombreuses incertitudes (propriétés du matériau, nombre de cycles à rupture, géométrie, chargement,...), la philosophie de dimensionnement en fatigue reste essentiellement déterministe. Les méthodes traditionnelles s'appuient sur l'utilisation de coefficients dits de "sécurité", codifiés et validés par retour d'expérience, dans le but d'assurer l'intégrité de la structure en couvrant les incertitudes inhérentes à la fatigue. Ces méthodes de l'ingénieur ont le mérite d'être simples d'application et de donner des solutions heureusement satisfaisantes du point de vue de la sécurité. Toutefois, elles ne permettent pas au concepteur de connaître la véritable marge de sécurité de la structure ainsi que l'influence des différents paramètres de conception sur la fiabilité. Les approches probabilistes peuvent être envisagées afin d'acquérir ces informations essentielles pour un dimensionnement optimal de la structure. Ces approches consistent à modéliser par des distributions statistiques l'aléa des paramètres entrant dans le calcul de la durée de vie afin d'approcher en sortie du modèle mécanique la réponse aléatoire de la structure.

Malgré leurs intérêts indéniables, les approches probabilistes restent très marginales dans l'industrie pour des raisons philosophiques (le risque de défaillance n'est plus caché derrière la notion rassurante de coefficient de "sécurité") et culturelles (probabilités et statistiques restent l'apanage des mathématiciens). Afin de promouvoir ces approches pour le dimensionnement en fatigue des structures, le projet DEFFI (**Dé**marche **F**iabiliste de conception en **F**atigue pour l'**I**ndustrie) a été initié par le CETIM en 2005 [Bignonnet and Lieurade, 2007; Bignonnet *et al.*, 2009; Ferlin *et al.*, 2009; Lefebvre *et al.*, 2009]. Dans sa continuité, le projet APPRoFi (**A**pproche mécano-**P**robabiliste **P**our la conception **Ro**buste en **F**ati**g**ue), financé par l'Agence Nationale de la Recherche et regroupant les laboratoires universitaires Roberval-UTC, LaMI-IFMA et LMT-ENS Cachan ainsi que

les industriels CETIM, Modartt, Phimeca et SNECMA, a été lancé avec pour objectif de développer une méthodologie globale d'évaluation de la fiabilité pour des structures existantes sollicitées en fatigue. Comme fil conducteur à ce projet, deux cas-tests sont fournis par SNECMA. Ces cas-tests sont constitués de modèles mécaniques numériques coûteux en temps de calcul et de données permettant de caractériser les incertitudes du chargement, de la géométrie de la structure, des propriétés du matériau ainsi que de son comportement en fatigue.

Objectifs

Dans le cadre du projet APPRoFi, les objectifs de cette thèse sont les suivants :

- définir une approche générale pour l'analyse probabiliste en fatigue. Ce point vise également à proposer des modélisations stochastiques pertinentes pour le chargement et la courbe $S - N$.
- développer des méthodes efficaces pour les analyses de fiabilité et de sensibilité. Ces méthodes doivent être parcimonieuses (économiques) du point de vue du nombre d'appels au modèle numérique et applicables au cas des faibles probabilités.
- traiter les deux cas-tests fournis par SNECMA.

Les apports de la thèse portant sur ces trois objectifs sont présentés succinctement dans ce résumé.

Approche générale pour l'analyse probabiliste en fatigue

Cette partie introduit l'approche probabiliste proposée dans le premier chapitre de thèse et qui représente une amélioration de la méthode probabiliste contrainte-résistance [Thomas *et al.*, 1999]. Cette dernière consiste à comparer deux distributions statistiques, à savoir la contrainte S et la résistance R afin soit de dimensionner une structure avec un objectif de fiabilité, soit de calculer la probabilité de défaillance d'une structure existante (voir Figure 1). Dans le cadre du calcul de la probabilité de défaillance, c'est-à-dire de la probabilité que $R \leq S$, la contrainte S représente les incertitudes du chargement, des propriétés du matériau ainsi que de la géométrie de la structure. La résistance R modélise, quant à elle, les incertitudes du comportement en fatigue du matériau. En établissant des lois pour S et R à partir de données expérimentales, la probabilité de défaillance peut facilement être calculée par intégration numérique. Toutefois, la valeur de cette probabilité est fortement liée aux choix des lois et il n'est pas possible de déterminer l'influence de chaque variable aléatoire sur la fiabilité de la structure étant donné que différents aléas sont inclus dans la distribution de S. A partir de cette constatation, une autre approche est proposée dans

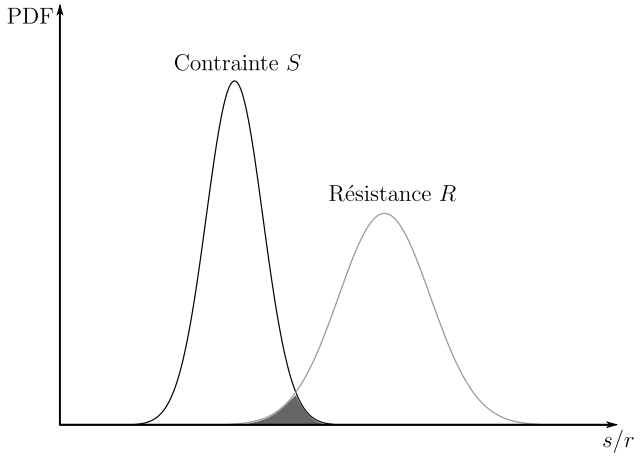

FIGURE 1 – Distributions S et R dans l'approche probabiliste contrainte-résistance. L'aire grise illustre le domaine des évènements défaillants.

le cadre du projet APPRoFi. Cette approche, illustrée en Figure 2, conserve les variables aléatoires du problème et ne nécessite plus de définir les distributions de S et R.

Les propriétés matériaux, la géométrie de la structure et le chargement sont respectivement modélisés par les vecteurs aléatoires $\mathbf{X}_m$, $\mathbf{X}_g$ et $\mathbf{X}_l$ définis à partir de données expérimentales. Le comportement en fatigue du matériau est représenté par un modèle probabiliste de courbes $S-N$ dont la courbe fractile est définie par la variable aléatoire U_f. La première étape de l'approche consiste à tirer aléatoirement une réalisation $\{\mathbf{x}_m, \mathbf{x}_g, \mathbf{x}_l, u_f\}$ des variables aléatoires. Un chargement virtuel $F(\mathbf{x}_l)$ est généré à partir du vecteur $\mathbf{x}_l$. Le concept d'Equivalent Fatigue (EF) [Thomas *et al.*, 1999] est utilisé afin de synthétiser ce chargement en un simple cycle d'amplitude constante notée $F_{eq}(\mathbf{x}_l, u_f, N_{eq})$ qui, répété N_{eq} fois, produit le même endommagement en fatigue que $F(\mathbf{x}_l)$. Ce cycle équivalent est ensuite appliqué au modèle numérique de la structure qui dépend des propriétés $\mathbf{x}_m$ du matériau et de la géométrie $\mathbf{x}_g$. L'amplitude du cycle de la réponse du modèle numérique est notée $\sigma_{eq}(\mathbf{x}_m, \mathbf{x}_g, \mathbf{x}_l, u_f, N_{eq})$. La valeur de la fonction de performance G caractérisant l'état de la structure étudiée et associée au scénario de défaillance en fatigue est calculée comme étant la différence entre la résistance $r(u_f, N_{eq})$ correspondant à la valeur de la courbe $S-N$ fractile à N_{eq} cycles et l'amplitude $\sigma_{eq}(\mathbf{x}_m, \mathbf{x}_g, \mathbf{x}_l, u_f, N_{eq})$. Une valeur négative ou nulle de G signifie que la réalisation est dans le domaine de défaillance, dans le cas contraire elle appartient au domaine de sûreté. Afin de déterminer la probabilité de défaillance et l'influence des variables aléatoires sur la fiabilité, une méthode de simulation type Monte Carlo est envisageable mais peut être avantageusement remplacée par une méthode de la famille AK-RM développée dans le cadre de cette thèse pour des raisons de temps de calcul.

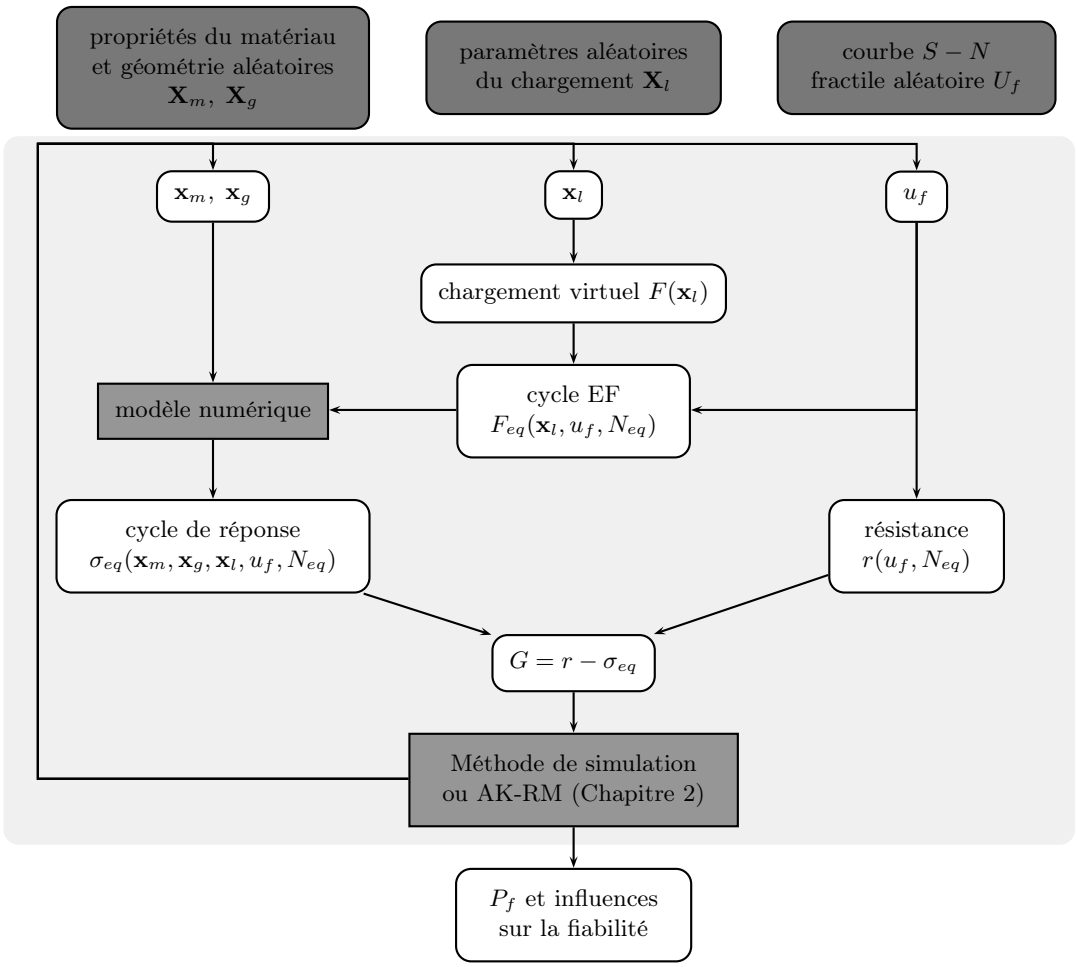

FIGURE 2 – Approche probabiliste implémentée dans le cadre du projet APPRoFi.

Calcul efficace de la probabilité de défaillance

Cette partie présente succinctement les méthodes proposées dans le second chapitre de cette thèse afin d'évaluer la fiabilité des structures dans un contexte industriel où le modèle mécanique numérique est coûteux en temps de calcul et où la probabilité de défaillance est supposée faible. Dans la suite, l'espace standard $\mathcal{U}^n$, où les variables aléatoires $\mathbf{U} = \{U_1, \ldots, U_n\}^t$ sont gaussiennes indépendantes de moyennes nulles et de variances unitaires, est considéré. L'équivalent de la fonction de performance G dans cet espace est noté $H(\mathbf{U}) \equiv G(T^{-1}(\mathbf{U}))$ où T est la transformation isoprobabiliste.

Evaluation par simulation de la probabilité de défaillance

Pour évaluer la probabilité de défaillance d'une structure, les méthodes de simulation demeurent des méthodes incontournables surtout pour traiter des problèmes dont l'état-limite $H(\mathbf{u}) = 0$ est complexe (forte non-linéarité, plusieurs points de défaillance, domaine

de défaillance non connexe, ...). La simulation de Monte Carlo (MCS) est la méthode de référence et permet de traiter théoriquement tout type de problème. Son principal inconvénient est le nombre d'appels à H nécessaires, surtout lorsque la probabilité recherchée est faible. Pour diminuer ce nombre d'appels, plusieurs méthodes sont envisageables. Une première approche peut être d'éviter les calculs superflus lorsque la monotonie de la fonction de performance est établie (souvent le cas pour des problèmes de mécanique des structures, voir De Rocquigny [2009]). Le tirage d'importance (IS) proposé par Melchers [1990] permet aussi de réduire considérablement le nombre d'appels à H sous l'hypothèse d'une topologie du domaine de défaillance faisant apparaître un maximum de densité de probabilité bien identifié, sans extremums secondaires. Ce point est couramment appelé "point de défaillance le plus probable". Enfin les Subset Simulations (SS) introduites par Au and Beck [2001] en fiabilité semblent être la méthode la plus aboutie pour réduire le nombre d'appels sans hypothèse sur la forme de l'état-limite.

Cependant, toutes ces méthodes sont difficilement envisageables pour traiter des problèmes industriels mettant en œuvre des fonctions de performance complexes et très coûteuses en temps de calcul (typiquement le cas des modèles éléments finis). Le point commun des méthodes de simulation est la nécessité de classer des points en fonction du signe de la fonction de performance (négatif ou nul = défaillant, positif = sûr). Partant de cette constatation, une stratégie de classification économique est proposée dans cette thèse. Cette technique basée sur un métamodèle de krigeage [Matheron, 1973; Sacks *et al.*, 1989] et appliquée aux différentes méthodes de simulation évoquées précédemment conduit à la création d'une nouvelle famille de méthodes appelée AK-RM pour *Active Learning and Kriging-based Reliability Methods*.

Principe de classification des méthodes AK-RM

L'objectif des méthodes AK-RM est de classer une population de points $\{\mathbf{u}^{(j)} \in \mathcal{U}^n,\ j = 1,\dots,N\}$ selon le signe de $H(\mathbf{u}^{(j)})$ avec le minimum d'évaluations de la fonction H. La stratégie de classification proposée réside dans l'utilisation d'un métamodèle de krigeage permettant à partir d'un plan d'expériences, c'est-à-dire à partir d'un ensemble d'observations de $H(\mathbf{u})$, de prédire la valeur de H notée $\mu_{\tilde{H}}(\mathbf{u}^*)$ en un point $\mathbf{u}^*$ pour lequel H n'a pas été évaluée. L'application du krigeage à la fiabilité est récente [Romero *et al.*, 2004; Kaymaz, 2005] mais de nombreux travaux [Bichon *et al.*, 2008; Ranjan *et al.*, 2008; Picheny *et al.*, 2010; Bect *et al.*, 2011; Dubourg, 2011] montrent l'intérêt croissant porté à ce type de métamodèle pour l'évaluation de la probabilité de défaillance. En plus de son caractère interpolant, le krigeage est de nature probabiliste et présente donc l'avantage par rapport aux autres métamodèles (surfaces de réponse quadratiques, chaos polynomial, support vector machine,...) de fournir un indicateur *a priori* de l'incertitude de prédiction sans calcul mécanique supplémentaire. Cet indicateur appelé variance de krigeage et noté $\sigma^2_{\tilde{H}}(\mathbf{u}^*)$ est très utile car il permet au travers de fonctions dites d'apprentissage d'enrichir

de façon itérative le plan d'expériences avec des points sélectionnés afin de raffiner le métamodèle dans une zone d'intérêt. Dans le cadre de la fiabilité, cette zone n'est autre que le voisinage de l'état-limite $H(\mathbf{u}) = 0$.

Pour une population de N points $\{\mathbf{u}^{(j)} \in \mathcal{U}^n,\ j = 1, \ldots, N\}$, la technique de classification proposée peut se résumer ainsi :

1. **Choisir un plan d'expériences initial** (environ 10 points) dans la population et faire les calculs correspondants de la fonction de performance H ;
2. **Construire le métamodèle de krigeage** à partir du plan d'expériences ;
3. **Evaluer la fonction d'apprentissage** : pour chaque point $\mathbf{u}^{(j)}$, prédire $\mu_{\tilde{H}}(\mathbf{u}^{(j)})$ et $\sigma^2_{\tilde{H}}(\mathbf{u}^{(j)})$, puis évaluer la fonction d'apprentissage $U(\mathbf{u}^{(j)}) = \lvert t - \mu_{\tilde{H}}(\mathbf{u}^{(j)})\rvert / \sigma_{\tilde{H}}(\mathbf{u}^{(j)})$ où $t = 0$ pour l'état-limite ;
4. **Apprentissage itératif ou arrêt de l'algorithme** 4.1. Si $\min_j(U(\mathbf{u}^{(j)})) \leq 2$, évaluer H au point $\mathbf{u}^\circ = \arg\min_j\ U(\mathbf{u}^{(j)})$ et ajouter ce point au plan d'expériences. Retourner à l'étape 2 pour construire le métamodèle avec le plan d'expériences enrichi ; 4.2. Sinon, arrêter l'algorithme et évaluer la probabilité de défaillance à partir du signe des moyennes de krigeage $\{\mu_{\tilde{H}}(\mathbf{u}^{(j)}),\ j = 1, \ldots, N\}$, représentatives du véritable signe de H en chacun de ces points.

Les étapes 3 et 4 de l'algorithme font appel à la fonction d'apprentissage U définie de façon à identifier les points de la population dont le signe de la fonction de performance est fortement incertain. Illustrée en Figure 3, cette fonction indique la distance, en nombre d'écarts-types de krigeage, entre la moyenne de krigeage et le seuil défini par $t = 0$:

$$U(\mathbf{u}) = \frac{\lvert t - \mu_{\tilde{H}}(\mathbf{u})\rvert}{\sigma_{\tilde{H}}(\mathbf{u})} \tag{1}$$

Sous l'hypothèse de gaussianité de la prédiction de krigeage, $1 - \Phi(U(\mathbf{u}))$ représente la probabilité que le signe de $H(\mathbf{u})$ soit différent du signe de $\mu_{\tilde{H}}(\mathbf{u})$ (Φ étant la fonction de répartition de la loi normale centrée réduite). Le point $\mathbf{u}^\circ$ où il est le plus intéressant d'évaluer la fonction de performance est donc celui qui minimise la fonction U. Cette évaluation est réalisée si la condition d'arrêt de l'apprentissage $\min_j U(\mathbf{u}^{(j)}) > 2$ à l'étape 4 n'est pas respectée. Cette condition signifie que le signe de $\mu_{\tilde{H}}$ en chaque point de la population est identique au signe de H correspondant avec un niveau de confiance supérieur à $\Phi(2) = 97.7\%$. Lorsque cette condition est respectée, il devient possible d'utiliser le signe des moyennes de krigeage $\{\mu_{\tilde{H}}(\mathbf{u}^{(j)}),\ j = 1, \ldots, N\}$ pour évaluer la probabilité de défaillance.

L'algorithme décrit dans cette section est mis en œuvre pour guider les méthodes de simulation évoquées précédemment. Les méthodes AK-MCS, AK-MCSm (m pour monotonie), AK-IS et AK-SS sont validées sur un ensemble d'exemples académiques. Les résultats montrent qu'elles sont parcimonieuses du point de vue du nombre d'appels à H et qu'elles fournissent des classifications très similaires (et même rigoureusement identiques dans la très grande majorité des cas) aux méthodes de simulation classiques.

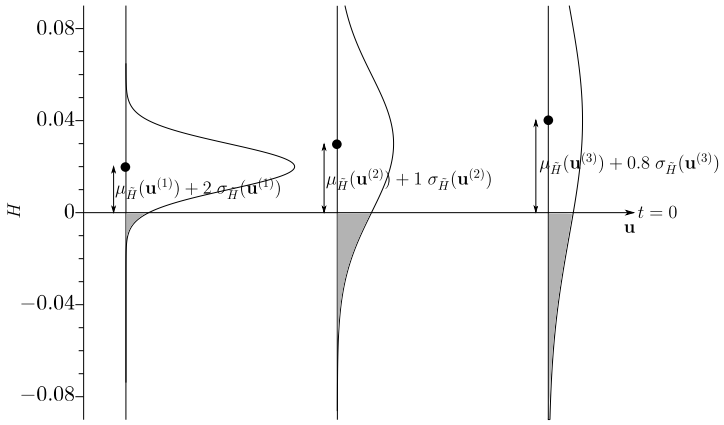

FIGURE 3 – Illustration de la fonction d'apprentissage U à évaluer en trois points différents $\mathbf{u}^{(1)}$, $\mathbf{u}^{(2)}$, $\mathbf{u}^{(3)}$ avec une moyenne de krigeage positive. La valeur de la fonction d'apprentissage en chacun de ces points est respectivement 2, 1 et 0.8. Les aires grisées représentent les probabilités $1 - \Phi(U(\mathbf{u}^{(j)}))$ que le signe de H soit différent de celui de $\mu_{\tilde{H}}$. Le point $\mathbf{u}^{(3)}$ est celui qui a la plus grande incertitude sur le signe de $H(\mathbf{u}^{(3)})$.

Applications et résultats

Le troisième chapitre de cette thèse traite des deux cas-tests du projet APPRoFi. Les incertitudes de chargement, des propriétés du matériau et de son comportement en fatigue sont considérées pour ces deux études (la géométrie est déterministe car il est montré qu'elle a peu d'influence sur la fiabilité ici). La modélisation du chargement est envisagée selon trois méthodes : une stratégie basée sur la définition de situations de vie élémentaires [Thomas *et al.*, 1999; Bignonnet *et al.*, 2009; Lefebvre *et al.*, 2009], une approche par coefficient de sévérité et une méthode modélisant la dispersion des matrices Rainflow avec des densités conjointes de probabilité [Nagode and Fajdiga, 1998, 2000, 2006; Nagode *et al.*, 2001; Nagode, 2012]. La modélisation du comportement en fatigue est réalisée, quant à elle, au moyen de courbes $S - N$ probabilistes issues de la littérature [AFNOR, 1991; Guédé, 2005; Guédé *et al.*, 2007; Perrin, 2008; Sudret, 2011]. L'approche probabiliste développée

dans le premier chapitre est implémentée afin de traiter la réponse aléatoire en fatigue des deux structures étudiées. Celle-ci est couplée aux méthodes AK-RM afin de permettre une évaluation de la fiabilité avec peu d'appels aux modèles numériques. De plus, le calcul mécanique déterministe est optimisé aux moyens de méthodes numériques avancées (méthode LATIN [Ladevèze, 1999] et stratégie multiparamétrique [Boucard and Champaney, 2003]) par le laboratoire LMT-ENS Cachan, partenaire du projet. La méthodologie globale du projet APPRoFi permet finalement d'évaluer la probabilité de défaillance en un temps convenable. Il est de plus montré par le calcul des facteurs d'importance que les modélisations du chargement et de la courbe $S - N$ sont les paramètres ayant le plus influence sur la fiabilité en fatigue au détriment des propriétés du matériau considérées, et cela pour la connaissance des données à disposition.

Conclusions et perspectives

Un schéma général de calcul pour l'analyse probabiliste en fatigue ainsi que des méthodes économiques d'évaluation de la fiabilité des structures ont été proposés dans ce travail de recherche. Ces méthodes de fiabilité, regroupées sous la dénomination AK-RM pour *Active Learning and Kriging-based Reliability Methods*, sont basées sur un métamodèle de krigeage permettant de prédire précisément le signe de la fonction de performance en chaque point d'une population sans avoir à effectuer un grand nombre de calculs mécaniques coûteux. Afin d'évaluer la fiabilité des deux cas-tests du projet APPRoFi, les incertitudes de chargement, des propriétés du matériau et de son comportement en fatigue ont été, dans un premier temps, modélisées à partir de méthodes issues de la littérature. Dans un second temps, ces incertitudes ont été propagées au travers du schéma général de calcul en fatigue grâce aux méthodes AK-RM. La probabilité de défaillance et les facteurs d'importance des deux cas-tests ont ainsi pu être évalués en un temps raisonnable. En effet, seulement 27 calculs mécaniques ont été nécessaires pour le cas du *blade support*, soit un temps de calcul total de $2,25$ heures en couplage avec les méthodes numériques du laboratoire LMT-ENS Cachan.

Ce travail de recherche ouvre de multiple perspectives. Tout d'abord, une étude plus approfondie des modélisations du chargement et de la courbe $S - N$ serait à envisager étant donné leurs influences sur la fiabilité. L'utilisation de processus Gaussiens [Pitoiset, 2001; Benasciutti and Tovo, 2005] ou de chaînes de Markov [Mattrand and Bourinet, 2011; Mattrand, 2011] pourrait, entre autre, représenter une alternative aux modélisations étudiées dans cette thèse pour le chargement.

De même, l'analyse de sensibilité réalisée au moyen des facteurs d'importance pourrait être complétée par une approche globale telle que les indices de Sobol'. Ces indices étant habituellement calculés par simulation de Monte Carlo, un métamodèle de krigeage pourrait être utilisé afin d'en diminuer le coût de calcul (voir Marrel *et al.* [2009]).

Une troisième idée serait l'introduction de coefficients partiels spécifiques aux structures étudiées en lieu et place des coefficients de "sécurité" traditionnels. La calibration de ces coefficients pour un objectif de fiabilité donné [Gayton *et al.*, 2004] permettrait de définir des règles de dimensionnement à la fois simples à suivre pour le concepteur, mais aussi plus adaptées aux structures à dimensionner.

Enfin, la résolution d'un problème d'optimisation sous contrainte de fiabilité pourrait être envisagée par l'intermédiaire des méthodes AK-RM sur la base des récentes avancées faites dans ce domaine avec un métamodèle de type krigeage [Bichon *et al.*, 2009; Dubourg, 2011; Dubourg *et al.*, 2011].

Contents

Introduction **1**

1 Structural design against fatigue failure **5**
1.1 Introduction . . . 6
1.2 Deterministic fatigue design . . . 7
1.2.1 Introduction . . . 7
1.2.2 Considerations in fatigue . . . 7
1.2.3 Fatigue design under a constant amplitude load . . . 11
1.2.4 Fatigue design under a variable amplitude load . . . 11
1.2.5 Equivalent fatigue concept . . . 15
1.2.6 Fatigue design codes in industry . . . 18
1.3 Probabilistic fatigue design . . . 19
1.3.1 Introduction . . . 19
1.3.2 Principles of the probabilistic approaches . . . 20
1.3.3 Basic statistical inference methods . . . 21
1.3.4 Modelling of in-service loads . . . 24
1.3.5 Probabilistic $S-N$ curves . . . 30
1.3.6 Probabilistic Stress-stRength approach . . . 35
1.3.7 Proposed approach in the context of the APPRoFi project . . . 47
1.4 Conclusion . . . 52
Chapter summary . . . 53

2 Active learning & Kriging-based Reliability Methods **55**
2.1 Introduction . . . 56
2.2 Isoprobabilistic transformation . . . 57
2.3 Sampling-based reliability methods . . . 58
2.3.1 Monte Carlo Simulation . . . 58
2.3.2 Monte Carlo Simulation under monotony . . . 59
2.3.3 Importance Sampling . . . 61
2.3.4 Subset Simulation . . . 64

2.3.5 Conclusion . . . 69
2.4 Kriging-based reliability methods . . . 69
2.4.1 Principles of metamodelling . . . 69
2.4.2 Kriging theory . . . 70
2.4.3 Active learning method . . . 73
2.4.4 Kriging prediction of the failure probability . . . 76
2.5 Active learning and Kriging-based Monte Carlo Simulation . . . 77
2.5.1 Motivation . . . 77
2.5.2 Procedure . . . 77
2.5.3 Validation . . . 78
2.5.4 Computational cost of the prediction step . . . 86
2.5.5 Conclusion . . . 88
2.6 Active learning and Kriging-based alternatives for small probability cases . . . 88
2.6.1 Active learning and Kriging based MCS under monotony . . . 88
2.6.2 Active learning and Kriging-based Importance Sampling . . . 92
2.6.3 Active learning and Kriging-based Subset Simulation . . . 98
2.7 Conclusion . . . 104
Chapter summary . . . 106

3 Application to the case studies of the APPRoFi project 107
3.1 Introduction . . . 108
3.2 Bolted joint in an aircraft engine . . . 108
3.2.1 Fatigue behaviour . . . 108
3.2.2 Load modelling . . . 111
3.2.3 Numerical model . . . 113
3.2.4 Reliability assessment . . . 114
3.2.5 Results . . . 115
3.3 Blade support case study . . . 115
3.3.1 Fatigue behaviour . . . 116
3.3.2 Material properties . . . 118
3.3.3 Load modelling . . . 119
3.3.4 Numerical model . . . 123
3.3.5 Reliability assessment . . . 124
3.3.6 Results . . . 125
3.4 Conclusion . . . 126

Conclusion 127

Bibliography 130

A List of abbreviations **141**

B List of notations **143**

B.1 General notations 143

B.2 Deterministic mechanical values 143

B.3 Random values 144

B.3.1 Scalar and statistical values 144

B.3.2 Vectorial values 144

B.3.3 Space notation and random functions 144

B.3.4 Random mechanical values 145

B.3.5 Kriging values 145

B.3.6 Reliability analysis products 145

C Parametric modelling of the load for the blade support case study **147**

Introduction

Context

Fatigue corresponds to the progressive deterioration of material strength under repeated loading and unloading. This phenomenon affects most of the structures that are currently operating, and represents approximately 90% of the in-service failures [Robert, 2009]. Its consideration is thus a priority when designing new structures. However, structural design is a complex task due to the significant number of uncertainties that are inherent to the fatigue phenonemon. For instance, the fatigue behaviour of materials is experimentally proven to be dispersed, and structures generally undergo variable stress levels depending on customer usage and operating conditions. Current procedures for designing structures against fatigue consist of deterministic approaches that are either codified in standards or based on the know-how acquired through experience feedback. These methods are grounded on the use of so-called safety factors in an attempt to ensure structural integrity while masking the inherent uncertainties and the lack of knowledge. Such factors are supposed to guarantee a reliability level which in practice cannot be assessed. Although these deterministic methods give mostly satisfactory solutions, they often lead to over-design, and consequently unnecessary expenditures. Within the scope of cost optimization, engineers are asked to design functional structures that remain safe while using a minimum quantity of raw materials. Such an objective can only be fulfilled through a better understanding of the structural behaviour. From this perspective, the safety margin and the most influent design parameters on structural reliability represent extremely valuable knowledge. Probabilistic approaches are a possible way to acquire this knowledge, as they enable the uncertainties of the different parameters involved in fatigue calculation to be propagated to the mechanical responses of structures. However, these approaches currently have few followers in industry due to the interdisciplinary skills required, as well as the cultural breakaway that they represent.

In 2005, CETIM launched the DEFFI project (***Dé**marche **F**iabiliste de conception en **F**atigue pour l'**I**ndustrie*) to promote the development of probabilistic approaches for mechanical fatigue design [see Bignonnet and Lieurade, 2007; Bignonnet *et al.*, 2009; Ferlin *et al.*, 2009; Lefebvre *et al.*, 2009]. In this project, the probabilistic Stress-stRength[†]

[†]The capital letters refer to the mathematical notation S for Stress and R for stRength.

approach [Thomas *et al.*, 1999] was applied to case studies from different industrial fields (railway, aerospace, aeronautics...). In 2008, the APPRoFi project (***A**pproche mécano-**P**robabiliste **P**our la conception **Ro**buste en **Fat**igue*), funded by ANR (***A**gence **N**ationale de la **R**echerche*) and bringing together academic partners (Laboratoire Roberval-UTC, LaMI-IFMA, LMT-ENS Cachan) and companies (CETIM, Modartt, Phimeca, SNECMA), was launched to make industrialists further aware of the potential benefits of probabilistic approaches in fatigue design. From a scientific point of view, the objective of the project is to implement a global methodology in order to determine, within a short space of time, the failure probability of already designed structures as well as the most influent design parameters on structural reliability. The project is based on two challenging case studies submitted by SNECMA. For each of these case studies, data are available on material tests (fatigue, tensile/compression), geometrical tolerances, and field measurements of the in-service loads. Computationally demanding finite element models simulating the mechanical behaviours of the structures are also provided. Starting from this set of information, the following points are identified as relevant directions to investigate in order to fulfil the scientific objective of the project:

1. **stochastic modelling of the material, geometry and load**. Statistical inference methods (frequentist and Bayesian) are applied to model the dispersion of the material properties and structure dimensions. Methods are also reviewed to depict the uncertainties of the in-service loads on the basis of field measurements. Point 1 is studied by Phimeca. Load modelling is also partly investigated by LaMI-IFMA.

2. **stochastic modelling of the fatigue behaviour**. In practice, the fatigue behaviour of a material is characterized by performing numerous experiments on smooth specimens. The results are then analysed in order to plot the $S-N$ curve of the material. Given that a large scatter is observed in the fatigue life when tests are performed at a similar stress level, the $S-N$ curve clearly presents a random nature. The objective of Point 2 explored by CETIM, LaMI-IFMA and Phimeca is the characterization of probabilistic $S-N$ curves modelling this uncertainty.

3. **efficient evaluation of the mechanical behaviour**. The evaluation of the numerical model simulating the mechanical behaviour of a structure is often a time-demanding process (typically the case of a finite element analysis which may take several minutes to several hours). Classical sampling-based reliability methods require a substantial number of model evaluations and are consequently inapplicable in a suitable amount of time. Numerical strategies are developed in this project to reduce the CPU time of succeeding model evaluations. Point 3 is researched by LMT-ENS Cachan and Laboratoire Roberval-UTC.

4. **efficient reliability assessment**. As mentioned above, classical sampling-based

reliability methods are incompatible with computationally demanding models. Alternative reliability methods based on metamodels are thus studied in Point 4 in order to considerably reduce the number of model evaluations required to assess the failure probability. On the one hand, Modartt investigates sparse grids. On the other hand, LaMI-IFMA proposes a family of methods based on a Kriging metamodel. These latter methods represent the main contribution of this thesis.

Thesis objectives

Within the APPRoFi project, the objectives of this thesis are:

- to define a general approach for probabilistic analysis in fatigue. This point also deals with the stochastic modellings of the in-service loads and fatigue behaviour on the basis of existing methods in the literature.
- to develop reliability methods that are parsimonious with respect to the number of numerical model evaluations and applicable to small failure probability cases.
- to handle the two case studies submitted by SNECMA.

Contents

This thesis is divided into three chapters, one for each of the objectives listed above. Chapter 1 is concerned with structural design against fatigue failure. The deterministic approaches are first detailed, and the use of safety factors in industry is briefly discussed. Following this, the principles of the probabilistic approach are introduced with statistical methods to model the uncertainties of the load and fatigue behaviour. The Stress-stRength approach implemented in the DEFFI project is then examined, and its limits are illustrated on an academic example. The alternative approach proposed in the frame of the APPRoFi project is finally explained.

Chapter 2 is devoted to the assessment of the failure probability for industrial applications. Sampling-based reliability methods are first reviewed. Given the considerable number of numerical model evaluations required by these sampling techniques, Kriging-based methods are proposed as more parsimonious alternatives. These methods form the AK-RM family (Active learning and Kriging-based Reliability Methods) and are validated on a chosen set of academic examples involving high non-linearity and small failure probabilities.

In Chapter 3, the different contributions of the thesis are applied to the case studies of the APPRoFi project. The uncertainties of the fatigue behaviour, material properties and load are considered. Their stochastic modellings are detailed, and methods of the AK-RM family are implemented to determine the failure probability and the influent parameters on structural reliability. The global methodology is proven to be operational and transferable in design offices in order to rapidly assess the reliability of structures.

1 Structural design against fatigue failure

Contents

1.1 Introduction 6
1.2 Deterministic fatigue design 7
1.2.1 Introduction 7
1.2.2 Considerations in fatigue 7
1.2.3 Fatigue design under a constant amplitude load 11
1.2.4 Fatigue design under a variable amplitude load 11
1.2.5 Equivalent fatigue concept 15
1.2.6 Fatigue design codes in industry 18
1.3 Probabilistic fatigue design 19
1.3.1 Introduction 19
1.3.2 Principles of the probabilistic approaches 20
1.3.3 Basic statistical inference methods 21
1.3.4 Modelling of in-service loads 24
1.3.5 Probabilistic $S-N$ curves 30
1.3.6 Probabilistic Stress-stRength approach 35
1.3.7 Proposed approach in the context of the APPRoFi project 47
1.4 Conclusion 52
Chapter summary 53

1.1 Introduction

The fatigue phenomenon is associated with the repeated loading and unloading of a material. The progressive deterioration of the material's strength resulting from the application of these cyclic loads, whose nominal stress values are below the ultimate strength and can be below the yield strength, is known as fatigue damage. This fatigue damage accounts for approximately 90% of the structural failures observed in service [Robert, 2009], making the consideration of the fatigue phenomenon a priority when designing new structures.

In a material, manufacturing defects are zones where plastic deformations may appear under very low nominal stresses. These plastic deformations are negligible for one stress cycle, but the succession of cycles produces an accumulation of microplasticity which may lead to the initiation of microscopic cracks. These cracks then propagate until they form a macroscopic crack that causes fracture. The process of fatigue damage is generally divided into three steps which are:

- the initiation of a macroscopic crack. This thesis focuses on this step, given that crack initiation is considered as the failure criterion for the structures studied in the APPRoFi project.
- the propagation of the macroscopic crack.
- the sudden fracture at the critical crack size.

The fatigue behaviour of structures is strongly affected by uncertainties. In addition to the unavoidable manufacturing defects, the applied loads are random, and the material properties present inherent scatters. The consideration of these uncertainties in the fatigue design process is necessary to devise reliable structures. A common practice in industry is the use of so-called safety factors in an attempt to ensure structural integrity while covering the inherent uncertainties. These factors based on practical experience or codified in standards are convenient to use, but they often lead to over-design. Additionally, the safety margin and the most influent design parameters on structural reliability which represent valuable information for the designer remain unknown. Starting from this observation, probabilistic approaches have been developed to contribute a better understanding of structural behaviours. These approaches are the main topic of this chapter which is organized as follows. Section 1.2 reviews important considerations in fatigue, and briefly presents the common deterministic fatigue design approaches employed in industry. Section 1.3 introduces the probabilistic approaches as a means to expand the knowledge of uncertainties in the mechanical response of structures. In this section, the statistical modellings of the in-service loads and $S-N$ curves are also discussed, and the probabilistic Stress-stRength approach by Thomas *et al.* [1999] is explained. Finally, the approach proposed in the APPRoFi project is presented as an alternative to calculate an accurate estimate of the failure probability as well as the influent parameters on structural reliability.

1.2 Deterministic fatigue design

1.2.1 Introduction

This part is structured as follows. Section 1.2.2 introduces important considerations in fatigue. Sections 1.2.3 and 1.2.4 present the deterministic fatigue design in the case of a constant amplitude load and a variable amplitude load respectively. Section 1.2.5 explains the equivalent fatigue concept. Finally, Section 1.2.6 briefly presents the deterministic design approaches that are employed in industry.

1.2.2 Considerations in fatigue

The present section is based on the books by Suresh [1998] and Lalanne [2002]. The reader may refer to them for further details and original references.

1.2.2.1 Constant amplitude load

The Constant Amplitude (CA)[†] load, depicted in Figure 1.1, is the simplest load in fatigue. Its replicated cycle features a mean σ_m and an amplitude σ_a. The cycle may also be defined with the extrema $\sigma_{\min} = \sigma_m - \sigma_a$ and $\sigma_{\max} = \sigma_m + \sigma_a$, or finally, by the stress range $\Delta\sigma$ and the stress (or load) ratio $\mathcal{R}$ that reads:

$$\mathcal{R} = \frac{\sigma_{\min}}{\sigma_{\max}} \tag{1.1}$$

Common stress ratio values are -1 and 0. $\mathcal{R} = -1$ refers to the fully reversed load which is characterized by a mean $\sigma_m = 0$ and a symmetric alternating amplitude σ'_a. $\mathcal{R} = 0$ refers to the zero-tension fatigue where the load is purely tensile ($\sigma_{\min} = 0$).

The load rate is assumed to have no effect on the fatigue behaviour if the frequency remains below 20 Hz [Robert, 2009]. This hypothesis enables the fatigue life to be expressed as a number of cycles.

1.2.2.2 $S - N$ curve

The fatigue behaviour of materials is characterized experimentally by applying a smooth specimen to a CA force load (or displacement) until failure, *i.e.* until a crack is initiated. The number of cycles to failure N thus obtained is carried forward into an $S - N$ diagram which typically consists of the alternating nominal stress amplitude undergone by the specimen (easily derived from the applied load and the specimen's cross-section) versus N. By plotting N for different stress levels, the $S - N$ curve, also known as the Wöhler

[†]A list of abbreviations is available in Appendix A. Note also that Appendix B provides a list of notations.

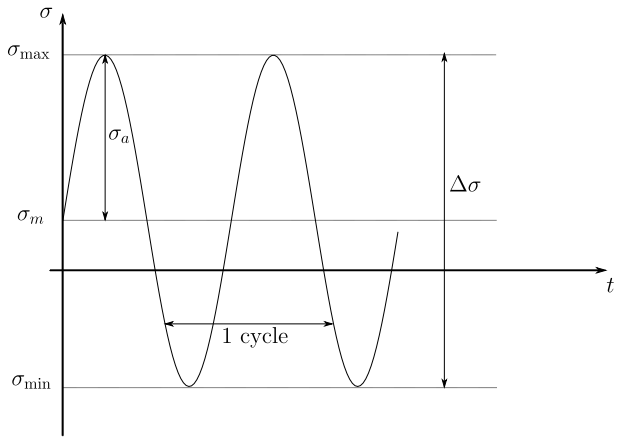

Figure 1.1: Characteristics of a constant amplitude load.

curve, is obtained (see Figure 1.2). This curve is generally expressed for $\mathcal{R} = -1$, and is commonly composed of three domains [Lalanne, 2002]:

I. The low cycle fatigue domain corresponds to the high stresses and relatively short lives, *i.e.* $N \leq 10^4 - 10^5$ cycles. In this domain, significant plastic deformations are observed. The plastic strain ϵ_p is usually related to N by using the so-called Manson-Coffin's relation:

$$\epsilon_p = C\ N^c \tag{1.2}$$

II. The high cycle fatigue domain with finite life (or zone of limited endurance) corresponds to stresses that are lower than those in domain I. The number of cycles to failure is between $10^4 - 10^5$ and $10^6 - 10^7$. In this domain, a linear relation is often assumed between $\log \sigma'_a$ and $\log N$. It is referred to as the Basquin's relation:

$$\sigma'_a = B\ N^b \tag{1.3}$$

In this thesis, b and B are called the Basquin's slope and the fatigue strength coefficient respectively.

III. The high cycle fatigue domain with infinite life corresponds to the number of cycles to failure that are greater than $10^6 - 10^7$. In this domain, a significant variation of slope is observed, and the curve tends towards a horizontal limit known as the fatigue limit σ_D. Stresses under this level never cause failure whatever the number of cycles.

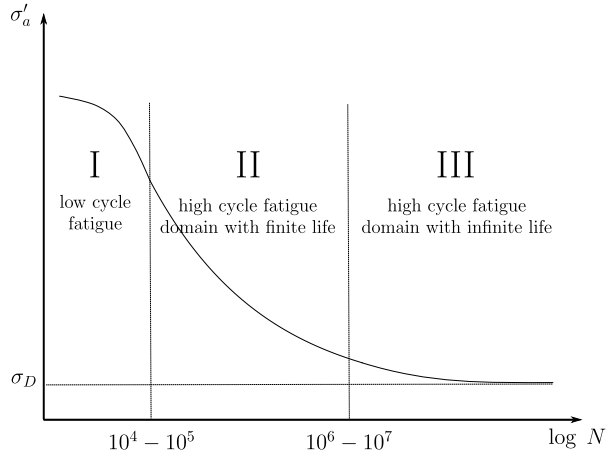

Figure 1.2: The domains of the $S - N$ curve.

Numerous relations exist in the literature [Lalanne, 2002] to associate the number of cycles to failure with the stress level (*e.g.* Bastenaire's, Stromeyer's, Weibull's,...). In this research work, the Basquin's relation is selected, as the study is restricted to the domain of high cycle fatigue with finite life. Note that a 'double' Basquin's relation may also be used to consider the change of slope between $\log \sigma'_a$ and $\log N$ in domain III.

A large scatter in fatigue life is observed when replicating several fatigue tests at a given stress level. The fatigue phenomenon is thus strongly affected by uncertainties which are mainly due to:

- the heterogeneity of materials. The fatigue strength, *i.e.* the value of the nominal stress at which failure occurs after N cycles, depends strongly on the chemical composition of some material grains in the critical zone where a crack will be initiated [Lalanne, 2002].
- the manufacturing quality (surface roughness, geometry).
- the casting defects such as inclusions.
- the conditions of tests (corrosion, temperature, the control of the applied load...).

The observed scatter is characterized with statistical tools, and the median curve (50% of the specimens tested at the given stress level fail at N) is generally plotted. The fatigue strength at a given N is often considered as a Gaussian random variable [Lalanne, 2002] (truncated to positive values). The number of cycles to failure at a given stress level is usually defined as a lognormal distribution [Lalanne, 2002; Guédé, 2005]. Note that the consideration of fatigue life scatter is further discussed in Section 1.3.5 with the introduction of probabilistic $S - N$ curves.

In contrast to a smooth specimen, a complex structure cannot be considered as being homogeneously affected by the applied load. Its geometry produces stress concentration zones, and the critical location, *i.e.* the location that first reaches failure, is likely to be located in these zones. The stress response undergone by the structure at this location must therefore be acquired in order to determine the fatigue life according to the $S-N$ curve of the material. In practice, the stress response of the structure is either derived from instrumenting the structure with sensors, or determined by applying field measurements of the in-service loads to the numerical model representing the structural behaviour. Another alternative is to conduct fatigue tests on real structures. The fatigue curve is then plotted in a diagram depicting the applied force (or displacement) versus the number of cycles to failure. However, conducting such fatigue tests is not always feasible due to prohibitive costs and structure size.

1.2.2.3 Mean stress effect on fatigue life

As mentioned previously, the $S-N$ curve is often drawn for a fully reversed load, but it may also be expressed for $\mathcal{R} \neq -1$. The fatigue behaviour is strongly affected by the mean value σ_m in the way that a positive mean (*i.e.* tensile stress) decreases the fatigue life, and conversely that a negative mean (*i.e.* compression stress) increases it as long as $|\sigma_m|$ is not too large. The mean effects can be represented in the Haigh diagram (see Figure 1.3) which depicts different combinations of the stress amplitude and mean stress providing a constant fatigue life. The three main expressions modelling the Haigh diagram are [Suresh, 1998]:

- The modified Goodman line:

$$\sigma_a = \sigma'_a \left(1 - \frac{\sigma_m}{R_m}\right) \tag{1.4}$$

  where R_m is the tensile strength.

- The Gerber parabola:

$$\sigma_a = \sigma'_a \left(1 - \left(\frac{\sigma_m}{R_m}\right)^2\right) \tag{1.5}$$

- The Söderbeg line:

$$\sigma_a = \sigma'_a \left(1 - \frac{\sigma_m}{R_y}\right) \tag{1.6}$$

  where R_y is the yield strength.

These expressions are used in order to convert a cycle having a stress ratio $\mathcal{R}_1$ into a cycle with $\mathcal{R}_2$ which is equivalent in terms of fatigue life. The mean stress effect on fatigue life is not considered in the same way for these three models. For instance, the Gerber

parabola implies that tensile and compressive mean stresses have the same impact on fatigue life, whereas the modified Goodman line considers that compressive mean stresses are beneficial to the fatigue life.

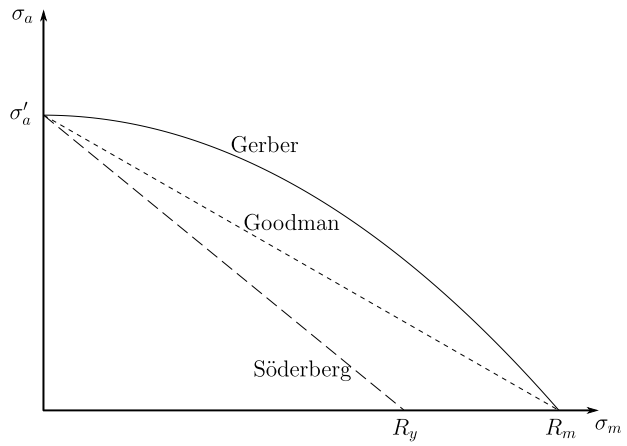

Figure 1.3: Different models of the Haigh diagram.

1.2.3 Fatigue design under a constant amplitude load

The objective of fatigue design under a CA load is to determine the fatigue life. Let a CA load be imposed on a smooth specimen. The nominal stress cycle deriving from this load is denoted by (σ_m, σ_a). Let the $S-N$ curve of the material be expressed for $\mathcal{R} = -1$. Figure 1.4 depicts the method which is as follows:

1. Convert the stress cycle (σ_m, σ_a) into its fully reversed equivalent $(\sigma_m = 0, \sigma'_a)$ using the Haigh diagram modelled for instance by the Gerber parabola.

2. Determine the number of cycles to failure corresponding to σ'_a with the $S-N$ curve of the material expressed for $\mathcal{R} = -1$.

1.2.4 Fatigue design under a variable amplitude load

Structures generally undergo Variable Amplitude (VA) stress responses rather than CA ones. As a result, the number of cycles that are applied is not as obvious, and cycle-counting techniques are necessary to identify them, as well as estimate their damage contributions. Figure 1.5 depicts the general procedure of the fatigue design approach. Let $F(t)$ be a VA force load applied to a structure. The design approach is as follows:

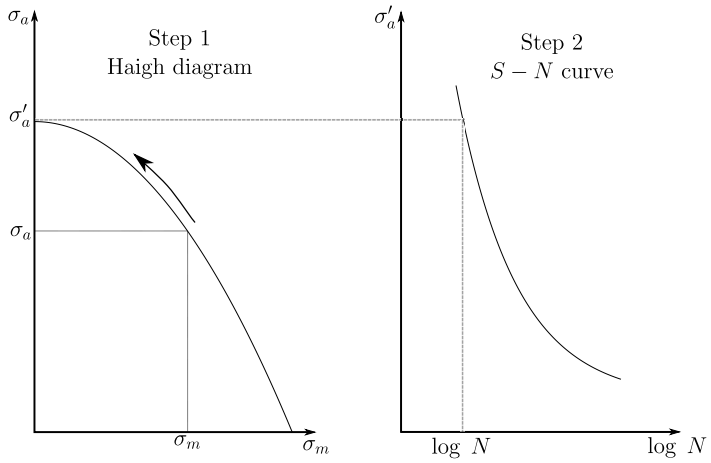

Figure 1.4: Fatigue design under a CA load.

1. Apply the load $F(t)$ to the numerical model of the structure which is characterized by a material and a geometry. The output of the model is the stress response $\sigma(t)$ at the critical location.

2. Decompose the stress history $\sigma(t)$ into cycles using the Rainflow-counting method (or other).

3. Convert the stress cycles into their $\mathcal{R} = -1$ equivalents using the Gerber parabola (or other).

4. Determine the fraction of damage of each stress cycle with the $S-N$ curve expressed for $\mathcal{R} = -1$.

5. Cumulate the fractions of damage with the Palmgren-Miner cumulative rule (see Section 1.2.4.2) to obtain the damage D.

6. Check if the damage causes failure with the design rule.

The Rainflow-counting method (Step 2) and the notion of damage (Step 4-6) are detailed below.

1.2.4.1 Rainflow-counting method

The Rainflow-counting method is widely used in industry to identify the cycles of a VA signal. The method was initially developed by Matsuishi and Endo [1968], and nowadays, different algorithmic versions coexist [Downing and Socie, 1982; Amzallag *et al.*, 1994]. However, the definition of a cycle as an hysteresis loop in the stress-strain plane (see Figure

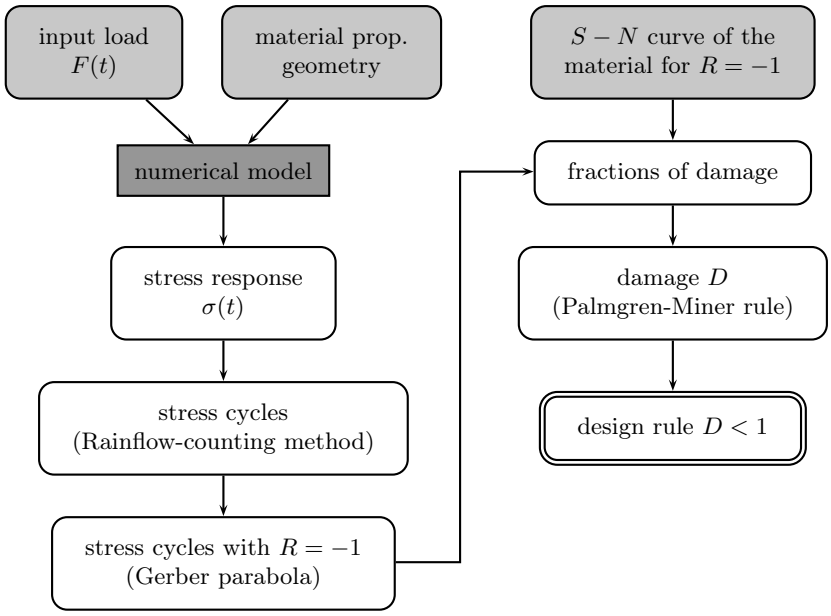

Figure 1.5: Fatigue design under a VA load.

1.6) is a shared principle. The four-point Rainflow-counting algorithm recommended by the French national organization for standardization [AFNOR, 1993] is as follows:

1. The sequence of N_{tp} local minima and maxima known as the turning points (or peaks and valleys) is extracted from the stress history $\sigma(t)$.

2. The position in the sequence of turning points is indexed by i. At the first iteration, $i = 1$.

3. The four successive turning points of the sequence are considered: σ_i, σ_{i+1}, σ_{i+2}, σ_{i+3}.

4. The following ranges are calculated: $\Delta_1 = |\sigma_{i+1} - \sigma_i|$, $\Delta_2 = |\sigma_{i+2} - \sigma_{i+1}|$, $\Delta_3 = |\sigma_{i+3} - \sigma_{i+2}|$.

5. If $\Delta_2 \leq \Delta_1$ and $\Delta_2 \leq \Delta_3$, the couple (σ_{i+1},σ_{i+2}) constitutes a cycle. Its mean $\sigma_m = (\sigma_{i+1} + \sigma_{i+2})/2$ and its amplitude $\sigma_a = |\sigma_{i+1} - \sigma_{i+2}|/2$ are calculated, and stored for further analysis. The points σ_{i+1} and σ_{i+2} are extracted from the sequence ($N_{tp} = N_{tp} - 2$), and σ_i and σ_{i+3} are now successive turning points. The algorithm goes back to Step 3 with $i = i - 2$ (or $i = 1$).

6. If the previous conditions are not satisfied, the algorithm goes back to Step 3 with $i = i + 1$.

The algorithm stops when $i + 3 > N_{tp}$. The turning points which have not been extracted from the sequence constitute the residue. The damage contribution of the residue is

significant as it contains the extreme turning points over the sequence. To extract this damage contribution, the four-point algorithm described above is run again in order to identify the cycles of a new sequence generated by repeating the residue. At the end of the procedure, the full decomposition of the stress history into cycles is obtained. Note that a counting threshold is often set in the Rainflow-counting method to avoid the consideration of small cycles and noise. Such a threshold may have an impact on fatigue life prediction. To conclude on this part, cycles are usually plotted in a 3D histogram, known as the Rainflow matrix, which represents the number of cycles ordered by mean and amplitude (see Figure 1.7).

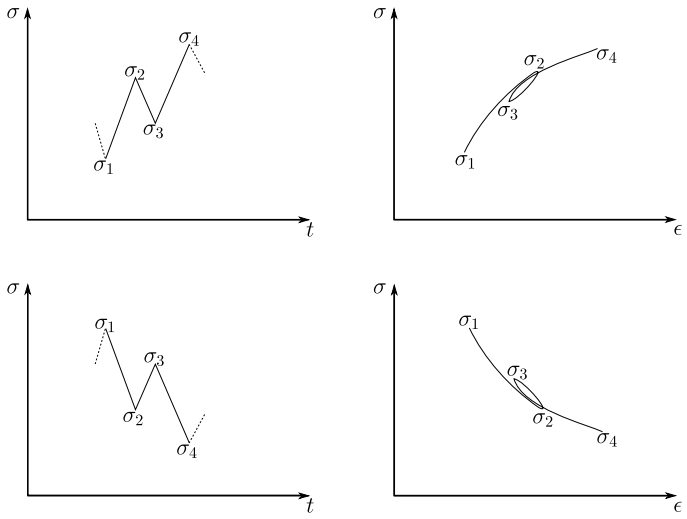

Figure 1.6: Sequence of turning points $(\sigma_1, \sigma_2, \sigma_3, \sigma_4)$ (on the left-hand side) with the corresponding hysteresis loop in the stress-strain plane (on the right-hand side). The segment (σ_2, σ_3) forms a cycle.

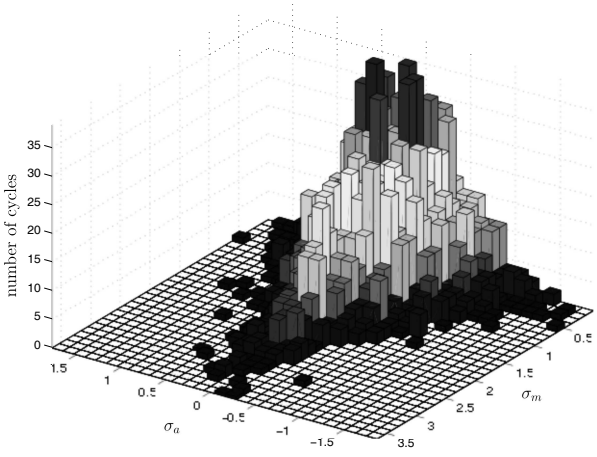

Figure 1.7: Example of Rainflow matrix.

1.2.4.2 Cumulative damage

In fatigue, the evolution of the material deterioration is quantified by the concept of damage denoted by D, which ranges between 0 (no deterioration) and 1 (failure). The fatigue life is frequently predicted with the Palmgren-Miner cumulative damage rule [Miner, 1945] that defines, for a stress level characterized by a mean $\sigma_{m,i}$ and an amplitude $\sigma_{a,i}$, the fraction of damage d_i as the ratio of the number n_i of cycles undergone by the structure to the number of cycles to failure N_i:

$$d_i = \frac{n_i}{N_i} \tag{1.7}$$

Note that N_i is derived from the $S-N$ curve. The Palmgren-Miner cumulative damage rule assumes that the order in which the cycles are undergone does not affect the fatigue life and that the fractions of damage can be added in a linear manner. The damage D then reads:

$$D = \sum_i d_i = \sum_i \frac{n_i}{N_i} \tag{1.8}$$

Failure occurs if the sum reaches 1. The design rule is thus $D < 1$ (see Figure 1.5).

1.2.5 Equivalent fatigue concept

In industry, fatigue design codes can also be deterministic stress-strength approaches as illustrated in Figure 1.8. The history $\sigma(t)$ of the stress response is summarized into a single stress value which is then compared with a given fatigue strength. The Equivalent Fatigue (EF) concept is commonly used to summarize the stress response. It converts a VA signal $\sigma(t)$ into a simple CA cycle which, repeated an arbitrary number of times N_{eq}, produces the same fatigue damage to the structure. This cycle is generally defined as fully reversed in order to be wholly characterized by its amplitude σ_{eq}. This amplitude is then compared with the fatigue strength r at N_{eq} cycles which is derived from the $S-N$ curve of the material expressed for $\mathcal{R} = -1$. The design rule thus becomes $\sigma_{eq} < r$. In this section, the EF concept is first applied to an assumed VA stress response at the critical location of the structure. It is then extended to a VA load imposed on the global structure as is usually the case for pre-dimensioning and test characterization.

1.2.5.1 Equivalent fatigue stress response

The stress response of a structure to an input VA load is assumed to be uniaxial at the critical location (or at least dominated by a direction). Its cycles are extracted, and the ith one is characterized by a mean $\sigma_{m,i}$, an amplitude $\sigma_{a,i}$ and a number of occurrences n_i. The damage induced by these cycles is denoted by D_R. Let D_{eq} be the damage produced by the EF cycle repeated N_{eq} times. Given an arbitrary N_{eq}, the symmetric alternating amplitude σ_{eq} must be determined so that $D_R = D_{eq}$.

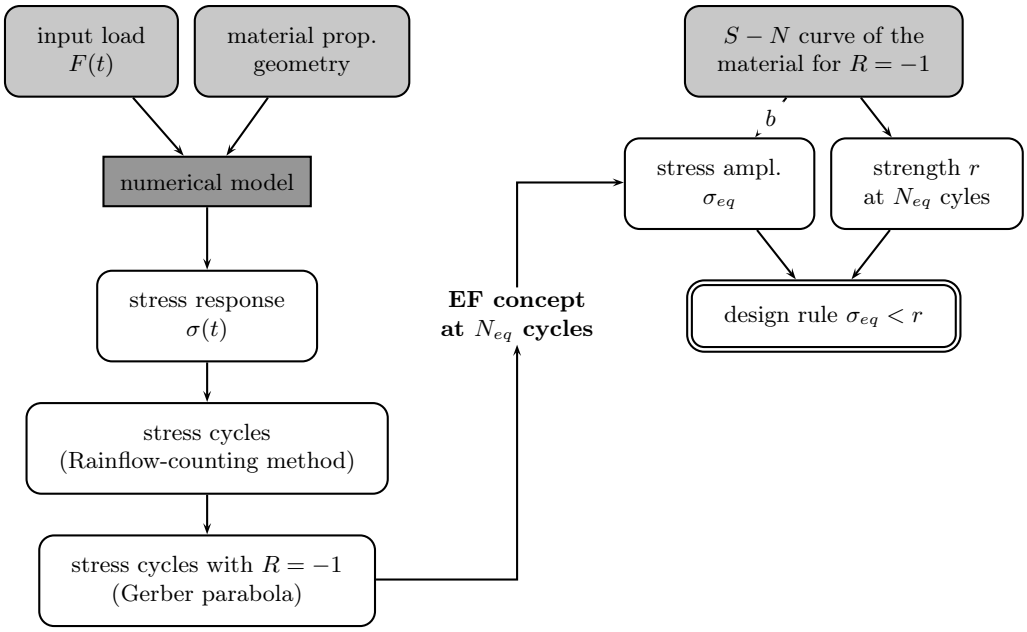

Figure 1.8: Deterministic stress-strength approach based on the EF concept.

On the one side, the damage D_R is calculated as explained in the previous section. For instance, assume that the Haigh diagram is modelled with the Gerber parabola, and that the $S - N$ curve is expressed as the Basquin's relation given in Eqn(1.3). Using the Palmgren-Miner cumulative rule, the damage D_R reads:

$$D_R = \sum_i n_i \left(\frac{\sigma_{a,i}}{B\left(1 - \left(\frac{\sigma_{m,i}}{R_m}\right)^2\right)} \right)^{-\frac{1}{b}} \tag{1.9}$$

On the other side, the damage D_{eq} simply reads:

$$D_{eq} = N_{eq} \left(\frac{\sigma_{eq}}{B} \right)^{-\frac{1}{b}} \tag{1.10}$$

The equivalence of the damages gives:

$$\sum_i n_i \left(\frac{\sigma_{a,i}}{\left(1 - \left(\frac{\sigma_{m,i}}{R_m}\right)^2\right)} \right)^{-\frac{1}{b}} = N_{eq}\ {\sigma_{eq}}^{-\frac{1}{b}} \tag{1.11}$$

In the literature [Thomas *et al.*, 1999; Veldkamp, 2006], N_{eq} is usually set to 10^6, but it may also be the number of cycles observed in the life of the structure. Given this arbitrary number of cycles, the EF amplitude is easily determined from Eqn.(1.11).

1.2.5.2 Equivalent fatigue load

The fatigue design approaches introduced previously require the knowledge of the stress response at the critical location of the structure. Often, in-service measurements provide the input loads, and the stress response history $\sigma(t)$ is derived from a time-demanding evaluation of the numerical model. Under some assumptions, the EF concept may also be used to summarize the load applied to the global structure instead of the stress response [Thomas *et al.*, 1999; Veldkamp, 2006; Genet, 2006]. In such a case, the EF cycle of the load is applied to the numerical model, and the cycle of stress response thus obtained is interpreted as being repeated N_{eq} times. The EF load is an extremely convenient tool as it avoids the time-demanding calculation of $\sigma(t)$. Additionally, it presents a large potential for other fatigue applications. For instance in Morel *et al.* [1993], the amplitude of the EF cycle is derived from field measurements, and then used as a setting value on a testing machine in order to perform simple but representative fatigue tests on real structures. The amplitude of the EF cycle may also be employed to compare different loads as it is a scalar representation of the load severity.

The equivalence of the damages D_R and D_{eq} must be assessed strictly from the loads that are independent from the geometry of the structure. Assume that a force load $F(t)$ is applied to the structure. The ith force cycle is characterized by a mean $F_{m,i}$, an amplitude $F_{a,i}$ and a number of occurrences n_i. Assume that the EF cycle is fully reversed, and features an amplitude F_{eq}. This amplitude must be determined so that $D_R = D_{eq}$. On the hypothesis that the global behaviour of the structure is elastic and quasi-static [Genet, 2006], the stress response at the critical location is proportional to the applied force:

$$\sigma(t) = \lambda\, F(t) \tag{1.12}$$

where λ depends on the structure's geometry and material. This linear assumption is acceptable in the case of a structure designed for high cycle fatigue, as macroscopic cyclic plasticity is not observed. According to Eqn.(1.12), the following relations can be written:

$$\begin{cases} \sigma_m = \lambda\, F_m \\ \sigma_a = \lambda\, F_a \\ \sigma_{eq} = \lambda\, F_{eq} \end{cases} \tag{1.13}$$

and the Basquin's relation becomes:

$$\lambda\, F'_a = B\, N^b \tag{1.14}$$

The damage D_{eq} expressed from the force thus reads:

$$D_{eq} = N_{eq} \left(\frac{\lambda\, F_{eq}}{B} \right)^{-\frac{1}{b}} \tag{1.15}$$

Concerning the damage D_R, Eqn.(1.9) requires the knowledge of the tensile strength R_m. The coefficient λ cannot be used to link the tensile strength to the 'tensile force' as plasticity occurs. An approximation is therefore made by considering the ratio K of the tensile strength to the stress at N_{eq} cycles:

$$K = \frac{R_m}{\sigma_{eq}} = \frac{R_m}{\lambda\, F_{eq}} \tag{1.16}$$

K depends on the fatigue behaviour of the material, and is commonly set to 2.5 for steels when $N_{eq} = 10^6$ cycles [Thomas *et al.*, 1999]. The damage D_R then reads:

$$D_R = \sum_i n_i \left(\frac{\lambda\, F_{a,i}}{B\left(1 - \left(\frac{F_{m,i}}{K\, F_{eq}}\right)^2\right)} \right)^{-\frac{1}{b}} \tag{1.17}$$

The equivalence of damages becomes:

$$\sum_i n_i \left(\frac{F_{a,i}}{\left(1 - \left(\frac{F_{m,i}}{K\, F_{eq}}\right)^2\right)} \right)^{-\frac{1}{b}} = N_{eq}\, {F_{eq}}^{-\frac{1}{b}} \tag{1.18}$$

λ and B are removed by expressing the equivalence, therefore, the structure's geometry is not involved in the expression of the EF amplitude. F_{eq} is assessed numerically using Newton's method to find the root of the following function $f(F_{eq})$:

$$f(F_{eq}) = 1 - \frac{{F_{eq}}^{\frac{1}{b}}}{N_{eq}} \sum_i n_i \left(\frac{F_{a,i}}{\left(1 - \left(\frac{F_{m,i}}{K\, F_{eq}}\right)^2\right)} \right)^{-\frac{1}{b}} \tag{1.19}$$

The function $f(F_{eq})$ is not defined for $F_{eq} = F_{m,i}/K$. It is recommended to set the initial point $F_{eq}^{(0)}$ of Newton's method so that $F_{eq}^{(0)} > \max_i(F_{m,i}/K)$.

1.2.6 Fatigue design codes in industry

The fatigue behaviour of structures is strongly affected by uncertainties [Svensson, 1997]. Tovo [2001] sorts these uncertainties into two fundamentally different categories that are:

- the inherent uncertainties of the material properties, loads, geometry and fatigue behaviour.
- the errors of the numerical model as well as in the estimation of the parameters.

The first category is the aleatoric uncertainties. They correspond to the parameters entering into mechanical modelling that are intrinsically random. The second category rep-

resents the epistemic uncertainties. In fatigue, they are caused by a lack of knowledge in the complex damage mechanism or by the shortage of experimental data. In contrast to the aleatoric uncertainties, they can, in principle, be reduced.

Most structures are designed against fatigue with deterministic approaches that are either codified in standards or based on practical experience. These approaches imply the use of so-called safety factors in an attempt to ensure the integrity of the structure while covering the inherent uncertainties mentioned above. Such factors are based on the know-how acquired through experience feedback, and are consequently highly subjective. In industry, two main fatigue design approaches exist:

- The first one is the application of the flowchart depicted in Figure 1.5 with safety rules. A codified load history is imposed on the structure, and the fraction of damage is calculated for each stress response cycle with a pessimistic $S-N$ curve. This curve can either be the isoprobabilistic $S-N$ curve representing the median shifted down by u_f (*e.g.* 3) standard deviations, or the most conservative curve obtained when multiplying the median one by a factor reducing the fatigue life and a factor augmenting the stress level [AFCEN, 2000].
- The second approach refers to the deterministic stress-strength approach. A design load representing the severity of the in-service loads is applied to the numerical model, and its stress response is compared to a conservative fatigue strength. Such a procedure may be grounded upon the EF concept as depicted in Figure 1.8.

For illustrations of such design approaches and safety factors, the reader is referred to codes such as the RCC-M standard [AFCEN, 2000] for nuclear applications, or the FEM1.001 [FEM, 1998] for lifting machines.

1.3 Probabilistic fatigue design

1.3.1 Introduction

As mentioned previously, safety factors are applied in deterministic fatigue design approaches to cover the uncertainties that are inherent to the fatigue phenomenon. Although these approaches mostly give satisfactory results, the use of safety factors often leads to over-design, *i.e.* excessive dimensions and masses. Within the scope of cost optimization, engineers are asked to design structures that are safe while using a minimum quantity of raw materials. Such a challenge can only be met through a better understanding of the structural behaviour. From this perspective, the knowledge of the safety margin and the most influent design factors on structural reliability is valuable for the design process. Deterministic methods are not sufficient to acquire this information, and probabilistic approaches are gradually finding their way into industrial research in order to provide answers to these recent expectations.

This part is devoted to these approaches. Section 1.3.2 explains the principles of the probabilistic approaches. Section 1.3.3 presents tools for inferring statistical distributions. Section 1.3.4 discusses methods for modelling the uncertainty of the in-service loads. Section 1.3.5 introduces the probabilistic $S-N$ curves to model the scatter of the fatigue behaviour. Section 1.3.6 explains the probabilistic Stress-stRength approach developed by Thomas *et al.* [1999]. Finally, Section 1.3.7 presents the approach implemented in the APPRoFi project.

1.3.2 Principles of the probabilistic approaches

In mechanics, probabilistic approaches are a way to consider the physical uncertainties affecting a structure [Ditlevsen and Madsen, 1996; Lemaire, 2009]. With such approaches, each parameter entering into mechanical modelling (*e.g.* structure dimensions, boundary conditions, material properties, fatigue behaviour...) is no longer a single value or number but a random variable. The mechanical response then becomes random, and its uncertainty can be quantified.

The present section is based on Lemaire [2009] and Sudret [2011]. Figure 1.9 depicts the general flowchart of a probabilistic approach. At first, **a deterministic model $\mathcal{M}$ (Step 1)** must be defined, and particularly its input parameters $\mathbf{x}$ and its response y. As mentioned above, the vector $\mathbf{x}$ is composed of the geometry, load and material parameters. In fatigue design, the response y may for instance be a damage value, a stress level or a number of cycles to failure.

Step 2 of the probabilistic approach is the **stochastic modelling** of uncertainties. The variabilities of $\mathbf{x}$ are modelled with Probability Density Functions (PDF) such as Gaussian, Weibull, uniform... The parameters are now random variables $\mathbf{X} = \mathbf{X}(\omega)^{\dagger}$. In practice, the PDFs are inferred from data sets that may be acquired by:

- quality controls for the geometry parameters.
- experience feedback and field measurements for the uncertainty of the in-service loads.
- multiple tests on structures and specimens for material properties and fatigue behaviour.

Classically, the parameters of the PDFs are adjusted by maximum likelihood estimation, and goodness-of-fit tests are conducted to determine whether the assumed distribution is valid (see Section 1.3.3 for further details on these statistical inference methods). Bayesian inference may also be used when the size of the data set is small and when there is *a priori*

[†]In this thesis, random parameters are written in capital letters. However, ω is sometimes used to underline the random nature of the quantity. For instance, the random stress level and the random number of cycles to failure are denoted by $\sigma(\omega)$ and $N(\omega)$ respectively.

information. It consists in determining a 'posterior' distribution according to the Bayes' rule, given a 'prior' believed distribution and the observation of data. Finally, when no data are available, recourse to expert judgement is required. A distribution and its parameters are simply assumed based on empirical knowledge.

Step 3 is the **propagation of uncertainty**. The response of the deterministic model is now a random variable $Y = \mathcal{M}(\mathbf{X})$ whose realizations are only known when evaluating $\mathcal{M}$ for a given realization $\mathbf{x}$ of $\mathbf{X}$. The propagation of uncertainty aims at characterizing the random response Y. Different analyses exist depending on the objective of the study. In the frame of this thesis, a structural reliability analysis is conducted. In such an analysis, a failure scenario of the structure is mathematically represented by a performance function $G(\mathbf{X})$ (or several) which is defined in order to give positive values in the safe domain and zero or negative values in the failure domain. The objective of the analysis is then to determine the failure probability $P_f = \text{Prob}(G(\mathbf{X}) \leq 0)$ through the use of reliability methods that are further discussed in Chapter 2. Note that the analysis also produces the importance factors or sensitivity indices which quantify the influence of the random input parameters on structural reliability. Finally, in the case of fatigue design, the performance function G can either be the difference between 1 and the cumulated damage, the difference between a fatigue strength and a stress level, or the difference between a reference number of cycles and the number of cycles to failure.

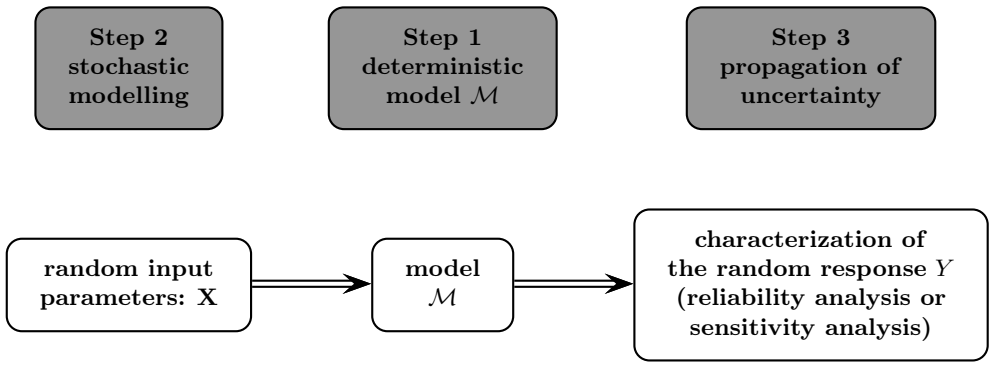

Figure 1.9: Steps of the probabilistic approach in mechanics.

1.3.3 Basic statistical inference methods

This section introduces some basic methods that are employed in this research work for modelling the uncertainty of the input parameters.

1.3.3.1 Maximum likelihood estimation

Statistical modelling aims at determining the stochastic model shared by a set of observations $\{x^{(1)}, \ldots, x^{(Q)}\}$ which are presumed to be independent and identically distributed.

To establish such a model, two types of methods exist in the literature: parametric methods and non-parametric methods. Within a parametric framework, a statistical distribution is assumed, and its parameters are inferred according to the observations. Conversely, non-parametric methods such as kernel density estimation [Saporta, 2006] do not rely on assumptions that the data are drawn from a given distribution. In the frame of this thesis, a parametric method known as Maximum Likelihood (ML) estimation [Fisher, 1950] is used.

Assume f_X to be the PDF of the random variable X whose available observations are denoted by $\{x^{(1)}, \dots, x^{(Q)}\}$. ML estimation aims at determining the parameters $\boldsymbol{\theta} = \{\theta_1, \dots, \theta_h\}$ of f_X according to the observations. For this purpose, the likelihood $\mathcal{L}$ is expressed as:

$$\mathcal{L}\left(\boldsymbol{\theta}; x^{(1)}, \dots, x^{(Q)}\right) = \prod_{i=1}^{Q} f_X\left(x^{(i)}; \boldsymbol{\theta}\right) \tag{1.20}$$

The ML estimate $\hat{\boldsymbol{\theta}}$ corresponds to the value of $\boldsymbol{\theta}$ that maximizes the likelihood. In practice, the log-likelihood is used in order to determine $\hat{\boldsymbol{\theta}}$. The optimization problem to solve then reads:

$$\hat{\boldsymbol{\theta}} = \arg\min \sum_{i=1}^{Q} -\ln f_X\left(x^{(i)}; \boldsymbol{\theta}\right) \tag{1.21}$$

In some cases, an explicit expression of the ML estimate may be derived. However, the optimization problem must often be solved numerically.

The selection of a PDF from a set of candidate models is done thanks to likelihood criteria such as AIC (Akaike Information Criterion) [Akaike, 1974] and BIC (Bayesian Information Criterion) [Schwarz, 1978]. These criteria measure the relative goodness of fit of models, and are based on the maximum value $\mathcal{L}_{\max}$ of the likelihood attained at $\hat{\boldsymbol{\theta}}$. AIC reads:

$$\mathrm{AIC} = -2 \ln \mathcal{L}_{\max} + 2\, h \tag{1.22}$$

where h denotes the number of components of $\boldsymbol{\theta}$. BIC reads:

$$\mathrm{BIC} = -2 \ln \mathcal{L}_{\max} + h \ln Q \tag{1.23}$$

where Q is recalled to be the number of available observations. The model to select is the one with the minimum AIC and BIC values. However, these criteria do not tell how well a model fits the data in an absolute sense. They can in fact only be used for comparing different models, and analysis must then be completed with goodness-of-fit tests to validate model hypotheses. These tests are introduced in the next section.

1.3.3.2 Goodness-of-fit tests

Goodness-Of-Fit (GOF) tests check whether there is evidence that a set of observations does not arise from a given statistical distribution. The null hypothesis usually denoted by H_0 corresponds to the position where the observations arise from the assumed distribution. Conversely, the alternative hypothesis H_1 is the position where the observations are not drawn from the assumed distribution. Let F_0 be the Cumulative Distribution Function (CDF) that is assumed, and $\hat{F}_Q$ be the empirical CDF of the observations. GOF tests quantify a distance between $\hat{F}_Q$ and F_0 known as the test statistic which is then compared with a critical value, in order to determine whether H_0 should be rejected or not (note that H_0 can never be proven). This critical value is associated with a significance level which corresponds to the probability of making an error by rejecting H_0. This probability is usually set to 5%. Another way of using GOF tests is to use the p-value in order to examine the strength of evidence that the set of observations provides against H_0. The p-value represents the probability of obtaining a test statistic at least as extreme as the value observed, assuming that H_0 is true. Hence the smaller the p-value, the stronger the evidence against H_0. Often, H_0 is rejected when the p-value is below the significance level.

The first GOF test considered in this research work is Kolmogorov-Smirnov's. Its statistic $\hat{D}$ reads:

$$\hat{D} = \max_{i\in\{1,\dots,Q\}} \left[\, |F_0(x^{(i)}) - \hat{F}_Q(x^{(i)})|, \; |F_0(x^{(i)}) - \hat{F}_Q(x^{(i-1)})| \, \right] \tag{1.24}$$

Under H_0, this statistic is asymptotically ($Q \to +\infty$) distributed as [Saporta, 2006]:

$$\text{Prob}(\sqrt{Q}\hat{D} > d) \to K(d) = \sum_{k=-\infty}^{+\infty} (-1)^k \exp(-2k^2d^2) \tag{1.25}$$

H_0 is then rejected if $\sqrt{Q}\hat{D}$ is higher than a critical value d_α (see Saporta [2006] for tables of d_α depending on the significance level).

The Anderson-Darling test [NIST/SEMATECH] is an alternative to the Kolmogorov-Smirnov test, and is often preferred for its ability to give more weight to the distribution tails. Its statistic $\hat{A}$ reads:

$$\hat{A} = -Q - \sum_{i=1}^{Q} \frac{2i-1}{Q} \left(\ln(F_0(x^{(i)})) + \ln(1 - F_0(x^{(Q-i+1)})) \right) \tag{1.26}$$

Contrary to the Kolmogorov-Smirnov test, the critical values of the Anderson-Darling test depend on the distribution which is assumed (see D'Agostino and Stephens [1986] for tables of critical values). The asymptotic distribution of the Anderson-Darling statistic presents a complex expression (see Marsaglia and Marsaglia [2004]). The calculation of the p-value is therefore relatively difficult, but one may use the package 'ADGofTest' [Gil Bellosta,

2011] of the programming language R which provides the p-value calculation based on the works by Marsaglia and Marsaglia [2004].

1.3.4 Modelling of in-service loads

The uncertainty of the in-service loads must be considered in the fatigue calculation so as to determine a correct structural design. Field measurements are generally conducted to examine this uncertainty. The problem tackled in this section is the determination of a stochastic model that matches the variability observed in a database of measurements. A load mix strategy dividing load histories into elementary life situations and the use of mixture models to represent Rainflow matrices are discussed here. It is important to note that this section is restricted to the methods studied in the frame of the APPRoFi project. Approaches such as the modelling of loads with stationary Gaussian processes [Pitoiset, 2001; Benasciutti and Tovo, 2005] or Markovian processes [Mattrand and Bourinet, 2011; Mattrand, 2011] are possible alternatives.

1.3.4.1 Load mix strategy

The load mix strategy [Thomas *et al.*, 1999; Bignonnet *et al.*, 2009; Lefebvre *et al.*, 2009] considers that in-service loads are mixtures of elementary life situations corresponding to specific usages of the structure. An elementary situation features:

- field measurements of the corresponding load which are generally converted into Rainflow matrices.
- a random percentage of occurrence during the structure's life span. Such information may be extracted from a customer survey or from field measurements of some parameters in addition to the load.

Table 1.1 presents the load mix strategy as described by Bignonnet *et al.* [2009]. $\mathcal{Q}^1$ and $\mathcal{Q}^2$ are quantities characterizing the structure's usage (*e.g.* the carried mass and speed). Two classes denoted by $\mathcal{Q}_1^i$ and $\mathcal{Q}_2^i$ are defined for each quantity $\mathcal{Q}^i$ (*e.g.* the class ≤ 500 kg and the class > 500 kg for the carried mass, or ≤ 100 km/h and > 100 km/h for the speed). Four elementary life situations then exist: $(\mathcal{Q}_1^1, \mathcal{Q}_1^2)$, $(\mathcal{Q}_1^1, \mathcal{Q}_2^2)$, $(\mathcal{Q}_2^1, \mathcal{Q}_1^2)$ and $(\mathcal{Q}_2^1, \mathcal{Q}_2^2)$. Several Rainflow matrices $\mathbb{M}_{j,k}^{(1)}$, $\mathbb{M}_{j,k}^{(2)}$,... representing the applied loads during realizations of the situation $(\mathcal{Q}_j^1, \mathcal{Q}_k^2)$ are derived from field measurements. Note that these Rainflow matrices are normalized to a given reference (*e.g.* 1 second or 1 km) in order to facilitate further use. For each class $\mathcal{Q}_j^i$, the ratio of the time spent in this class to the structure's life span is modelled with a random percentage of occurrence P_j^i which is usually considered as uniform [Lefebvre *et al.*, 2009]. A Rainflow matrix $\mathbb{L}$ representing a virtual life of the structure is generated by selecting a realization $\{p_1^1, p_2^1, p_1^2, p_2^2\}$ of the

four random percentages $\{P_1^1, P_2^1, P_1^2, P_2^2\}$ and a Rainflow matrix to consider for each elementary situation (see the circled matrices in Table 1.1). The matrix $\mathbb{L}$ then reads:

$$\mathbb{L} = C \left(p_1^1 \, p_1^2 \, \mathbb{M}_{1,1}^{(4)} + p_1^1 \, p_2^2 \, \mathbb{M}_{1,2}^{(2)} + p_2^1 \, p_1^2 ; \mathbb{M}_{2,1}^{(1)} + p_2^1 \, p_2^2 \, \mathbb{M}_{2,2}^{(3)} \right) \tag{1.27}$$

where C is a coefficient transposing the normalized Rainflow matrices to the structure's estimated life span.

Elementary life sit.	Random percentages	Rainflow matrices
$(\mathcal{Q}_1^1, \mathcal{Q}_1^2)$	$P_1^1 \times P_1^2$	$\mathbb{M}_{1,1}^{(1)}$; $\mathbb{M}_{1,1}^{(2)}$; $\mathbb{M}_{1,1}^{(3)}$; $\boxed{\mathbb{M}_{1,1}^{(4)}}$
$(\mathcal{Q}_1^1, \mathcal{Q}_2^2)$	$P_1^1 \times P_2^2$	$\mathbb{M}_{1,2}^{(1)}$; $\boxed{\mathbb{M}_{1,2}^{(2)}}$; $\mathbb{M}_{1,2}^{(3)}$
$(\mathcal{Q}_2^1, \mathcal{Q}_1^2)$	$P_2^1 \times P_1^2$	$\boxed{\mathbb{M}_{2,1}^{(1)}}$
$(\mathcal{Q}_2^1, \mathcal{Q}_2^2)$	$P_2^1 \times P_2^2$	$\mathbb{M}_{2,2}^{(1)}$; $\mathbb{M}_{2,2}^{(2)}$; $\boxed{\mathbb{M}_{2,2}^{(3)}}$

Table 1.1: Illustration of the load mix strategy.

Two types of random variables are necessary in the load mix strategy: the percentages of occurrence and the discrete variables enabling the selection of a Rainflow matrix for each elementary life situation. The percentages characterizing the classes of a quantity $\mathcal{Q}^i$ are inevitably correlated, since their sum must be 100%. In the case depicted in Table 1.1, P_2^i can be defined as fully dependent on P_1^i, *i.e.* $P_2^i = 100 - P_1^i$, and consequently only two random percentages (P_1^1 and P_1^2) are sufficient to model all the occurences. For applications with a higher-than-two number of classes, the modelling of the percentages is more complex and requires simplifying hypotheses. An approach for three classes, for instance, could be to consider two percentages as uniform distributions and the third as the difference between 100 and their sum (assuming the sum is below 100). Note that the third percentage does not follow a uniform distribution in such an approach. The second type of random variables involved in the load mix strategy consists of the discrete variables enabling the selection of a Rainflow matrix for each elementary life situation. In the illustration shown in Table 1.1, three discrete variables are necessary, one for each of the following elementary life situations: $(\mathcal{Q}_1^1, \mathcal{Q}_1^2)$, $(\mathcal{Q}_1^1, \mathcal{Q}_2^2)$ and $(\mathcal{Q}_2^1, \mathcal{Q}_2^2)$.

In addition to the complex definition of the percentages, the load mix strategy presents two main limits for structural reliability analysis. First, a large number of random variables must be handled when numerous elementary life situations are defined. Second, the consideration of discrete random variables in reliability is difficult, except for sampling-based methods, but such methods are often inapplicable due to their high computational cost (see Chapter 2).

1.3.4.2 Mixture models of Rainflow matrices

Field measurements are generally conducted in a short period of time, and consequently, all the cycles the structure may undergo during its life are not observed. The parametric modelling of Rainflow matrices with unimodal joint PDFs is a solution to extrapolate more damaging cycles. Nevertheless, Rainflow matrices are multimodal when load histories are non-stationary random processes, and a simple joint PDF is thus not always sufficient [Nagode *et al.*, 2001]. This section introduces the concept of mixture models for the particular case of Rainflow matrices, and is mainly based on the works by Nagode and Fajdiga [1998, 2000, 2006]; Nagode *et al.* [2001]; Nagode [2012]. Note that after Nagode *et al.* [2001], Rainflow matrices are considered in this section as representations of the number of cycles ordered by mean σ_m and range $\Delta\sigma$ (instead of amplitude).

For convenience, let $\mathbf{S}$ be the random vector $\{S_m, S_r\}^t = \{\sigma_m(\omega), \Delta\sigma(\omega)\}^t$ where $S_m = \sigma_m(\omega)$ is the random mean and $S_r = \Delta\sigma(\omega)$ is the random range. A realization of this random vector is denoted by $\mathbf{s} = \{\sigma_m, \Delta\sigma\}^t$. A Rainflow matrix can be defined as a weighted sum of component distributions:

$$f_{\mathbf{S}}(\mathbf{s}; \mathbf{w}, \boldsymbol{\theta}^{(1)}, \ldots, \boldsymbol{\theta}^{(z)}) = \sum_{l=1}^{z} w^{(l)} \; f_{\mathbf{S}}^{(l)}(\mathbf{s}; \boldsymbol{\theta}^{(l)}) \tag{1.28}$$

where $\boldsymbol{\theta}^{(l)}$ are the parameters of the lth component distribution $f_{\mathbf{S}}^{(l)}(\mathbf{s}; \boldsymbol{\theta}^{(l)})$, and where the mixing weights are denoted by $\mathbf{w} = \{w^{(1)}, \ldots, w^{(z)}\}^t$ with $w^{(l)} \geq 0$ for $l = 1, \ldots, z$ and $\sum_{l=1}^{z} w^{(l)} = 1$. The component distributions are presumed as being conditionally independent. Hence, $f_{\mathbf{S}}^{(l)}(\mathbf{s}; \boldsymbol{\theta}^{(l)})$ reads:

$$f_{\mathbf{S}}^{(l)}(\mathbf{s}; \boldsymbol{\theta}^{(l)}) = f_{S_m}^{(l)}(\sigma_m; \boldsymbol{\theta}_{S_m}^{(l)}) \times f_{S_r}^{(l)}(\Delta\sigma; \boldsymbol{\theta}_{S_r}^{(l)}) \tag{1.29}$$

where $f_{S_m}^{(l)}(\sigma_m; \boldsymbol{\theta}_{S_m}^{(l)})$ denotes the distribution of the random mean and $f_{S_r}^{(l)}(\Delta\sigma; \boldsymbol{\theta}_{S_r}^{(l)})$ the distribution of the random range for the lth component.

Nagode *et al.* [2001] propose mixture models composed of Gaussian distributions for means and two-parameter Weibull distributions for ranges. An illustration of such mixture models is depicted in Figure 1.10. The Gaussian distribution of means corresponding to the lth component reads:

$$f_{S_m}^{(l)}(\sigma_m; \boldsymbol{\theta}_{S_m}^{(l)}) = \frac{1}{\sqrt{2\pi}\sigma_{S_m}^{(l)}} \exp\left(-\frac{1}{2} \frac{\left(\sigma_m - \mu_{S_m}^{(l)}\right)^2}{{\sigma_{S_m}^{(l)}}^2} \right) \tag{1.30}$$

where $\boldsymbol{\theta}_{S_m}^{(l)}$ is the vector containing the mean $\mu_{S_m}^{(l)}$ and the standard deviation $\sigma_{S_m}^{(l)}$ of the random mean S_m for the lth component. Ranges are modelled with Weibull distributions because the PDF support is $\mathbb{R}_+$. The Weibull distribution of ranges corresponding to the

lth component reads:

$$f_{S_r}^{(l)}(\Delta\sigma;\boldsymbol{\theta}_{S_r}^{(l)}) = \frac{h_{S_r}^{(l)}}{\lambda_{S_r}^{(l)}}\left(\frac{\Delta\sigma}{\lambda_{S_r}^{(l)}}\right)^{\kappa_{S_r}^{(l)}-1}\exp\left(-\left(\frac{\Delta\sigma}{\lambda_{S_r}^{(l)}}\right)^{\kappa_{S_r}^{(l)}}\right) \tag{1.31}$$

where $\boldsymbol{\theta}_{S_r}^{(l)}$ is the vector containing the shape parameter $\kappa_{S_r}^{(l)}$ and the scale parameter $\lambda_{S_r}^{(l)}$ of the random range S_r for the lth component. As expressed in Eqn.(1.29), S_m and S_r corresponding to the lth component stand for independent variables. However, it is underlined by Nagode *et al.* [2001] that a global correlation between mean and range can be modelled by selecting an appropriate number of component distributions.

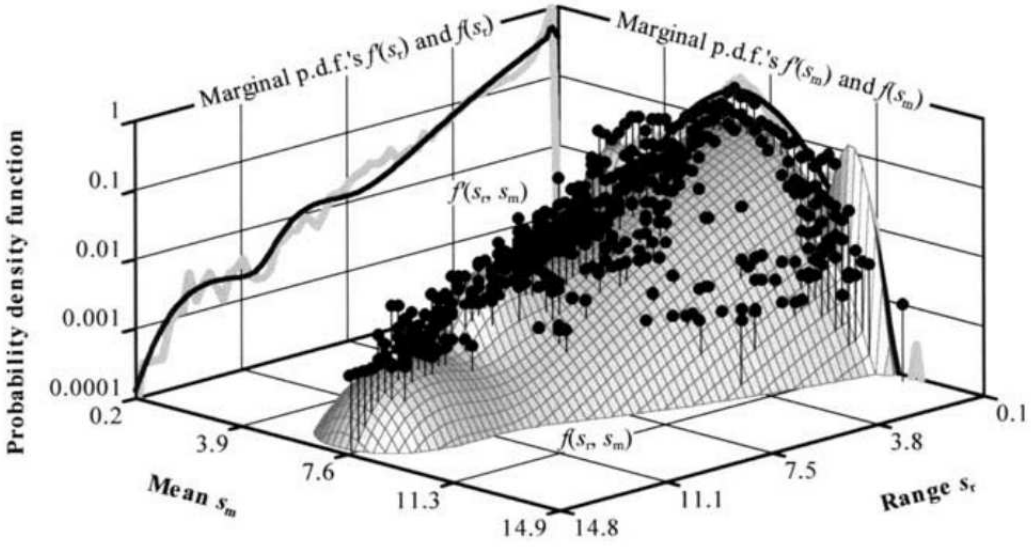

Figure 1.10: Illustration of a mixture model from Nagode *et al.* [2001]. The black dots represent the cycles. The mixture model contains five component distributions.

In order to establish a mixture model, the number of component distributions z, the mixing weights $\mathbf{w}$ and the parameters $\{\boldsymbol{\theta}^{(l)},\ l = 1,\ldots,z\}$ have to be determined. Such an analysis may be conducted with the REBMIX algorithm [Nagode and Fajdiga, 1998, 2000, 2006; Nagode *et al.*, 2001]. Note that the R package called 'rebmix' [Nagode and Fajdiga, 2011a,b] provides an implementation of the algorithm whose principles are presented below. The reader is referred to Nagode [2012] for further details.

Principles of the REBMIX algorithm

For the sake of clarity, the algorithm, depicted in Figure 1.11, is described on a simple one-dimensional Rainflow matrix, *i.e.* a histogram into which n fully reversed (mean = 0) stress cycles are sorted according to the range. In the general case of a Rainflow matrix ordered by mean and range, the procedure is similar.

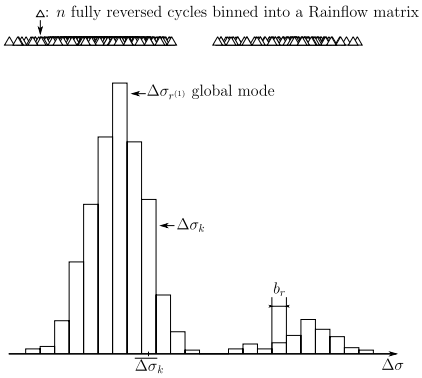

(a) Determination of the global mode for the first component distribution ($l = 1$).

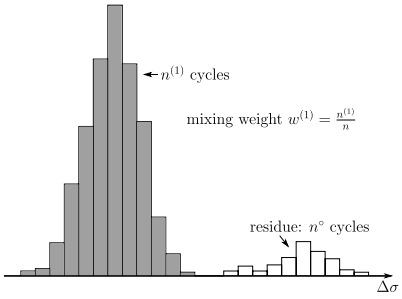

(b) Identification of the $n^{(1)}$ cycles (in grey) belonging to the first component distribution using the iterative clustering procedure and the rough estimation of the component parameters.

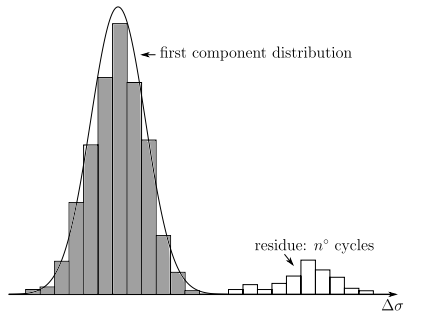

(c) Inference of the distribution's parameters using ML estimation.

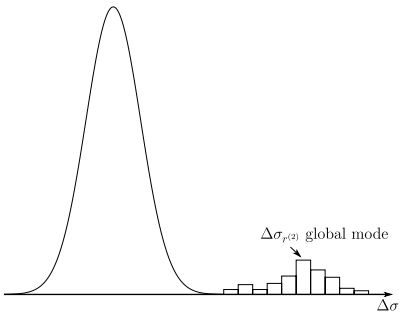

(d) Determination of the global mode for the second component distribution ($l = 2$).

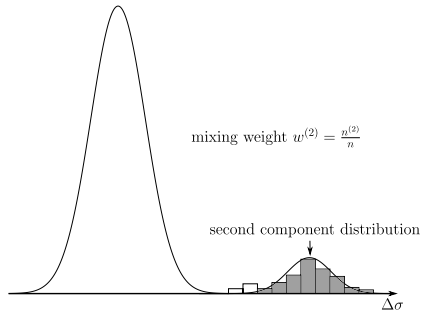

(e) Identification of the $n^{(2)}$ cycles (in grey) belonging to the second component distribution and inference of the distribution's parameters.

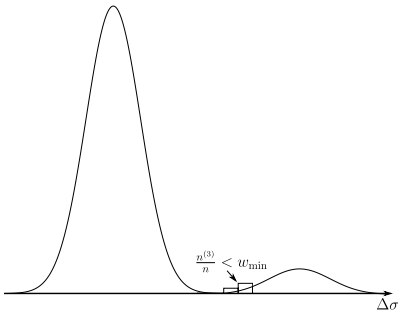

(f) Mixture model. The final residue is assigned to the second component distribution according to the Bayes decision rule.

Figure 1.11: Bases of the REBMIX algorithm after Nagode and Fajdiga [2006].

For this simplified study, the objective is to define the one-dimensional Rainflow matrix ordered by range as a weighted sum of component distributions:

$$f_{S_r}(\Delta\sigma; \mathbf{w}, \boldsymbol{\theta}_{S_r}^{(1)}, \ldots, \boldsymbol{\theta}_{S_r}^{(z)}) = \sum_{l=1}^{z} w^{(l)} \; f_{S_r}^{(l)}(\Delta\sigma; \boldsymbol{\theta}_{S_r}^{(l)}) \tag{1.32}$$

Let the range axis be discretized into classes $\Delta\sigma_k$ of width b_r. The centre of the bin $\Delta\sigma_k$ is denoted by $\overline{\Delta\sigma}_k$. The number of cycles falling into the bin $\Delta\sigma_k$ is n_k, and the corresponding relative frequency reads $f_k = n_k/n$. The number of cycles belonging to the lth component distribution is $n^{(l)}$. The number of cycles of the lth component falling into the bin $\Delta\sigma_k$ is denoted by $n_k^{(l)}$, and the corresponding relative frequency reads $f_k^{(l)} = n_k^{(l)}/n^{(l)}$. The mixing weight $w^{(l)}$ associated with the lth component is calculated as:

$$w^{(l)} = \frac{n^{(l)}}{n} \tag{1.33}$$

Initially, l is set to 1, $n_k^{(l)}$ to n_k, $n^{(l)}$ to n, and $f_k^{(l)}$ to f_k. The algorithm starts with the **determination of the global mode** (see Figure 1.11(a)), *i.e.* the bin $\Delta\sigma_{r^{(l)}}$ at which:

$$\Delta\sigma_{r^{(l)}} = \arg\max_k f_k^{(l)} \tag{1.34}$$

This global mode characterizes the lth component distribution.

An iterative **clustering procedure** is then applied to determine the $n^{(l)}$ cycles belonging to the lth component distribution (see Figure 1.11(b)). The algorithm is provided in Nagode [2012]. This procedure is based on the deviation $e_k^{(l)}$ between $n_k^{(l)}$ and the component frequency at $\overline{\Delta\sigma}_k$:

$$e_k^{(l)} = n_k^{(l)} - f_{S_r}^{(l)}(\overline{\Delta\sigma}_k; \boldsymbol{\theta}_{S_r}^{(l)}) \; b_r \; n^{(l)} \tag{1.35}$$

The most deviating cycles are gradually transferred to the residue, and the mixing weight $w^{(l)}$ is recalculated using the updated number $n^{(l)}$ in Eqn.(1.33). At the end of the procedure, the residue is composed of the n° cycles that do not belong to the lth component distribution.

At each iteration of the clustering procedure, a **rough estimation of the component parameters** $\boldsymbol{\theta}_{S_r}^{(l)} = \{\kappa_{S_r}^{(l)}, \lambda_{S_r}^{(l)}\}^t$ enables the calculation of $f_{S_r}^{(l)}(\overline{\Delta\sigma}_k; \boldsymbol{\theta}_{S_r}^{(l)})$ in Eqn.(1.35). This rough estimation is based on the expression of constraints that prevent the component distribution from moving away from its global mode. The first constraint ensures the equivalence of the relative frequencies at the global mode:

$$f_{S_r}^{(l)}\left(\overline{\Delta\sigma}_{r^{(l)}}; \boldsymbol{\theta}_{S_r}^{(l)}\right) \; b_r = f_{r^{(l)}}^{(l)} \tag{1.36}$$

The second constraint makes the global mode of the component distribution coincide with

$\overline{\Delta\sigma}_{r^{(l)}}$:

$$\left.\frac{\partial f_{S_r}^{(l)}\left(\Delta\sigma;\boldsymbol{\theta}_{S_r}^{(l)}\right)}{\partial\Delta\sigma}\right|_{\overline{\Delta\sigma}_{r^{(l)}}} = 0 \tag{1.37}$$

The parameters $\boldsymbol{\theta}_{S_r}^{(l)}$ are estimated using Eqns.(1.36) and (1.37). Note that in the case of a Rainflow matrix ordered by mean and range, additional constraints are required. They are obtained from the equivalences of the component conditional relative frequencies at the global mode [Nagode and Fajdiga, 2006; Nagode, 2012].

Once the $n^{(l)}$ cycles belonging to the lth component distribution have been identified, and the mixing weight $w^{(l)}$ has been calculated, **ML estimation** is applied in order to refine the parameters of the component distribution (see Figure 1.11(c)). l is then set to $l+1$, and the same method is conducted to determine the new lth component distribution on the basis of the $n^{(l)} = n^{\circ}$ cycles of the residue (see Figure 1.11(d) and Figure 1.11(e)). The algorithm is run until the weight $n^{(l)}/n$ is below a critical weight $w_{\min}$ which is set to avoid over-fitting (see Figure 1.11(f)). When this stopping condition is met, the remaining cycles are assigned to the existing components using the Bayes decision rule [Nagode, 2012], and the mixing weights and component parameters are recalculated. Note that the user may also set a maximum number of component distributions. The most adequate mixture model according to criteria such as AIC and BIC can be determined by repeating the procedure with various maximum numbers of component distributions.

The parametric modelling examined in this section provides a continuous description of the Rainflow matrices which may for instance be used to improve the load mix strategy explained in Section 1.3.4.1. Within such an enhanced strategy, the elementary life situations feature mixture models instead of discrete Rainflow matrices.

1.3.5 Probabilistic $S-N$ curves

As mentioned previously, the fatigue behaviour of materials is highly subjected to uncertainties. This section introduces the probabilistic $S-N$ curves as a way to model the scatter observed in a data set of fatigue tests. It focuses on the ESOPE model that is codified in the standard A03-405 [AFNOR, 1991], as well as the works by Guédé [2005]; Guédé *et al.* [2007]; Perrin [2008]. The reader may also refer to Sudret [2011] for further details on these models. In practice, a probabilistic $S-N$ curve features:

- a deterministic model $\mathcal{D}$ (or $\mathcal{D}^{-1}$) characterizing the median trend as $\sigma_{50\%} = \mathcal{D}(N)$ or $N_{50\%} = \mathcal{D}^{-1}(\sigma)$. This model may, for instance, be the Basquin's relation which is recalled to read $\sigma_{50\%} = B\,N^b$ for a given number of cycles N, or $N_{50\%} = (\sigma/B)^{1/b}$ for a given stress level σ.

- a statistical distribution to model the scatter around the median trend. Such a distribution may, for instance, be Gaussian or lognormal, and its dispersion may

be represented by either a constant standard deviation or a constant coefficient of variation at any N or σ.

Let $\mathbb{E} = \{(\sigma^{(i)}, N^{(i)}),\ i = 1, \ldots, Q\}$ be a data set of fatigue tests where $\sigma^{(i)}$ is the nominal stress undergone by a specimen and $N^{(i)}$ the corresponding number of cycles to failure. ESOPE and Guédé's models are explained below.

1.3.5.1 ESOPE

The ESOPE model [AFNOR, 1991] depicted in Figure 1.12(a) is based on the works by Bastenaire [1960]. Let $F(\sigma, N)$ be the function characterizing the probability that the specimen fails before N cycles under the stress level σ. At a given N, this function is assumed to vary in σ as the CDF of a Gaussian random variable with mean $\mu_{SN}(N)$ and standard deviation $\sigma_{SN}(N)$. The mean $\mu_{SN}(N)$ corresponds to the deterministic model $\mathcal{D}(N)$, and $\sigma_{SN}(N)$ is supposed to be constant at any N, *i.e.* $\sigma_{SN}(N) = \sigma_{SN}$. As a result, $F(\sigma, N)$ reads:

$$F(\sigma, N) = \Phi\left(\frac{\sigma - \mathcal{D}(N)}{\sigma_{SN}}\right) \tag{1.38}$$

where Φ is the standard Gaussian CDF (zero mean and unit variance). In the case of the Basquin's relation, $F(\sigma, N)$ becomes:

$$F(\sigma, N) = \Phi\left(\frac{\sigma - B\ N^b}{\sigma_{SN}}\right) \tag{1.39}$$

Given that $F(\sigma, N)$ is the CDF of a Gaussian random variable, an isoprobability $S - N$ curve reads:

$$\sigma = B\ N^b + u_f\ \sigma_{SN} \tag{1.40}$$

where u_f is a realization of the standard Gaussian variable U_f which represents the random isoprobability $S - N$ curve.

The ESOPE model is characterized by the parameters $\boldsymbol{\theta} = \{B, b, \sigma_{SN}\}^t$. As recommended in the standard A03-405 [AFNOR, 1991], ML estimation is applied to estimate these parameters according to the data set $\mathbb{E}$. Let $N(\sigma, \omega)$ be the random number of cycles to failure under a stress level σ. Its PDF $f_N(\sigma, N)$ reads:

$$f_N(\sigma, N) = \frac{\partial F(\sigma, N)}{\partial N} \tag{1.41}$$

The likelihood $\mathcal{L}$ is expressed as:

$$\mathcal{L}\left(B, b, \sigma_{SN}; \mathbb{E}\right) = \prod_{i=1}^{Q} f_N\left(\sigma^{(i)}, N^{(i)}; B, b, \sigma_{SN}\right) \tag{1.42}$$

The optimization problem consists in numerically finding the optimum $\hat{\boldsymbol{\theta}} = \{\hat{B}, \hat{b}, \hat{\sigma}_{SN}\}^t$

that reads:

$$\hat{\boldsymbol{\theta}} = \arg\min_{\boldsymbol{\theta}\in\mathbb{R}^3} \left(-\ln \mathcal{L}\left(B, b, \sigma_{SN}; \mathbb{E}\right)\right) \tag{1.43}$$

The solution of such a problem strongly depends on the starting point of the optimization procedure. In this research work, a two-step procedure is implemented. First, the least squares method is applied to determine rough estimates of B and b. The standard deviation σ_{SN} is estimated by calculating the distance between the curve obtained by the least squares method and the observations of $\mathbb{E}$. Second, the ML estimation is performed thanks to a simulated annealing algorithm whose starting point is the solution of the least squares method.

Once the ESOPE model is fully determined, the initial hypothesis on the statistical distribution must be validated *a posteriori*. A GOF test is performed to check whether there is evidence against:

$$U_f = \frac{\sigma - B\ N^b}{\sigma_{SN}} \sim \mathcal{N}(0,1) \tag{1.44}$$

where $\mathcal{N}(0,1)$ is the Gaussian distribution of parameters 0 (mean) and 1 (variance).

Figure 1.12(b) depicts an alternative model called ESOPE 2 in this thesis. For this model, the coefficient of variation δ_{SN} is supposed to be constant at any N (instead of the standard deviation σ_{SN}). The function $F(\sigma, N)$ of ESOPE 2 then reads:

$$F(\sigma, N) = \Phi\left(\frac{\sigma - B\ N^b}{\delta_{SN}\ B\ N^b}\right) \tag{1.45}$$

The isoprobability $S-N$ curve becomes:

$$\sigma = (1 + u_f\ \delta_{SN})\ B\ N^b \tag{1.46}$$

It is important to note that given Eqn.(1.46), all the isoprobability $S-N$ curves feature the same Basquin's slope b. Finally, the GOF test conducted *a posteriori* checks whether there is evidence against:

$$U_f = \frac{\sigma - B\ N^b}{\delta_{SN}\ B\ N^b} \sim \mathcal{N}(0,1) \tag{1.47}$$

1.3.5.2 Guédé's model

In ESOPE, the distribution of the number of cycles to failure $N(\sigma, \omega)$ under the stress level σ is not explicit. Guédé [2005]; Guédé *et al.* [2007] propose an alternative to ESOPE which consider $\ln N(\sigma, \omega)$ as a Gaussian random variable with parameters $\mu_N(\sigma)$ and $\sigma_N(\sigma)$. The model is depicted in Figure 1.13. Assuming that the random variables $\ln N(\sigma, \omega)$ at different stress levels are perfectly correlated, a single standard Gaussian random variable

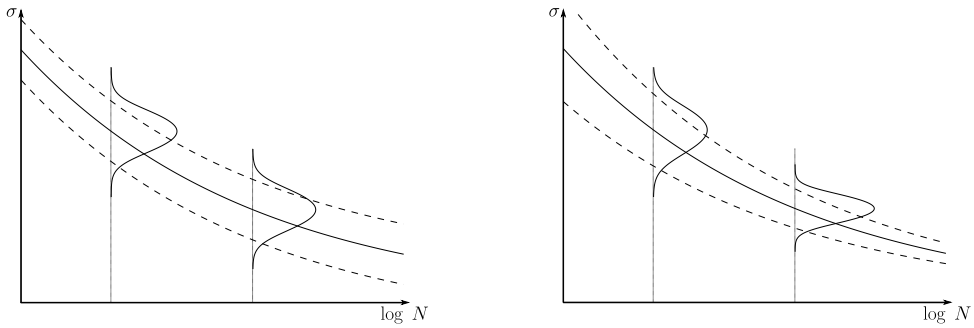

(a) ESOPE. (b) ESOPE 2.

Figure 1.12: ESOPE and ESOPE 2. The solid line represents the median curve (50% probability to fail at the stress level σ given N cycles). The dashed lines are the isoprobability $S-N$ curves defined at 2.5% and 97.5%, *i.e.* $u_f = \mp 1.96$.

U_f is sufficient to model the scatter as:

$$\ln N(\sigma, \omega) = \mu_N(\sigma) + U_f \; \sigma_N(\sigma) \tag{1.48}$$

The mean $\mu_N(\sigma)$ corresponds to the deterministic model $\mathcal{D}^{-1}(\sigma)$. In the case of the Basquin's relation, it reads:

$$\mu_N(\sigma) = A + a \; \ln \sigma \tag{1.49}$$

where $a = 1/b$ and $A = -\ln(B)/b$. The scatter in N is supposed to be correctly modelled with a constant coefficient of variation δ_N at any stress level:

$$\sigma_N(\sigma) = \delta_N \; \mu_N(\sigma) \tag{1.50}$$

As a result, $\ln N(\sigma, \omega)$ becomes:

$$\ln N(\sigma, \omega) = \mu_N(\sigma) \, (1 + U_f \; \delta_N) \tag{1.51}$$

An isoprobability $S-N$ curve is simply obtained by selecting a realization u_f of the standard Gaussian random variable U_f.

Guédé's model features the parameters $\boldsymbol{\theta} = \{A, a, \delta_N\}^t$. The PDF $f_N(\sigma, N)$ of the number of cycles to failure $N(\sigma, \omega)$ under the stress level σ is explicitly known as:

$$f_N(\sigma, N) = \frac{1}{\delta_N (A + a \; \ln \sigma) N} \phi \left(\frac{\ln N - (A + a \; \ln \sigma)}{\delta_N (A + a \; \ln \sigma)} \right) \tag{1.52}$$

where ϕ is the standard Gaussian PDF. ML estimation is applied to estimate the para-

meters of the model according to the data set $\mathbb{E}$. The likelihood $\mathcal{L}$ is expressed as:

$$\mathcal{L}\left(A, a, \delta_N; \mathbb{E}\right) = \prod_{i=1}^{Q} f_N\left(\sigma^{(i)}, N^{(i)}; A, a, \delta_N\right) \tag{1.53}$$

Note that censored data, *i.e.* fatigue tests which have been stopped before failure, can be considered in the ML estimation [Perrin, 2008; Sudret, 2011]. For a given censored test (σ^*, N^*), the value of the PDF $f_N(\sigma^*, N^*; A, a, \delta_N)$ is replaced in the ML estimation with $1 - F_N(\sigma^*, N^*; A, a, \delta_N)$ where F_N is the CDF of $N(\sigma, \omega)$ that reads:

$$F_N(\sigma^*, N^*; A, a, \delta_N) = \Phi\left(\frac{\ln N^* - (A + a\ \ln \sigma^*)}{\delta_N (A + a\ \ln \sigma^*)}\right) \tag{1.54}$$

Finally, the GOF test conducted *a posteriori* checks whether there is evidence against:

$$U_f = \frac{\ln N(\sigma, \omega) - (A + a\ \ln \sigma)}{\delta_N\ (A + a\ \ln \sigma)} \sim \mathcal{N}(0, 1) \tag{1.55}$$

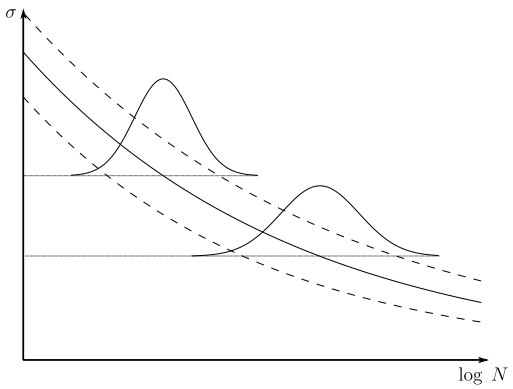

Figure 1.13: Guédé's model. The solid line represents the median curve (50% probability to fail at N cycles given the stress level σ). The dashed lines are the isoprobability $S - N$ curves defined at 2.5% and 97.5%.

1.3.5.3 Selection of the most adequate model

Given that the models are determined using ML estimation, likelihood criteria AIC and BIC are relevant means for model selection [Perrin, 2008]. Additionally, the GOF tests provide p-values which can be used to rank the initial hypotheses of the models. The combination of AIC, BIC and the p-value thus represents a helpful approach for selecting the most adequate model.

1.3.6 Probabilistic Stress-stRength approach

1.3.6.1 Structural design calculation

The probabilistic Stress-stRength approach [Thomas *et al.*, 1999; Bignonnet and Thomas, 2004] is an engineering tool for designing new structures against fatigue with a given reliability objective (or targeted failure probability). It consists of comparing two statistical distributions, namely S and R, the former modelling the uncertainty of the in-service loads while the latter models the uncertainty in the mechanical properties of the structure to design. These distributions are commonly called Stress for S and stRength for R. As depicted in Figure 1.14, the aim of the approach is to ascertain the mean strength μ_R which ensures a reliability objective P_f°, considering that the distribution S is known to be characterized by a mean μ_S and a standard deviation σ_S and that the Strength R presents an inherent scatter in the form of a coefficient of variation δ_R. It is important to firstly outline that the probabilistic Stress-stRength approach was implemented in the DEFFI project [Bignonnet and Lieurade, 2007; Bignonnet *et al.*, 2009; Ferlin *et al.*, 2009; Lefebvre *et al.*, 2009] which is mentioned in introduction of this thesis.

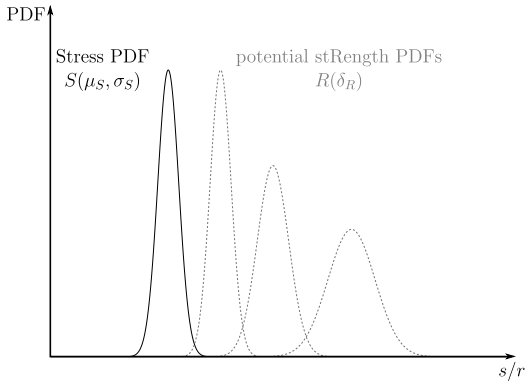

Figure 1.14: Potential stRength distributions depending on its inherent scatter δ_R, the Stress distribution and the reliability objective.

Stress-Strength Interference analysis

In the probabilistic Stress-stRength approach, the failure scenario is mathematically represented by the performance function G given as follows:

$$G(R, S) = R - S \tag{1.56}$$

Failure occurs when the performance function is negative, *i.e.* when S is larger than R as illustrated in Figure 1.15. The failure probability P_f consequently reads:

$$P_f = \text{Prob}(G(R, S) \leq 0) = \text{Prob}(R - S \leq 0) \tag{1.57}$$

Within the frame of the probabilistic Stress-stRength approach, the Stress-Strength Interference (SSI) analysis [Booker *et al.*, 2001] is applied to assess this failure probability. This very simple and convenient engineering tool assumes that both S and R are known and independent PDFs. Consequently, the failure probability simply reads:

$$P_f = \int_{-\infty}^{+\infty} f_S(s) F_R(s) \mathrm{d}s \tag{1.58}$$

where f_S is the assumed PDF of S and F_R is the assumed CDF of R. The failure probability may be calculated using any numerical integration technique, but in some cases, analytical expressions are directly available [Lemaire, 2009]. For instance, on the hypothesis that S and R are Gaussian distributions, the failure probability becomes:

$$P_f = \Phi\left(-\frac{\mu_R - \mu_S}{\sqrt{\sigma_R^2 + \sigma_S^2}}\right) \tag{1.59}$$

where σ_R is the standard deviation of R. Thomas *et al.* [1999] mention that S may either be a Gaussian, lognormal or Weibull distribution, whereas R is Gaussian given that it is a combination of many variables (see the following paragraph on stRength distribution). The next step is the capitalization of available data in order to determine the parameters of the distributions S and R.

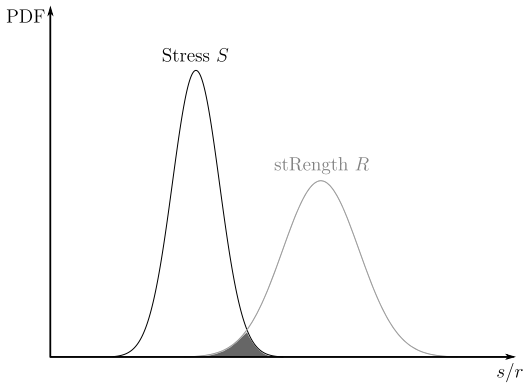

Figure 1.15: Stress-Strength Interference analysis. The dark area depicts the failure events.

Stress distribution

Figure 1.16 illustrates the general procedure for modelling the uncertainty of the in-service loads. Beforehand, field measurements are conducted to obtain representative histories of the different loads imposed on the structure. Let us assume that these recordings are force histories $F(t)$, but they can be defined in any other load quantity, *e.g.* in terms of displace-

ment. On the basis of these force histories, modelling techniques such as those detailed in Section 1.3.4 are applied to model the uncertainties with random load parameters $\mathbf{X}_l$ (*e.g.* random percentages of occurrence). By drawing a realization $\mathbf{x}_l$ of these random parameters, a virtual load is generated. The damage contribution (or severity) of this virtual load is then summarized into an EF cycle of amplitude $F_{eq}(\mathbf{x}_l, b, N_{eq})$ repeated N_{eq} times. Numerous realizations of the random parameters are drawn, and a large number of F_{eq} values is thus obtained. The distribution S modelling the variability of F_{eq} is considered in this section as Gaussian, because such an assumption provides an analytical expression of the failure probability when combined with a Gaussian stRength (see Eqn.(1.59)).

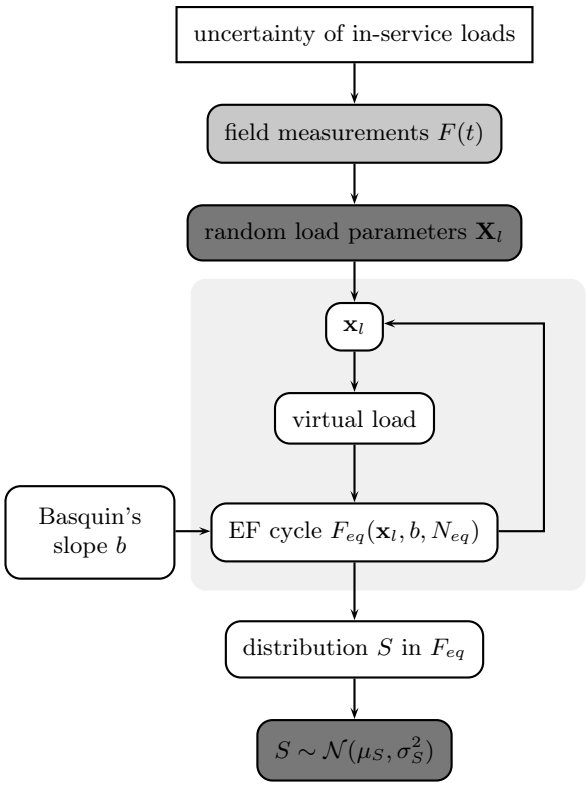

Figure 1.16: Definition of the Stress distribution S.

StRength distribution

The stRength R represents the uncertainty of the mechanical properties (material properties, fabrication process) having fatigue damage consequences for the structure to design. To enable a comparison with S, R is defined as the distribution of the fatigue strength in force at N_{eq} cycles. The objective here is to determine the coefficient of variation $\delta_R = \sigma_R/\mu_R$ interpreting the relative scatter of the fabrication process and its fatigue damage consequences. Remember that the designer's final aim is to set μ_R, given the inherent scatter of R, the distribution S and the reliability objective P_f°. The general

procedure to determine R and the coefficient δ_R is depicted in Figure 1.17. Fatigue tests performed on specimens and on structures which are similar to the one being designed are collected in order to provide sufficient knowledge. On a stRength$-N$ diagram, the data sets at different numbers of cycles are combined into one group at N_{eq} cycles following the concept of Equivalent Fatigue strength (EF strength) [Hanaki *et al.*, 2010] depicted in Figure 1.18. The empirical mean m_R and the unbiased estimate s_R^* of the standard deviation are then calculated from the group at N_{eq} cycles. Given that the number N_t of tested samples is usually small, the confidence in the stRength distribution R may be weak. Thomas *et al.* [1999] consider that an acceptable mean value can be estimated with $N_t \geq 8$ samples: $\mu_R = m_R$. Assuming that R is a Gaussian random variable and that $\mu_R = m_R$, the standard deviation is set as the upper bound of the confidence interval defined by the risk γ:

$$\sigma_R^{\gamma,N_t} = s_R^* \sqrt{\frac{N_t - 1}{k_{N_t-1;\gamma/2}}} \tag{1.60}$$

where $k_{N_t-1;\gamma}$ is the χ^2 quantile. The quantity of interest, *i.e.* δ_R^{γ,N_t}, is derived from the standard deviation and the mean. The distribution R is thus characterized only by δ_R^{γ,N_t}. As mentioned previously, R is always considered as Gaussian.

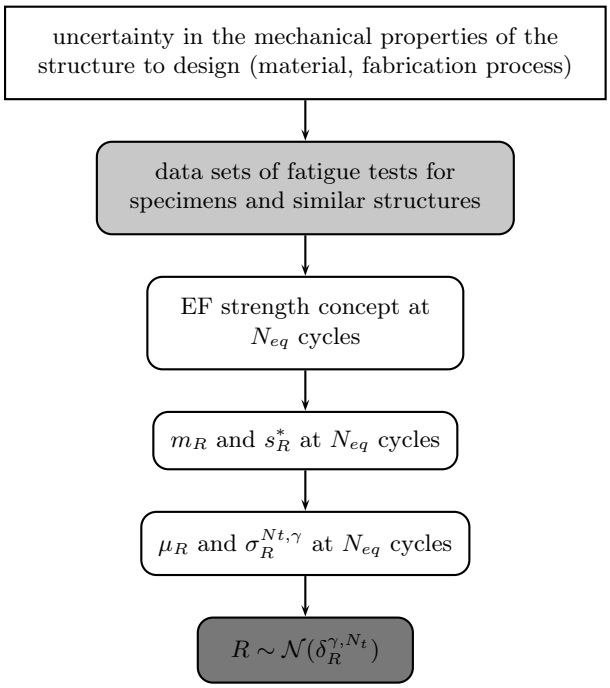

Figure 1.17: Definition of the stRength distribution R.

Risk analysis

An EF cycle of reference is arbitrarily selected in the distribution S (see Figure 1.19). Its

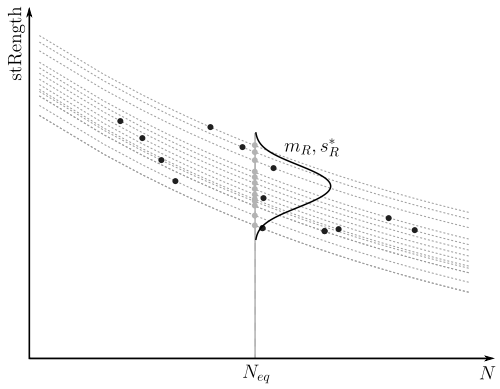

Figure 1.18: Concept of Equivalent Fatigue strength. The black dots represent the available data set of fatigue tests. These samples at different numbers of cycles are projected to N_{eq} cycles, parallel to the median $S-N$ curve of the material. The group of grey dots is thus obtained, and the empirical mean m_R and unbiased estimate s_R^* of the standard deviation can be calculated at N_{eq}.

amplitude is denoted by F_n, and its severity is defined as the positive α quantile:

$$F_n = \mu_S + \alpha\, \sigma_S \tag{1.61}$$

The probability of exceeding F_n is then:

$$\text{Prob}(s > F_n) = 1 - \Phi\left(\frac{F_n - \mu_S}{\sigma_S}\right) = \Phi(-\alpha) \tag{1.62}$$

Typical probabilities are 10^{-2}, 10^{-3}, 5×10^{-4}. F_n represents neither a certain type of situation nor the most severe observed load. It is an arbitrary amplitude that enables the conversion of the failure probability calculation into a simple specification procedure. F_n is associated with an acceptance criterion in stRength defined at κ standard deviations below the mean stRength (see Figure 1.19):

$$\mu_R = F_n + \kappa \sigma_R^{\gamma, N_t} \tag{1.63}$$

The relative mean strength m_R^* is defined as:

$$m_R^* = \frac{\mu_R}{F_n} = \frac{1}{1 - \kappa \delta_R^{\gamma, N_t}} \tag{1.64}$$

S and R are recalled to be Gaussian distributions. By introducing F_n and the coefficient of variation δ_S of S in Eqn.(1.59), the targeted failure probability P_f° can be rewritten as:

$$P_f^\circ = \Phi\left(-\frac{\mu_R - \mu_S}{\sqrt{\left(\mu_R\ \delta_R^{\gamma,N_t}\right)^2 + \left(\mu_S\ \delta_S\right)^2}}\ \frac{F_n}{F_n}\right) \tag{1.65}$$

It is then recast as:

$$P_f^\circ = \Phi\left(-\frac{m_R^* - \frac{1}{1+\alpha\ \delta_S}}{\sqrt{\left(m_R^*\ \delta_R^{\gamma,N_t}\right)^2 + \left(\frac{\delta_S}{1+\alpha\ \delta_S}\right)^2}}\right) \tag{1.66}$$

In Eqn.(1.66), the parameters α, δ_S, δ_R^{γ,N_t} are known. The relative mean strength m_R^* can thus be assessed for a given reliability objective P_f°.

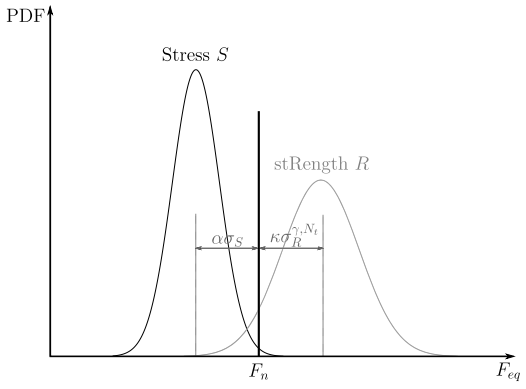

Figure 1.19: Reference EF cycle defined by F_n.

Figure 1.20 depicts an example of the structural design calculation from the designer's point of view. In practice, the reference EF cycle with amplitude F_n is applied to the numerical model. In this illustration, the numerical model output used for fatigue calculation is assumed to be the maximum principal stress σ_{I} at the critical location. The designer checks that the point $(N_{eq}, \sigma_{\mathrm{I}})$ is below the isoprobability $S-N$ curve of the material that corresponds to the median curve shifted down by κ standard deviations (κ determined using Eqn.(1.64)). In this example, the failure probability is below P_f° as the gap is positive.

Conclusion

The probabilistic Stress-stRength approach detailed in this section is particularly well adapted for industrial applications in the field of high cycle fatigue with linear mechanical behaviour. Under some assumptions, it enables new structures to be designed with a given

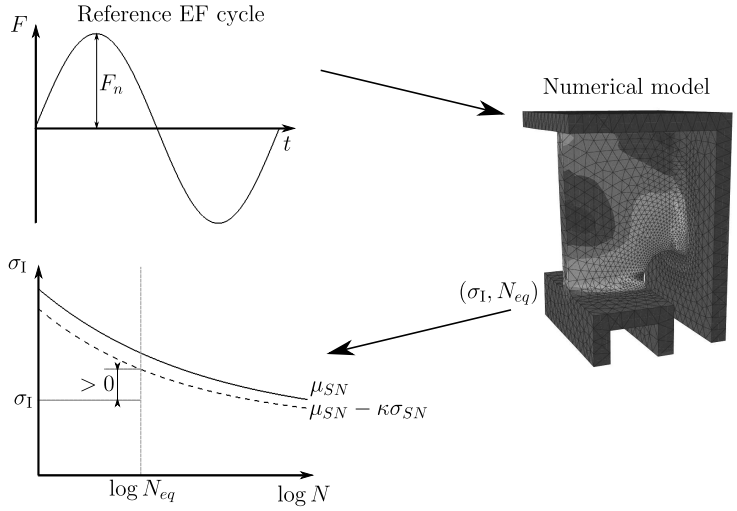

Figure 1.20: Illustration of the structural design calculation. The numerical model is from Relun [2011].

reliability objective. The probabilistic Stress-stRength approach consists of comparing the distributions S and R that respectively model the uncertainty of the in-service loads and the uncertainties in the mechanical properties of the structure to design. On the one hand, S is characterized by a mean and a standard deviation, and on the other, R features an inherent scatter in the form of its coefficient of variation. SSI analysis is applied in order to provide an expression of the targeted failure probability which depends on the distributions assumed for S and R (typically Gaussian). Finally, the mean strength μ_R is determined by considering the inherent scatter of the stRength, the distribution S and the reliability objective. In the frame of this thesis, the objective is not to ascertain the optimum design of a new structure but to assess the failure probability of an already designed structure. The adaption of the probabilistic Stress-stRength approach to this case is explained in the next section.

1.3.6.2 Reliability assessment

Two adaptions of the probabilistic Stress-stRength approach to reliability assessment can be devised depending on available data. The simplest alternative is formulated in terms of a load quantity (*e.g.* in force). In such a case, S remains the distribution of the EF amplitude F_{eq}, but R is this time fully characterized by its parameters μ_R and σ_R which are determined according to data sets of fatigue tests on the structure. Assumptions are made on the distributions followed by S and R, and SSI analysis is applied to assess the failure probability using Eqn.(1.58). Note that the numerical model of the structure is not required in this adaption. However, the fatigue behaviour of the structure is often unknown since conducting fatigue tests on a structure is usually unfeasible due to prohibitive costs or

structure size. It is then necessary to resort to the second adaption which simply requires data sets of tests performed on smooth specimens in order to characterize the $S-N$ curve and other material properties. Note that experimental data on the structure's geometry may also be considered. The second adaption is depicted in Figure 1.21. Its different steps are described in the following paragraphs.

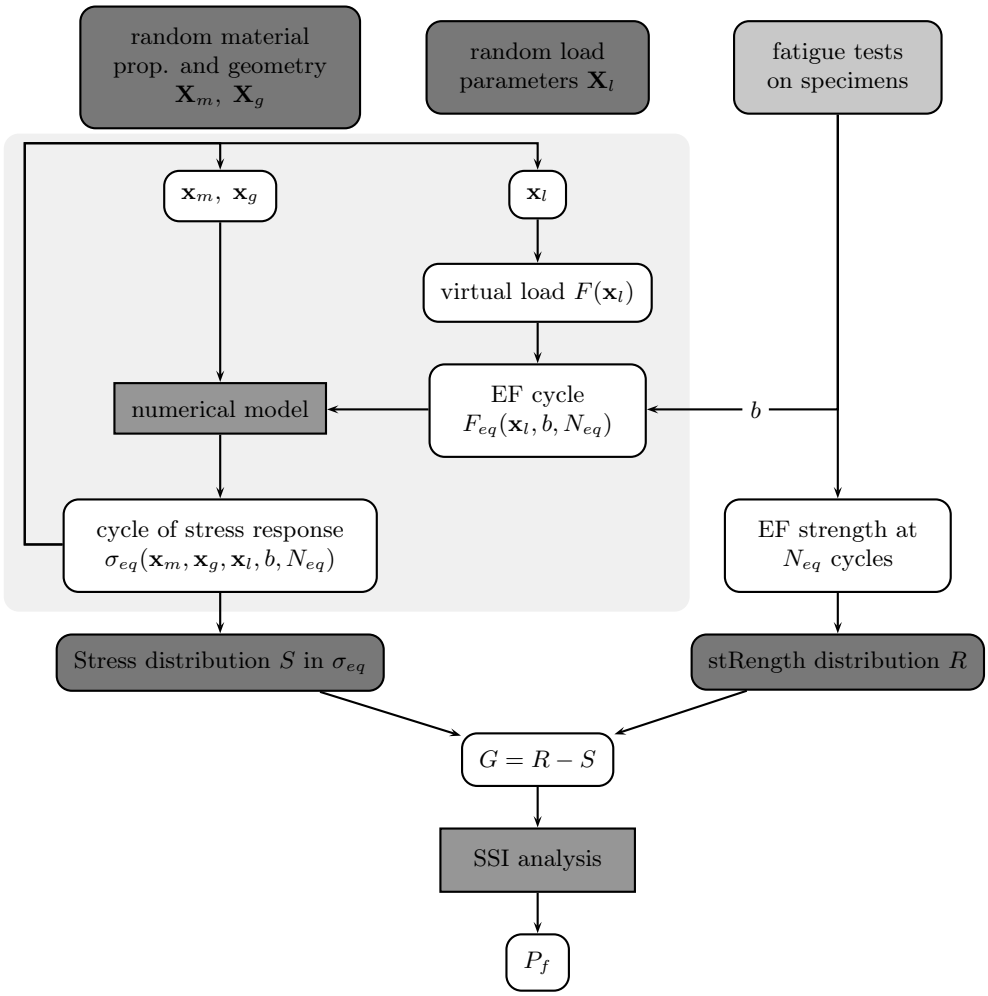

Figure 1.21: Probabilistic Stress-stRength approach for reliability assessment.

Stress distribution

The uncertainties of the material properties, geometry and applied loads are statistically modelled with the random vectors respectively denoted by $\mathbf{X}_m$, $\mathbf{X}_g$ and $\mathbf{X}_l$. The first step of the procedure is the selection of a realization $\{\mathbf{x}_m, \mathbf{x}_g, \mathbf{x}_l\}$. A virtual load $F(\mathbf{x}_l)$ is generated with $\mathbf{x}_l$, and the corresponding EF cycle of amplitude $F_{eq}(\mathbf{x}_l, b, N_{eq})$ repeated N_{eq} times is calculated using the Basquin's slope b of the $S-N$ curve. The EF cycle is then applied to the numerical model which depends on $\mathbf{x}_m$ and $\mathbf{x}_g$. A cycle of stress response

is thus derived from the model evaluation. Assuming that the $S-N$ curve is provided for $\mathcal{R}=-1$, this cycle is converted into its fully reversed equivalent whose amplitude is $\sigma_{eq}(\mathbf{x}_m, \mathbf{x}_g, \mathbf{x}_l, b, N_{eq})$. Several values of σ_{eq} are derived from the evaluation of the numerical model for various realizations of the random variables. The observed dispersion in σ_{eq} is modelled with a statistical distribution which corresponds to the Stress S.

stRength distribution

The uncertainty in the fatigue behaviour of the material is modelled with the stRength distribution R. The EF strength concept presented in Section 1.3.6.1 is applied to determine the scatter of the fatigue strength at N_{eq} cycles. As mentioned previously, a Gaussian distribution is usually assumed for R [Lalanne, 2002].

SSI analysis

Given the distributions S and R, the failure probability is assessed using the SSI analysis, and particularly Eqn.(1.58).

Limits

The application of the probabilistic Stress-stRength approach to reliability assessment present two main limits. First, the influence of each random variable on structural reliability cannot be determined since $\mathbf{X}_m$, $\mathbf{X}_g$ and $\mathbf{X}_l$ are gathered in S (remember that the knowledge of the most influent variables represents a valuable information for the design process). Second, the failure probability is extremely sensitive to the distribution that S is assumed to follow. In this section, a simple example gives evidence of these two limits.

The beam case study illustrated in Figure 1.22 is subjected to a force $F(t)$ in C. Assuming that the structure remains in the elastic domain, the maximal stress in A reads:

$$\sigma(t) = \frac{F(t)}{4(w\ v - v^2)} + \frac{6\ F(t)\ l\ w}{w^4 - (w-2\ v)^4} \tag{1.67}$$

where v and w define the cross-section of the beam and l its length. $\sigma(t)$ is supposed to be the stress response used for fatigue calculation. In other words, Eqn.(1.67) is the numerical model representing the mechanical behaviour of the case study.

The uncertainties of the geometry, force and fatigue behaviour of the material are considered in this example. Table 1.2 reports the different random variables. The deterministic parameters v, w and l are replaced with Gaussian variables V, W and L respectively. The uncertainty of the force F is modelled with a simplified load mix strategy (see Section 1.3.4.1) involving only two elementary life situations. The most severe situation features a Rainflow matrix $\mathbb{M}_1$ and a random percentage of occurrence P_1 which is considered as uniform in the interval $[0; 60\%]$. The second situation is characterized by a Rainflow matrix $\mathbb{M}_2$ and a random percentage $P_2 = 100 - P_1$. The Rainflow matrices are modelled with

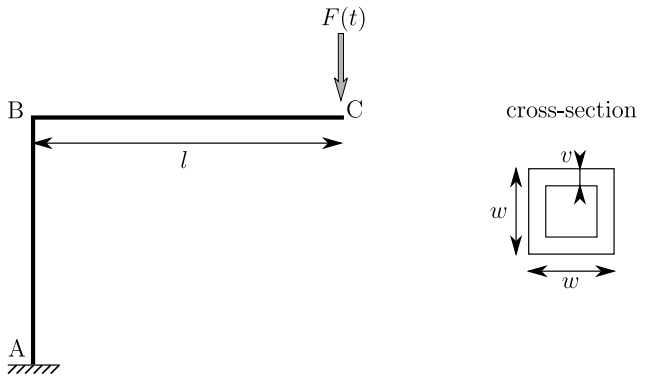

Figure 1.22: Characteristics of the beam case study.

independent joint Gaussian PDFs whose parameters are given in Table 1.3. The extreme Rainflow matrices providing the number of cycles ordered by mean F_m and amplitude F_a are depicted in Figure 1.23. Instead of sampling in the joint PDFs, the axes F_m and F_a are arbitrarily discretized in order to represent the different cycles imposed on the structure. The number of occurrences of each cycle is obtained by reading the n axis which corresponds to the value of the joint Gaussian PDF multiplied by a constant C (applied to define a suitable life span). A virtual Rainflow matrix $\mathbb{L}(p_1)$ representing a potential service life of the structure is generated by drawing a realization p_1 of P_1:

$$\mathbb{L}(p_1) = p_1 \, \mathbb{M}_1 + (1 - p_1) \, \mathbb{M}_2 \tag{1.68}$$

The virtual Rainflow matrix $\mathbb{L}(p_1)$ is then summarized into an EF cycle of symmetric alternating amplitude $F_{eq}(p_1, b, N_{eq})$ repeated $N_{eq} = 10^6$ times. Note that for the calculation of the EF cycle, the Basquin's slope b is -0.3, and the ratio K of the tensile strength to the stress at $N_{eq} = 10^6$ cycles (see Eqn.(1.16)) is set to 2.5. Once determined, the EF cycle is applied to the numerical model characterized by a selected geometry $\{v, w, l\}$. The fully reversed cycle of the stress response in A is obtained using Eqn.(1.67). It features an amplitude $\sigma_{eq}(v, w, l, p_1, b, N_{eq})$ and is interpreted as a cycle being repeated $N_{eq} = 10^6$ times. Several values of σ_{eq} are calculated for various realizations of the random variables. The dispersion observed is modelled with the distribution S which is then compared to the distribution R of the EF strength at $N_{eq} = 10^6$ cycles.

This case study is devised to be representative of the complex structures examined in this thesis. A small failure probability ($\approx 10^{-6}$) is thus defined, and the evaluation of the numerical model, *i.e.* Eqn.(1.67), is considered as time-demanding. The latter condition limits the number of σ_{eq} values that can be evaluated in a practical amount of time, therefore the Stress distribution must be determined with a relatively small number of σ_{eq} values. In this study, three sets, each composed of only 100 σ_{eq} values, are considered (see Figure 1.24). ML estimation is applied to determine the parameters of the Gaussian,

Variable	Distribution	Parameters
V (mm)	Gaussian	$\mu_V = 3$; $\delta_V = 3\%$
W (mm)	Gaussian	$\mu_W = 50$; $\delta_W = 3\%$
L (mm)	Gaussian	$\mu_L = 10^3$; $\delta_L = 3\%$
P_1 (%)	Uniform	$[0; 60]$
R (MPa)	Gaussian	$\mu_R = 180$; $\delta_R = 10\%$

Table 1.2: Random variables of the beam case study.

		Mean	Std. dev.
$\mathbb{M}_1$	F_m (N)	0	30
	F_a (N)	700	50
$\mathbb{M}_2$	F_m (N)	0	50
	F_a (N)	250	50

Table 1.3: Parameters of the independent joint Gaussian PDFs of the Rainflow matrices $\mathbb{M}_1$ and $\mathbb{M}_2$.

lognormal and Weibull distributions fitting these sets. GOF tests are also conducted to determine how well the assumed distributions fit the sets. The Anderson-Darling test is selected since it gives more weight to the distribution tails where failure occurs. SSI analyses are applied to assess the failure probability. The First Order Reliability Method (FORM) is also applied to determine the influences of the Stress and stRength on structural reliability (see Section 2.3.3.2). For this application, the elasticities of the Hasofer-Lind reliability index $\beta = -\Phi^{-1}(P_f)$ with respect to the standard deviations σ_S and σ_R of the Stress and stRength distributions are quantified. The elasticity value E_{σ_i} must be interpreted as the percentage by which the Hasofer-Lind reliability index is increased when the standard deviation of the ith random variable is raised by 1%.

Table 1.4 reports the results of the first set. The values of the likelihood criteria are extremely similar, but the Gaussian distribution giving a failure probability of 4.9×10^{-6} seems the most adequate model according to its p-value. For the second set (see Table 1.5), the highest p-value is obtained for the Gaussian distribution, but the lognormal distribution seems to be a relevant alternative according to AIC and BIC. The choice of the distribution has a significant impact on the estimation of the failure probability, since P_f is either 1.5×10^{-6} or 12×10^{-6}. For the third set (see Table 1.6), the Weibull distribution gives the best results, and the failure probability is 0.23×10^{-6}. This study shows that the accuracy of the probabilistic Stress-stRength approach for reliability assessment is

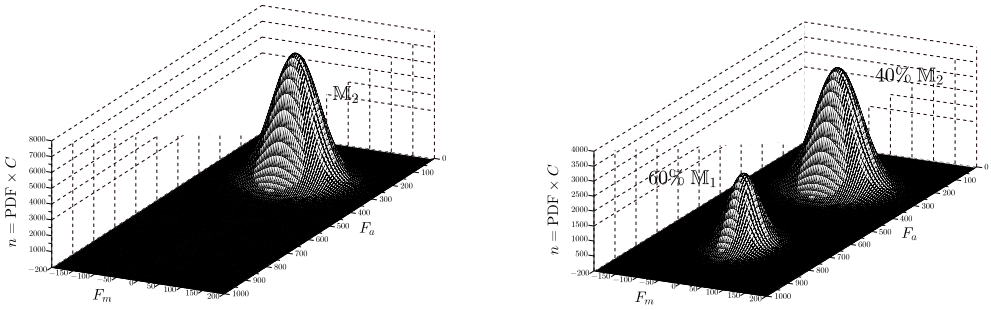

(a) Least severe matrix $\mathbb{L}(0)$.

(b) Most severe matrix $\mathbb{L}(60)$.

Figure 1.23: Extreme Rainflow matrices obtained as mixtures of $\mathbb{M}_1$ and $\mathbb{M}_2$.

strongly affected by the number of model evaluations which can be performed in a practical amount of time. In addition, confidence in the failure probability is extremely limited, since the interference between Stress and stRength is at the extremes of the poorly known distribution tails. For this case study, the order of magnitude of the failure probability seems to be between 10^{-5} and 10^{-7}, which represents a relatively wide interval. To finish, it can be noted for this case study that the elasticities of the Hasofer-Lind reliability index show that the standard deviation of the stRength has more impact on structural reliability than the standard deviation of the Stress when the latter is modelled with a Gaussian or Weibull distribution. An opposite behaviour is observed with a lognormal Stress.

Stress distribution	AIC	BIC	p-value	P_f	E_{σ_R}	E_{σ_S}
Gaussian	818	823	0.81	4.9×10^{-6}	-0.61	-0.39
Lognormal	820	826	0.65	53×10^{-6}	-0.33	-0.63
Weibull	819	825	0.66	1.6×10^{-6}	-0.76	-0.36

Table 1.4: First set - Impact of the Stress distribution S on the failure probability and elasticities of the Hasofer-Lind reliability index.

Stress distribution	AIC	BIC	p-value	P_f	E_{σ_R}	E_{σ_S}
Gaussian	797	802	0.45	1.5×10^{-6}	-0.66	-0.34
Lognormal	796	801	0.37	12×10^{-6}	-0.40	-0.56
Weibull	802	807	0.40	0.63×10^{-6}	-0.79	-0.32

Table 1.5: Second set - Impact of the Stress distribution S on the failure probability and elasticities of the Hasofer-Lind reliability index.

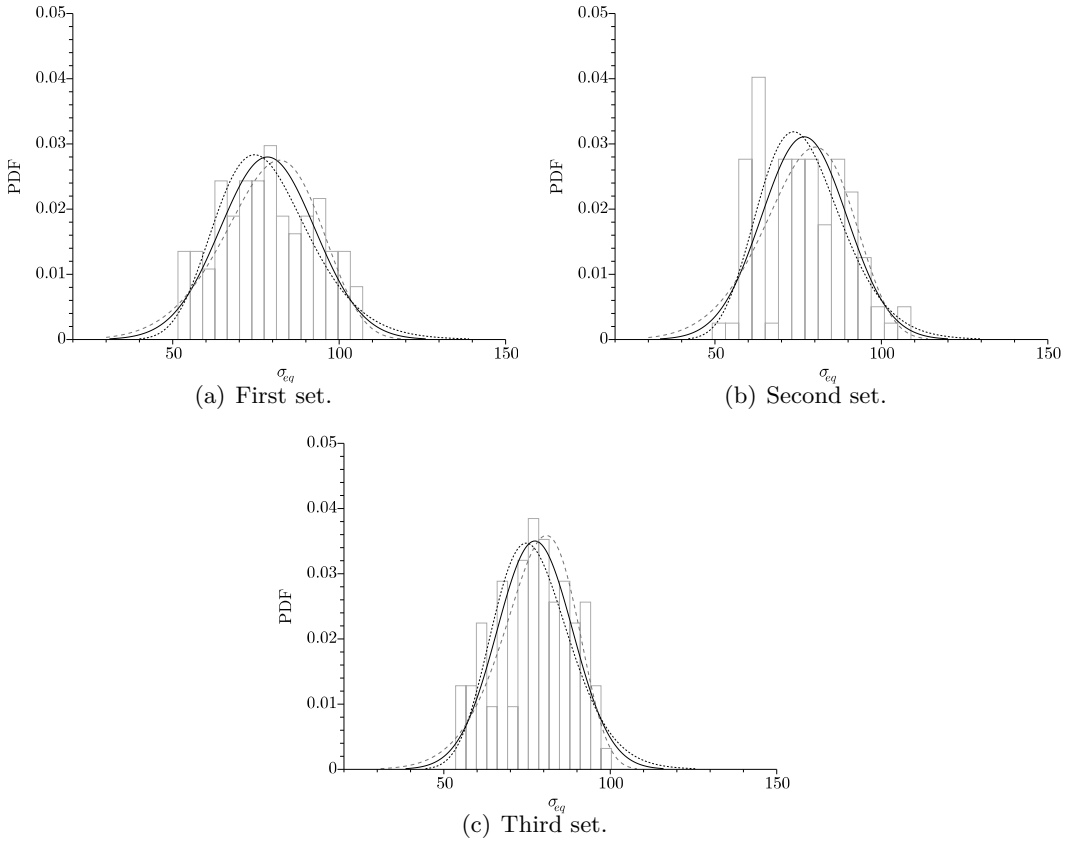

(a) First set.

(b) Second set.

(c) Third set.

Figure 1.24: Fitting of probability distributions to the three empirical sets of 100 σ_{eq} observations. The solid line is Gaussian. The dashed line is Weibull. The dotted line is lognormal.

Stress distribution	AIC	BIC	p-value	P_f	E_{σ_R}	E_{σ_S}
Gaussian	773	779	0.69	0.72×10^{-6}	-0.71	-0.29
Lognormal	779	784	0.29	5.0×10^{-6}	-0.48	-0.49
Weibull	771	776	0.92	0.23×10^{-6}	-0.84	-0.23

Table 1.6: Third set - Impact of the Stress distribution S on the failure probability and elasticities of the Hasofer-Lind reliability index.

1.3.7 Proposed approach in the context of the APPRoFi project

1.3.7.1 Motivation

In the previous section, it has been shown that the probabilistic Stress-stRength approach for reliability assessment provides failure probability values which are sensitive to the assumption made on the distribution followed by the Stress. Additionally, the influence of each random variable on structural reliability cannot be determined since the uncertainties

of the material properties, geometry and load are gathered in S. In the frame of the APPRoFi project, a more general probabilistic approach [Echard *et al.*, 2011c; Gayton *et al.*, 2011] is proposed to overcome the limits of the Stress-stRength approach. First, the SSI analysis is replaced with a more robust reliability method in order to assess the failure probability with a suitable confidence level. Second, the random variables are kept separate throughout the whole approach process so as to enable the determination of the random variables' influences on structural reliability. It is also important to note the uncertainty of the fatigue behaviour is considered through various probabilistic $S-N$ curve models instead of the EF strength concept. Specific behaviour of materials can thus be considered, and the most adequate $S-N$ curve model can be selected using likelihood criteria and p-values of GOF tests.

1.3.7.2 Procedure

The approach is depicted in Figure 1.25. The uncertainties of the material properties, geometry and applied loads are statistically modelled with random vectors respectively denoted by $\mathbf{X}_m$, $\mathbf{X}_g$ and $\mathbf{X}_l$. The uncertainty in the fatigue behaviour of the material is modelled with a random variable U_f, which represents the random isoprobability $S-N$ curve (see Section 1.3.5). Note that the deterministic model of the $S-N$ curve is assumed as the Basquin's relation. The first step of the approach is the selection of a realization $\{\mathbf{x}_m, \mathbf{x}_g, \mathbf{x}_l, u_f\}$ of the random parameters. A virtual load $F(\mathbf{x}_l)$ is generated with $\mathbf{x}_l$, and the corresponding EF cycle of symmetric alternating amplitude $F_{eq}(\mathbf{x}_l, u_f, N_{eq})$ repeated N_{eq} times is calculated using the Basquin's slope $b(u_f)$ of the isoprobability $S-N$ curve determined by u_f. The EF cycle is then applied to the numerical model which depends on $\mathbf{x}_m$ and $\mathbf{x}_g$. The output $\sigma_{eq}(\mathbf{x}_m, \mathbf{x}_g, \mathbf{x}_l, u_f, N_{eq})$ of the numerical model is compared to the strength value $r(u_f, N_{eq})$ of the isoprobability $S-N$ curve at N_{eq} cycles in order to determine whether the selected realization leads to failure. The failure probability is finally assessed by repeating the different steps presented above with various realizations. Sampling techniques such as Monte Carlo Simulation are a possibility to estimate the failure probability, but they are inapplicable in the case of a computationally demanding numerical model since they require a substantial number of model evaluations. In Chapter 2, alternatives are proposed to assess the failure probability in a parsimonious way with regard to the number of model evaluations. These alternatives called Active learning and Kriging-based Reliability Methods (AK-RM) can be seen as 'guided' sampling techniques, as they iteratively determine which evaluation should be carried out to best improve the accuracy of the failure probability estimate.

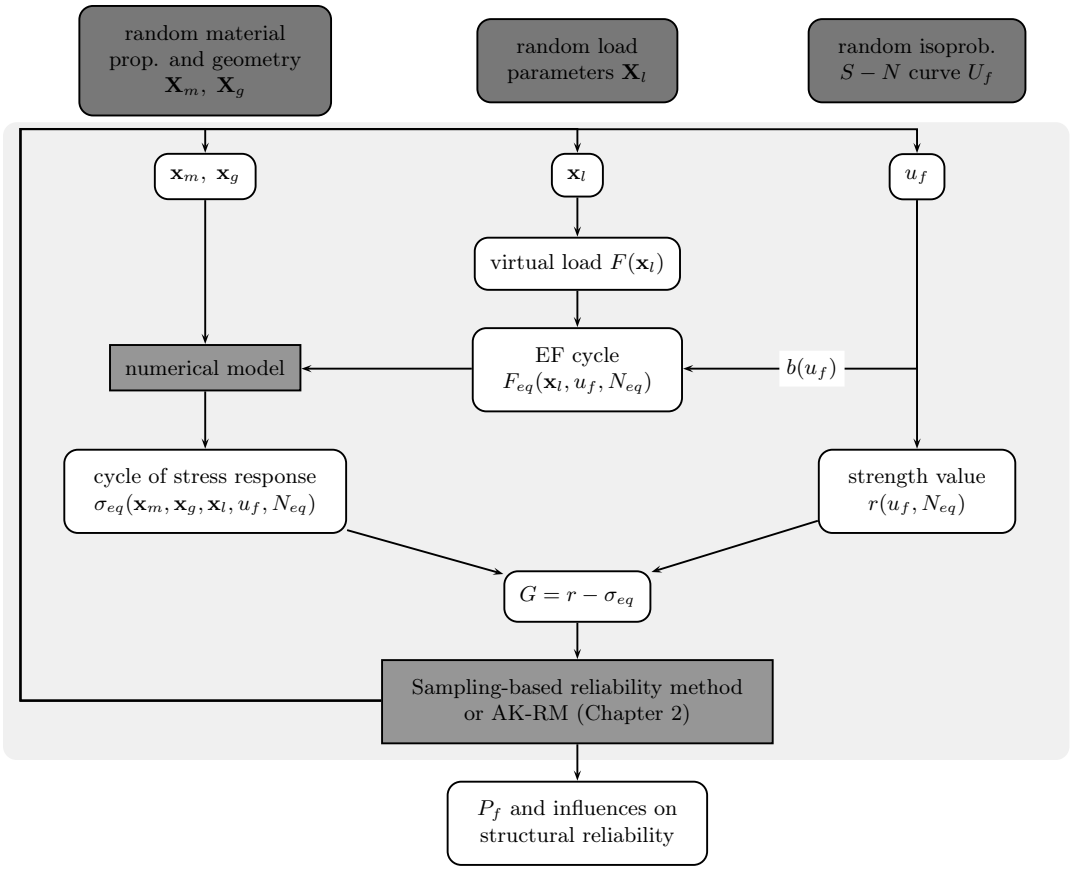

Figure 1.25: Probabilistic approach implemented in the APPRoFi project.

1.3.7.3 Important remarks

In the frame of the probabilistic approach implemented in the APPRoFi project, the performance function G is formulated in terms of stress, but an equivalent formulation is also possible in terms of number of cycles. In the latter formulation, the flowchart of Figure 1.25 is slightly changed. For a given realization of the random variables, the stress response amplitude $\sigma_{eq}(\mathbf{x}_m, \mathbf{x}_g, \mathbf{x}_l, u_f, N_{eq})$ is carried forward into an $S-N$ diagram for determining the number of cycles to failure $N(\sigma_{eq})$ which depends on the isoprobability $S-N$ curve defined by u_f. The performance function then simply consists of the difference between $N(\sigma_{eq})$ and N_{eq} (remember that the stress response cycle is interpreted as a cycle being repeated N_{eq} times).

The performance function can also be expressed in terms of damage. In such a formulation, the EF concept is removed, and the cycles extracted from $F(\mathbf{x}_l)$ are directly applied to the numerical model. The damage $D(\mathbf{x}_m, \mathbf{x}_g, \mathbf{x}_l, u_f)$ induced by the stress response $\sigma(\mathbf{x}_m, \mathbf{x}_g, \mathbf{x}_l)$ is calculated using the Palmgren-Miner rule as well as an isoprobability $S-N$ curve defined by u_f. The performance function is then the difference between 1 and $D(\mathbf{x}_m, \mathbf{x}_g, \mathbf{x}_l, u_f)$. This is the framework adopted by Guédé [2005].

The following comments can be made on the range of applications of these formulations:

- The formulations in terms of stress and number of cycles are equivalent for any mechanical behaviour.
- For problems involving a linear mechanical behaviour, the formulations in terms of stress and number of cycles are similar to the formulation in terms of damage.
- In the case of a very limited and localized plasticity, the formulations in terms of stress and number of cycles represent acceptable approximations of the damage formulation (remember the linear assumption of the EF concept).
- For non-linear applications, only the damage formulation provides usable fatigue calculation results.
- Although damage formulation can be applied to any fatigue problem, it is nonetheless a high computational effort. For a given realization of the random variables, all the cycles extracted from $F(\mathbf{x}_l)$ must be applied to the numerical model. In the formulations in terms of stress and number of cycles, a simpler calculation is sufficient as the stress response is only determined for the EF cycle summarizing $F(\mathbf{x}_l)$.

1.3.7.4 Illustration on the beam case study

The probabilistic approach implemented in the APPRoFi project is illustrated on the beam case study already examined in Section 1.3.6.2. ESOPE 2 model is considered for the probabilistic $S-N$ curve in order to define the same stRength distribution R as the one reported in Table 1.2. Given that ESOPE 2 model presents a constant Basquin's slope b for all the isoprobability $S-N$ curves (see Eqn.(1.46)), the calculation of the EF amplitude no longer depends on the realization u_f, and the approach can be simplified by directly considering the stRength distribution R at N_{eq} cycles on the right-hand side of Figure 1.25.

For this illustration, the failure probability is assessed using Importance Sampling (IS) and AK-IS. Importance Sampling is a sampling-based method that requires a relatively large number of numerical model evaluations. Its application to the beam case study aims at providing a reference estimate of the failure probability. AK-IS is the member of the AK-RM family that constitutes a 'guided' Importance Sampling. To be relevant, AK-IS must provide an accurate estimate of the failure probability with the least possible number of numerical model evaluations. The reader is referred to Chapter 2 for details and validation of the AK-RM reliability methods which represent the major contribution of this thesis.

Table 1.7 reports the reliability results. Importance Sampling requires $N_E = 5 \times 10^4$ evaluations of the numerical model to assess the failure probability with a coefficient of

variation of $\delta = 2\%$. AK-IS only requires $N_E = 82$ evaluations to provide the same failure probability estimate. The probabilities assessed using SSI analyses in Section 1.3.6.2 are also reported in Table 1.7 for the most adequate models according to the likelihood criteria. It can be seen that the SSI analysis conducted on the third set with a Weibull distribution provides the closest failure probability value. For this application, AK-IS enables the failure probability to be accurately assessed with less model evaluations than the SSI analyses.

In Section 1.3.6.2, only the influences of the Stress and stRength on structural reliability could be determined. With the proposed approach, the elasticities with respect to the standard deviations σ_V, σ_W, σ_L, σ_R and the upper bound $b_{P_1} = 60\%$ of P_1 can be calculated. Table 1.8 reports these elasticities. The standard deviations of the geometry variables are seen to have a limited impact in comparison to the upper bound b_{P_1} of the load parameter P_1 and the standard deviation of R. It is also observed that E_{σ_R} is relatively close to the elasticities observed when the Stress S is modelled with a Weibull distribution in the probabilistic Stress-stRength approach (see Tables 1.4, 1.5 and 1.6).

Reliability method	N_E	P_f	δ %
IS	5×10^4	0.74×10^{-6}	2.00
AK-IS	82	0.74×10^{-6}	2.00
SSI - First set (Gauss)	100	4.9×10^{-6}	-
SSI - Second set (lognormal)	100	12×10^{-6}	-
SSI - Third set (Weibull)	100	0.23×10^{-6}	-

Table 1.7: Reliability results on the example of the beam case study. AK-IS is compared with Importance Sampling and the SSI analyses conducted in Section 1.3.6.2. N_E refers to the number of numerical model evaluations. δ is the coefficient of variation of the failure probability estimator.

Geometry			Load	Fatigue
E_{σ_V}	E_{σ_W}	E_{σ_L}	$E_{b_{P_1}}$	E_{σ_R}
-0.039	-0.070	-0.004	-0.310	-0.811

Table 1.8: Elasticities of the Hasofer-Lind reliability index with respect to the standard deviations of V, W, L and R and the upper bound $b_{P_1} = 60\%$ of the uniform percentage P_1.

1.4 Conclusion

In this chapter, probabilistic approaches have been discussed as a possible alternative to the current deterministic fatigue design approaches based on so-called safety factors. After presenting the principles of the probabilistic approaches in mechanics, different methods for modelling the inherent uncertainties of the fatigue phenomenon have been examined. First, the modelling of the in-service loads has been considered through a mix strategy of elementary life situations and a mixture of joint PDFs. Second, the uncertainty in the fatigue behaviour of materials has been tackled with the use of probabilistic $S-N$ curves. Following this discussion on stochastic modelling, the probabilistic Stress-stRength approach has been introduced as a tool for either designing new structures against fatigue with a given reliability objective or estimating the failure probability of an already designed structure. This approach is grounded upon the EF concept for summarizing the damage content of the load into an easily manageable cycle, and SSI analysis for quantitatively predicting structural reliability. The Stress-stRength approach represents a practical engineering tool, but as illustrated in this chapter, confidence in its failure probability value is extremely limited as an assumption must be made on the distribution followed by the Stress. Additionally, this approach does not allow to determine the influence of each random variable on structural reliability. Starting from these observations, a more general probabilistic approach has been proposed in the frame of the APPRoFi project. This approach remains based on the EF concept, but replaces the SSI analysis with more robust reliability methods discussed further in Chapter 2. In addition, the uncertainty of the fatigue behaviour is considered through probabilistic $S-N$ curve models instead of the EF strength concept. The application of this approach to a simple structural reliability problem has demonstrated that an accurate failure probability estimate and the influences of random variables can be determined for a smaller computational cost than that of the probabilistic Stress-stRength approach. Finally, note that the proposed approach, grounded upon the EF concept, is restricted to applications involving high cycle fatigue or very limited and localized plasticity. Its range of applications can be widened by expressing the performance function in terms of damage, but the numerical model evaluation is more time-demanding in this case.

Chapter summary

Structures are generally designed against fatigue failure with deterministic approaches based on so-called safety factors in an attempt to ensure the structural integrity while covering the inherent uncertainties (material, loads, geometry, lack of knowledge in the damage mechanism...). These factors are based on the know-how acquired through experience feedback, and are consequently highly subjective. The use of safety factors often leads to over-design and masks any information about the safety margin and the influent design parameters on structural reliability. Probabilistic approaches are a means to provide the designer with this missing information. The probabilistic Stress-stRength approach [Thomas *et al.*, 1999] is a practical engineering tool that is currently used in some design offices for either designing a structure against fatigue with a given reliability objective, or assessing the failure probability of an already designed structure. It basically consists of comparing two statistical distributions, namely the Stress and the stRength. The limits of the approach are that its failure probability value is extremely sensitive to the assumption made on the distribution followed by the Stress, and the influences of the random variables on structural reliability cannot be determined. A more general probabilistic approach is proposed in the frame of the APPRoFi project to overcome these two limits. The Stress and stRength distributions are no longer defined, and the different random variables are kept separate throughout the whole reliability process. The approach is coupled with specific reliability methods devised to determine the failure probability and the influent random variables with only a limited number of numerical model evaluations. These reliability methods are detailed in Chapter 2.

2 Active learning & Kriging-based Reliability Methods

Contents

2.1 Introduction . . . 56
2.2 Isoprobabilistic transformation . . . 57
2.3 Sampling-based reliability methods . . . 58
2.3.1 Monte Carlo Simulation . . . 58
2.3.2 Monte Carlo Simulation under monotony . . . 59
2.3.3 Importance Sampling . . . 61
2.3.4 Subset Simulation . . . 64
2.3.5 Conclusion . . . 69
2.4 Kriging-based reliability methods . . . 69
2.4.1 Principles of metamodelling . . . 69
2.4.2 Kriging theory . . . 70
2.4.3 Active learning method . . . 73
2.4.4 Kriging prediction of the failure probability . . . 76
2.5 Active learning and Kriging-based Monte Carlo Simulation . . . 77
2.5.1 Motivation . . . 77
2.5.2 Procedure . . . 77
2.5.3 Validation . . . 78
2.5.4 Computational cost of the prediction step . . . 86
2.5.5 Conclusion . . . 88
2.6 Active learning and Kriging-based alternatives for small probability cases . . . 88
2.6.1 Active learning and Kriging based MCS under monotony . . . 88
2.6.2 Active learning and Kriging-based Importance Sampling . . . 92
2.6.3 Active learning and Kriging-based Subset Simulation . . . 98
2.7 Conclusion . . . 104
Chapter summary . . . 106

2.1 Introduction

In the frame of this thesis, the physical space is denoted by $\mathcal{X}^n \subseteq \mathbb{R}^n$. $\mathbf{X} = \{X_1, \ldots, X_n\}^t$ denotes the physical random vector of which a realization is written $\mathbf{x} = \{x_1, \ldots, x_n\}^t \in \mathcal{X}^n$. The structural response is characterized by the performance function G depending on the random vector $\mathbf{X}$. At a given realization $\mathbf{x}$, its evaluation gives a scalar value which enables the definition of:

- the safe domain $\mathcal{S} = \Big\{\mathbf{x} = \{x_1, \ldots, x_n\}^t \in \mathcal{X}^n : G(\mathbf{x}) > 0\Big\}$,
- and its complement, the failure domain $\mathcal{F} = \Big\{\mathbf{x} = \{x_1, \ldots, x_n\}^t \in \mathcal{X}^n : G(\mathbf{x}) \leq 0\Big\}$.

Structural reliability analysis aims at assessing the failure probability P_f that reads:

$$P_f = \text{Prob}(G(\mathbf{X} \leq 0)) \tag{2.1}$$

By introducing the joint PDF $f_{\mathbf{X}}(\mathbf{x})$ of the random variables, the probability is recast as:

$$P_f = \int_{\mathcal{F}} f_{\mathbf{X}}(\mathbf{x}) \mathrm{d}x_1 \ldots \mathrm{d}x_n \tag{2.2}$$

To assess the failure probability of a structure, sampling-based reliability methods are very popular, especially as they can deal with complex limit states (high non-linearity, non-convex and/or disconnected domains of failure, system reliability...). Monte Carlo Simulation, the most general approach, can, in theory, deal with any structural reliability problems. However, its computational cost makes it inapplicable in the case of small failure probabilities. Some alternatives such as Importance Sampling [Melchers, 1990] and Subset Simulation [Au and Beck, 2001] considerably reduce this cost, but the number of performance function evaluations that is required remains incompatible with computationally demanding numerical models (*e.g.* finite element models). This observation has led to the development of metamodels which are fast-to-evaluate representations of the performance function. As a contribution to this field of research, a family of four Active learning and Kriging-based Reliability Methods (AK-RM) [Echard *et al.*, 2011a; Gayton and Echard, 2012] are proposed in this thesis to deal with computationally demanding models and small failure probabilities.

This chapter is organized as follows. Section 2.2 recalls the widely used isoprobabilistic transformation. Section 2.3 reviews Monte Carlo Simulation, as well as its classical alternatives which are more efficient for dealing with small failure probabilities. Section 2.4 introduces metamodels, particularly Kriging, as a means to conduct reliability analyses for a significantly smaller computational cost. Section 2.5 describes the general approach of AK-RM, namely AK-MCS. Section 2.6 exposes its three alternatives (AK-MCSm, AK-IS, AK-SS) that are more efficient for small failure probability cases.

2.2 Isoprobabilistic transformation

The isoprobabilistic transformation T aims at simplifying the joint PDF $f_{\mathbf{X}}(\mathbf{x})$ in the integral expression of the failure probability, Eqn.(2.2). By definition, this transformation preserves the probability. It associates the physical random variables $\mathbf{X}$ with independent Gaussian ones characterized by zero means and unit variances. The latter variables are commonly denoted by $\mathbf{U}$ and referred to as standard Gaussians. The performance function in the standard space $\mathcal{U}^n$ is denoted by H and reads:

$$H(\mathbf{U}) \equiv G(T^{-1}(\mathbf{U})) \tag{2.3}$$

The failure domain in the standard space is $\mathcal{F} = \{\mathbf{u} = \{u_1, \ldots, u_n\}^t \in \mathcal{U}^n : H(\mathbf{u}) \leq 0\}$. By using the isoprobabilistic transformation T, the failure probability is recast as:

$$P_f = \int_{\mathcal{F}} \phi_n(\mathbf{u}) \mathrm{d}u_1 \ldots \mathrm{d}u_n \tag{2.4}$$

where ϕ_n is the n-dimensional standard Gaussian PDF.

For independent physical random variables, the isoprobabilistic transformation T is simply derived, variable by variable, from the equality of the cumulative probabilities between the physical realization x_i and the corresponding u_i in the standard space:

$$x_i \overset{T}{\rightarrow} u_i = T_i(x_i) \;\Leftrightarrow\; \Phi(u_i) = F_{X_i}(x_i) \tag{2.5}$$

where Φ and F_{X_i} are the CDFs of U_i and X_i respectively. T is then the composition of two CDFs:

$$x_i \overset{T}{\rightarrow} u_i = \Phi^{-1}(F_{X_i}(x_i)) \tag{2.6}$$

Reciprocally, the inverse transformation T^{-1} reads:

$$u_i \overset{T^{-1}}{\rightarrow} x_i = F_{X_i}^{-1}(\Phi(u_i)) \tag{2.7}$$

In the case of correlated variables, u_i cannot be associated with x_i variable by variable. The transformation T_i then becomes a function of $\mathbf{x}$:

$$u_i = T_i(\mathbf{x}) \tag{2.8}$$

As suggested by Der Kiureghian and Liu [1986], the transformation T can be characterized by the Nataf transformation [Nataf, 1962]. Let $\mathbf{X} = \{X_1, \ldots, X_n\}^t$ be random variables that are correlated. The correlation matrix is denoted by $\mathbb{C}$. Using Eqn.(2.6), the correlated Gaussian variables $\bar{\mathbf{U}}$ with zero means and unit variances are obtained as follows:

$$\bar{u}_i = \Phi^{-1}(F_{X_i}(x_i)) \tag{2.9}$$

Let $\breve{\mathbb{C}}$ denote the correlation matrix of the variables $\breve{\mathbf{U}}$. The element $\breve{\mathbb{C}}_{i,j}$ is linked to the element $\mathbb{C}_{i,j}$ by [Lemaire, 2009]:

$$\mathbb{C}_{i,j} = \int_{-\infty}^{+\infty}\int_{-\infty}^{+\infty}\left(\frac{F_{X_i}^{-1}(\Phi(\breve{u}_i)) - \mu_{X_i}}{\sigma_{X_i}}\right)\left(\frac{F_{X_j}^{-1}(\Phi(\breve{u}_j)) - \mu_{X_j}}{\sigma_{X_j}}\right)\phi_2(\breve{u}_i, \breve{u}_j, \breve{\mathbb{C}}_{i,j})\mathrm{d}\breve{u}_i\mathrm{d}\breve{u}_j \tag{2.10}$$

where μ_{X_i} (respectively μ_{X_j}) is the mean of X_i (resp. X_j) and σ_{X_i} (resp. σ_{X_j}) is the standard deviation of X_i (resp. X_j). The elements of $\breve{\mathbb{C}}$ are numerically determined using Eqn.(2.10). Note that semi-empirical equations linking $\mathbb{C}_{i,j}$ and $\breve{\mathbb{C}}_{i,j}$ exist in the literature [Der Kiureghian and Liu, 1986] to ease calculations. Once determined, the matrix $\breve{\mathbb{C}}$ is recast as:

$$\breve{\mathbb{C}} = \mathbb{L}\mathbb{L}^t \tag{2.11}$$

where $\mathbb{L}$ is the lower triangular matrix of the Cholesky decomposition. The independent standard Gaussian variables are finally obtained by:

$$u_i = T_i(\mathbf{x}) = \sum_j \mathbb{L}_{i,j}^{-1}\ \breve{u}_j = \sum_j \mathbb{L}_{i,j}^{-1}\ \Phi^{-1}(F_{X_j}(x_j)) \tag{2.12}$$

Note that the characterization of the dependence between random variables can be generalized with the concept of copulas, the Nataf transformation in fact making the hypothesis of a Gaussian copula [Lebrun and Dutfoy, 2009].

2.3 Sampling-based reliability methods

2.3.1 Monte Carlo Simulation

By introducing the indicator function $I_{\mathcal{F}}(\mathbf{u}) = \{1 \text{ if } H(\mathbf{u}) \leq 0 \text{ and } 0 \text{ otherwise}\}$, Eqn.(2.4) becomes [Ditlevsen and Madsen, 1996; Lemaire, 2009]:

$$P_f = \int_{\mathcal{U}^n} I_{\mathcal{F}}(\mathbf{u})\phi_n(\mathbf{u})\mathrm{d}u_1 \ldots \mathrm{d}u_n = \mathrm{E}\left[I_{\mathcal{F}}(\mathbf{U})\right] \tag{2.13}$$

where E[.] is the mathematical expectation. Simulation methods are often applied to estimate this integral. The most popular is the Monte Carlo Simulation (MCS) which constitutes a numerical integration method relying on repeated random sampling, as illustrated in Figure 2.1. Given N_{MCS} independent copies $\{\mathbf{U}^{(j)},\ j = 1, \ldots, N_{\mathrm{MCS}}\}$ of $\mathbf{U}$ distributed according to ϕ_n, the estimator $\hat{P}_f$ of the failure probability reads:

$$P_f \approx \hat{P}_f = \frac{1}{N_{\mathrm{MCS}}}\sum_{j=1}^{N_{\mathrm{MCS}}} I_{\mathcal{F}}\left(\mathbf{U}^{(j)}\right) \tag{2.14}$$

Its coefficient of variation δ is expressed as follows:

$$\delta = \sqrt{\frac{1 - P_f}{N_{\text{MCS}}\, P_f}} \tag{2.15}$$

The major drawback of Monte Carlo Simulation is the large number of points at which H should be evaluated, in order to obtain a suitable coefficient of variation of $\hat{P}_f$. Eqn.(2.15) shows that assessing a probability of 10^{-p} with a targeted $\delta = 10\%$ requires $N_{\text{MCS}} = 10^{p+2}$ evaluations. Monte Carlo Simulation is consequently inapplicable to problems involving small probabilities and time-demanding performance function evaluations.

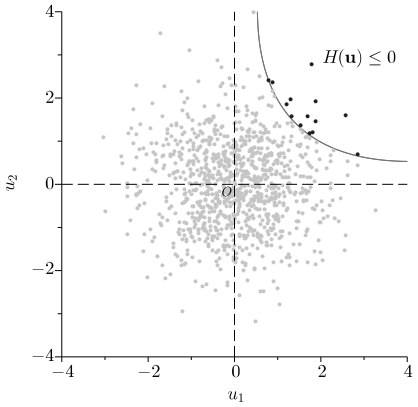

Figure 2.1: Monte Carlo Simulation. The black dots represent points located in the failure domain $\mathcal{F}$.

2.3.2 Monte Carlo Simulation under monotony

In many mechanical structures, the performance function happens to be monotonic with respect to its random input variables. De Rocquigny [2009] notes that an insufficient attention is brought to monotony in structural reliability analysis, and formulates its basic features. He further proposes Monotonic Reliability Methods which consist in progressively narrowing some robust upper and lower bounds on the failure probability through an adaptive sampling.

A performance function $H^{\dagger}$, as depicted in Figure 2.2, is globally monotonic if:

$$\forall i,\ \exists s_i \in \{-1;1\},\ a \geq 0,\ \mathbf{u} \in \mathcal{U}^n,\ H(u_1, \ldots, u_i + s_i\, a, \ldots, u_n) \leq H(u_1, \ldots, u_i, \ldots, u_n) \tag{2.16}$$

[†]Note that monotony in $\mathcal{X}^n$ is preserved in $\mathcal{U}^n$ in case of independent physical variables, due to the fact that the isoprobabilistic transformation is then the composition of two CDFs that are, by definition, monotonically increasing functions.

where s_i characterizes the monotonic trend in the ith direction. Suppose H is evaluated at a point $\mathbf{u}^{(1)}$ which is found to lie in $\mathcal{S}$. The sub-domain $E^+_{\mathbf{u}^{(1)}}$ delimited by the 'corner' $\mathbf{u}^{(1)}$ necessarily constitutes an ensured safe domain. Conversely, for a point $\mathbf{u}^{(2)}$ lying in $\mathcal{F}$, the sub-domain $E^-_{\mathbf{u}^{(2)}}$ bordered by $\mathbf{u}^{(2)}$ forms an ensured failure domain. Such features enable the definition of robust lower and upper bounds on the failure probability as follows [De Rocquigny, 2009]:

$$\text{Prob}(\mathbf{u} \in E^+) \leq P_f \leq 1 - \text{Prob}(\mathbf{u} \in E^-) \tag{2.17}$$

where $E^+ = \bigcup_j E^+_{\mathbf{u}^{(j)}}$ and $E^- = \bigcup_k E^-_{\mathbf{u}^{(k)}}$. The evaluation of H at a point lying in the margin between E^+ and E^- constitutes a definite improvement to the bounds on P_f. A simple accept-reject Monte Carlo Simulation or a more sophisticated sampling strategy can be used to generate new points in the margin.

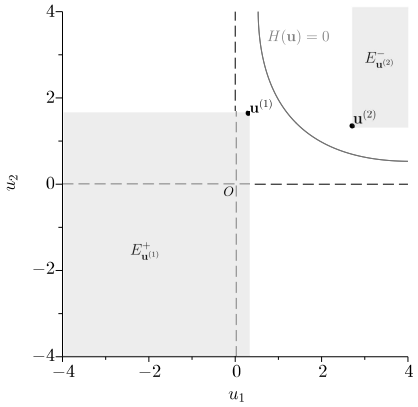

Figure 2.2: Ensured sub-domains $E^+_{\mathbf{u}^{(1)}}$ and $E^-_{\mathbf{u}^{(2)}}$ on the hypothesis that H is monotonic. Evaluations of H at points lying in these sub-domains are worthless.

In this paragraph, the procedure of Monte Carlo Simulation under monotony (MCSm) is restricted to the classification of a fixed sample population into the safe and failure subsets. The calculation of the lower and upper bounds on the failure probability is then not considered. Let H be a monotonic performance function in the standard space. The algorithm is as follows:

1. Generate a population $\mathbb{P}_{\text{MCS}}$ according to ϕ_n, and composed of N_{MCS} points.

2. Evaluate H at a point in $\mathbb{P}_{\text{MCS}}$. This point may be drawn uniformly from the population, but the selection of a location close to the limit state is recommended. In some cases, the nature of some random variables can be determined intuitively. Such information is helpful to better select a point to evaluate. Assuming monotony, an increase of the load variables (*e.g.* the size of a flaw) or a decrease of the resistance

variables (*e.g.* tensile strength) from a current safe location leads to a new location which is closer to the limit state.

3. Count the points lying in E^+ and E^-. They are respectively denoted by N^+ and N^-.

4. Remove the points lying in E^+ and E^- from $\mathbb{P}_{\text{MCS}}$ as they represent worthless evaluations. N_R denotes the number of points lying in the margin. The procedure goes back to Step 2 while $N_R > 0$.

5. Calculate the failure probability estimate as N^-/N_{MCS}. The coefficient of variation δ of the estimator is obtained using Eqn.(2.15).

In conclusion, the consideration of monotony clearly enables a drastic reduction in the number of performance function evaluations in comparison to Monte Carlo Simulation. Nevertheless, H is inevitably evaluated at a substantial number of points in the vicinity of the limit state, and the convergence thus remains slow.

2.3.3 Importance Sampling

2.3.3.1 Concept of most probable failure point

The Hasofer-Lind reliability index β [Hasofer and Lind, 1974] corresponds to the distance between the origin O of the standard space and the closest failure point to O denoted by $P^\star$. The PDF is maximized in the failure domain at $P^\star$ which is commonly referred to as the Most Probable Failure Point (MPFP) [†]. Its location $\mathbf{u}^\star = \{u_1^\star, \ldots, u_n^\star\}^t$ is determined by solving the following constraint optimization problem:

$$\beta = \sqrt{(\mathbf{u}^{\star t}\ \mathbf{u}^\star)} = \min_{H(\mathbf{u})\leq 0} \sqrt{(\mathbf{u}^t\ \mathbf{u})} \tag{2.18}$$

Hasofer-Lind-Rackwitz-Fiessler (HLRF) algorithm [Rackwitz and Fiessler, 1978] and its improved version (iHLRF) by Zhang and Der Kiureghian [1995] are commonly implemented to find $P^\star$. Note that the Hasofer-Lind reliability index is conventionally set as negative if O lies in the failure domain.

2.3.3.2 First order reliability method

Calculation of the failure probability

The probability density function in $\mathcal{F}$ is, by definition, maximum at $P^\star$. Additionally, in the presence of a limited number of random variables, the density decreases rapidly when the distance from the origin increases. Following these statements, the First Order

[†] note the discussion about naming $P^\star$ in Lemaire [2009].

Reliability Method (FORM), illustrated on an example in Figure 2.3, consists in replacing the limit state $H(\mathbf{u}) = 0$ by an hyper-plane at $P^\star$ that reads:

$$\tilde{H}(\mathbf{u}) = \sum_{i=1}^{n} \alpha_i \, u_i + \beta = 0 \tag{2.19}$$

where $\{\alpha_i, \; i = 1, \ldots, n\}$ are the direction cosines of the vector $P^\star O$, *i.e.* $\alpha_i = -u_i^\star/\beta$. The hyper-plane is orthogonal to the vector $P^\star O$, so the failure probability can consequently be approximated by:

$$\tilde{P}_f = \Phi(-\beta) \tag{2.20}$$

Concerning small failure probabilities, FORM is an efficient alternative to Monte Carlo Simulation, as its number of performance function evaluations N_{FORM} remains significantly smaller than N_{MCS}. Nevertheless, the previously cited optimization algorithms to find $P^\star$ are gradient-based, and FORM thus loses efficiency in high-dimensional problems. Furthermore, the potential error made with the linearization of the limit state is unknown, so additional sampling is therefore required to validate the approximation of the failure probability.

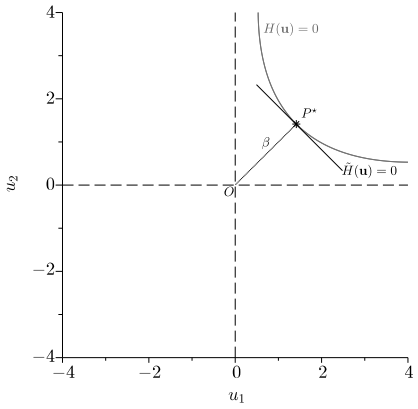

Figure 2.3: FORM linear approximation of the limit state at the MPFP $P^\star$.

Importance factors in reliability

FORM analysis also provides importance factors for the Hasofer-Lind reliability index with respect to the random variables and their distribution parameters (mean, standard deviation, correlation between two variables...). These factors offer a way to rank the influence of the input random variables on reliability. The most significant variables should be controlled to ensure structural integrity, while those playing a small role can be set to deterministic values in order to simplify the analysis. This section is restricted to the importance factors with respect to the distribution parameters. The parameter of the ith

random variable is denoted by p_i. The sensitivity of the Hasofer-Lind reliability index with respect to p_i is denoted by S_{p_i} and reads [Lemaire, 2009]:

$$S_{p_i} = \left.\frac{\partial \beta}{\partial p_i}\right|_{\mathbf{u}^\star} \tag{2.21}$$

S_{p_i} represents the value by which β is increased when p_i is raised by 1. It can be recast as:

$$S_{p_i} = \left.\frac{\partial \beta}{\partial u_i}\right|_{\mathbf{u}^\star} \left.\frac{\partial u_i}{\partial p_i}\right|_{\mathbf{u}^\star} = \left.\frac{\partial \beta}{\partial u_i}\right|_{\mathbf{u}^\star} \left.\frac{\partial T_i(x_j)}{\partial p_i}\right|_{\mathbf{x}^\star} \tag{2.22}$$

where the variable U_i is deduced from the X_j using the isoprobabilistic transformation T_i. By definition of the direction cosines, the sensitivity becomes:

$$S_{p_i} = -\alpha_i \left.\frac{\partial T_i(x_j)}{\partial p_i}\right|_{\mathbf{x}^\star} \tag{2.23}$$

For correlated variables, the Nataf transformation, introduced in Section 2.2, can be applied. In the case of independent random variables, Eqn.(2.6) enables the sensitivity to be recast as follows:

$$S_{p_i} = -\alpha_i \frac{1}{\phi(u_i^\star)} \left.\frac{\partial F_{X_i}(x_i)}{\partial p_i}\right|_{\mathbf{x}^\star} \tag{2.24}$$

For independent Gaussian random variables, sensitivities with respect to the mean S_{μ_i} and standard deviation S_{σ_i} simply read:

$$S_{\mu_i} = \frac{\alpha_i}{\sigma_i} \tag{2.25}$$

$$S_{\sigma_i} = -\frac{\beta\, \alpha_i^2}{\sigma_i} \tag{2.26}$$

Note that sensitivities with respect to standard deviations are negative if $\beta > 0$, thus increasing a standard deviation always diminishes the reliability of the structure.

In the end, normalized sensitivities are often introduced to enable the comparison between variables and parameters. They are known as elasticities and read:

$$E_{p_i} = \frac{p_i}{\beta} S_{p_i} \tag{2.27}$$

E_{p_i} then represents the percentage by which β is increased when p_i is raised by 1%.

2.3.3.3 Probability assessment using Importance Sampling

As already mentioned, additional sampling is required in order to validate the FORM approximation of the failure probability. The variance reduction technique known as Importance Sampling (IS) is commonly applied for this purpose [Melchers, 1990]. Importance Sampling relies on the hypothesis that the weight of the failure probability is located in

the vicinity of a unique MPFP. If such a hypothesis holds, sampling points centred on $P^\star$, as illustrated in Figure 2.4, is more efficient than sampling around the origin of standard space. The probability of a failure event is in fact larger, and its variance is significantly reduced. Given the sampling PDF φ_n, the failure probability can be recast as follows:

$$P_f = \int_{\mathcal{U}^n} I_{\mathcal{F}}(\mathbf{u}) \, \frac{\phi_n(\mathbf{u})}{\varphi_n(\mathbf{u})} \varphi_n(\mathbf{u}) \mathrm{d}u_1 \dots \mathrm{d}u_n \tag{2.28}$$

φ_n is often defined, in the standard space, as a n-dimensional Gaussian distribution centred on the MPFP with uncorrelated components and unit variances. Note that other values may also be considered for the variances, so as to tighten or spread out the conditioning. Given N_{IS} independent copies $\{\bar{\mathbf{U}}^{(j)},\ j = 1, \dots, N_{\mathrm{IS}}\}$ of the random vector $\bar{\mathbf{U}}$ distributed according to φ_n, the estimator $\hat{P}_f$ of the failure probability reads:

$$P_f \approx \hat{P}_f = \frac{1}{N_{\mathrm{IS}}} \sum_{j=1}^{N_{\mathrm{IS}}} I_{\mathcal{F}}\left(\bar{\mathbf{U}}^{(j)}\right) \frac{\phi_n\left(\bar{\mathbf{U}}^{(j)}\right)}{\varphi_n\left(\bar{\mathbf{U}}^{(j)}\right)} \tag{2.29}$$

Its variance $\mathrm{Var}[\hat{P}_f]$ is expressed as:

$$\mathrm{Var}[\hat{P}_f] = \frac{1}{N_{\mathrm{IS}}} \left(\frac{1}{N_{\mathrm{IS}}} \sum_{j=1}^{N_{\mathrm{IS}}} \left(I_{\mathcal{F}}\left(\bar{\mathbf{U}}^{(j)}\right) \left(\frac{\phi_n\left(\bar{\mathbf{U}}^{(j)}\right)}{\varphi_n\left(\bar{\mathbf{U}}^{(j)}\right)} \right)^2 \right) - \hat{P}_f^2 \right) \tag{2.30}$$

The coefficient of variation δ of $\hat{P}_f$ is given as the following ratio:

$$\delta = \frac{\sqrt{\mathrm{Var}[\hat{P}_f]}}{P_f} \tag{2.31}$$

Importance Sampling based on the sampling PDF φ_n as defined in this section should only be conducted if the MPFP is well isolated and that no secondary minima exist in other areas of space. In such a case, Importance Sampling drastically reduces the number of points to evaluate. Note that Importance Sampling can also be applied with other sampling PDFs.

2.3.4 Subset Simulation

Subset Simulation (SS), introduced in structural reliability by Au and Beck [2001], is another efficient alternative to Monte Carlo Simulation regarding small failure probabilities. Its basic idea, illustrated in Figure 2.5, is to express the failure probability as a product of larger conditional probabilities by introducing some intermediate events. Let H be the performance function in the standard space and $\mathcal{F} = \{\mathbf{u} \in \mathcal{U}^n : H(\mathbf{u}) \leq 0\}$ be the failure domain. Let a decreasing sequence of sub-domains $\mathcal{F}_1, \mathcal{F}_2 \dots, \mathcal{F}_m$ be, so that

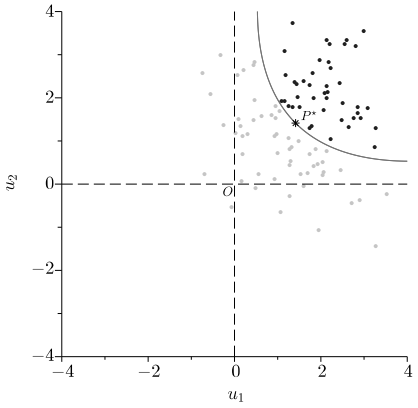

Figure 2.4: Importance Sampling centred on the MPFP $P^\star$.

$\mathcal{F}_1 \supset \mathcal{F}_2 \supset \ldots \supset \mathcal{F}_m = \mathcal{F}$ where $\mathcal{F}_k = \{\mathbf{u} \in \mathcal{U}^n : H(\mathbf{u}) \leq H_k\}$. The failure probability is then expressed as the product of the conditional probabilities:

$$P_f = \text{Prob}(\mathbf{u} \in \mathcal{F}_1) \prod_{k=2}^{m} \text{Prob}(\mathbf{u} \in \mathcal{F}_k | \mathbf{u} \in \mathcal{F}_{k-1}) \tag{2.32}$$

In practice, the thresholds $\{H_k,\ k = 1, \ldots, m\}$ are determined for obtaining conditional probabilities close to 0.1 [Au and Beck, 2001]. Such a value represents a reasonable trade-off between the number of simulation levels m and the number of performance function evaluations.

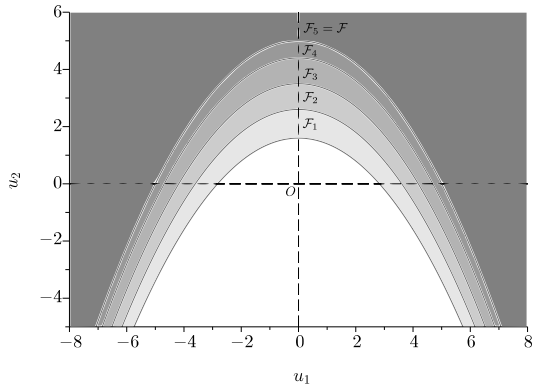

Figure 2.5: Sequence of five simulation levels in Subset Simulation.

Figure 2.6 depicts the Subset Simulation procedure. The first simulation level is a Monte Carlo Simulation (see Figure 2.6(a)). A population $\mathbb{P}_1$ of N_1 points is generated according to ϕ_n. The performance function is evaluated at each point of the population,

and the threshold H_1 is determined (see Figure 2.6(b)) so that the probability estimate reads:

$$\hat{P}_1 = \frac{1}{N_1} \sum_{j=1}^{N_1} I_{\mathcal{F}_1} \left(\mathbf{u}^{(j)} \right) \approx 0.1 \tag{2.33}$$

where $I_{\mathcal{F}_1}(\mathbf{u}^{(j)}) = \{1 \text{ if } H(\mathbf{u}^{(j)}) \leq H_1 \text{ and } 0 \text{ otherwise}\}$. According to Eqn.(2.15), the coefficient of variation δ_1 of the probability estimator reads:

$$\delta_1 = \sqrt{\frac{1 - \text{Prob}(\mathbf{u} \in \mathcal{F}_1)}{N_1 \, \text{Prob}(\mathbf{u} \in \mathcal{F}_1)}} \tag{2.34}$$

At the kth simulation level ($k = 2, \ldots, m$), a Markov Chain Monte Carlo sampling technique is first applied to generate a population $\mathbb{P}_k$ following the conditional distribution $\phi_n(.|\mathbf{u} \in \mathcal{F}_{k-1})$ from the seeds, *i.e.* from the $[0.1 \times N_{k-1}]$ points lying in $\mathcal{F}_{k-1}$. Figure 2.6(c) depicts such a population for $k = 2$. Au and Beck [2001] propose a modified version of the Metropolis-Hastings algorithm [Metropolis *et al.*, 1953; Hastings, 1970] to generate $\mathbb{P}_k$. Let $\mathbf{u}^{(1)}$ be a seed distributed according to $\phi_n(.|\mathbf{u} \in \mathcal{F}_{k-1})$. A chain of points $\mathbf{u}^{(1)}, \mathbf{u}^{(2)}, \ldots$ lying in $\mathcal{F}_{k-1}$ is generated by simulating $\mathbf{u}^{(l+1)}$ from the state $\mathbf{u}^{(l)}$. The algorithm is as follows:

1. Generate a candidate state $\breve{\mathbf{u}}^{(l+1)}$: a point $\breve{\mathbf{v}}^{(l+1)}$ is simulated according to a n-dimensional PDF centred on the current state $\mathbf{u}^{(l)}$ and denoted by $p(.|\mathbf{u}^{(l)} \in \mathcal{F}_{k-1})$. Such a distribution is expressed as a product of independent PDFs $\{p_i(.|\mathbf{u}^{(l)} \in \mathcal{F}_{k-1}),\ i = 1, \ldots, n\}$ that are uniform with a width between 1 and 3 (usually 2). The ratio $t_i = \phi(\breve{v}_i^{(l+1)})/\phi(u_i^{(l)})$ is calculated. $\breve{u}_i^{(l+1)}$ is set to $\breve{v}_i^{(l+1)}$ with probability $\min\{1, t_i\}$ and to $u_i^{(l)}$ with the remaining probability $1 - \min\{1, t_i\}$. This step can be seen as a random walk in the neighbourhood of the current state $\mathbf{u}^{(l)}$.

2. Accept/reject the candidate state: the performance function is evaluated at the candidate state $\breve{\mathbf{u}}^{(l+1)}$. It is accepted as the state $\mathbf{u}^{(l+1)}$ if it lies in $\mathcal{F}_{k-1}$, *i.e.* if $H(\breve{\mathbf{u}}^{(l+1)}) \leq H_{k-1}$. Otherwise, it is rejected and the chain remains in the current state: $\mathbf{u}^{(l+1)} = \mathbf{u}^{(l)}$.

3. Add the state $\mathbf{u}^{(l+1)}$ to the population $\mathbb{P}_k$.

4. Replicate the algorithm several times with the $[0.1 \times N_{k-1}]$ seeds until $N_k \geq N_{k-1}$.

Given the population $\mathbb{P}_k$, the threshold H_k is determined (see Figure 2.6(d)) so that the estimate $\hat{P}_k$ of the conditional probability $\text{Prob}(\mathbf{u} \in F_k | \mathbf{u} \in F_{k-1})$ reads:

$$\hat{P}_k = \frac{1}{N_k} \sum_{j=1}^{N_k} I_{F_k} \left(\mathbf{u}^{(j)} \right) \approx 0.1 \tag{2.35}$$

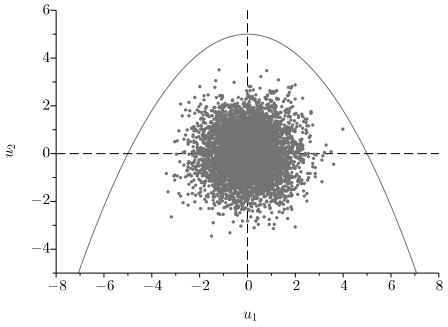

(a) Generation of a population $\mathbb{P}_1$ using ϕ_2.

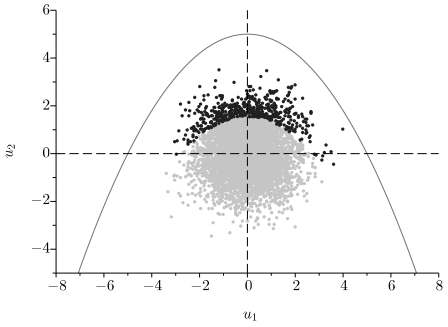

(b) The performance function is evaluated at each point of $\mathbb{P}_1$ and the threshold H_1 is determined.

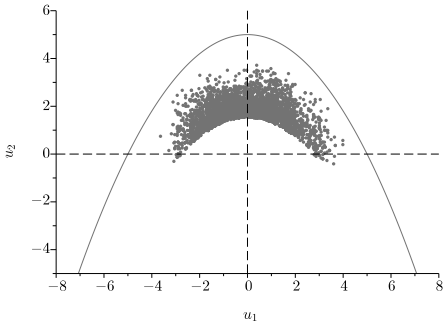

(c) The modified Metropolis-Hastings algorithm is employed to generate a population $\mathbb{P}_2$ following the conditional distribution $\phi_2(.|\mathbf{u} \in \mathcal{F}_1)$.

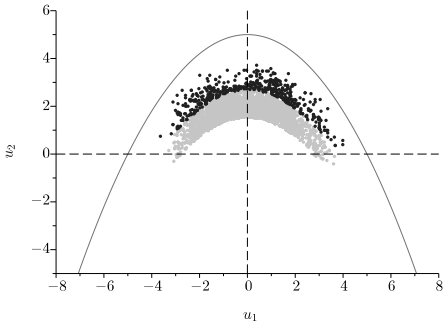

(d) The threshold H_2 is determined.

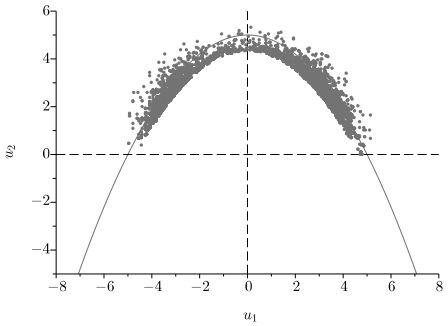

(e) After 4 simulation levels, a population $\mathbb{P}_5$ is generated following the conditional distribution $\phi_2(.|\mathbf{u} \in \mathcal{F}_4)$.

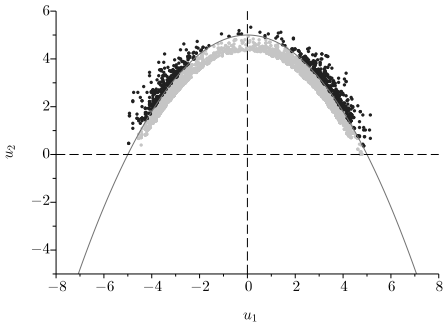

(f) The threshold H_5 is negative. It is then set to $H_5 = 0$. $\hat{P}_5$ is calculated and the failure probability is estimated by the product of the intermediate probabilities.

Figure 2.6: Subset Simulation procedure.

The coefficient of variation δ_k of the probability estimator is:

$$\delta_k = \sqrt{\frac{1 - \text{Prob}(\mathbf{u} \in F_k | \mathbf{u} \in F_{k-1})}{N_k \, \text{Prob}(\mathbf{u} \in F_k | \mathbf{u} \in F_{k-1})}(1 + \gamma_k)} \tag{2.36}$$

where γ_k is a factor accounting for the correlation between the N_k points. The last level is illustrated in Figure 2.6(e) and Figure 2.6(f). When the threshold H_k is negative, k is set to m and $H_m = 0$. The failure probability estimate is finally obtained, on the basis of Eqn.(2.32), by:

$$\hat{P}_f = \prod_{k=1}^{m} \hat{P}_k \tag{2.37}$$

The coefficient of variation δ of the failure probability estimator is given by:

$$\delta = \sqrt{\sum_{k=1}^{m} \delta_k^2} \tag{2.38}$$

Unlike Importance Sampling, Subset Simulation enables the detection of secondary minima in other areas of space. Generality is thus preserved. Nevertheless, it inevitably leads to a higher number of performance function evaluations. A slight modification of Subset Simulation, known as iSubset, is proposed by Defaux *et al.* [2010] to reduce the computational cost. Given that numerous simulation levels are unnecessary when an order of magnitude of the failure probability is known, Conditional Sampling [Bernard and Fogli, 1987] is performed at the first simulation level. Such a sampling, depicted in Figure 2.7, is characterized by an exclusion hyper-sphere centred on the origin of space with radius β_e to set.

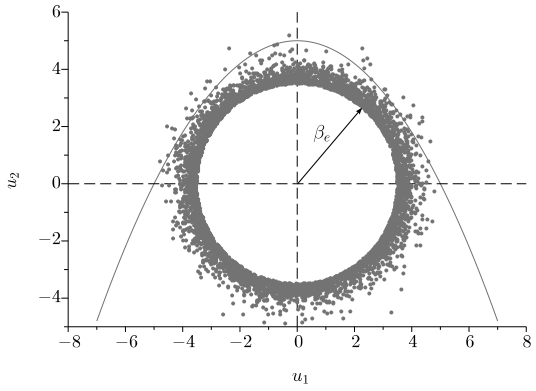

Figure 2.7: First simulation level in iSubset.

2.3.5 Conclusion

In this section, various sampling-based reliability methods have been introduced to handle problems involving small failure probabilities. Other alternatives such as Directional Sampling [Ditlevsen *et al.*, 1988] are acknowledged by the author but not considered in the frame of this thesis.

2.4 Kriging-based reliability methods

Performance functions generally depend on responses of numerical models simulating the mechanical behaviours of structures. Despite considerable advances in computer technology over the last two decades, a single evaluation of such models remains time-demanding (several minutes to several hours) due to the continuous need for more faithful representations to the real mechanical behaviours. Numerous calls to performance functions are consequently not possible in a short space of time. In addition, structures encountered in industry are fortunately designed with codified rules leading to large safety margins, *i.e.* small failure probabilities. The sampling-based reliability methods reviewed in the previous section are possible solutions to assess small probabilities, but they are inapplicable with computationally demanding models, in so far as they still require a substantial number of performance function evaluations. This statement motivates the use of metamodelling as a means to conduct structural reliability analyses in a more practical amount of time.

2.4.1 Principles of metamodelling

Metamodels are widespread in computational sciences and employed to predict the outcome of a time-demanding function at any point, providing that the outcomes at a few other points are known. These latter points are usually called the Design Of numerical Experiments (DOE). Metamodels are attractive tools because they are fast to evaluate in comparison with the actual functions. However, the selection of the DOE is of high importance. The DOE must contain a sufficient number of points in order to ensure an accurate approximation of the function, but it must also keep this number to a minimum so as to remain affordable at a low cost. This latter condition is often referred to as the parsimony constraint.

In structural reliability analysis, the metamodel $\tilde{H}$ of the performance function H in the standard space (or $\tilde{G}$ for G in the physical space) is built to provide an approximate failure domain $\tilde{\mathcal{F}} = \{\mathbf{u} \in \mathcal{U}^n : \tilde{H}(\mathbf{u}) \leq 0\}$. The integral formula of the failure probability is then approximated by:

$$P_f \approx \int_{\tilde{\mathcal{F}}} \phi_n(\mathbf{u}) \mathrm{d}u_1 \dots \mathrm{d}u_n \tag{2.39}$$

In practice, the failure probability is assessed by applying a sampling-based reliability

method to the metamodel of the performance function. Note that a bias may be introduced in the probability if the metamodel is not sufficiently refined.

Among metamodels, Quadratic Response Surfaces [Bucher and Bourgund, 1990; Das and Zheng, 2000; Gayton *et al.*, 2003] are the most popular although they are limited to local interpolation. Polynomial Chaos [Ghanem and Spanos, 1991; Sudret and Der Kiureghian, 2002] is an alternative to avoid this problem. However, the definitions of the DOE and of the polynomial degrees are delicate issues [Blatman and Sudret, 2010]. More recently, reliability methods based on Support Vector Machine have also been proposed [Hurtado, 2004; Bourinet *et al.*, 2011]. Finally, Kriging (also known as Gaussian process) is investigated in this thesis for its stochastic and interpolation features (discussed in Section 2.4.2.3). Its efficiency has been proven in structural reliability analysis [Romero *et al.*, 2004; Kaymaz, 2005; Bichon *et al.*, 2008, 2009, 2011; Ranjan *et al.*, 2008; Picheny *et al.*, 2010; Bect *et al.*, 2011; Dubourg, 2011; Dubourg *et al.*, 2011] and in related domains such as uncertainty analysis and global sensitivity analysis [Kennedy *et al.*, 2006; O'Hagan, 2006; Marrel *et al.*, 2009].

2.4.2 Kriging theory

Kriging, pioneered by Krige [1951] and then theorized by Matheron [1973], considers the performance function H as a realization of a Gaussian process $\mathcal{H}(\mathbf{u})$. The first step of Kriging is the determination of the Gaussian process parameters according to the DOE. Then, the best linear unbiased predictor is applied in order to estimate the outcome of the performance function at an unobserved point. For more details on Kriging theory, the reader may refer to Dubourg [2011, Chapter 1].

2.4.2.1 Identification of the Gaussian process

The model of the Gaussian process $\mathcal{H}(\mathbf{u})$ is expressed as [Sacks *et al.*, 1989]:

$$\mathcal{H}(\mathbf{u}) = Y(\mathbf{u}, \boldsymbol{\eta}) + \mathcal{Z}(\mathbf{u}) \tag{2.40}$$

where:

- $Y(\mathbf{u}, \boldsymbol{\eta})$ is the deterministic part giving an approximation of the response in mean. It represents the trend of Kriging, and corresponds to a regression model that reads:

$$Y(\mathbf{u}, \boldsymbol{\eta}) = \mathbf{y}(\mathbf{u})^t \, \boldsymbol{\eta} \tag{2.41}$$

  where $\mathbf{y}(\mathbf{u}) = \{y_1(\mathbf{u}), \ldots, y_b(\mathbf{u})\}^t$ is the vector of the basis functions and $\boldsymbol{\eta} = \{\eta_1, \ldots, \eta_b\}^t$ the vector of the regression coefficients. In this thesis, an ordinary trend is favoured for Kriging, meaning that $Y(\mathbf{u}, \boldsymbol{\eta})$ is reduced to a scalar η. This regression model is often sufficient, and other models do not necessarily bring any

substantial gain according to Bichon *et al.* [2011]. The following equations in this section are based on the assumption of ordinary Kriging.

- $\mathcal{Z}(\mathbf{u})$ is a stationary Gaussian process with zero mean and covariance between two points of space $\mathbf{u}$ and $\mathbf{v}$ that reads:

$$\operatorname{cov}\left(\mathcal{Z}(\mathbf{u}), \mathcal{Z}(\mathbf{v})\right) = \sigma^2_{\mathcal{Z}} R_{\boldsymbol{\theta}}(\mathbf{u}, \mathbf{v}) \tag{2.42}$$

  where $\sigma^2_{\mathcal{Z}}$ is the process variance and $R_{\boldsymbol{\theta}}$ is the correlation function characterized by its set of parameters $\boldsymbol{\theta} = \{\theta_1, \ldots, \theta_n\}^t$.

In this thesis, the anisotropic Gaussian model is selected to represent the correlation function:

$$R_{\boldsymbol{\theta}}(\mathbf{u}, \mathbf{v}) = \prod_{i=1}^{n} \exp\left[-\theta_i (u_i - v_i)^2\right] \tag{2.43}$$

This model is dominant in engineering literature [Santner *et al.*, 2003; Bichon *et al.*, 2008; Ranjan *et al.*, 2008]. Note that the Matérn correlation function is a more flexible alternative that is gradually finding its way in structural reliability analysis [Dubourg, 2011], but its use increases the computational cost [Bichon *et al.*, 2011].

Let a DOE be defined by a set of N_E points $\mathbb{D} = \{\mathbf{u}^{(1)}, \ldots, \mathbf{u}^{(N_E)}\}^t$ and their respective observations $\mathbf{h} = \{H(\mathbf{u}^{(1)}), \ldots, H(\mathbf{u}^{(N_E)})\}^t$. The scalars η and σ_z^2 are estimated by [Jones *et al.*, 1998]:

$$\hat{\eta} = \frac{\mathbf{1}^t_{N_E} \mathbb{R}^{-1}_{\boldsymbol{\theta}} \mathbf{h}}{\mathbf{1}^t_{N_E} \mathbb{R}^{-1}_{\boldsymbol{\theta}} \mathbf{1}_{N_E}} \tag{2.44}$$

and:

$$\hat{\sigma_{\mathcal{Z}}}^2 = \frac{\left(\mathbf{h} - \hat{\eta}\mathbf{1}_{N_E}\right)^t \mathbb{R}^{-1}_{\boldsymbol{\theta}} \left(\mathbf{h} - \hat{\eta}\mathbf{1}_{N_E}\right)}{N_E} \tag{2.45}$$

where $\mathbb{R}_{\boldsymbol{\theta}_{i,j}} = R_{\boldsymbol{\theta}}(\mathbf{u}^{(i)}, \mathbf{u}^{(j)})$ is the correlation matrix of the points in $\mathbb{D}$ and $\mathbf{1}_{N_E}$ denotes the N_E-length column vector of ones. $\hat{\eta}$ and $\hat{\sigma_{\mathcal{Z}}}^2$ in Eqn.(2.44) and Eqn.(2.45) depend on the parameter $\boldsymbol{\theta}$ through the matrix $\mathbb{R}_{\boldsymbol{\theta}}$. This parameter is obtained by ML estimation [Lophaven *et al.*, 2002a]:

$$\hat{\boldsymbol{\theta}} = \arg \min_{\boldsymbol{\theta}} \left(\det \mathbb{R}_{\boldsymbol{\theta}}\right)^{\frac{1}{N_E}} \hat{\sigma_{\mathcal{Z}}}^2 \tag{2.46}$$

In the DACE Matlab/Scilab Kriging toolbox [Lophaven *et al.*, 2002a] employed in this thesis, a pattern search approach known as the modified Hooke and Jeeves method is proposed in order to solve the optimization problem. Full details on the algorithm and performance tests may be found in Lophaven *et al.* [2002b]. Note that the artificial bee colony algorithm [Karaboga, 2005; Karaboga and Basturk, 2007] has recently been proposed by Luo *et al.* [2012] as an efficient alternative to the current optimization procedure in DACE.

2.4.2.2 Kriging prediction

In the previous section, the parameters of the Gaussian process have been determined. The next step is the prediction of the outcome $H(\mathbf{u}^*)$ at an unobserved point $\mathbf{u}^*$. Beforehand, let $\mathbf{r}(\mathbf{u}^*)$ denote the correlation vector between $\mathbf{u}^*$ and the points in $\mathbb{D}$. Hence:

$$\mathbf{r}(\mathbf{u}^*) = \{R_{\boldsymbol{\theta}}(\mathbf{u}^*, \mathbf{u}^{(1)}), \dots, R_{\boldsymbol{\theta}}(\mathbf{u}^*, \mathbf{u}^{(N_E)})\}^t \tag{2.47}$$

The Best Linear Unbiased Predictor (BLUP), denoted by $\tilde{H}(\mathbf{u}^*)$, is a Gaussian random variable:

$$\tilde{H}(\mathbf{u}^*) \sim \mathcal{N}\left(\mu_{\tilde{H}}(\mathbf{u}^*), \sigma^2_{\tilde{H}}(\mathbf{u}^*)\right) \tag{2.48}$$

with Kriging mean [Jones *et al.*, 1998]:

$$\mu_{\tilde{H}}(\mathbf{u}^*) = \hat{\eta} + \mathbf{r}(\mathbf{u}^*)^t \mathbb{R}_{\boldsymbol{\theta}}^{-1} \left(\mathbf{h} - \hat{\eta}\mathbf{1}_{N_E}\right) \tag{2.49}$$

and Kriging variance [Jones *et al.*, 1998]:

$$\sigma^2_{\tilde{H}}(\mathbf{u}^*) = \hat{\sigma_{\mathcal{Z}}}^2 \left(1 - \mathbf{r}(\mathbf{u}^*)^t \mathbb{R}_{\boldsymbol{\theta}}^{-1} \mathbf{r}(\mathbf{u}^*) + \frac{\left(1 - \mathbf{1}_{N_E}^t \mathbb{R}_{\boldsymbol{\theta}}^{-1} \mathbf{r}(\mathbf{u}^*)\right)^2}{\mathbf{1}_{N_E}^t \mathbb{R}_{\boldsymbol{\theta}}^{-1} \mathbf{1}_{N_E}}\right) \tag{2.50}$$

2.4.2.3 Noteworthy features

Kriging presents two intrinsic features that motivate its application to structural reliability problems in this thesis:

- **Interpolation**: Figure 2.8(a) shows that the predictor interpolates the observations $\mathbf{h}$, *i.e.* $\forall i,\ \mathbf{u}^{(i)} \in \mathbb{D},\ \mu_{\tilde{H}}(\mathbf{u}^{(i)}) = H(\mathbf{u}^{(i)})$. The proof of this begins by noting that, for a point $\mathbf{u}^{(i)} \in \mathbb{D}$, the correlation vector $\mathbf{r}(\mathbf{u}^{(i)})$ is equivalent to the ith column of $\mathbb{R}_{\boldsymbol{\theta}}$. Hence, the correlation vector reads:

  $$\mathbf{r}\left(\mathbf{u}^{(i)}\right) = \mathbb{R}_{\boldsymbol{\theta}} \mathbf{e}_i \tag{2.51}$$

  where $\mathbf{e}_i$ is the unit vector which is one for its ith row and zero for the others. Eqn.(2.49) then becomes:

  $$\mu_{\tilde{H}}\left(\mathbf{u}^{(i)}\right) = \hat{\eta} + \mathbf{e}_i^t \left(\mathbf{h} - \hat{\eta}\mathbf{1}_{N_E}\right) = \mathbf{e}_i^t \mathbf{h} = H\left(\mathbf{u}^{(i)}\right) \tag{2.52}$$

  Furthermore, Kriging variance is zero as Eqn.(2.50) changes to:

  $$\sigma^2_{\tilde{H}}\left(\mathbf{u}^{(i)}\right) = \hat{\sigma_{\mathcal{Z}}}^2 \left(1 - \mathbf{r}(\mathbf{u}^{(i)})^t \mathbf{e}_i + \frac{\left(1 - \mathbf{1}_{N_E}^t \mathbf{e}_i\right)^2}{\mathbf{1}_{N_E}^t \mathbb{R}_{\boldsymbol{\theta}}^{-1} \mathbf{1}_{N_E}}\right) = 0 \tag{2.53}$$

- **Measure of the prediction uncertainty**: At a given point, Kriging not only provides a prediction (Kriging mean) of the function outcome, but also a measure of the prediction uncertainty (Kriging variance). As illustrated in Figure 2.8(b), the Kriging variance may be used to find a point (or several) whose observation(s) would lead to a substantial improvement in the metamodel's accuracy. An iterative enrichment of the DOE with wisely chosen points thus seems a relevant approach to respect the parsimony constraint, *i.e.* to establish an accurate metamodel with a limited number of function evaluations. Such an approach is commonly referred to as an active learning method, and is further discussed in the next section.

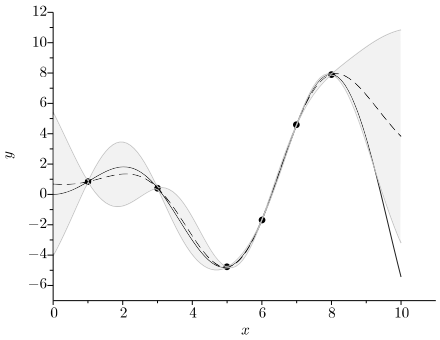

(a) Kriging metamodel interpolating the observations.

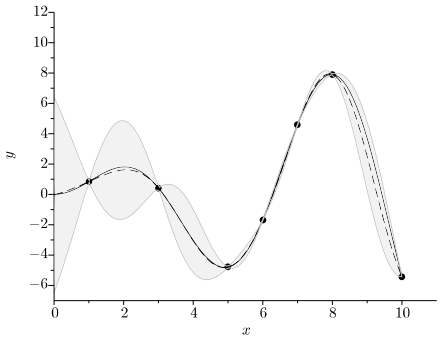

(b) Global prediction improved by evaluating $y = x\sin(x)$ at the point having the largest Kriging variance, *i.e.* $x = 10$.

Figure 2.8: Illustrations of Kriging. The solid line is the function $y = x\sin(x)$. The dashed line depicts the Kriging mean. The observations of the DOE are represented by the black dots. The light grey area corresponds to the 95% confidence interval, *i.e.* $\mu_{\tilde{H}}(x) \pm 1.96\,\sigma_{\tilde{H}}(x)$.

2.4.3 Active learning method

As far as the author is aware, Romero *et al.* [2004] are the first in applying Kriging to structural reliability problems. In this early paper, the DOE of the Kriging metamodel evolves following progressive lattice samplings, and consequently, does not consider the additional information brought by the Kriging variance. The same statement can be made regarding the method proposed by Kaymaz [2005]. Following these pioneering works, Kriging is applied in an active learning scheme, where the DOE is iteratively enriched with points selected through the evaluation of a learning function [Bichon *et al.*, 2008; Ranjan *et al.*, 2008; Picheny *et al.*, 2010; Bect *et al.*, 2011; Dubourg, 2011; Echard *et al.*, 2011a]. The general procedure of active learning can be summarized as follows:

1. Build the Kriging metamodel of H with an initial DOE.

2. Find the point leading to the optimum of the learning function.

3. Enrich the DOE by evaluating H at such a point.

4. Build the new Kriging metamodel and go back to Step 2.

In structural reliability analysis, only points in the vicinity of the limit state $H(\mathbf{u}) = 0$ represent relevant observations to refine the metamodel. Learning functions, discussed in the following section, are specifically developed to find such points.

2.4.3.1 Learning function

Several learning functions are available in the literature related to structural reliability. This section is restricted to the introduction of two functions that are easy to implement and fast to evaluate.

Expected feasibility function

The active learning scheme of the Efficient Global Reliability Analysis (EGRA) [Bichon *et al.*, 2008] relies on the Expected Feasibility Function (EFF). Inspired by the contour estimation work in Ranjan *et al.* [2008], EFF expresses the expectation that the actual outcome of the performance function in a point $\mathbf{u}$ is expected to satisfy the equality constraint $H(\mathbf{u}) = t$ [Bichon *et al.*, 2011] ($t = 0$ for the limit state). The function reads:

$$\mathrm{EFF}(\mathbf{u}) = \mathrm{E}\left[\epsilon(\mathbf{u}) - \min(|\tilde{H}(\mathbf{u}) - t|, \epsilon(\mathbf{u}))\right] \tag{2.54}$$

where ϵ is set to focus the search in $t \pm \epsilon$. In Bichon *et al.* [2008], ϵ is proportional to the Kriging standard deviation at each point: $\epsilon(\mathbf{u}) = 2\sigma_{\tilde{H}}(\mathbf{u})$. By integrating over $t \pm \epsilon$, the expectation becomes:

$$\begin{aligned}\mathrm{EFF}(\mathbf{u}) \;=\; & \mu_{\tilde{H}}(\mathbf{u})\left[2\Phi\left(\tfrac{t-\mu_{\tilde{H}}(\mathbf{u})}{\sigma_{\tilde{H}}(\mathbf{u})}\right) - \Phi\left(\tfrac{t-\epsilon(\mathbf{u})-\mu_{\tilde{H}}(\mathbf{u})}{\sigma_{\tilde{H}}(\mathbf{u})}\right) - \Phi\left(\tfrac{t+\epsilon(\mathbf{u})-\mu_{\tilde{H}}(\mathbf{u})}{\sigma_{\tilde{H}}(\mathbf{u})}\right)\right] \\ & -\sigma_{\tilde{H}}(\mathbf{u})\left[2\phi\left(\tfrac{t-\mu_{\tilde{H}}(\mathbf{u})}{\sigma_{\tilde{H}}(\mathbf{u})}\right) - \phi\left(\tfrac{t-\epsilon(\mathbf{u})-\mu_{\tilde{H}}(\mathbf{u})}{\sigma_{\tilde{H}}(\mathbf{u})}\right) - \phi\left(\tfrac{t+\epsilon(\mathbf{u})-\mu_{\tilde{H}}(\mathbf{u})}{\sigma_{\tilde{H}}(\mathbf{u})}\right)\right] \\ & +\epsilon(\mathbf{u})\left[\Phi\left(\tfrac{t+\epsilon(\mathbf{u})-\mu_{\tilde{H}}(\mathbf{u})}{\sigma_{\tilde{H}}(\mathbf{u})}\right) - \Phi\left(\tfrac{t-\epsilon(\mathbf{u})-\mu_{\tilde{H}}(\mathbf{u})}{\sigma_{\tilde{H}}(\mathbf{u})}\right)\right]\end{aligned} \tag{2.55}$$

High values of EFF are obtained for points having Kriging means close to the threshold t, as well as points having large Kriging variances. The performance function is thus evaluated at the location where EFF is maximized. The search of the optimum point is further discussed in Section 2.4.3.2.

Learning function U

Inspired by Kushner's criterion [1964] and the lower confidence bounding function [Cox and John, 1997] in optimization, the learning function U [Echard *et al.*, 2009] is proposed

to focus the search in the vicinity of the limit state. At an unobserved point $\mathbf{u}$, it reads:

$$U(\mathbf{u}) = \frac{|t - \mu_{\tilde{H}}(\mathbf{u})|}{\sigma_{\tilde{H}}(\mathbf{u})} \tag{2.56}$$

As depicted in Figure 2.9, U measures the distance in standard deviations between the Kriging mean and the threshold t (set to 0 for the limit state). Since Gaussianity is assumed by Eqn.(2.48), $1 - \Phi(U(\mathbf{u}))$ for $t = 0$ represents the probability that $H(\mathbf{u})$ has an opposite sign (negative/positive) from $\mu_{\tilde{H}}(\mathbf{u})$. A small value of $U(\mathbf{u})$ leads to a large probability, and consequently, the performance function should be evaluated at the point where U is minimized.

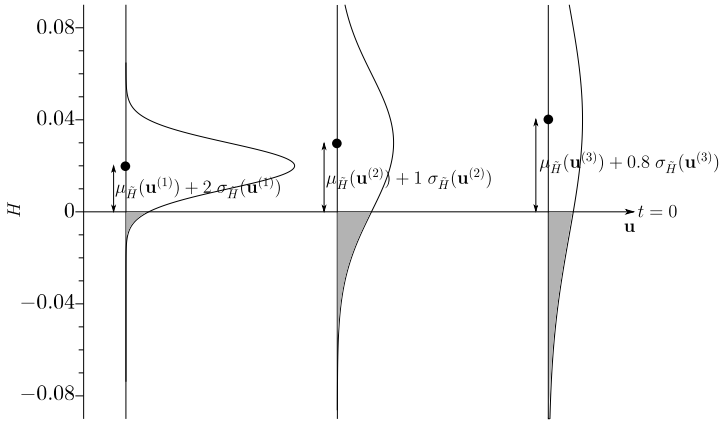

Figure 2.9: Illustration of the learning function U for three points $\mathbf{u}^{(1)}$, $\mathbf{u}^{(2)}$, $\mathbf{u}^{(3)}$ with positive Kriging means. The values of U are respectively 2, 1 and 0.8. The grey areas represent the probabilities $1 - \Phi(U(\mathbf{u}^{(j)}))$. The performance function H should be evaluated at the point $\mathbf{u}^{(3)}$.

Other alternatives

More sophisticated criteria such as the targeted Integrated Mean-Squared Error (tIMSE) [Picheny *et al.*, 2010] and the Stepwise Uncertainty Reduction (SUR) [Bect *et al.*, 2011] are available in the literature. Comparative studies of these learning functions have been undertaken by Bect *et al.* [2011] and Li *et al.* [2011]. SUR is seen to converge the fastest to a rough estimate of the failure probability, but its computational cost is larger than EFF and U. In addition, the number of evaluations performed with U is rather comparable to SUR's when a refined estimate of the failure probability is targeted [Li *et al.*, 2011]. Within this thesis, the learning function U thus seems acceptable for its simplicity and efficiency.

2.4.3.2 Search of the optimum

Learning functions are highly multimodal and consequently, finding the optimum is a complex task. EGRA resorts to the gradient-free DIRECT (DIviding RECTangles) global optimization algorithm [Jones *et al.*, 1993; Gablonsky, 2001]. It consists of an iterative division of the search domain into hyper-rectangles. The learning function EFF is calculated at the hyper-centres, and the potentially optimal hyper-rectangles, determined according to their size and EFF value, are sequentially divided. For further details on the algorithm, the interested reader is referred to the DIRECT Matlab toolbox [Finkel, 2003]. In this thesis, the optimization is solved numerically by computing the learning function at each point of a fixed population. Such a choice is seen as sufficient for the new reliability methods devised in this research work (see Section 2.5).

2.4.4 Kriging prediction of the failure probability

In practice, the failure probability of Eqn.(2.39) is assessed by applying a sampling-based reliability method to the refined metamodel of the performance function. For a given population, Kriging offers two estimates of the failure probability:

- an estimate based on the mean values. The predicted failure domain is $\tilde{\mathcal{F}} = \{\mathbf{u} \in \mathcal{U}^n : \mu_{\tilde{H}}(\mathbf{u}) \leq 0\}$, and the Kriging mean indicator function $I_{\tilde{\mathcal{F}}}(\mathbf{u}) = \{1 \text{ if } \mu_{\tilde{H}}(\mathbf{u}) \leq 0 \text{ and } 0 \text{ otherwise}\}$ is introduced to assess $\tilde{P}_f$.

- an estimate based on the full probabilistic information held in the Kriging predictions [Picheny *et al.*, 2010; Dubourg, 2011]. The predicted failure domain becomes $\tilde{\mathcal{F}} = \{\mathbf{u} \in \mathcal{U}^n : \tilde{H}(\mathbf{u}) \leq 0\}$, and the probabilistic indicator function $I_{\tilde{\mathcal{F}}}(\mathbf{u}) = \{\Phi(U(\mathbf{u})) \text{ if } \mu_{\tilde{H}}(\mathbf{u}) \leq 0 \text{ and } 1-\Phi(U(\mathbf{u})) \text{ otherwise}\}$ is introduced to assess $\tilde{P}_f$. Note that U is not defined at the points of the DOE, but the sign of the performance function value is known in such points. Finally, $\Phi(U(\mathbf{u}))$ is 1 (respectively 0) when $U(\mathbf{u})$ tends to $+\infty$ (respectively 0), thus both estimates converge to the same $\tilde{P}_f$.

In this thesis, the failure probability is estimated with the Kriging mean values. Hence in the rest of the document, the predicted failure domain is defined as $\tilde{\mathcal{F}} = \{\mathbf{u} \in \mathcal{U}^n : \mu_{\tilde{H}}(\mathbf{u}) \leq 0\}$, and $I_{\tilde{\mathcal{F}}}(\mathbf{u})$ refers to the Kriging mean indicator function. Note that the second estimate is also calculated to observe the convergence in Section 2.5.3.

2.5 Active learning and Kriging-based Monte Carlo Simulation

2.5.1 Motivation

Kriging-based methods such as EGRA [Bichon *et al.*, 2008] are mostly two-stage procedures, where the construction of the Kriging metamodel through an active learning scheme (stage 1) is completely independent from the subsequent sampling-based reliability analysis (stage 2). Since stage 1 is performed regardless of the probability density, the performance function may be observed in some areas that will not be covered by the random sampling of stage 2. These observations consequently represent unnecessary evaluations that can be avoided by merging both stages. In this thesis, a single-stage procedure is thus devised to avoid these evaluations. The method is referred to as an Active learning and Kriging-based Monte Carlo Simulation (AK-MCS) [Echard *et al.*, 2009, 2010a,b, 2011a,b]. Following the classification concept [Hurtado, 2004], AK-MCS uses a Kriging metamodel to classify a fixed Monte Carlo population into the safe and failure subsets, *i.e.* into the points having positive performance function values and the points having negative performance function values. The function U is evaluated at each point of the population, and the Kriging metamodel is adaptively refined by evaluating the performance function at the point leading to the smallest value of $U(\mathbf{u})$. AK-MCS can be seen as a 'guided' Monte Carlo Simulation, where the sign of each point in the population is deduced from a Kriging metamodel built with only a few wisely chosen observations of the performance function.

2.5.2 Procedure

Let N_E denote the number of performance function evaluations. Figure 2.10 depicts the procedure which is as follows:

1. **Generate a population $\mathbb{P}_{\text{MCS}}$ according to ϕ_n[†].** It consists of the points $\{\mathbf{u}^{(j)} = \{u_1^{(j)}, \ldots, u_n^{(j)}\}^t,\ j = 1, \ldots, N_{\text{MCS}}\}$ to classify into the safe and failure subsets. These points also represent candidates for future performance function evaluations.

2. **Define the initial DOE.** The performance function is evaluated at various points in $\mathbb{P}_{\text{MCS}}$. In the original paper, around ten ($N_E \approx 10$) are uniformly drawn from the population of candidates. However, such a selection may not lead to a sufficient spread of the DOE due to the high density of candidates near the origin of space. To convey a larger amount of information about the behaviour of the performance function, space-filling designs such as Latin Hyper-cube Sampling [McKay *et al.*,

[†]For consistency of the document, the method is explained in the standard space but its application in $\mathcal{X}^n$ is also possible.

1979] seem more suitable. Another alternative may, for instance, be a uniform sampling of various points (*e.g.* 3) in each of the following subsets: $\{\mathbf{u} \in \mathbb{P}_{\text{MCS}} : \|\mathbf{u}\| < 1\}$, $\{\mathbf{u} \in \mathbb{P}_{\text{MCS}} : 2 \leq \|\mathbf{u}\| < 3\}$, $\{\mathbf{u} \in \mathbb{P}_{\text{MCS}} : 3 \leq \|\mathbf{u}\| < 4\}$... Note that the number of observations is purposely small at first, since the DOE is iteratively enriched in the subsequent active learning loop.

3. **Perform the Kriging classification loop.**

   (a) **Build the Kriging metamodel.** An ordinary Kriging metamodel with anisotropic Gaussian correlation is built from the N_E observations. DACE Matlab/Scilab toolbox [Lophaven *et al.*, 2002a] is used in this research work.

   (b) **Predict outcomes and assess $\tilde{P}_f$.** The Kriging predictions of the points in $\mathbb{P}_{\text{MCS}}$ are computed: $\{\mu_{\tilde{H}}(\mathbf{u}^{(j)}),\ \sigma_{\tilde{H}}(\mathbf{u}^{(j)}),\ j = 1, \ldots, N_{\text{MCS}}\}$. The Kriging mean indicator function (see Section 2.4.4) is introduced in Eqn.(2.14) to estimate the failure probability $\tilde{P}_f$. The Kriging probabilistic indicator function may also be used to provide a second estimate.

   (c) **Evaluate the learning function U and find $\mathbf{u}^\circ = \arg \min_{\mathbf{u} \in \mathbb{P}_{\text{MCS}}} U(\mathbf{u})$.** The function U is evaluated at the $[N_{\text{MCS}} - N_E]$ unobserved points of $\mathbb{P}_{\text{MCS}}$. The point $\mathbf{u}^\circ \in \mathbb{P}_{\text{MCS}}$ leading to the smallest value of $U(\mathbf{u})$ is easily found.

   (d) **Test the stopping condition on learning.** The condition reads: $U(\mathbf{u}^\circ) \geq 2$. This arbitrary value refers to a 97.7% confidence level on the sign of the performance function outcome. The author recommends deactivating the condition in the early iterations, due to the fact that the procedure might wrongly stop with an insufficient DOE. Experience has shown that the stopping condition can be activated, once the DOE includes both safe and failure points.

   (e) **Enrich the DOE.** If the stopping condition is not satisfied, the DOE is enriched by evaluating $H(\mathbf{u}^\circ)$. Hence $N_E = N_E + 1$, and the procedure goes back to Step 3a to build the new Kriging metamodel.

4. **End.** If the stopping condition is met, each point of the population is considered to be classified with a sufficient confidence level. $\tilde{P}_f$ corresponds to the probability estimated in Step 3b during the last loop. The coefficient of variation δ is calculated using Eqn.(2.15). Note that if the coefficient of variation is too large, a new population is generated, and the Kriging classification loop (Step 3) continues until the stopping condition is satisfied again.

2.5.3 Validation

For the purpose of validating AK-MCS, examples which cover a wide variety of limit states (high non-linearity, moderate number of random variables, non-convex and/or disconnec-

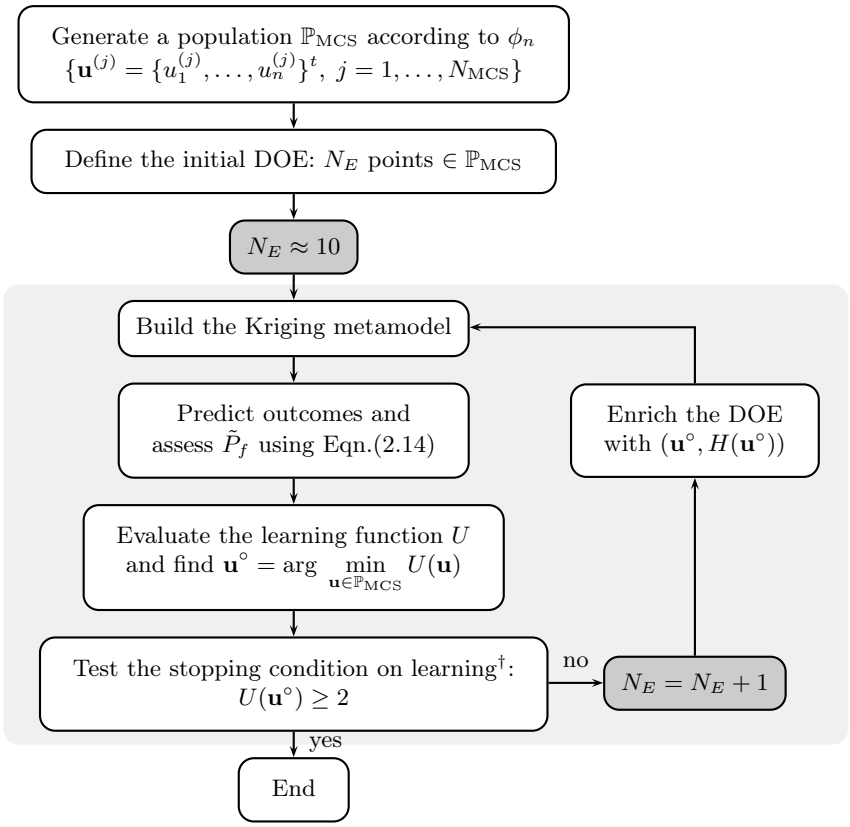

†The stopping condition is activated, once the DOE includes both safe and failure points.

Figure 2.10: AK-MCS procedure. The light grey rectangle represents the Kriging classification loop (Step 3).

ted domains of failure) are studied in this section. The reader may refer to Echard *et al.* [2009, 2010a,b, 2011a,b] for further applications.

2.5.3.1 Two-dimensional series system with four branches

The first example is a series system with four branches, also studied by Waarts [2000]; Schueremans and Van Gemert [2005]. The performance function reads as follows:

$$H(U_1, U_2) = \min \left\{ \begin{array}{l} 3 + \frac{(U_1 - U_2)^2}{10} - \frac{(U_1 + U_2)}{\sqrt{2}}; \\ 3 + \frac{(U_1 - U_2)^2}{10} + \frac{(U_1 + U_2)}{\sqrt{2}}; \\ (U_1 - U_2) + \frac{6}{\sqrt{2}}; \\ (U_2 - U_1) + \frac{6}{\sqrt{2}} \end{array} \right\} \tag{2.57}$$

where U_1 and U_2 are standard Gaussian distributed random variables. The problem is represented in Figure 2.11. In this example, the population to classify into the safe and failure subsets is composed of $N_{\text{MCS}} = 10^6$ points. The initial DOE of AK-MCS is defined

as ten points that are uniformly drawn from the population. The robustness of AK-MCS is tested by applying the method to 100 different populations.

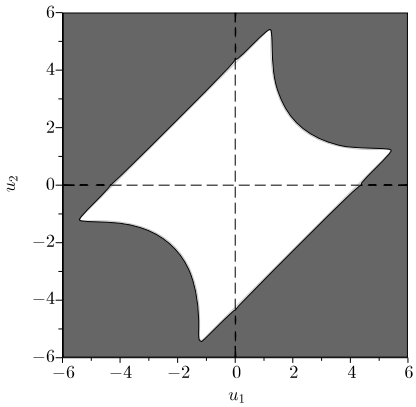

Figure 2.11: Safe (white) and failure (dark) domains on the example of the series system with four branches.

The number of performance function evaluations (N_E) for the 100 AK-MCS runs is represented in Figure 2.12. It ranges between 86 and 127, which is significantly less than the number of points to classify (N_{MCS}). In Table 2.1, the number of points misclassified by AK-MCS in each of the 100 populations is reported. The classification is found to be exact in 61 cases, meaning that the AK-MCS estimate of the failure probability is strictly similar to the Monte Carlo estimate. Among the remaining 39 cases, the largest error, *i.e.* 3, is negligible in comparison with N_{MCS}. In this example, AK-MCS with a median DOE of 102 observations is shown to be equivalent to a Monte Carlo Simulation of 10^6 points (see Table 2.2 for the median reliability results).

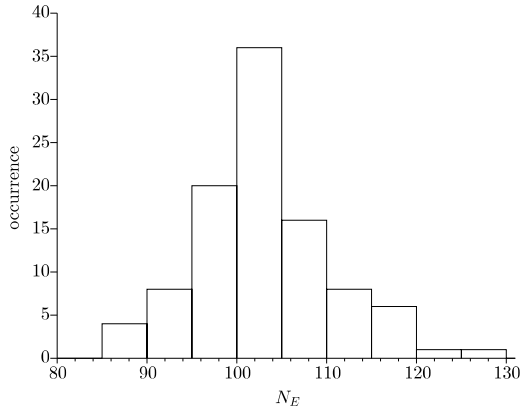

Figure 2.12: Number of performance function evaluations (N_E) for 100 runs of AK-MCS on the example of the series system with four branches.

Misclassified points	Occurrence
0	61
1	27
2	7
3	5

Table 2.1: Number of misclassified points for 100 runs of AK-MCS on the example of the series system with four branches.

Method	N_E	P_f ($\times 100$)	$\delta\%$ ($\times 100$)
MCS	10^6	4.4591×10^{-3}	1.525
AK-MCS	102	4.4587×10^{-3}	1.527

Table 2.2: Median reliability results of Monte Carlo Simulation and AK-MCS over 100 simulated populations on the example of the series system with four branches.

Figure 2.13(a) depicts an example of a population classified by AK-MCS. Figure 2.13(b) gives the corresponding DOE. In accordance with the definition of the learning function, the observations are mainly located in the close vicinity of the actual limit state. It can also be seen that the accuracy of the predicted limit state, *i.e.* $\mu_{\tilde{H}}(\mathbf{u}) = 0$, is high among the points of the population but decreases in areas such as the intersections of the four branches that are not covered by the random sampling. These intersections are low probability zones whose impact on the failure probability is negligible. Two-stage procedures such as EGRA, which construct the Kriging metamodel regardless of the probability density, would unnecessarily enrich the DOE with numerous points in the vicinity of these discontinuities. Nevertheless, it is important to note that bounds can be adjusted in EGRA in order to limit the domain of interest. For instance, $[-5; 5] \times [-5; 5]$ would be sufficient to avoid the consideration of these intersections. Note also that EGRA has recently been improved to deal with system reliability problems such as this example [Bichon *et al.*, 2011].

Figure 2.14(a) depicts the evolution of the two estimates of the failure probability, *i.e.* the estimate based on the Kriging mean values and the estimate based on the full probabilistic information held in the Kriging predictions (see Section 2.4.4). Both tend towards a similar value after 70 evaluations. However, at this iteration, 72 points are still incorrectly classified by AK-MCS. Figure 2.14(b) depicts the evolution of the learning function's minimum value. For this AK-MCS run, the stopping condition is met after $N_E = 117$ evaluations, and no misclassified points remain. As a conclusion, an extremely accurate classification is guaranteed with the stopping condition $U(\mathbf{u}^\circ) \geq 2$, but the user

may stop the procedure when the convergence of the two estimates is visually reached, as long as a less refined result is acceptable.

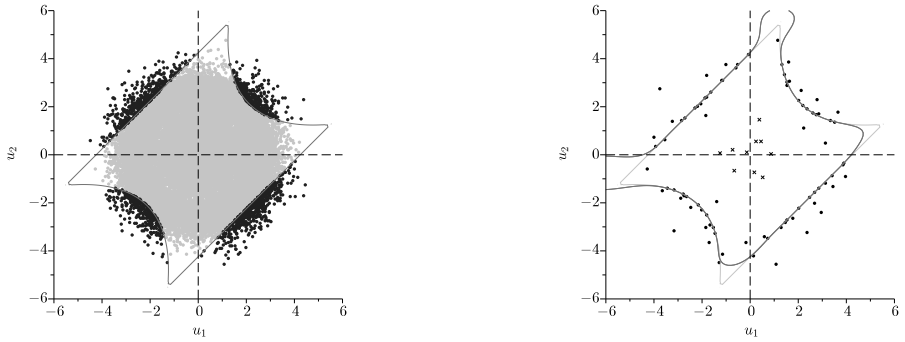

(a) Classification by AK-MCS. The light grey dots depict the points having a positive Kriging mean (safe), the black dots present a negative Kriging mean (failure).

(b) Final DOE of AK-MCS. The crosses are the initial DOE, and the dots represent the points iteratively added to the DOE. The dark line depicts the predicted limit state $\mu_{\tilde{H}}(\mathbf{u}) = 0$.

Figure 2.13: Illustration of AK-MCS on the example of the series system with four branches.

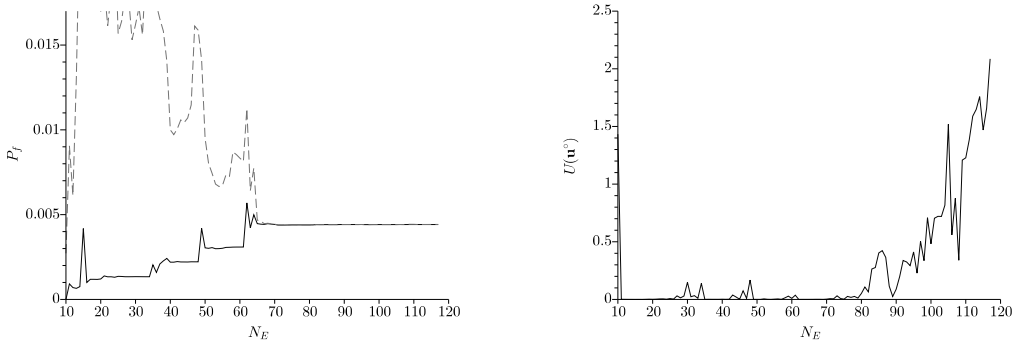

(a) Evolution of the failure probability estimates. The solid line is the estimate based on the Kriging mean values. The dashed line depicts the estimate based on the full probabilistic information held in the Kriging predictions.

(b) Evolution of the learning function's minimum value, *i.e.* $U(\mathbf{u}^\circ)$.

Figure 2.14: Evolutions of the failure probability estimates and learning function's minimum value on the example of the series system with four branches.

2.5.3.2 Modified Rastrigin function

The second example is based on the so-called Rastrigin function [Törn and Zilinskas, 1989]. This function is slightly modified to give a non-linear limit state involving non-convex and

disconnected domains of failure (see Figure 2.15). The performance function reads:

$$H(U_1, U_2) = 10 - \sum_{i=1}^{2} \left(U_i^2 - 5\cos\left(2\pi\, U_i\right) \right) \tag{2.58}$$

where U_1 and U_2 are standard Gaussian variables. The population to classify into the safe and failure subsets is composed of $N_{\text{MCS}} = 2.5 \times 10^4$ points. The initial DOE of AK-MCS is defined as ten points that are uniformly drawn from the population.

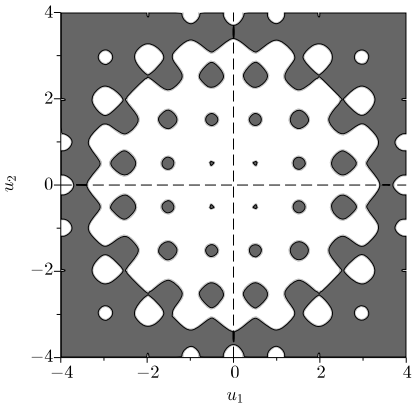

Figure 2.15: Safe (white) and failure (dark) domains on the example of the modified Rastrigin function example.

The results are given in Table 2.3. 391 evaluations of the performance function are sufficient to correctly classify the population into the safe and failure subsets (see Figure 2.16(a)). Figure 2.16(b) shows that the points of the DOE are located in the vicinity of the different frontiers. In Figure 2.17(a), the failure probability estimate based on the Kriging mean values is progressively improved. Such a behaviour can be related to the gradual discovery of new failure zones. The two failure probability estimates are also seen to tend towards a similar value after 360 evaluations of the performance function. At this iteration, 40 points are still misclassified by AK-MCS. The evolution of the learning function's minimum value is given in Figure 2.17(b). As mentioned previously, the user may stop the procedure when the convergence of the two estimates is visually reached, as long as a less refined result is acceptable.

Method	N_E	P_f	$\delta\%$
MCS	2.5×10^4	7.43×10^{-2}	2.23
AK-MCS	391	7.43×10^{-2}	2.23

Table 2.3: Reliability results on the example of the modified Rastrigin function.

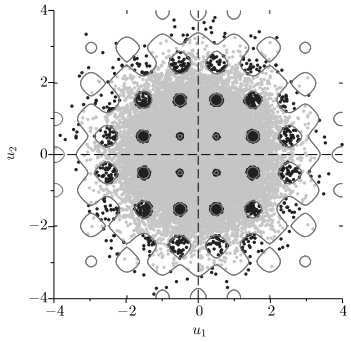

(a) Classification by AK-MCS. The light grey dots depict the points having a positive Kriging mean (safe), the black dots present a negative Kriging mean (failure).

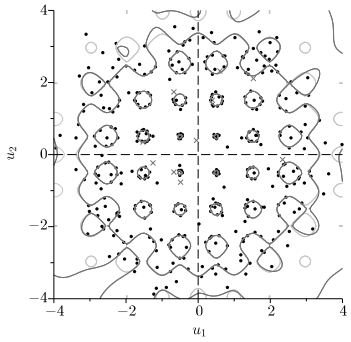

(b) Final DOE of AK-MCS. The crosses are the initial DOE and the dots represent the points iteratively added to the DOE. The dark line depicts the predicted limit state $\mu_{\tilde{H}}(\mathbf{u}) = 0$.

Figure 2.16: Illustration of AK-MCS on the example of the modified Rastrigin function.

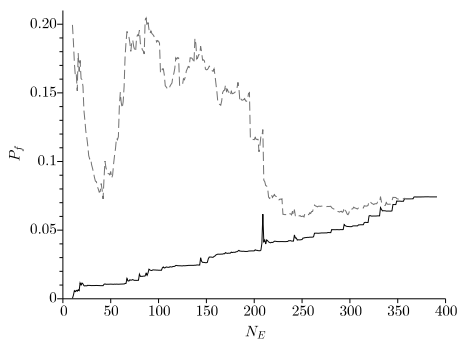

(a) Evolution of the failure probability estimates. The solid line is the estimate based on the Kriging mean values. The dashed line depicts the estimate based on the full probabilistic information held in the Kriging predictions.

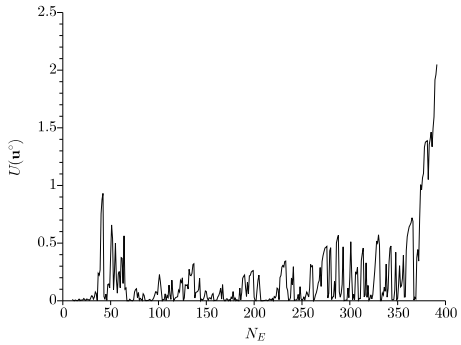

(b) Evolution of the learning function's minimum value, *i.e.* $U(\mathbf{u}^\circ)$.

Figure 2.17: Evolutions of the failure probability estimates and learning function's minimum value on the example of the modified Rastrigin function.

2.5.3.3 Maximal deflection of a truss structure

The final example is a truss structure, proposed by Blatman and Sudret [2010], that is illustrated in Figure 2.18. This application involves a moderate number of independent random variables that are the Young moduli E_1 and E_2, the cross-section areas A_1 and A_2, and the applied loads P_p for $p = 1, \ldots, 6$. The characteristics of the random variables are listed in Table 2.4. The response of the truss model is the deflection V_1 at midspan.

Given a threshold $V_{\max}$, the performance function reads:

$$G(E_1, E_2, A_1, A_2, P_p) = V_{\max} - V_1 \tag{2.59}$$

Three thresholds $V_{\max} = \{10;\ 11;\ 12\}$ (cm) are considered so as to study the influence of the probability level. One population is generated for each threshold. Their respective sizes $N_{\text{MCS}} = \{3.5 \times 10^4;\ 2 \times 10^5;\ 10^6\}$ are determined to give an approximately 2.5% coefficient of variation on the Monte Carlo estimator. The initial DOE of AK-MCS is defined as ten points uniformly drawn from the population.

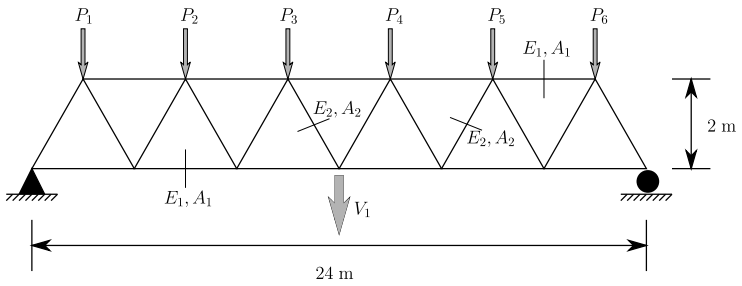

Figure 2.18: Truss structure with 23 members.

Variable	Distribution	Mean	Std. dev.
E_1, E_2(Pa)	Lognormal	2.1×10^{11}	2.1×10^{10}
A_1(m^2)	Lognormal	2.0×10^{-3}	2.0×10^{-4}
A_2(m^2)	Lognormal	1.0×10^{-3}	1.0×10^{-4}
$P_1 - P_6$(N)	Gumbel	5.0×10^4	7.5×10^3

Table 2.4: Random variables for the example of the truss structure.

The reliability results are reported in Table 2.5. For the three thresholds, no points are misclassified by AK-MCS. Its failure probability estimates are then strictly similar to Monte Carlo estimates. For a constant δ, the probability level is seen to have a limited effect on the number of performance function evaluations as N_E only varies between 110 and 128.

Figure 2.19(a) depicts, for the threshold $V_{\max} = 10$, the failure probability estimates that are either based on the Kriging mean values or on the full probabilistic information held in the Kriging predictions. In the previous examples, a large difference between them is observed in the early iterations. For the truss structure, the estimates are extremely similar, even before convergence. Stopping the procedure before observing this convergence may lead to an inaccurate reliability result. To avoid this, the original stopping condition depicted in Figure 2.19(b) should be preferred.

Method	$V_{\max}$	N_E	P_f
MCS	10	3.5×10^4	4.33×10^{-2}
	11	2×10^5	8.38×10^{-3}
	12	10^6	1.53×10^{-3}
AK-MCS	10	110	4.33×10^{-2}
	11	128	8.38×10^{-3}
	12	124	1.53×10^{-3}

Table 2.5: Reliability results for $\delta \approx 2.5\%$ on the example of the truss structure.

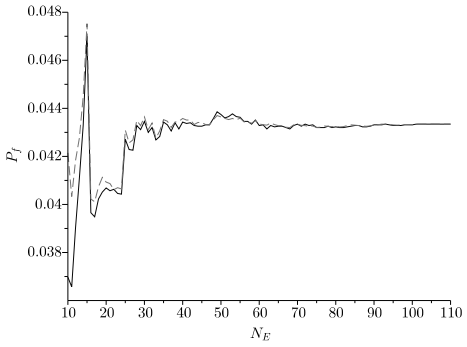

(a) Evolution of the failure probability estimates. The solid line is the estimate based on the Kriging mean values. The dashed line depicts the estimate based on the full probabilistic information held in the Kriging predictions.

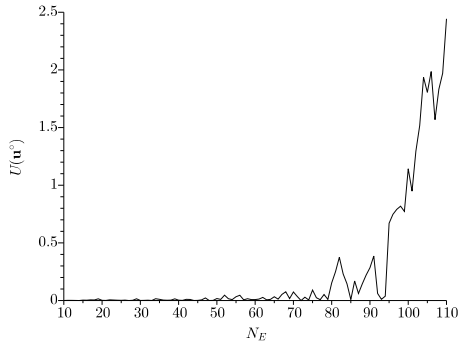

(b) Evolution of the learning function's minimum value, *i.e.* $U(\mathbf{u}^\circ)$.

Figure 2.19: Evolutions of the failure probability estimates and learning function's minimum value on the example of the truss structure for the threshold $V_{\max} = 10$.

2.5.4 Computational cost of the prediction step

In the previous part, AK-MCS is proven to be parsimonious with respect to the number of performance function evaluations. The computational cost of the prediction step in the AK-MCS procedure (Step 3b in Section 2.5.2) is now investigated so as to provide recommendations on AK-MCS' range of applications.

Consider the following n-dimensional problem proposed by Rackwitz [2001]:

$$G(X_1, \ldots, X_n) = \left(n + 3\sigma\sqrt{n}\right) - \sum_{i=1}^{n} X_i \tag{2.60}$$

where X_i for $i = 1, \ldots, n$ are lognormal distributed random variables with mean value $\mu = 1$, and standard deviation $\sigma = 0.2$. The computational cost of the prediction step

depends on the dimension of space (n), the size of the DOE at the current AK-MCS iteration (N_E), and the size of the population to predict (N_{MCS}). A set of 18 situations are simulated by combining the following values for the tuning parameters:

- dimension of space: $n = \{2;\ 10\}$,
- size of the DOE at the current AK-MCS iteration: $N_E = \{10;\ 100;\ 400\}$,
- size of the population to predict: $N_{\text{MCS}} = \{10^4;\ 10^5;\ 10^6\}$.

The 18 simulations are conducted with a Intel Q9550 processor at 2.83 Ghz. Table 2.6 and Table 2.7 report the results in terms of the total CPU time, *i.e.* the sum of the CPU time consumed by all of the CPUs utilized by the simulation. On the one hand, the CPU time is obviously affected in a major way by the number of points in the population N_{MCS}. On the other hand, N_E and n play relatively minor roles, at least in the studied ranges of variation. According to these results, AK-MCS should be performed with a maximum of 10^5 points to ensure a suitable computational cost. Failure probabilities higher than 10^{-3} can then be assessed with a reasonable coefficient of variation. Finally, note that the parallel computing of the prediction step is also an easily-implementable solution in order to reduce the time seen by the user.

N_{MCS} \ N_E	10	100	400
10^4	< 1	1	4
10^5	2	8	38
10^6	13	82	370

Table 2.6: CPU time in seconds of the Kriging prediction for a dimension of space $n = 2$ (*e.g.* for $N_{\text{MCS}} = 10^5$ and $N_E = 100$, the CPU time is 8 seconds). The simulations are conducted with a Intel Q9550 processor at 2.83 Ghz.

N_{MCS} \ N_E	10	100	400
10^4	< 1	3	13
10^5	3	25	97
10^6	33	240	955

Table 2.7: CPU time in seconds of the Kriging prediction for a dimension of space $n = 10$ (*e.g.* for $N_{\text{MCS}} = 10^5$ and $N_E = 100$, the CPU time is 25 seconds). The simulations are conducted with a Intel Q9550 processor at 2.83 Ghz.

2.5.5 Conclusion

In this section, an Active learning and Kriging-based Monte Carlo Simulation (AK-MCS) has been introduced. This 'guided' Monte Carlo Simulation is an iterative procedure where a Kriging metamodel is used to classify a fixed population into the safe and failure subsets. A learning function is devised to adaptively refine the metamodel. The validation of the method on a set of examples shows that it provides an accurate classification of the population while remaining parsimonious with respect to the number of performance function evaluations (< 400 for the studied cases). In addition, its concept is similar to crude Monte Carlo Simulations, making it an easily intelligible approach. Its implementation based on a Kriging toolbox such as DACE is also very accessible. Finally, it is important to mention that AK-MCS has been successfully applied for the mechanical and the thermo-chemical reliability assessments of an intensified heat exchanger reactor [Boniface, 2010]. In Boniface's PhD thesis, AK-MCS demonstrates the limits of FORM and Quadratic Responses Surfaces.

2.6 Active learning and Kriging-based alternatives for small probability cases

In spite of its parsimony regarding the number of performance function evaluations, AK-MCS cannot be applied to applications involving small failure probabilities (at least not in a short time). Three extensions of the original algorithm are thus proposed to handle this case. With AK-MCS, they form the Active learning and Kriging-based Reliability Methods, or AK-RM family [Gayton and Echard, 2012].

2.6.1 Active learning and Kriging based MCS under monotony

The first extension is proposed in the case of monotonic performance functions. The Monte Carlo Simulation under monotony, exposed in Section 2.3.2, may be improved considerably thanks to the Kriging classification loop of AK-MCS. The iterative selection by the learning function U of new points in the vicinity of the limit state allows a drastic reduction of the margin between the ensured safe and failure sub-domains. As a Kriging prediction is necessary only for the few points lying in this margin, the computational cost of the prediction step is substantially reduced. This extension is called AK-MCSm (m standing for monotony).

2.6.1.1 Procedure

Let H be a monotonic performance function in the standard space. The ensured safe and failure sub-domains are respectively denoted by E^+ and E^-. Figure 2.20 depicts the procedure which is as follows:

1. **Generate a population $\mathbb{P}_{\text{MCS}}$ according to ϕ_n.** The points are denoted by $\{\mathbf{u}^{(j)} = \{u_1^{(j)}, \ldots, u_n^{(j)}\}^t,\ j = 1, \ldots, N_{\text{MCS}}\}$.

2. **Perform crude MCSm until $N_E \approx 10$.** MCS under monotony is run as explained in Section 2.3.2. The number of points in $\mathbb{P}_{\text{MCS}}$ and lying in the margin between E^+ and E^- is N_R. N^+ and N^- refer to the number of points in the ensured safe and failure sub-domains respectively.

3. **Perform the Kriging classification loop.**

   (a) **Build the Kriging metamodel.** The metamodel is built from the N_E observations. Note that the initial DOE consists of the ≈ 10 points evaluated by crude MCSm at Step 2.

   (b) **Predict outcomes and assess $\tilde{P}_f$.** The Kriging predictions of the N_R points lying in the margin are computed: $\{\mu_{\tilde{H}}(\mathbf{u}^{(j)}), \sigma_{\tilde{H}}(\mathbf{u}^{(j)}),\ j = 1, \ldots, N_R\}$. The estimate $\tilde{P}_f$ of the failure probability reads:

   $$\tilde{P}_f = \frac{N^- + \sum_{j=1}^{N_R} I_{\tilde{\mathcal{F}}}\left(\mathbf{u}^{(j)}\right)}{N_{\text{MCS}}} \tag{2.61}$$

   where $I_{\tilde{\mathcal{F}}}(\mathbf{u})$ is the Kriging mean indicator function.

   (c) **Evaluate the learning function U and find $\mathbf{u}^\circ$.** The function U is evaluated at the remaining N_R points. The point $\mathbf{u}^\circ$ leading to the smallest value of $U(\mathbf{u})$ is easily found.

   (d) **Test the stopping condition on learning.** The condition reads: $U(\mathbf{u}^\circ) \geq 2$. It is activated once the DOE includes both safe and failure points.

   (e) **Enrich the DOE.** If the stopping condition is not satisfied, the DOE is enriched by evaluating $H(\mathbf{u}^\circ)$, and $N_E = N_E + 1$.

   (f) **Update N_R, N^+ and N^-.** Either E^+ or E^- is enlarged due to the new observation $H(\mathbf{u}^\circ)$. The values of N_R, N^+ and N^- are updated. The procedure goes back to Step 3a to build the new Kriging metamodel.

4. **End.** If the stopping condition is met, each point of the population is considered to be classified with a sufficient confidence level. $\tilde{P}_f$ corresponds to the probability estimated in Step 3b during the last loop. The coefficient of variation δ is calculated using Eqn.(2.15). Note that if the coefficient of variation is too large, a new population of points lying in the margin between E^+ and E^- is generated by means of an accept/reject Monte Carlo sampling. The Kriging classification loop (Step 3) then continues until the stopping condition is satisfied again.

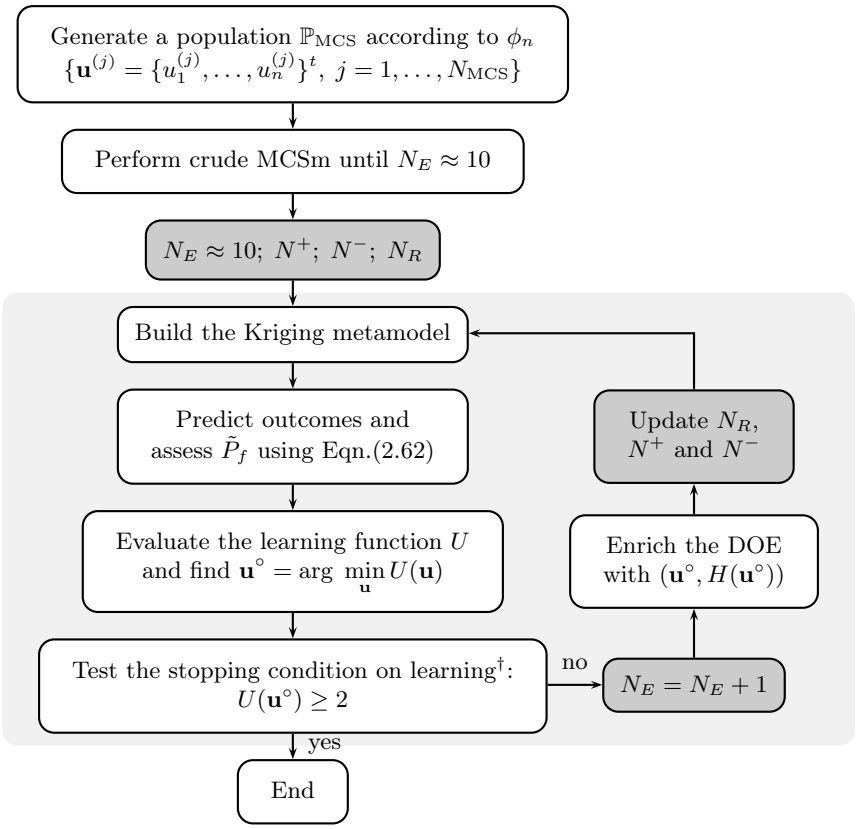

†The stopping condition is activated, once the DOE includes both safe and failure points.

Figure 2.20: AK-MCSm procedure. The light grey rectangle represents the Kriging classification loop (Step 3).

2.6.1.2 Illustration

AK-MCSm is illustrated on an elementary $R - S$ case:

$$G(R, S) = R - S \tag{2.62}$$

where R and S are independent random variables. R is Gaussian with mean of 11 and unit variance. S is uniform in the interval $[6; 7.2]$. The problem, depicted in Figure 2.21, is considered in the standard space with the monotonic performance function $H(U_R, U_S)$. An initial population of 10^6 points is generated according to ϕ_2. Crude MCSm is performed until $N_E = 10$, and the Kriging classification loop is run until the stopping condition is satisfied. Subsequently, 10^6 new points are simulated using ϕ_2 and among them, only those lying in the margin between E^+ and E^- are kept, so as to be also classified with the Kriging loop. This procedure is repeated until the coefficient of variation of the failure probability estimator is below $\leq 2.5\%$. To check its robustness, AK-MCSm is run for 100 different initial populations.

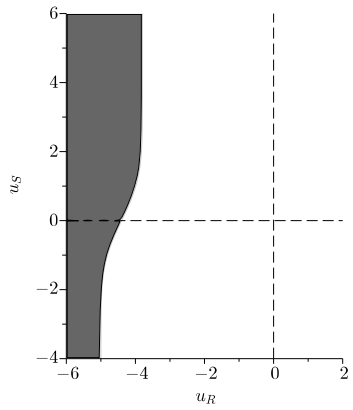

Figure 2.21: Safe (white) and failure (dark) domains of the elementary $R - S$ case.

The median reliability results are reported in Table 2.8. For this application, AK-MCSm with a median DOE of 24 observations is equivalent to a Monte Carlo Simulation of 1.14×10^8 points. Additionally, its computational cost is acceptable, since a median CPU time of 106 seconds is measured. Note that AK-MCS is inapplicable, due to the significant size of the population. Figure 2.22 shows the number of points misclassified by AK-MCSm in each of the 100 populations. 84 cases present less than 4 misclassified points, and the maximum value, *i.e.* 18, is negligible in comparison with the 1.14×10^8 points. Figure 2.23 illustrates the final DOE for a given run of AK-MCSm. The Kriging classification loop is seen to add points mainly in the vicinity of the limit state.

Method	N_E ($\times 100$)	P_f ($\times 100$)	CPU time in s ($\times 100$)
MCS	1.14×10^8	1.41×10^{-5}	-
AK-MCSm	24	1.41×10^{-5}	106

Table 2.8: Median reliability results of Monte Carlo Simulation and AK-MCSm over 100 simulated populations on the elementary $R - S$ case. The targeted coefficient of variation is $\delta \leq 2.5\%$. The median CPU time is given over 100 runs performed with a Intel Q9550 processor at 2.83 Ghz.

2.6.1.3 Conclusion

AK-MCSm is a simple but efficient extension of AK-MCS for the case of monotonic performance functions. It reduces the computational cost of the prediction step considerably, and small failure probability cases can thus be handled in a short space of time.

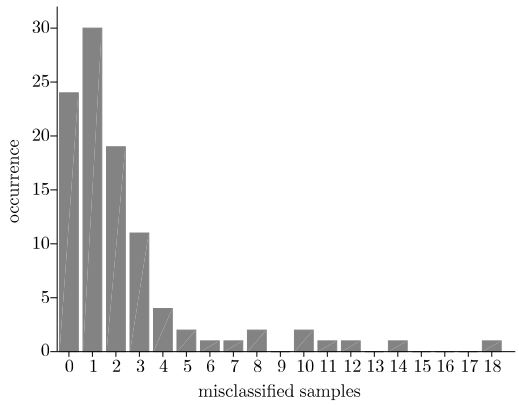

Figure 2.22: Number of misclassified points for 100 runs of AK-MCSm on the elementary $R - S$ case.

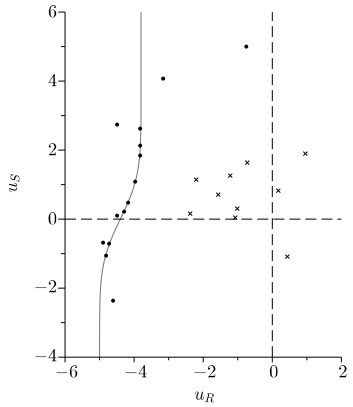

Figure 2.23: Final DOE of AK-MCSm on the elementary $R - S$ case. The crosses depict the 10 evaluations made with crude Monte Carlo Simulation under monotony at Step 2. The dots represent the 14 points added with the Kriging classification loop (Step 3). The dark line depicts the predicted limit state.

2.6.2 Active learning and Kriging-based Importance Sampling

The application of the Kriging classification loop to a fixed population centred on the MPFP is also an alternative to assess small failure probabilities. This approach represents an improvement on the crude Importance Sampling technique with a Kriging metamodel. It is referred to as AK-IS [Echard *et al.*, 2011c, 2012]. By analogy with Importance Sampling, AK-IS relies on the assumptions that the MPFP is well isolated and that no secondary minima exist in other areas of space.

2.6.2.1 Procedure

Let H be the performance function in the standard space. Figure 2.24 depicts the AK-IS procedure which is as follows:

1. **'Roughly' search the MPFP.** The HLRF algorithm (or other) is performed in order to find the MPFP $P^\star$. The performance function H is evaluated at $N_E = N_{\text{FORM}}$ points. Note that a precise $P^\star$ is not required. Performing a few iterations of HLRF is sufficient to move sufficiently the centre of the population.

2. **Generate a population $\mathbb{P}_{\text{IS}}$ according to φ_n.** It is recalled that the sampling PDF φ_n is the n-dimensional Gaussian distribution centred on the approximated $P^\star$ with uncorrelated components and unit variances. The points in the population $\mathbb{P}_{\text{IS}}$ are denoted by $\{\bar{\mathbf{u}}^{(j)} = \{\bar{u}_1^{(j)}, \dots, \bar{u}_n^{(j)}\}^t,\ j = 1, \dots, N_{\text{IS}}\}$.

3. **Perform the Kriging classification loop.**

   (a) **Build the Kriging metamodel.** The metamodel is built from the N_E observations. Note that the initial DOE consists of the N_{FORM} points evaluated at Step 1. It may also be uniformly drawn from the population $\mathbb{P}_{\text{IS}}$ as in AK-MCS.

   (b) **Predict outcomes and assess $\tilde{P}_f$.** The Kriging predictions of the N_{IS} points are computed: $\{\mu_{\tilde{H}}(\bar{\mathbf{u}}^{(j)}), \sigma_{\tilde{H}}(\bar{\mathbf{u}}^{(j)}),\ j = 1, \dots, N_{\text{IS}}\}$. The estimate $\tilde{P}_f$ of the failure probability is assessed using Eqn.(2.29) with the Kriging mean indicator function $I_{\tilde{\mathcal{F}}}(\bar{\mathbf{u}})$.

   (c) **Evaluate the learning function U and find $\bar{\mathbf{u}}^\circ = \arg\min_{\bar{\mathbf{u}} \in \mathbb{P}_{\text{IS}}} U(\bar{\mathbf{u}})$.** The function U is evaluated at the unobserved points of $\mathbb{P}_{\text{IS}}$. The point $\bar{\mathbf{u}}^\circ \in \mathbb{P}_{\text{IS}}$ leading to the smallest value of $U(\bar{\mathbf{u}})$ is easily found.

   (d) **Test the stopping condition on learning.** The condition reads: $U(\bar{\mathbf{u}}^\circ) \geq 2$. It is activated once the DOE includes both safe and failure points.

   (e) **Enrich the DOE.** If the stopping condition is not satisfied, the DOE is enriched by evaluating $H(\bar{\mathbf{u}}^\circ)$. Hence $N_E = N_E + 1$, and the procedure goes back to Step 3a to build the new Kriging metamodel.

4. **End.** If the stopping condition is met, each point of the population is considered to be classified with a sufficient confidence level. $\tilde{P}_f$ corresponds to the probability estimated in Step 3b during the last loop. The coefficient of variation δ is calculated using Eqn.(2.31). Note that if the coefficient of variation is too large, a new population is generated according to φ_n and the Kriging classification loop (Step 3) continues until the stopping condition is satisfied again. At the end of the procedure, the MPFP can be updated with the failure point which is the closest to the origin of the standard space according to the Kriging predictions. The importance factors are then calculated, as exposed in Section 2.3.3.2.

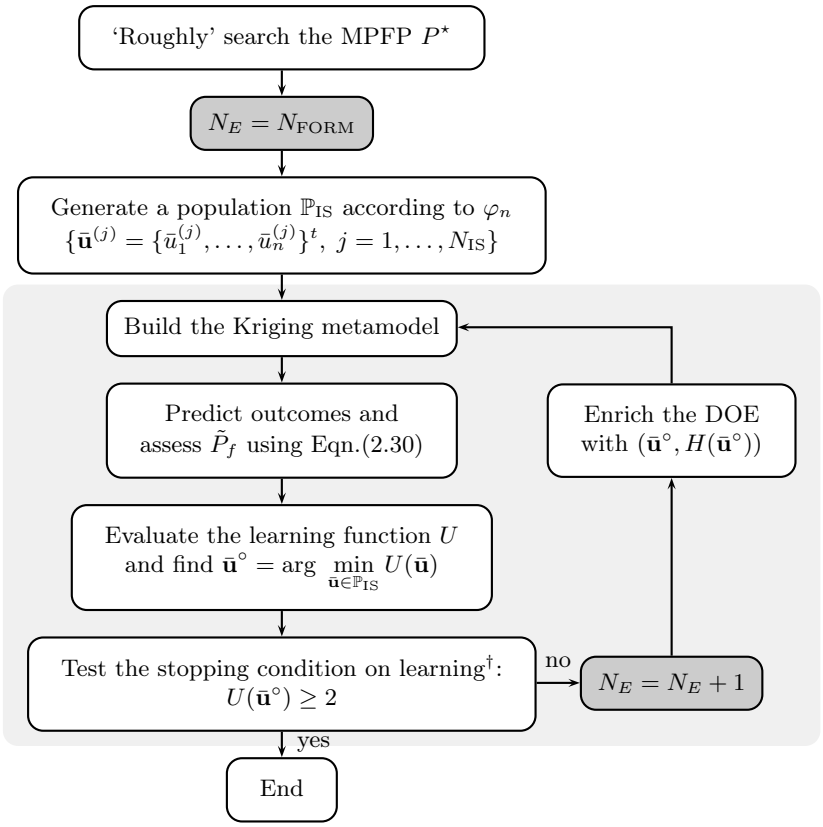

†The stopping condition is activated, once the DOE includes both safe and failure points.

Figure 2.24: AK-IS procedure. The light grey rectangle represents the Kriging classification loop (Step 3).

2.6.2.2 Two-dimensional non-linear performance function

AK-IS is first validated on a two-dimensional non-linear performance function H that reads:

$$H(U_1, U_2) = 0.5(U_1 - 2)^2 - 1.5(U_2 - 5)^3 - 3 \tag{2.63}$$

where U_1 and U_2 are standard Gaussian distributed random variables. The problem is depicted in Figure 2.25. The HLRF algorithm is performed in order to find the single MPFP. The number of HLRF iterations i_{FORM} varies from 3 to 6 in order to observe the effect of the precision of $P^\star$ on the probability assessed by AK-IS. The corresponding $P_3^\star$ to $P_6^\star$ are illustrated in Figure 2.26. The population to classify into the safe and failure subsets is composed of $N_{\text{IS}} = 10^4$ points. The robustness of AK-IS is tested by applying it to 4 sets of 100 different populations, one set for each i_{FORM} value.

Table 2.9 reports the number of points misclassified by AK-IS. The maximum error is 3 which is negligible in comparison with N_{IS}. Given the small number of misclassified points, the AK-IS failure probability estimates are very similar to the corresponding Importance

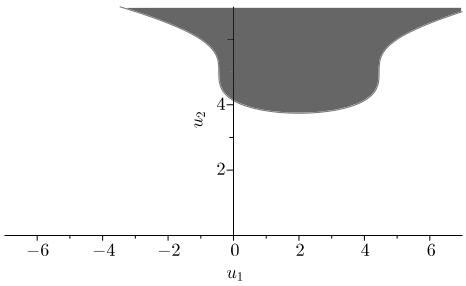

Figure 2.25: Safe (white) and failure (dark) domains on the example of the two-dimensional non-linear performance function.

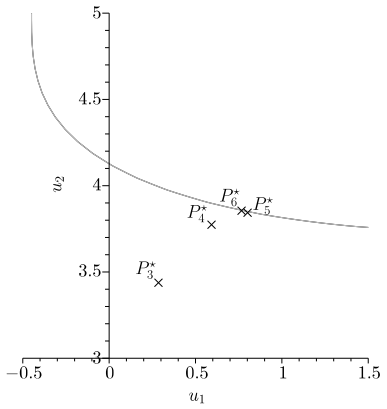

Figure 2.26: Locations of the MPFP $P^\star_{i_{\mathrm{FORM}}}$ on the example of the two-dimensional non-linear performance function.

Sampling estimates. The median reliability results are reported in Table 2.10. For the different levels of i_{FORM}, N_E is seen to be significantly less than N_{IS}. It is also observed, for this example, that a less precise $P^\star$ has a very slight impact on the number of evaluations $[N_E - N_{\mathrm{FORM}}]$. It thus seems suitable to limit the HLRF algorithm to a few iterations. Note that the small increase in the coefficient of variation δ when the number of HLRF iterations is reduced may be compensated by a larger population $\mathbb{P}_{\mathrm{IS}}$. Finally, it is important to mention that AK-IS is extremely fast, since the median CPU time of the AK-IS runs is only 5 seconds with a Intel Q9550 processor at 2.83 Ghz.

Misclassified points	Occurrence			
	$i_{\text{FORM}} = 3$	$i_{\text{FORM}} = 4$	$i_{\text{FORM}} = 5$	$i_{\text{FORM}} = 6$
0	96	99	94	94
1	4	1	5	3
2	0	0	1	2
3	0	0	0	1

Table 2.9: Number of points misclassified by AK-IS on the example of the two-dimensional non-linear performance function. AK-IS is applied to 4 sets of 100 different populations, one set for each i_{FORM}.

Method	i_{FORM}	$N_E{}^{\dagger}(\times 100)$	P_f $(\times 100)$	$\delta\%$ $(\times 100)$
FORM	6	19	4.21×10^{-5}	-
IS	6	$19 + 10^4$	2.86×10^{-5}	2.39
AK-IS	6	$19 + 7$	2.86×10^{-5}	2.39
AK-IS	5	$16 + 7$	2.86×10^{-5}	2.39
AK-IS	4	$13 + 8$	2.88×10^{-5}	2.48
AK-IS	3	$10 + 8$	2.87×10^{-5}	2.94

$^{\dagger}N_E$ for IS and AK-IS is separated into the number required by FORM + the number for the Kriging classification loop.

Table 2.10: Median reliability results over 100 runs of AK-IS for each i_{FORM} on the example of the two-dimensional non-linear performance function.

2.6.2.3 Dynamic response of a non-linear oscillator

The second example deals with a non-linear undamped single degree of freedom oscillator that is depicted in Figure 2.27 [Rajashekhar and Ellingwood, 1993; Gayton *et al.*, 2003; Schueremans and Van Gemert, 2005]. The performance function reads:

$$G(C_1, C_2, M, R, T_1, F_1) = 3\,R - \left| \frac{2\,F_1}{M\,\omega_0^2} \sin\left(\frac{\omega_0^2\,T_1}{2}\right) \right| \tag{2.64}$$

with $\omega_0 = \sqrt{(C_1 + C_2)\,/M}$. The random variables are listed in Table 2.11. Note that the distribution of the force F_1 has changed in comparison to the previously cited research papers in order to define a small failure probability, namely one that cannot be assessed in a short space of time with AK-MCS. A reference failure probability estimate is set as the median calculated over 100 runs of Monte Carlo Simulation with $N_{\text{MCS}} = 1.8 \times 10^8$ points. AK-IS is applied to 100 populations, each composed of $N_{\text{IS}} = 10^4$ points.

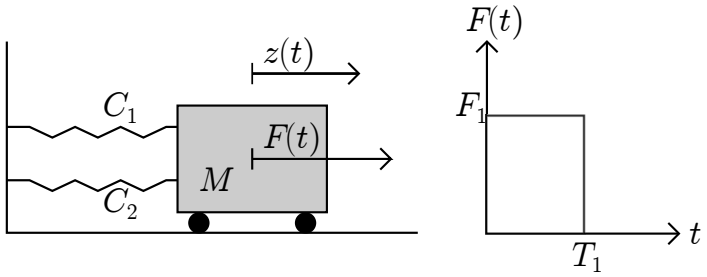

Figure 2.27: Dynamic response of a non-linear oscillator.

Variable	Distribution	Mean	Std. dev.
M	Gaussian	1	0.05
C_1	Gaussian	1	0.1
C_2	Gaussian	0.1	0.01
R	Gaussian	0.5	0.05
T_1	Gaussian	1	0.2
F_1	Gaussian	0.6	0.1

Table 2.11: Random variables on the example of the non-linear oscillator.

The median reliability results are reported in Table 2.12. The methods give relatively close estimates of the failure probability, but AK-IS confirms the FORM approximation with only 38 additional evaluations of the performance function. The number of misclassified points for the 100 AK-IS runs are listed in Table 2.13. These errors are clearly not significant.

Method	N_E ($\times 100$)	P_f ($\times 100$)	$\delta\%$ ($\times 100$)
MCS	1.8×10^8	9.09×10^{-6}	2.47
FORM	29	9.76×10^{-6}	-
IS	$29 + 10^{4\dagger}$	9.13×10^{-6}	2.29
AK-IS	$29 + 38^{\dagger}$	9.13×10^{-6}	2.29

$^{\dagger}N_E$ for AK-IS is separated into the number required by FORM + the number for the Kriging classification loop.

Table 2.12: Median reliability results over 100 runs of AK-IS on the example of the non-linear oscillator.

Misclassified points	Occurrence
0	97
1	3

Table 2.13: Number of misclassified points for 100 runs of AK-IS on the example of the non-linear oscillator.

2.6.2.4 Conclusion

AK-IS is the extension of AK-MCS to a population centred on the MPFP. The number of points to predict is considerably reduced in comparison with AK-MCS, and consequently, small failure probabilities can be assessed in a very short space of time. Nevertheless, AK-IS is limited to cases where the MPFP is well isolated, and where no secondary minima exist in other areas of space.

2.6.3 Active learning and Kriging-based Subset Simulation

The last extension implements the Kriging classification loop within a Subset Simulation (see Section 2.3.4) to reduce the computational cost of the two following steps:

- the evaluation of the performance function at the points in the first population $\mathbb{P}_1$.
- the evaluation of the performance function at the simulated candidate states in Step 2 of the modified Metropolis-Hastings algorithm.

In both cases, what matters is the position of the points in comparison with a given threshold H_k (above or below) and not the performance function value. The Kriging classification loop is appropriate to provide such information in a parsimonious way. This extension is called AK-SS, and can be seen as an intermediary approach between the general AK-MCS and the more specific AK-IS.

2.6.3.1 Procedure

Figure 2.28 depicts the AK-SS procedure. Let H be the performance function in the standard space. Let a decreasing sequence of sub-domains $\tilde{\mathcal{F}}_1$ to $\tilde{\mathcal{F}}_m$ be, so that $\tilde{\mathcal{F}}_1 \supset \tilde{\mathcal{F}}_2 \supset \ldots \supset \tilde{\mathcal{F}}_m = \tilde{\mathcal{F}}$ where $\tilde{\mathcal{F}}_k = \left\{\mathbf{u} \in \mathcal{U}^n : \mu_{\tilde{H}}(\mathbf{u}) \leq \mu_{\tilde{H}_k}\right\}$.

First simulation level, $k = 1$

The first simulation level in Subset Simulation is a Monte Carlo Simulation. AK-MCS is thus performed with some modifications to consider the threshold $\mu_{\tilde{H}_1}$. It goes as follows:

1. **Generate a population** $\mathbb{P}_1$ **using** ϕ_n**.** The points in $\mathbb{P}_1$ are denoted by $\{\mathbf{u}^{(j)} = \{u_1^{(j)}, \ldots, u_n^{(j)}\}^t,\ j = 1, \ldots, N_1\}$.

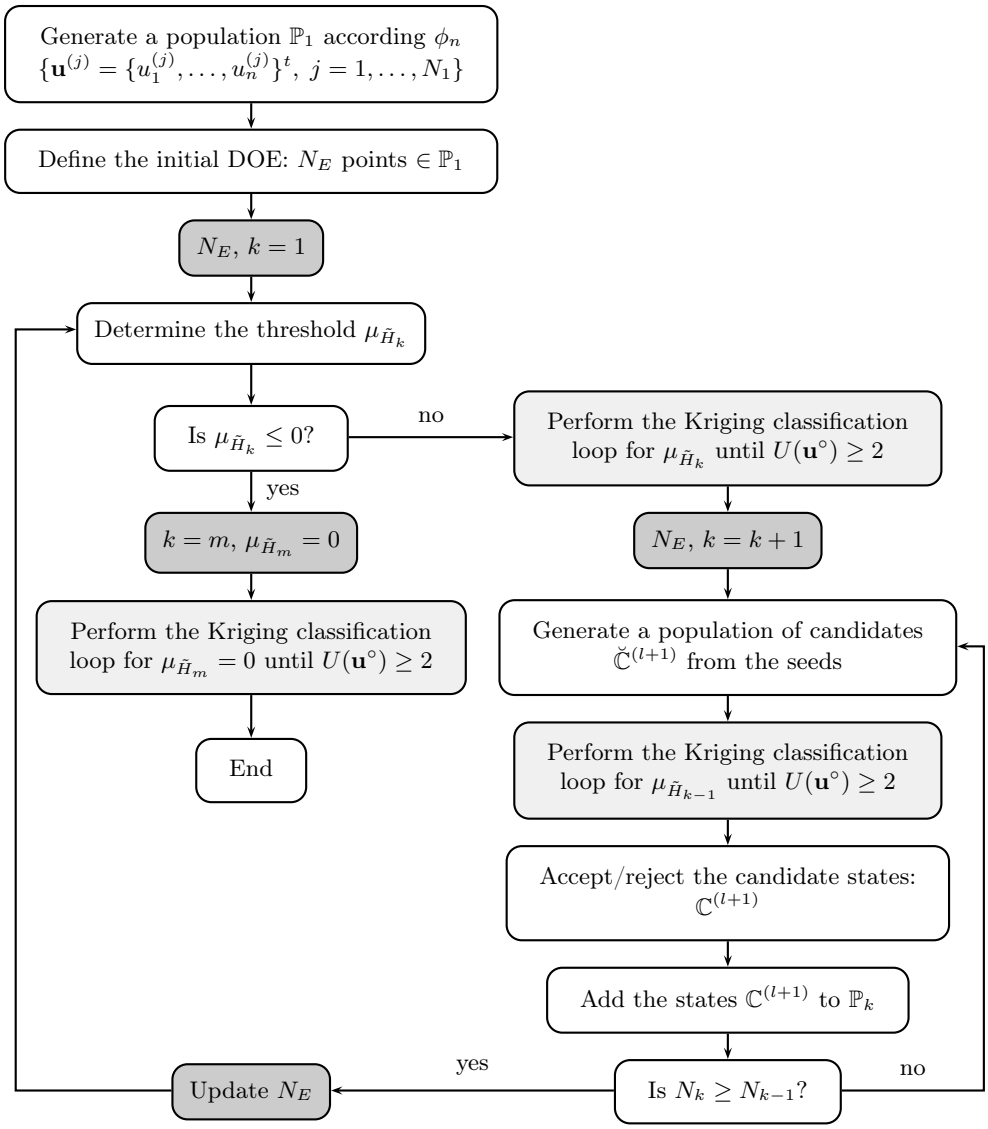

Figure 2.28: AK-SS procedure.

2. **Define the initial DOE.** The definition of the initial DOE is important as the threshold $\mu_{\tilde{H}_1}$ will be determined in Step 3 using a metamodel which has not yet been adaptively refined. A relatively correct representation of the behaviour of the performance function in the domain covered by $\mathbb{P}_1$ is thus beneficial at this early stage. Latin Hyper-cube Sampling or the design proposed in Step 1 of AK-MCS procedure (see Section 2.5.2) are possibilities.

3. **Determine the threshold $\mu_{\tilde{H}_1}$.**

   (a) **Build the Kriging metamodel.** The metamodel is built from the N_E observations.

(b) **Predict outcomes.** The Kriging predictions of the N_1 points are computed: $\{\mu_{\tilde{H}}(\mathbf{u}^{(j)}), \sigma_{\tilde{H}}(\mathbf{u}^{(j)}),\ j = 1, \ldots, N_1\}$.

(c) **Determine $\mu_{\tilde{H}_1}$.** The threshold $\mu_{\tilde{H}_1}$ characterizing the sub-domain $\tilde{\mathcal{F}}_1$ is determined so that:

$$\tilde{P}_1 = \frac{1}{N_1} \sum_{j=1}^{N_1} I_{\tilde{\mathcal{F}}_1} \left(\mathbf{u}^{(j)} \right) \approx 0.1 \tag{2.65}$$

where $I_{\tilde{\mathcal{F}}_1}(\mathbf{u}) = \{1 \text{ if } \mu_{\tilde{H}}(\mathbf{u}) \leq \mu_{\tilde{H}_1} \text{ and 0 otherwise}\}$.

4. **Is $\mu_{\tilde{H}_1} \leq 0$?.** The threshold $\mu_{\tilde{H}_1}$ is set to 0 if found negative.

5. **Perform the Kriging classification loop.**

(a) **Build the Kriging metamodel.** The metamodel is built from the N_E observations.

(b) **Predict outcomes and assess $\tilde{P}_1$.** The Kriging predictions of the N_1 points are computed: $\{\mu_{\tilde{H}}(\mathbf{u}^{(j)}), \sigma_{\tilde{H}}(\mathbf{u}^{(j)}),\ j = 1, \ldots, N_1\}$. The estimate $\tilde{P}_1$ is then improved using Eqn.(2.65).

(c) **Evaluate the learning function U and find $\mathbf{u}^\circ = \arg \min_{\mathbf{u} \in \mathbb{P}_1} U(\mathbf{u})$.** To consider the threshold $\mu_{\tilde{H}_1}$, the function U is modified as:

$$U(\mathbf{u}) = \frac{|\mu_{\tilde{H}_1} - \mu_{\tilde{H}}(\mathbf{u})|}{\sigma_{\tilde{H}}(\mathbf{u})} \tag{2.66}$$

It is evaluated at the $[N_1 - N_E]$ unobserved points of $\mathbb{P}_1$. The point $\mathbf{u}^\circ$ leading to the smallest value of $U(\mathbf{u})$ is easily found.

(d) **Test the stopping condition on learning.** The condition reads: $U(\mathbf{u}^\circ) \geq 2$. It is activated once the DOE includes points on both sides of $\mu_{\tilde{H}_1}$.

(e) **Enrich the DOE.** If the stopping condition is not satisfied, the DOE is enriched by evaluating $H(\mathbf{u}^\circ)$. Hence $N_E = N_E + 1$, and the procedure goes back to Step 5a to build the new Kriging metamodel.

6. If the stopping condition is met, each point of the population is considered to be classified to the threshold $\mu_{\tilde{H}_1}$ with a sufficient confidence level. $\tilde{P}_1$ corresponds to the probability estimated in Step 5b during the last loop. The coefficient of variation δ_1 is calculated using Eqn.(2.34). If $\mu_{\tilde{H}_1} = 0$, the procedure is finished. Otherwise, the simulation level is set to $k = k+1$, *i.e.* $k = 2$, and a new population is generated as explained in the next paragraph.

It is important to note that, following the principle of iSubset (see Section 2.3.4), the population of the first simulation level may also be derived from Conditional Sampling.

Generation of the population for the kth simulation level, $k = \{2, \dots, m\}$
The modified Metropolis-Hastings algorithm is applied to generate a population $\mathbb{P}_k$ following the conditional distribution $\phi_n(.|\mathbf{u} \in \tilde{\mathcal{F}}_{k-1})$. It is recalled that in crude Subset Simulation, the performance function is evaluated at each simulated candidate state to know whether it lies in $\tilde{\mathcal{F}}_{k-1}$ or not. The Kriging classification loop is applied to avoid these evaluations. The procedure is as follows:

I. **Generate a population of candidate states $\breve{\mathbb{C}}^{(l+1)}$ from the seeds.** This is similar to Step 1 of the modified Metropolis-Hastings algorithm, explained in Section 2.3.4. The population is composed of $[\tilde{P}_1 \times N_{k-1}]$ candidate states (assuming that this number is an integer).

II. **Perform the Kriging classification loop.**

   (a) **Build the Kriging metamodel.** The metamodel is built from the N_E observations.

   (b) **Predict outcomes.** The Kriging predictions of the candidate states are computed.

   (c) **Evaluate the learning function U and find $\mathbf{u}^\circ = \arg \min_{\mathbf{u} \in \breve{\mathbb{C}}^{(l+1)}} U(\mathbf{u})$.** The following function U is considered:

$$U(\mathbf{u}) = \frac{|\mu_{\tilde{H}_{k-1}} - \mu_{\tilde{H}}(\mathbf{u})|}{\sigma_{\tilde{H}}(\mathbf{u})} \tag{2.67}$$

   The function is evaluated at each of the unobserved candidate states of $\breve{\mathbb{C}}^{(l+1)}$ in order to determine whether they are classified with a sufficient confidence level. The candidate state $\mathbf{u}^\circ$ leading to the smallest value of $U(\mathbf{u})$ is easily found.

   (d) **Test the stopping condition on learning.** The condition reads: $U(\mathbf{u}^\circ) \geq 2$.

   (e) **Enrich the DOE.** If the stopping condition is not satisfied, the DOE is enriched by evaluating $H(\mathbf{u}^\circ)$. Hence $N_E = N_E + 1$, and the procedure goes back to Step IIa to build the new Kriging metamodel.

III. **Accept/reject the candidate states.** If the stopping condition is met, each candidate state of $\breve{\mathbb{C}}^{(l+1)}$ is considered to be classified to the threshold $\mu_{\tilde{H}_{k-1}}$ with a sufficient confidence level. The candidate states are accepted if they lie in $\tilde{\mathcal{F}}_{k-1}$, otherwise they are rejected, *i.e.* the Markov chains remain in the current state. The population $\mathbb{C}^{(l+1)}$ of the states is thus obtained.

IV. **Add the states $\mathbb{C}^{(l+1)}$ to $\mathbb{P}_k$.** The algorithm is then repeated with $l = l + 1$ until $N_k \geq N_{k-1}$.

Calculation of $\tilde{P}_k$ for simulation levels $k = \{2, \ldots, m\}$
For a simulation level $k > 1$, the procedure is slightly different from the first simulation level. In Step 1, the population $\mathbb{P}_k$ is generated with the modified Metropolis-Hastings, explained above. Step 2 is removed, as the DOE is composed of N_E observations that have already been made in the previous simulation levels. In Step 3c, the threshold $\mu_{\tilde{H}_k}$ characterizing the sub-domain $\tilde{\mathcal{F}}_k$ is determined so that $\tilde{P}_k = 0.1$. If found negative, $\mu_{\tilde{H}_k}$ is set to 0. In Step 5, the learning function U becomes:

$$U(\mathbf{u}) = \frac{|\mu_{\tilde{H}_k} - \mu_{\tilde{H}}(\mathbf{u})|}{\sigma_{\tilde{H}}(\mathbf{u})} \tag{2.68}$$

The last difference is the calculation of the coefficient of variation δ_k using Eqn.(2.36). The procedure continues until $\mu_{\tilde{H}_k} = \mu_{\tilde{H}_m} = 0$. The failure probability is then assessed using Eqn.(2.37), and the coefficient of variation of the estimate is calculated with Eqn.(2.38).

2.6.3.2 Illustration

AK-SS is illustrated on the example of the parabolic limit state proposed by Der Kiureghian and Dakessian [1998]. The performance function reads:

$$H(U_1, U_2) = a - U_2 - b(U_1 - c)^2 \tag{2.69}$$

where U_1 and U_2 are standard normal distributed random variables, $a = 5$, $b = 0.2$ and $c = 0$. Note that the latter parameters differ slightly from the original paper. Parameters a and b are set to define a small failure probability ($\approx 10^{-5}$); one that cannot be assessed in a short space of time with AK-MCS. Parameter c is set to give a symmetric limit state (see Figure 2.29) and consequently two MPFPs. In such a case, AK-IS leads to a biased failure probability estimate as only one MPFP is identified. AK-SS is proposed as a more general approach that can deal with such reliability problems more precisely. A reference failure probability estimate is defined as the median calculated over 100 runs of Subset Simulation with an initial population of $N_1 = 10^5$ points. AK-SS is conducted with the same initial populations. The Kriging classification loop is also implemented within iSubset. Its exclusion hyper-sphere presents a radius $\beta_e = 3.5$.

The median reliability results are reported in Table 2.14. The median failure probability estimates of the three methods are extremely similar. However, the number of performance function evaluations is reduced from 5×10^5 to 38 for AK-SS and 27 for AK-SS+iSubset. The iSubset trick also enables a decrease of the CPU time by 42% in comparison with AK-SS. Figure 2.30(a) depicts the final DOE for a given run of AK-SS. The Kriging classification loop is seen to add points mainly in the vicinity of the different thresholds. The same comment can be made on the DOE of AK-SS+iSubset shown in Figure 2.30(b).

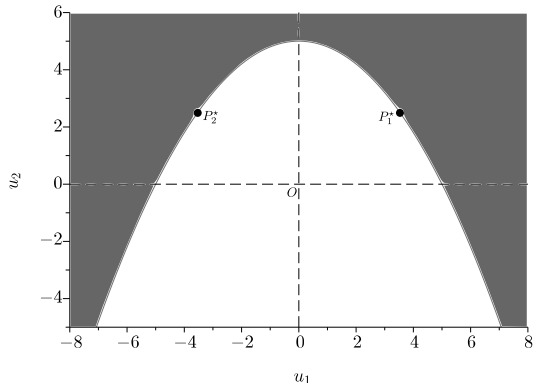

Figure 2.29: Parabolic limit state with its symmetric MPFPs $P_1^\star$ and $P_2^\star$. The dark area represents the failure domain.

Method	N_E ($\times 100$)	P_f ($\times 100$)	$\delta\%$ ($\times 100$)	CPU time in s ($\times 100$)
SS	5×10^5	1.91×10^{-5}	3.42	-
AK-SS	38	1.90×10^{-5}	3.28	260
AK-SS+iSubset†	27	1.92×10^{-5}	3.27	150

†The radius of the hyper-sphere is $\beta_e = 3.5$.

Table 2.14: Median reliability results over 100 runs of AK-SS and AK-SS+iSubset on the example of the parabolic limit state. The median CPU time is given for 100 runs performed with a Intel Q9550 processor at 2.83 Ghz.

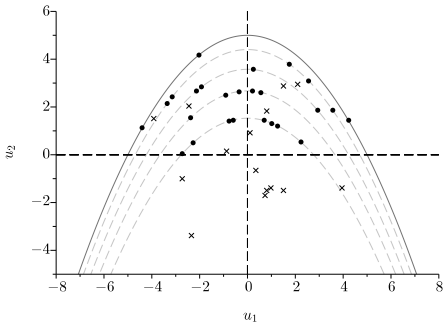

(a) Final DOE of an AK-SS run. Five simulation levels are observed.

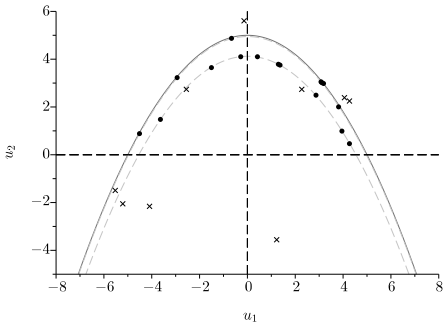

(b) Final DOE of an AK-SS+iSubset run. Three simulation levels are observed (the second one is extremely close to the limit state).

Figure 2.30: Illustration of AK-SS and AK-SS+iSubset on the example of the parabolic limit state. The crosses depict the initial DOE. The dots represent the points iteratively added to the DOE with the Kriging classification loop. The solid line is the limit state. The dashed lines are the different thresholds $H(\mathbf{u}) = \mu_{\tilde{H}_k}$.

2.6.3.3 Conclusion

AK-SS corresponds to the implementation of the Kriging classification loop within Subset Simulation. Unlike AK-IS, AK-SS is not based on any assumption of the limit state's shape. Nevertheless, it requires more predictions and performance function evaluations. The computational cost of AK-SS may be improved by performing the first simulation level with Conditional Sampling, as in iSubset. Finally, AK-SS can be seen as an intermediary approach between the general AK-MCS and the more specific AK-IS.

2.7 Conclusion

A family of Kriging-based reliability methods called AK-RM has been presented in this chapter. These methods represent improvements on various classical sampling techniques through the addition of an iterative Kriging classification loop. The basic idea is to use the predictions of the Kriging metamodel in order to classify a fixed population into its safe and failure subsets, using the least possible number of performance function evaluations. A specific learning function identifies the evaluations that should be carried out to adaptively refine the metamodel in the vicinity of the limit state. To a certain extent, the AK-RM family can be seen as 'guided' sampling techniques. Their validations on a set of examples show that they are accurate classifiers, while remaining parsimonious with respect to the number of performance function evaluations.

The first method of the AK-RM family (see Figure 2.31) is AK-MCS, which corresponds to the combination of the Kriging classification loop with Monte Carlo Simulation. Although it is the most general approach, it becomes computationally demanding for failure probabilities below 10^{-3}. Alternatives are thus introduced to consider such reliability levels. Given that the performance function of many structures happens to be monotonic with respect to its random variables, AK-MCSm is suggested to take advantage of this monotony. AK-IS is another approach that classifies points simulated in the vicinity of the MPFP. The computational cost is considerably reduced, but the approach relies on the hypothesis that the weight of the failure probability is well located. Finally, AK-SS based on Subset Simulation is proposed as an intermediary method between the general AK-MCS and the more specific AK-IS.

Note that the adaption of the Kriging classification loop to the case of multiple failure modes (or system reliability) is currently being studied. It is also important to mention that the principles of AK-RM have recently been applied to the tolerance Inspection of Large Surfaces (AK-ILS) [Dumas *et al.*, 2012, 2013]. Inspired by the learning function U, AK-ILS iteratively identifies the points that should be measured in order to determine with the least number of measurements the conformity (or non-conformity) of the surface being inspected.

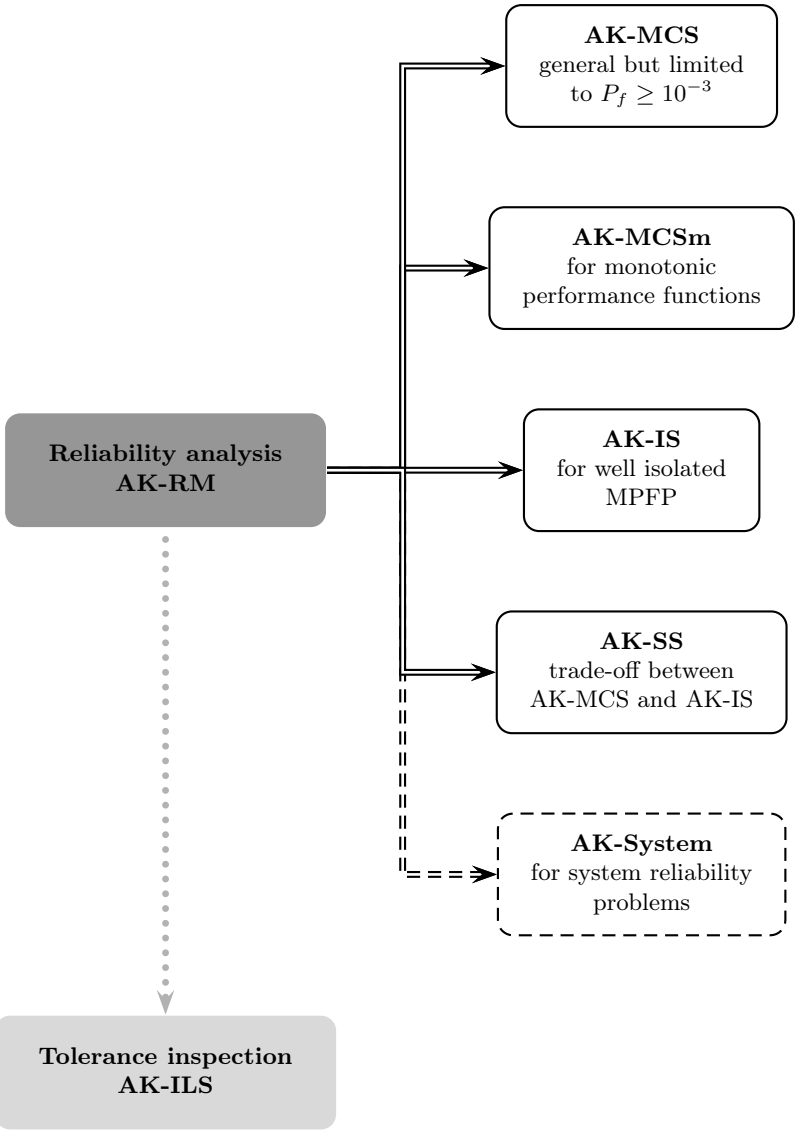

Figure 2.31: AK-RM family and current extensions.

Chapter summary

In industry, structures are designed with large safety margins, so that failure has a small probability of occurring. Furthermore, performance functions characterizing structural failure scenarios often depend on responses of numerical models whose evaluations are time-demanding. As a consequence, the classical sampling-based reliability methods such as Monte Carlo Simulation cannot be applied. Following this statement, metamodelling is proposed in this chapter as a means to conduct structural reliability analyses in a more practical amount of time. Metamodels are fast-to-evaluate approximations of the performance function. They require a Design Of numerical Experiments (DOE), *i.e.* a set of points where the values of the computationally demanding performance function are known. The selection of the DOE is of high importance, as it must contain a sufficient number of points to build an accurate metamodel, but must also keep this number to a minimum so as to remain practical in a short space of time. In this chapter, the Kriging metamodel is selected because it presents two crucial features. First, it interpolates the points in the DOE. Second, it provides a measure of the prediction uncertainty (the Kriging variance). The latter feature enables the use of Kriging in an active learning scheme which is an iterative enrichment of the DOE with well selected points. Within the frame of structural reliability analysis, the best points to select are located in the vicinity of the limit state. A learning function named U and based on the Kriging variance is specifically proposed in this chapter to identify these points. Finally, this learning function is employed within four Active learning and Kriging-based Reliability Methods (AK-RM) to deal with problems involving computationally demanding models and small failure probabilities. The validation of these methods on a set of examples shows that they provide accurate failure probability estimates while remaining parsimonious with respect to the number of performance function evaluations.

3 Application to the case studies of the APPRoFi project

Contents

3.1 Introduction 108
3.2 Bolted joint in an aircraft engine 108
3.2.1 Fatigue behaviour 108
3.2.2 Load modelling 111
3.2.3 Numerical model 113
3.2.4 Reliability assessment 114
3.2.5 Results 115
3.3 Blade support case study 115
3.3.1 Fatigue behaviour 116
3.3.2 Material properties 118
3.3.3 Load modelling 119
3.3.4 Numerical model 123
3.3.5 Reliability assessment 124
3.3.6 Results 125
3.4 Conclusion 126

3.1 Introduction

This chapter is devoted to the application of the probabilistic approach exposed in Chapter 1 to two case studies submitted by SNECMA within the frame of the APPRoFi project. These case studies involve computationally demanding numerical model and small failure probabilities. To enable a prompt reliability assessment, the global methodology developed in the APPRoFi project is applied. The probabilistic approach explained in Chapter 1 forms the backbone of this methodology. The computational cost of the structural reliability analysis is then reduced in two ways. First, the CPU time of the numerical model evaluation is optimized by LMT-ENS Cachan. The LATIN method [Ladevèze, 1999] is used in order to diminish the time spent for a single model evaluation. A multiparametric strategy [Boucard and Champaney, 2003] is also applied in order to decrease the time demand of succeeding computations. For further details on these two numerical methods, the reader may refer to Relun [2011] whose thesis also contributes to the APPRoFi project. Second, Kriging-based reliability methods presented in Chapter 2 are applied to determine the failure probability and the influent parameters on structural reliability with a limited number of numerical model evaluations.

Note that, for confidentiality reasons, axis graduations are not displayed and no order of magnitude of the failure probability is mentioned.

3.2 Bolted joint in an aircraft engine

The first case study is proposed by SNECMA's aviation branch. It deals with a bolted joint of blisks (also known as bladed disks and integrally bladed rotors) located in a jet engine. One of these blisks undergoes high stresses in the vicinity of an oil evacuation hole. The aim of the study is to determine the probability of crack initiation at this geometric discontinuity due to fatigue loads. Figure 3.1 depicts the flowchart of the probabilistic approach for this case study. The different steps of this flowchart are discussed below.

3.2.1 Fatigue behaviour

Probabilistic $S-N$ curves are implemented in this thesis to model the dispersion observed in a data set of 361 purely tensile ($\mathcal{R} = 0$) fatigue tests provided by SNECMA. The deterministic model of the $S-N$ curves is selected as a 'double' Basquin's relation, where the change of slope is set to an arbitrary number of cycles N_C. The deterministic model is expressed as the median range $\Delta\sigma_{50\%}$:

$$\Delta\sigma_{50\%} = \begin{cases} B_i \, N^{b_i} \text{ for } N \leq N_C \\ B_s \, N^{b_s} \text{ for } N > N_C \end{cases} \tag{3.1}$$

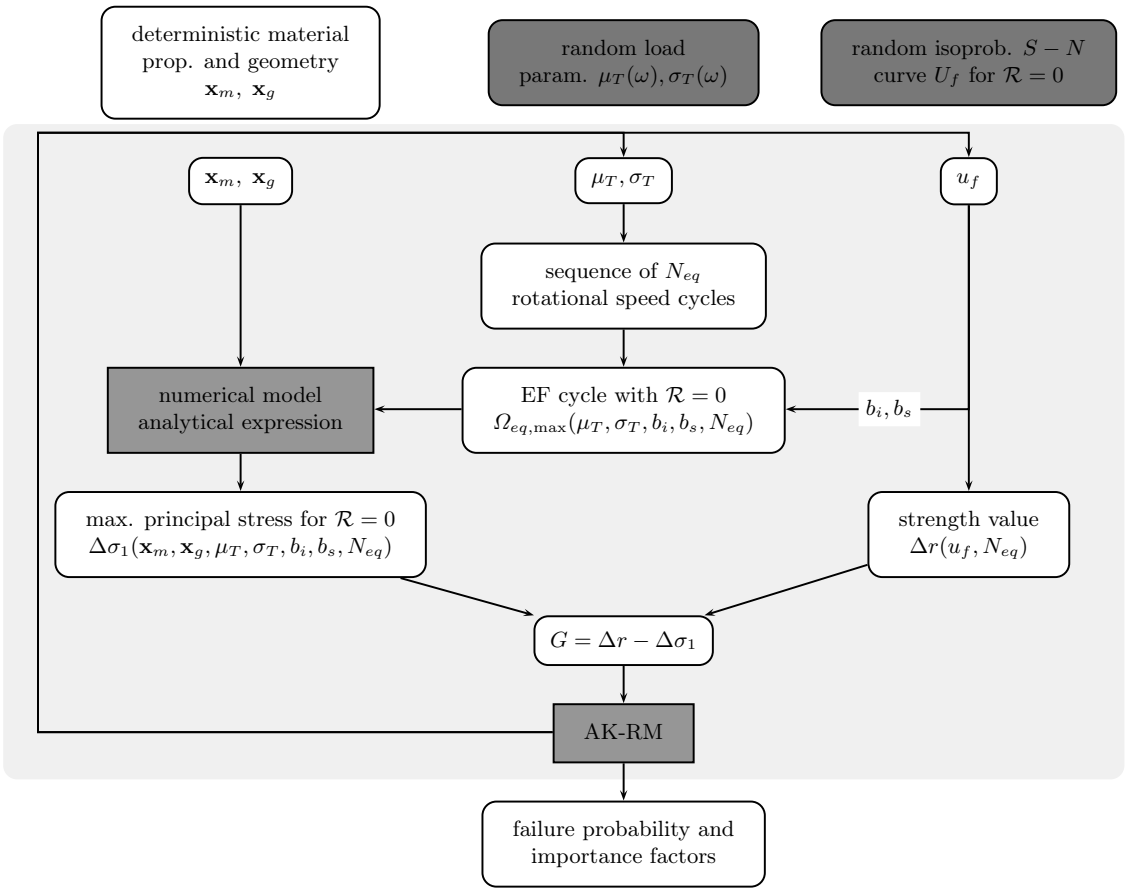

Figure 3.1: Probabilistic approach for the bolted joint case study.

The parameters of the three probabilistic $S-N$ curve models discussed in Section 1.3.5 are inferred according to the data set. ESOPE, ESOPE 2 and Guédé's model are depicted in Figure 3.2. Relatively different behaviours are observed for these three $S-N$ curve models. The impact of modelling on the strength value for three numbers of cycles to failure N_1, N_2 and N_3 is quantified in Table 3.1. The median curves are seen to be rather similar (particularly ESOPE 2 and Guédé's model), but the isoprobability curves at 2.5% and 97.5% present significant differences. Model selection is done using AIC, BIC and the p-values of Kolmogorov-Smirnov tests. Table 3.2 reports the values of these criteria. ESOPE 2 is selected in the frame of this study, due to the fact that it presents the smallest AIC and BIC values and that there is not enough evidence to reject its initial hypothesis at a sensible level (5%). As mentioned in Section 1.3.5, all the isoprobability $S-N$ curves of ESOPE 2 feature the same Basquin's slopes b_i and b_s, *i.e.* $b_i(U_f) = b_i$, and $b_s(U_f) = b_s$ (U_f is recalled to denote the random isoprobability $S-N$ curve).

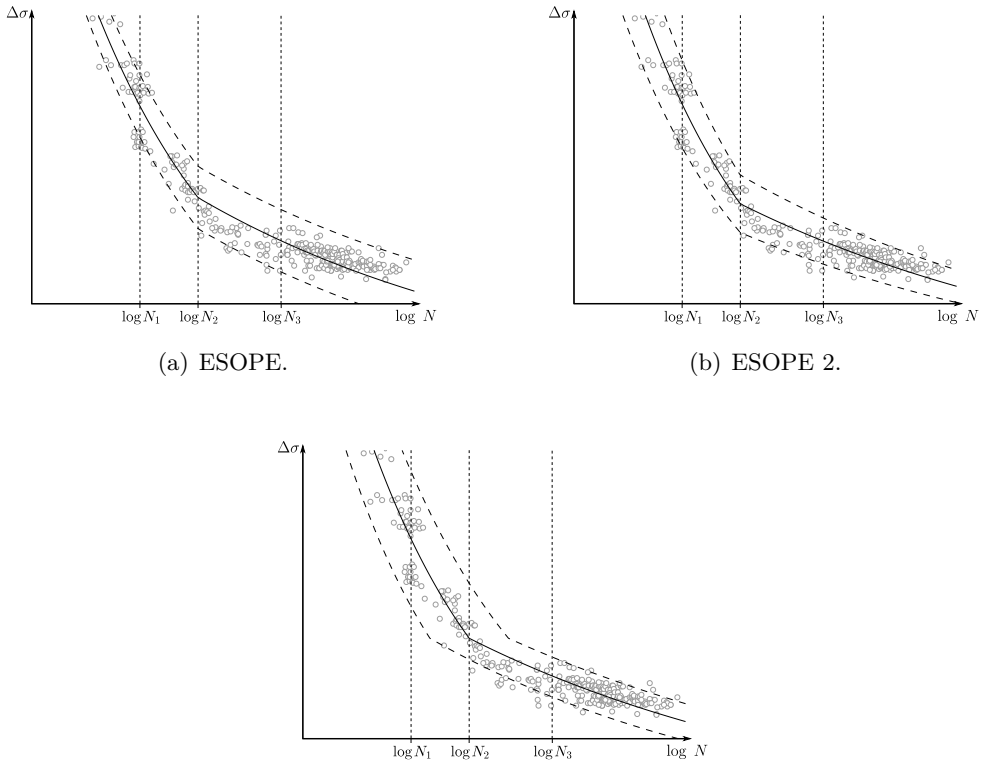

(a) ESOPE.

(b) ESOPE 2.

(c) Guédé's model.

Figure 3.2: Fitting of ESOPE, ESOPE 2 and Guédé's models to the fatigue tests for the bolted joint case study. The solid line represents the median trend. The dashed lines are the isoprobability $S-N$ curves defined at 2.5% and 97.5%.

Model	N_1			$N_2 = N_C$			N_3		
	2.5%	50%	97.5%	2.5%	50%	97.5%	2.5%	50%	97.5%
ESOPE	1.00	1.00	1.00	1.00	1.00	1.00	1.00	1.00	1.00
ESOPE 2	0.96	1.01	1.05	0.98	0.97	0.96	1.06	1.00	0.95
Guédé	0.87	1.01	1.12	1.03	0.97	1.08	1.08	1.00	0.93

Table 3.1: Impact of the $S-N$ curve model on the strength value for the bolted joint case study. The results for different lives N_1, N_2 and N_3 (see Figure 3.2) are normalized to the strength value found using ESOPE. The percentages $(2.5\%, 50\%, 97.5\%)$ refer to the isoprobability curves.

Model	AIC	BIC	p-value
ESOPE	9103	9119	5×10^{-4}
ESOPE 2	8980	8996	0.09
Guédé	9011	9027	0.13

Table 3.2: Measures of the relative goodness of fit of the probabilistic $S-N$ curve models for the bolted joint case study.

3.2.2 Load modelling

The bolted joint of blisks is subjected to various loadings including preloads and centrifugal, radial and axial loads of the blades. Deterministic sensitivity studies conducted by LMT-ENS Cachan prove that the centrifugal load is the main source of fatigue damage and that the variations of the other loads have no significant impact on the structural response. The latter loads are thus set as deterministic, and only the uncertainty of the centrifugal load is considered in this study.

The centrifugal load is derived from the rotational speed Ω which is associated with the thrust that must be generated in order to make the aircraft move. Given that the greatest thrust is observed at takeoff, the fatigue load is defined as a sequence of N_{eq} cycles $(0,\ \Omega_{i,\max})$ where N_{eq} is the number of flights performed by the engine during its design life and $\Omega_{i,\max}$ the maximum rotational speed observed at the ith takeoff (see Figure 3.3). The load sequence presents variable ranges which are in fact due to the climatic fluctuations of temperature at takeoff[†]. In this study, the load sequence is assumed to be a mix of five missions $\{\mathrm{A}, \mathrm{B}, \mathrm{C}, \mathrm{D}, \mathrm{E}\}$ characterized by maximum rotational speeds $\mathbf{\Omega} = \{\Omega^{\mathrm{A}}_{\max}, \Omega^{\mathrm{B}}_{\max}, \Omega^{\mathrm{C}}_{\max}, \Omega^{\mathrm{D}}_{\max}, \Omega^{\mathrm{E}}_{\max}\}^t$ at takeoff and temperatures $\mathbf{T} = \{T^{\mathrm{A}}, T^{\mathrm{B}}, T^{\mathrm{C}}, T^{\mathrm{D}}, T^{\mathrm{E}}\}^t$.

[†]The thrust generated by the jet engine is inversely proportional with ambient temperature. The rotational speed required for reaching takeoff thrust is then linked to temperature in the following way: the higher temperature, the higher the rotational speed.

Table 3.3 reports the characteristics of these missions. To consider the uncertainties of the centrifugal load, the percentages of occurrence $\{p^{\mathrm{A}}, p^{\mathrm{B}}, p^{\mathrm{C}}, p^{\mathrm{D}}, p^{\mathrm{E}}\}$ of the missions are random variables. No load data are provided to determine the scatter of these percentages, but according to SNECMA flight experts, an aircraft mostly takes off from a given base and is consequently subjected to rather similar temperatures at takeoff throughout its design life. Following this statement, the bolted joint of blisks is exposed to a dominant mission (or rotational speed), and secondary missions are less and less frequent as their corresponding temperatures at takeoff are further from the temperature of the dominant mission. For a given aircraft, the temperature at takeoff can be modelled by a squared exponential function. This function is considered as being a Gaussian PDF $f_T(t)$ (see Figure 3.4). Given a mean μ_T and a standard deviation σ_T, the values $\{f_T(T^{\mathrm{A}}), f_T(T^{\mathrm{B}}), f_T(T^{\mathrm{C}}), f_T(T^{\mathrm{D}}), f_T(T^{\mathrm{E}})\}$ of the Gaussian PDF can be calculated, and each percentage of occurrence p^m for $m = \mathrm{A}, \ldots, \mathrm{E}$ can be defined as:

$$p^m = \frac{f_T(T^m)}{\sum_{i=\mathrm{A}}^{\mathrm{E}} f_T(T^i)} \tag{3.2}$$

Following Eqn.(3.2), the percentages are fully characterized by the PDF's parameters μ_T and σ_T. Setting these parameters as random variables thus enables random percentages to be defined. In agreement with SNECMA engineers, the mean $\mu_{\mathrm{T}}(\omega)$ is considered as a uniform random variable on the interval $[\min(\mathbf{T}) - 5; \max(\mathbf{T}) + 5]$, and the standard deviation $\sigma_T(\omega)$ as a Gaussian variable of mean 16 and variance 4.

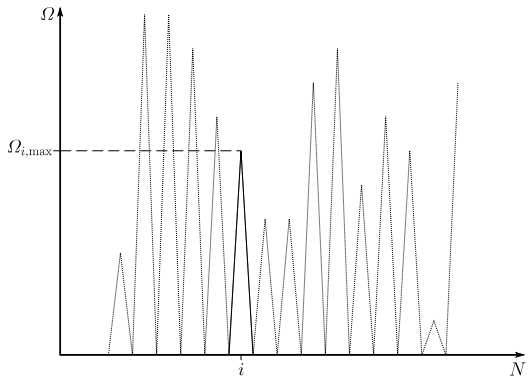

Figure 3.3: Sequence of cycles in maximum rotational speed Ω at takeoff.

By drawing a realization $\{\mu_{\mathrm{T}}, \sigma_T\}$, a sequence of N_{eq} rotational speed cycles is generated. This sequence is composed of $N_{eq} \times p^{\mathrm{m}}(\mu_{\mathrm{T}}, \sigma_T)$ cycles $(0, \Omega^{\mathrm{m}}_{\max})$ for each $m = \mathrm{A}, \ldots, \mathrm{E}$. Using the deterministic Basquin's slopes b_i and b_s, the virtual sequence is transformed into an EF cycle $(0,\ \Omega_{eq,\max}(\mu_{\mathrm{T}}, \sigma_T, b_i, b_s, N_{eq}))$ repeated N_{eq} times.

Mission	A	B	C	D	E
$\Omega_{\max}$	1.028	1.012	1.000	0.990	0.975
T	33.1	14.4	0	-11.2	-28.7

Table 3.3: Missions characterized by their maximum rotational speeds $\Omega_{\max}$ and temperatures T at takeoff. The rotational speeds are normalized to $\Omega^{\mathrm{C}}_{\max}$. The temperature is given as the difference with T^{C}.

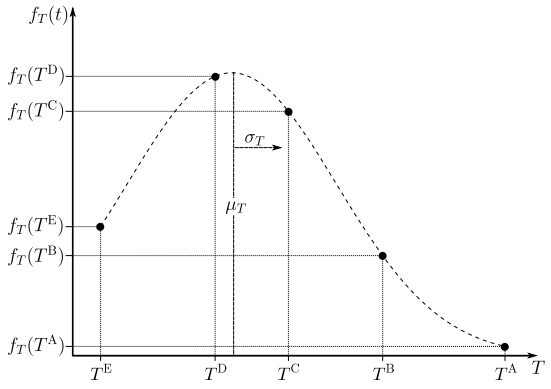

Figure 3.4: Gaussian distribution of the temperature at takeoff for a given aircraft. The distribution is characterized by a mean μ_T and a standard deviation σ_T. The values $\{f_T(T^{\mathrm{A}}), f_T(T^{\mathrm{B}}), f_T(T^{\mathrm{C}}), f_T(T^{\mathrm{D}}), f_T(T^{\mathrm{E}})\}$ are used to define the percentages of occurrence following Eqn.(3.2).

3.2.3 Numerical model

In a preliminary sensitivity analysis by LMT-ENS Cachan, the material properties and geometry of the numerical model are proven to have no significant impact on the structural response, thus they are considered as deterministic parameters respectively denoted by $\{\mathbf{x}_m, \mathbf{x}_g\}$. The EF cycle $(0,\ \Omega_{eq,\max}(\mu_{\mathrm{T}}, \sigma_T, b_i, b_s, N_{eq}))$ is applied to the numerical model. The output of interest is the cycle of the maximum principal stress $(\sigma_{\mathrm{I,min}}, \sigma_{\mathrm{I,max}})$ interpreted as a cycle being undergone N_{eq} times by the bolted joint of blisks. This cycle features a maximum value $\sigma_{\mathrm{I,max}}(\mathbf{x}_m, \mathbf{x}_g, \mu_T, \sigma_T, b_i, b_s, N_{eq})$ which is reached when $\Omega_{eq,\max}(\mu_{\mathrm{T}}, \sigma_T, b_i, b_s, N_{eq})$ is applied, and a minimum value $\sigma_{\mathrm{I,min}}(\mathbf{x}_m, \mathbf{x}_g)$ for a rotational speed of zero. Given that deterministic preloads are also applied to the numerical model, $\sigma_{\mathrm{I,min}}(\mathbf{x}_m, \mathbf{x}_g)$ differs from 0 when the engine is not in operation. Therefore, the stress cycle is not purely tensile ($\mathcal{R} \approx -0.05$), and a mean correction is necessary to enable fatigue calculation. To convert the stress cycle into its purely tensile equivalent, a model of the Haigh diagram is to be assumed and the tensile strength of the material must be known. In agreement with SNECMA engineers, the mean correction is not performed.

Hence, $\sigma_{\mathrm{I,min}}(\mathbf{x}_m, \mathbf{x}_g)$ is said to be 0, and the range $\Delta\sigma_{\mathrm{I}}(\mathbf{x}_m, \mathbf{x}_g, \mu_T, \sigma_T, b_i, b_s, N_{eq})$ thus corresponds to $\sigma_{\mathrm{I,max}}(\mathbf{x}_m, \mathbf{x}_g, \mu_T, \sigma_T, b_i, b_s, N_{eq})$.

Numerical model evaluations by LMT-ENS Cachan show that a linear relation can be assumed between $\sigma_{\mathrm{I,max}}(\mathbf{x}_m, \mathbf{x}_g, \mu_T, \sigma_T, b_i, b_s, N_{eq})$ ($\equiv \Delta\sigma_{\mathrm{I}}(\mathbf{x}_m, \mathbf{x}_g, \mu_T, \sigma_T, b_i, b_s, N_{eq})$) and $\Omega_{eq,\mathrm{max}}(\mu_T, \sigma_T, b_i, b_s, N_{eq})$ in the interval $[\Omega^{\mathrm{E}}_{\mathrm{max}}; \Omega^{\mathrm{A}}_{\mathrm{max}}]$ (see Figure 3.5). Given that the geometry and the material properties are deterministic, the relation remains the same for any realization of the random variables. The numerical model is therefore replaced with an analytical expression whose computational cost is free.

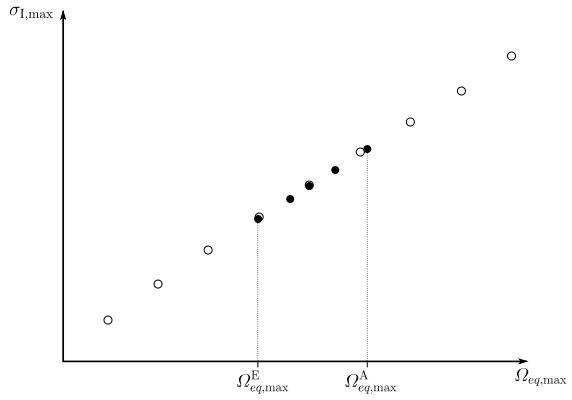

Figure 3.5: Numerical model evaluations (white dots) by LMT-ENS Cachan showing that a linear relation exist between $\sigma_{\mathrm{I,max}}$ and $\Omega_{eq,\mathrm{max}}$ in the interval $[\Omega^{\mathrm{E}}_{\mathrm{max}}; \Omega^{\mathrm{A}}_{\mathrm{max}}]$ (black dots).

3.2.4 Reliability assessment

Table 3.4 recapitulates the random variables of the reliability problem. The performance function G compares the range $\Delta\sigma_{\mathrm{I}}(\mathbf{x}_m, \mathbf{x}_g, \mu_T, \sigma_T, b_i, b_s, N_{eq})$ with the drawn strength range $\Delta r(u_f, N_{eq})$ at N_{eq} cycles. AK-IS and AK-SS are implemented to pilot structural reliability analyses. Given that the model is replaced with an analytical expression, Importance Sampling and Subset Simulation are also applied to confirm results.

Random variable	Denomination	Distribution	Parameters
$\mu_T(\omega)$	Mean of $f_T(T)$	Uniform	$[\min(\mathbf{T}) - 5; \max(\mathbf{T}) + 5]$
$\sigma_T(\omega)$	Std. dev. of $f_T(T)$	Gaussian	$\mu_{\sigma_T} = 16$; $\sigma_{\sigma_T} = 2$
U_f	Isoprob. $S-N$ curve	Gaussian	$\mu_{U_f} = 0$; $\sigma_{U_f} = 1$

Table 3.4: Random variables of the bolted joint case study.

3.2.5 Results

The reliability results are reported in Table 3.5. A population of 1.2×10^4 points centred on the approximated MPFP is classified using AK-IS and Importance Sampling. Similar probabilities are obtained, but AK-IS requires only 54 evaluations of the performance function. AK-SS and SS are performed to verify whether the MPFP is well isolated. For computational reasons, AK-SS is performed with an initial population of 2×10^4 points, whereas SS is performed with a significantly larger initial population. The results prove that the MPFP is indeed isolated.

Method	N_E	P_f^{norm}	δ
FORM	9	1.00	-
IS	1.2×10^4	0.66	2.41%
SS	3.5×10^6	0.65	2.10%
AK-IS	54	0.66	2.41%
AK-SS	451	0.66	10.56%

Table 3.5: Reliability results for the case study of the bolted joint. The failure probabilities are normalized to the FORM approximation.

The elasticities of the Hasofer-Lind reliability index with respect to the standard deviations of $\mu_T(\omega)$, $\sigma_T(\omega)$ and U_f are reported in Table 3.6. For this case study, the $S-N$ curve model is the most influent parameter on structural reliability.

Load		Fatigue
$E_{\sigma_{\mu_T}}$	$E_{\sigma_{\sigma_T}}$	$E_{\sigma_{U_f}}$
-3.4×10^{-2}	-3.7×10^{-4}	-0.973

Table 3.6: Elasticities of the Hasofer-Lind reliability index with respect to the standard deviations of $\mu_T(\omega)$, $\sigma_T(\omega)$ and U_f for the case study of the bolted joint.

3.3 Blade support case study

The blade support case study (see Figure 3.6) is an aerospace application which has already been considered in the DEFFI project [Bignonnet and Lieurade, 2007; Bignonnet *et al.*, 2009; Ferlin *et al.*, 2009; Lefebvre *et al.*, 2009]. During its design life, the blade support is shear-loaded by random fatigue displacements in its transverse direction. The aim of the study is to determine the probability of crack initiation due to these fatigue loads. Figure

3.7 depicts the flowchart of the probabilistic approach for this case study. The different step of this flowchart are discussed below.

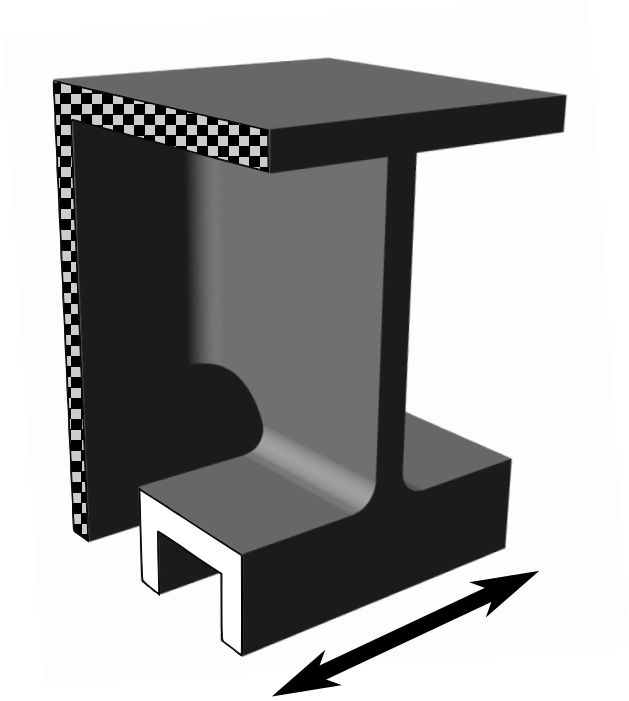

Figure 3.6: Blade support case study. The displacement is applied to the white surface. Its direction is represented by the arrow. The chequered area is fixed (no displacement allowed in any direction).

3.3.1 Fatigue behaviour

A data set of 80 fatigue tests conducted with fully reversed cycles is provided by SNECMA. The $S-N$ curves are plotted as the Smith-Watson-Topper (SWT) strength (Smith *et al.*, 1970, see Section 3.3.5 for its definition) in terms of the number of cycles to failure. The deterministic model of the $S-N$ curves is selected as the Basquin's relation. ESOPE, ESOPE 2 and Guédé's model are depicted in Figure 3.8. The impact of the model on the SWT strength value for three numbers of cycles is quantified in Table 3.7. The three models are extremely similar for the median curve and short lives (N_1). For higher numbers of cycles, the differences increase dramatically. AIC, BIC and the p-values of Kolmogorov-Smirnov tests are reported in Table 3.8. ESOPE 2 is selected for its AIC and BIC values. Additionally, the p-values of the three models are relatively high, meaning that there is not enough evidence to reject their initial hypotheses. As mentioned in Section 1.3.5, all the isoprobability $S-N$ curves of ESOPE 2 feature the same Basquin's slope $b(U_f) = b$.

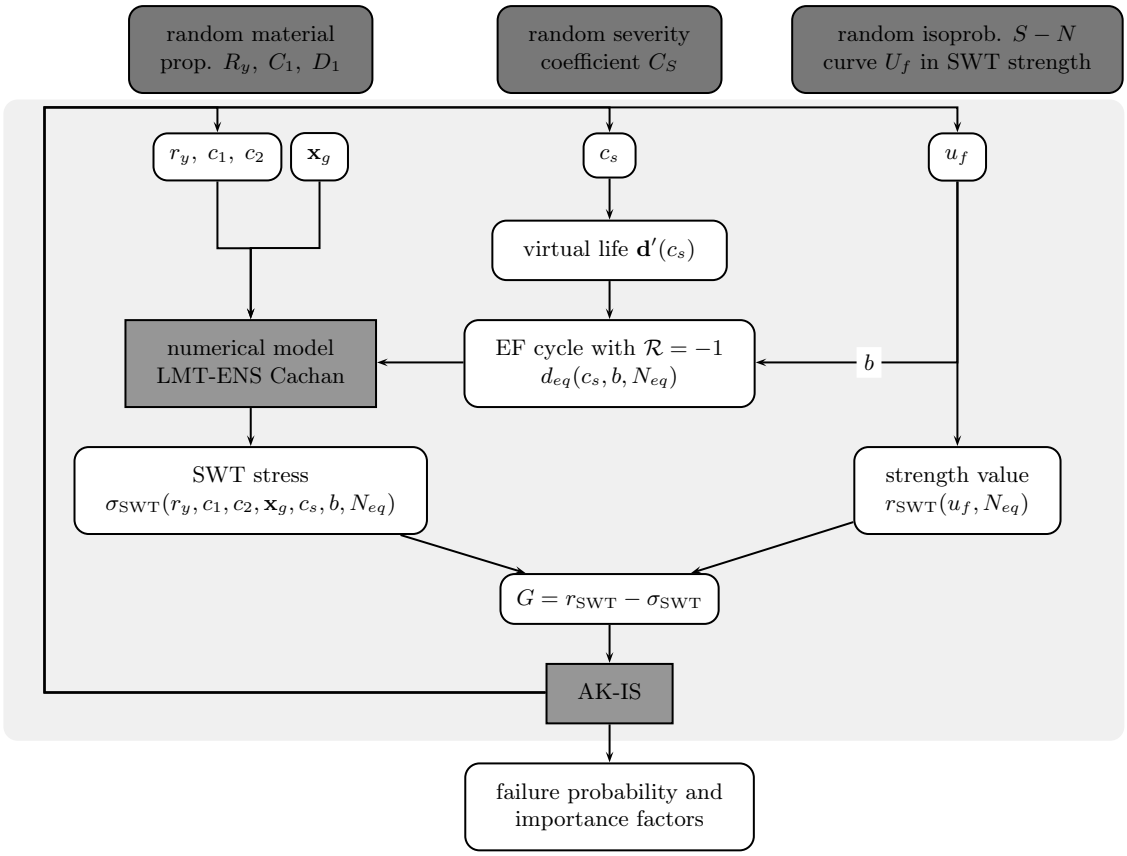

Figure 3.7: Probabilistic approach for the blade support case study.

Model	N_1 2.5%	N_1 50%	N_1 97.5%	$N_2 = N_{eq}$ 2.5%	$N_2 = N_{eq}$ 50%	$N_2 = N_{eq}$ 97.5%	N_3 2.5%	N_3 50%	N_3 97.5%
ESOPE	1.00	1.00	1.00	1.00	1.00	1.00	1.00	1.00	1.00
ESOPE 2	0.99	1.01	1.02	1.19	1.01	0.92	1.73	1.02	0.80
Guédé	0.99	1.01	1.01	1.08	1.00	0.96	1.44	0.99	0.87

Table 3.7: Impact of the $S-N$ curve model on the SWT strength value for the blade support case study. The results for different lives N_1, N_2 and N_3 (see Figure 3.8) are normalized to the strength value found using ESOPE. The percentages $(2.5\%, 50\%, 97.5\%)$ refer to the isoprobability curves.

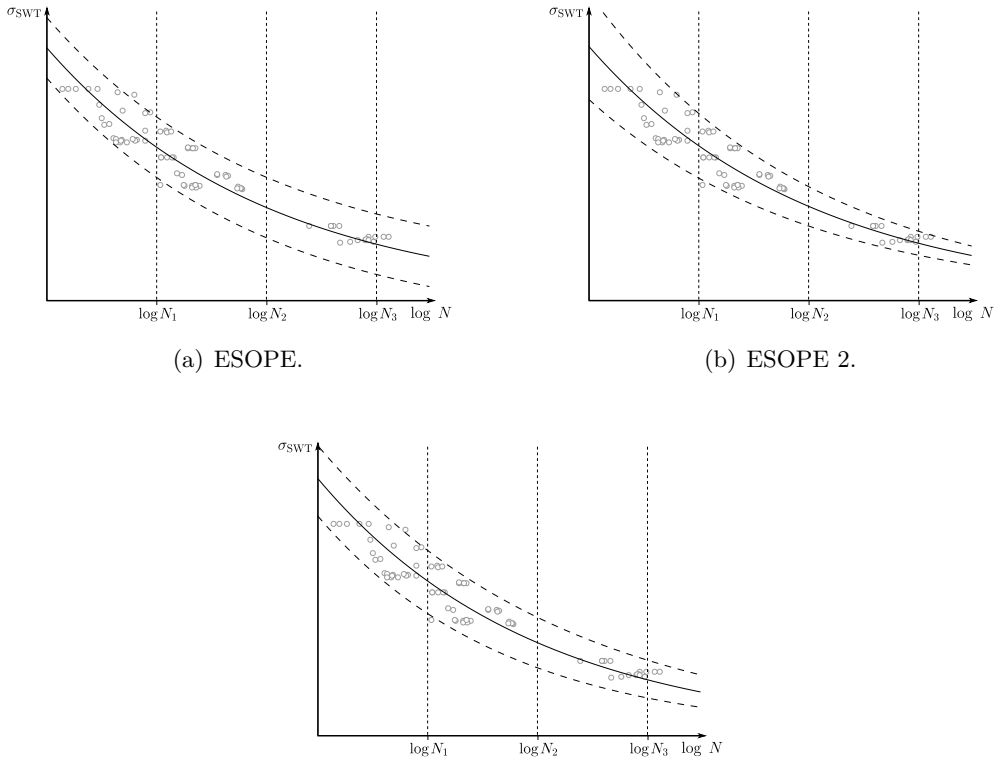

(a) ESOPE.

(b) ESOPE 2.

(c) Guédé's model.

Figure 3.8: Fitting of ESOPE, ESOPE 2 and Guédé's models to the fatigue tests for the blade support case study. The solid line represents the median trend. The dashed lines are the isoprobability $S-N$ curves defined at 2.5% and 97.5%.

Model	AIC	BIC	p-value
ESOPE	1402	1409	0.67
ESOPE 2	1380	1387	0.41
Guédé	1389	1396	0.41

Table 3.8: Measures of the relative goodness of fit of the probabilistic $S-N$ curve models for the blade support case study.

3.3.2 Material properties

The elastic-plastic behaviour of the material is characterized by the law of Chaboche [1989]:

$$\sigma = R_y + \frac{C_1}{C_2} \tanh\left(C_2\ \epsilon_p\right) \tag{3.3}$$

where the yield strength R_y and the hardening parameters C_1 and C_2 are random variables, and where the plastic strain amplitude ϵ_p is obtained through the numerical model evaluation (see Section 3.3.4). Prior distributions of R_y, C_1 and C_2 and stabilized hysteresis loops at different strain levels are provided. For each of these loops, relevant information is extracted using the method described in [Lemaitre *et al.*, 2009, Chapter 6]. Bayesian inference is then used by Phimeca to establish the statistical distribution followed by R_y. The prior distributions followed by C_1 and C_2 are also updated by Phimeca using Bayesian techniques [Perrin, 2008]. The material properties are assumed to be lognormal variables, and a strong correlation is set between C_1 and C_2. A realization of the random material properties is denoted by $\{r_y, c_1, c_2\}$.

3.3.3 Load modelling

Nine displacement histories $d(t)$ (see Figure 3.9(a)) representing entire life spans of the structure are available to quantify the uncertainty of the in-service loads. In addition to the displacement, the course of the carrier rocket is characterized by its speed V, incidence angle I and yaw angle Y (see Figure 3.9(b)). In this section, the modelling implemented in the DEFFI project is first discussed. The alternative selected within the frame of the APPRoFi project is then explained. Note that the load modelling is also discussed in Appendix C with a parametric method following Nagode's mixture models (Section 1.3.4.2). Developed after the APPRoFi project, this alternative was not applied to assess structural reliability.

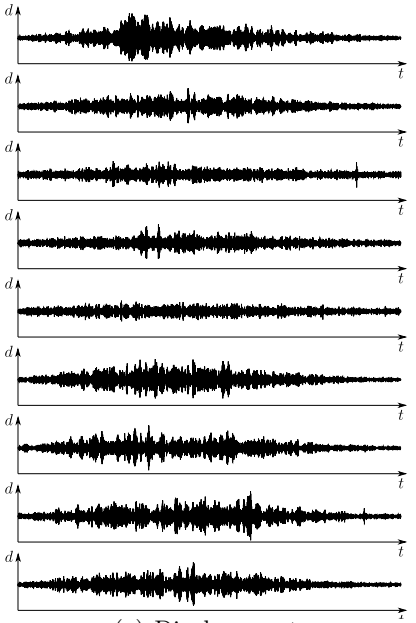

(a) Displacement.

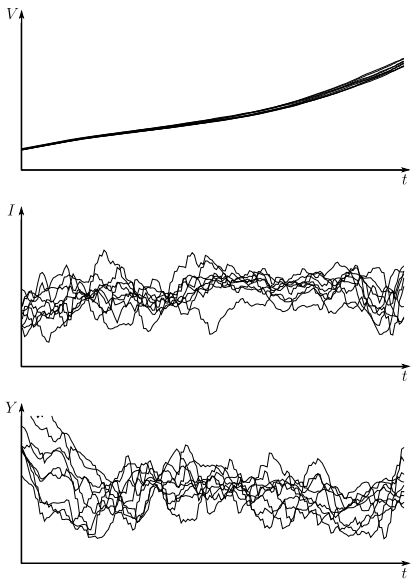

(b) Speed, incidence angle and yaw angle of the carrier rocket.

Figure 3.9: Available histories.

3.3.3.1 Load mix strategy in the DEFFI project

In agreement with SNECMA engineers, the displacement is assumed to depend strictly on the quantities V, I and Y. Such an assumption enables the load mix strategy presented in Section 1.3.4.1 to be applied. It is recalled that this strategy is grounded upon the definition of elementary life situations whose percentages of occurrence are random. To characterize these elementary situations, each of the quantities V, I and Y is divided into three arbitrary classes (or intervals) as illustrated in Figure 3.10. The classes are V_1, V_2, V_3 for speed, I_1, I_2, I_3 for the incidence angle, and Y_1, Y_2, Y_3 for the yaw angle. Such a division creates 27 elementary life situations, each one being denoted by (V_v, I_i, Y_y) for $v = 1, 2, 3$, $i = 1, 2, 3$ and $y = 1, 2, 3$. The nine displacement histories are decomposed into these 27 situations, and the Rainflow-counting method is processed to obtain Rainflow matrices. A total of 198 matrices is extracted using this method.

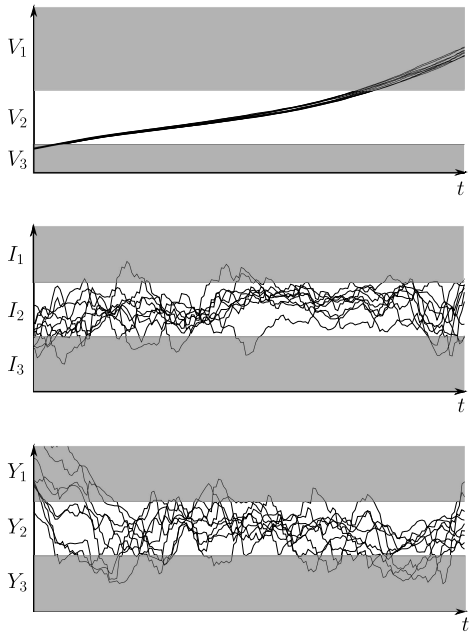

Figure 3.10: Definition of the different classes in speed, incidence angle and yaw angle.

For each class, nine values of the ratio of time spent in this class to the structure's life span can be calculated according to the displacement histories. The scatter of these nine values are modelled by a random percentage of occurrence. In the DEFFI project, the percentages of the classes I_1, I_2, Y_1 and Y_2 are assumed to be uniform random variables, and the percentages of I_3 and Y_3 are defined as the corresponding rests (to get 100%). The percentages of V_1, V_2 and V_3 are deterministic given that their scatters are not significant (see Figure 3.10).

A Rainflow matrix representing a virtual life of the structure is generated by selecting a realization of the percentages and a Rainflow matrix for each elementary life situation.

Up to 31 random variables are thus involved in the generation of such a virtual life: four random percentages and up to 27 discrete variables for selecting the different Rainflow matrices. This number of random variables represents a significant effort in structural reliability analysis, and the consideration of discrete variables is also difficult in metamodelling. For these reasons, a different model is implemented in the APPRoFi project.

3.3.3.2 Severity coefficient-based model

The model implemented in the APPRoFi project focuses strictly on displacement. The cycles of each displacement history are extracted using the Rainflow-counting method (see Figure 3.11), and a mean correction is applied in order to convert each cycle into its fully reversed equivalent[†]. As a result, the ith recording (for $i = 1, \ldots, 9$) can now be represented as a vector $\mathbf{d}'^{(i)}$ containing the symmetric alternating displacement amplitudes of its different fully reversed cycles. The vectors $\{\mathbf{d}'^{(i)},\ i = 1, \ldots, 9\}$ are depicted by their empirical CDFs in Figure 3.12. They present relatively smooth shapes. The empirical mean m_l of the symmetric alternating displacement amplitude at a probability level l (l varying between 0 and 1) can be calculated as:

$$m_l = \frac{1}{9} \sum_{i=1}^{9} d_l'^{(i)} \tag{3.4}$$

where $d_l'^{(i)}$ refers to the symmetric alternating displacement amplitude of the ith vector having a probability level equal to l (see Figure 3.12). The unbiased estimate s_l^* of the standard deviation reads:

$$s_l^* = \frac{1}{8} \sum_{i=1}^{9} \left(d_l'^{(i)} - m_l \right)^2 \tag{3.5}$$

Following this, the scatter of the symmetric alternating amplitude $d_l'(\omega)$ at a probability level l (see Figure 3.13) is assumed to be modelled by:

$$d_l'(\omega) = m_l + C_S(\omega)\ s_l^* \tag{3.6}$$

where $C_S = C_S(\omega)$ is a standard Gaussian random variable called severity coefficient. The random variables $d_k'(\omega), d_l'(\omega), \ldots,$ at different probability levels are assumed to be perfectly correlated, thus a single realization c_s of C_S enables an entire CDF of the symmetric alternating amplitude to be constructed, as shown in Figure 3.13.

A virtual life $\mathbf{d}'(c_s) = \{d_0'(c_s), \ldots, d_l'(c_s), \ldots, d_1'(c_s)\}$ is generated by discretizing the CDF into N_f regularly-distributed probability levels. Given that the numbers of cycles observed in the nine recordings is very similar, N_f is considered as deterministic. Using

[†]Note that Figure 3.11 which depicts the extracted cycles in an isometric plot shows that the mean values of the cycles could have also been simply neglected.

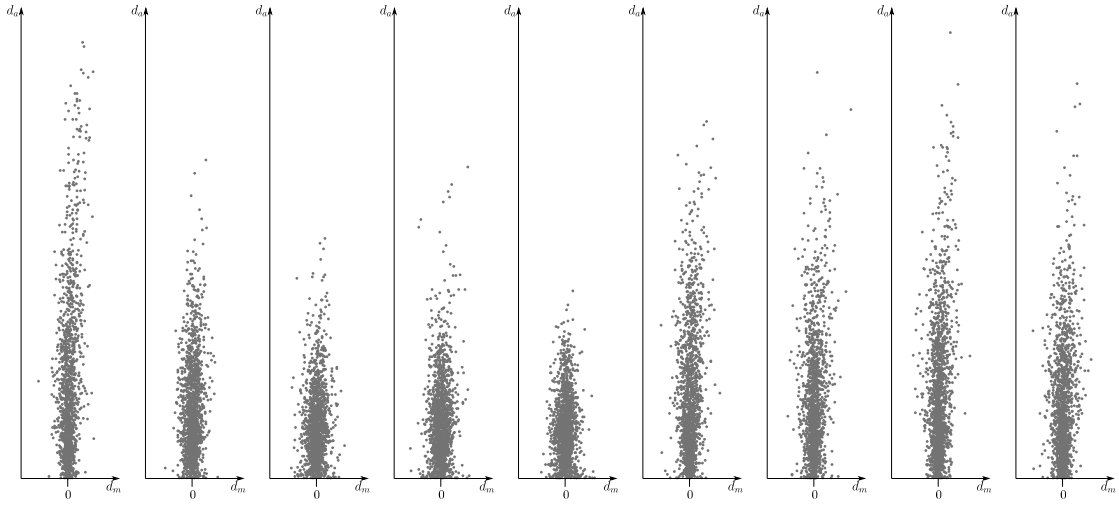

Figure 3.11: Extracted cycles of the nine displacement histories depicted in an isometric plot of the mean d_m and amplitude d_a.

the Basquin's slope b of the $S-N$ curve, the virtual life is finally summarized into an EF cycle (fully reversed) repeated N_{eq} times, and characterized by an amplitude $d_{eq}(c_s, b, N_{eq})$. Figure 3.14 depicts an empirical distribution of the EF amplitude $d_{eq}(c_s, b, N_{eq})$ obtained with the severity coefficient-based modelling. The distribution is more spread out than the observed values.

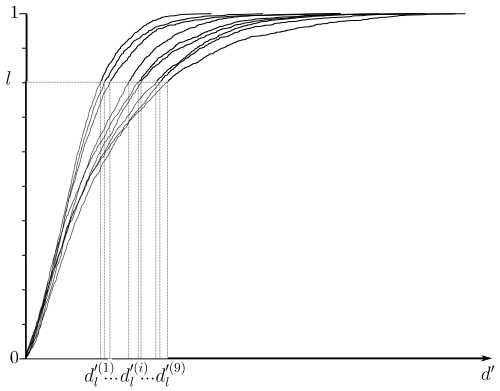

Figure 3.12: Empirical CDFs of the vectors $\{\mathbf{d}'^{(i)},\ i = 1, \ldots, 9\}$. At a probability level l, m_l and s_l^* are calculated using the symmetric alternating displacement amplitudes $\{d_l'^{(i)},\ i = 1, \ldots, 9\}$.

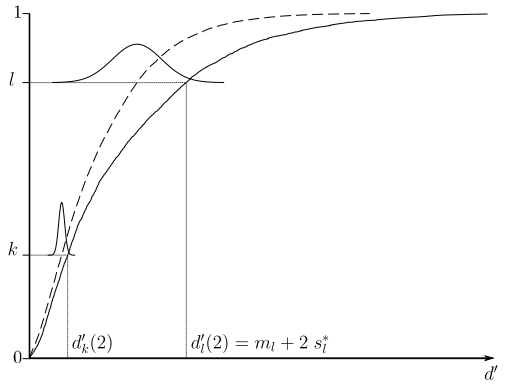

Figure 3.13: CDF of the symmetric alternating amplitude for two values of the severity coefficient. The dashed line depicts the mean CDF obtained for $c_s = 0$. The solid line represents the CDF defined by $c_s = 2$.

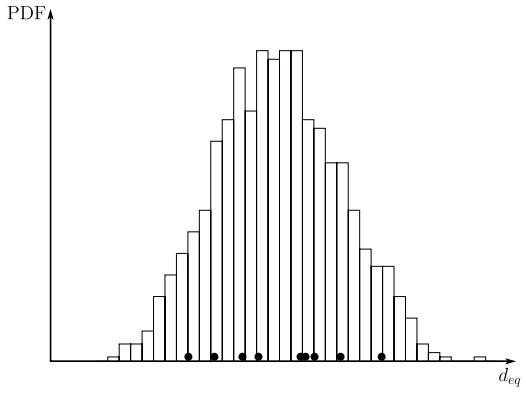

Figure 3.14: Empirical distribution of $1,000$ EF amplitudes d_{eq} at N_{eq} cycles. The black dots represent the EF amplitudes summarizing the nine displacement histories.

3.3.4 Numerical model

The EF cycle is applied to the numerical model simulating the elastic-plastic mechanical behaviour of the blade support. The numerical model is characterized by a realization $\{r_y, c_1, c_2\}$ of the material properties and a geometry $\mathbf{x}_g$, which is considered as deterministic given that a preliminary sensitivity analysis has proven that its influence on structural response is minor. The outputs of the numerical model are the elastic strain amplitude $\epsilon_e(r_y, c_1, c_2, \mathbf{x}_g, c_s, b, N_{eq})$, the plastic strain amplitude $\epsilon_p(r_y, c_1, c_2, \mathbf{x}_g, c_s, b, N_{eq})$ and the maximum stress $\sigma_{\max}(r_y, c_1, c_2, \mathbf{x}_g, c_s, b, N_{eq})$.

LMT's multiparametric strategy and LATIN method [Relun, 2011] are employed to reduce the CPU time of numerical model evaluations. For a single evaluation, the LATIN solver appears to be competitive with the commercial code Abaqus [Relun, 2011]: the CPU time using the LATIN method takes 800 seconds when considering a $141,450$ degrees of freedom mesh and 48 time steps to solve the elastic-plastic problem, whereas Abaqus takes $1,200$ seconds (both computations are performed with a Intel Xeon W5650 processor at 2.6 Ghz - 6 cores). For succeeding numerical model evaluations, LMT's multiparametric strategy is seen to reduce the CPU time down to 40 seconds for small variations of the material parameters.

A remote procedure call (see Figure 3.15) is set by Relun [2011] to enable communication between the probabilistic approach implemented by LaMI in Clermont-Ferrand, and the efficient numerical model of LMT in Cachan. The AK-IS reliability method, implemented for this case study, identifies the realization of the random variables, which, at the current process stage, is relevant to compute. The realization is then automatically sent to LMT's numerical model, which, after evaluation, sends the values ϵ_e, ϵ_p, and $\sigma_{\max}$ back for fatigue calculation. No user intervention is required throughout the entire reliability assessment.

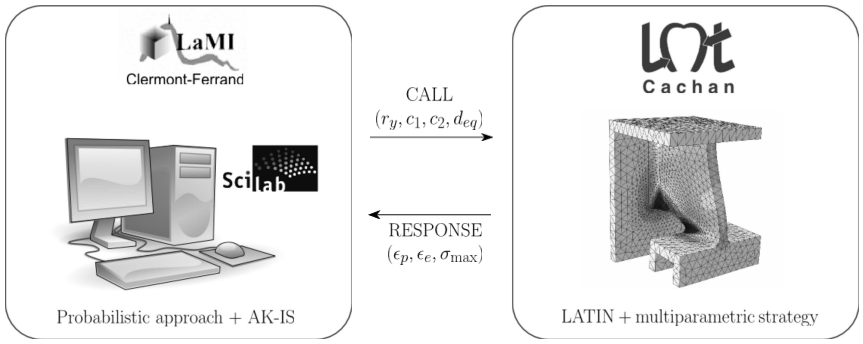

Figure 3.15: Remote procedure call between LaMI's methodology and LMT's numerical model.

3.3.5 Reliability assessment

Table 3.9 recapitulates the random variables of the reliability problem. For a given realization of these random variables, the Smith-Watson-Topper (SWT) stress $\sigma_{\text{SWT}} = \sigma_{\text{SWT}}(r_y, c_1, c_2, c_s, b, N_{eq})$ on the stabilized cycle is calculated using the different outputs of the numerical model:

$$\sigma_{\text{SWT}} = \sqrt{E\,\sigma_{\max}\,(\epsilon_p + \epsilon_e)} \tag{3.7}$$

where E is the Young's modulus. The performance function G compares the realization of the SWT stress with the selected SWT strength $r_{\text{SWT}}(u_f, N_{eq})$ at N_{eq} cycles. As mentioned previously, AK-IS is implemented to pilot the structural reliability analysis.

Random variable	Denomination	Distribution
R_y	Yield strength	Lognormal
C_1	Hardening parameter 1	Lognormal
C_2	Hardening parameter 2	Lognormal
C_S	Severity coefficient	Gaussian
U_f	Isoprob. $S-N$ curve	Gaussian

Table 3.9: Random variables of the blade support case study.

3.3.6 Results

Table 3.10 reports the reliability results. FORM approximation requires 19 evaluations of the performance function. Note that the finite difference approximation of the gradient does not require a new call to the numerical model for the component U_f, since the calculation of the EF load does not depend on U_f. Hence, only 16 evaluations are time-demanding. The Kriging procedure in AK-IS requires 11 additional computations to classify a population of $N_{\text{IS}} = 10^4$ points simulated in the vicinity of the approximated MPFP. The limit state seems to be linear as the failure probabilities obtained by FORM and AK-IS are extremely similar. Within the frame of this case study, the Kriging classification procedure validates the FORM approximation with only a few additional evaluations.

Method	N_E	P_f^{norm}	δ
FORM	16	1	-
AK-IS	27	1.01	2.5%

Table 3.10: Reliability results for the blade support case study. The failure probabilities are normalized to the FORM approximation.

The computational gain of AK-IS compared to crude IS is about 370 ($10,016/27$). Performing crude IS with the numerical model from Abaqus would require 139 days. With AK-IS, the CPU time would drop to 9 hours ($27 \times 1,200$ seconds). Note that the prediction step of AK-IS takes less than 3 seconds which is negligible in comparison with the numerical model evaluation. Finally, by combining AK-IS with LMT's methods, the failure probability is assessed in 2.25 hours, given that the computational gain of the LATIN + multiparametric strategy is 4 for this application. This case study proves that combining parsimonious reliability methods with numerical strategies that reduce the CPU time of succeeding model evaluations is of interest.

AK-IS enables the calculation of the direction cosines $\{\alpha_i,\ i = R_y, C_1, C_2, C_S, U_f\}$ of

the vector $P^{\star}O$. The values are reported in Table 3.11. The severity coefficient C_S and the $S-N$ curve model are the most influent parameters on structural reliability. The minor impact of the material random variables is due to the fact that the global structure remains in the elastic domain.

Material			Load	Fatigue
$-\alpha^2_{R_y}$	$-\alpha^2_{C_1}$	$-\alpha^2_{C_2}$	$-\alpha^2_{C_S}$	$-\alpha^2_{U_f}$
-2.5×10^{-5}	-1.6×10^{-5}	-0.4×10^{-5}	-0.270	-0.729

Table 3.11: Sensitivities $-\alpha_i^2$ of the different random variables for the blade support case study.

3.4 Conclusion

In this chapter, the probabilistic approach outlined in Chapter 1 and the parsimonious reliability methods of the AK-RM family introduced in Chapter 2 have successfully been coupled to handle the two case studies submitted by SNECMA within the frame of the APPRoFi project. The methodology has been completed with LMT's numerical methods with the aim of reducing the CPU time of succeeding model evaluations. For the blade support case study, prompt reliability assessment has been proven possible despite time-demanding model evaluations and small failure probability. Additionally, it has been shown for these case studies that structural reliability in fatigue is mainly affected by the load and the $S-N$ curve, thus attention should be turned to their modellings and the definition of tools for model selection.

Conclusion and future work

Conclusion

Fatigue in structural design is currently considered with deterministic approaches grounded on the use of so-called safety factors. Although these deterministic approaches give mostly satisfactory solutions, they often lead to over-design and are not sufficient to provide the designer with the safety margin and the most influent design parameters on structural reliability. To acquire this additional information, probabilistic approaches are a possible alternative. The research as presented in this document represents a part of the global probabilistic methodology developed in the ANR-funded project called APPRoFi, and which aims at assessing the reliability of already designed structures within a short space of time.

The first contribution of this research work is the definition of a general probabilistic approach for fatigue analysis (Chapter 1). The proposed approach is an improvement on the probabilistic Stress-stRength method [Thomas *et al.*, 1999] which represents a practical engineering tool for assessing structural reliability in the context of fatigue. The main limit of this method is the sensitivity of the failure probability estimate to the necessary assumptions made on the distributions followed by the Stress and the stRength. Furthermore, the influences of random variables on structural reliability cannot be assessed since these variables are carried either by the Stress or the stRength distribution. The proposed approach overcomes these limits by keeping the different random variables separate from each other. The advantages of this approach over the probabilistic Stress-stRength method are demonstrated through an academic example. The approach is proven to enable the assessment of a more accurate failure probability estimate, as well as a determination of the random variables' influences on structural reliability.

In the proposed approach, the failure probability can be assessed using sampling-based reliability methods, but these are inapplicable in the case of a computationally demanding numerical model since they require a substantial number of model evaluations. This thesis thus proposes a family of reliability methods (Chapter 2) that are more parsimonious with respect to the number of model evaluations. These methods named AK-RM (Active learning and Kriging-based Reliability Methods) represent improvements on various classical sampling techniques through the use of a Kriging metamodel. They are based on a Kriging

classification loop that iteratively identifies the model evaluation which should be carried out to enhance the classification of a given population into its safe and failure subsets. The first proposed reliability method is called AK-MCS and corresponds to the combination of the Kriging classification loop with Monte Carlo Simulation. It is applicable to structural reliability problems involving high non-linearity and disconnected domains of failure, but the computational cost of its prediction step is observed to dramatically increase for failure probabilities below 10^{-3}. Alternatives are thus proposed to consider smaller failure probabilities. AK-MCSm is first suggested to take advantage of the possible monotony of the performance function with respect to its random input variables. AK-IS is a second alternative that consists in classifying a population simulated in the vicinity of the most probable failure point. The computational cost of the Kriging procedure is greatly reduced, but the approach relies on the hypothesis that the weight of the failure probability is well located. Finally, AK-SS representing an improvement on Subset Simulation is proposed as an intermediary method between the general AK-MCS and the more specific AK-IS.

The last point of this thesis is the application of the proposed probabilistic approach to the case studies of the APPRoFi project (Chapter 3). In these case studies, the uncertainties of the in-service loads, fatigue behaviour and material properties are statistically modelled. The load uncertainty is examined using a mix strategy based on random percentages of occurrences, a random severity coefficient-based approach, and a parametric modelling of Rainflow matrices. The uncertainty of the fatigue behaviour is considered through the implementation of three probabilistic $S-N$ curve models which are ranked according to likelihood criteria and goodness-of-fit tests. Structural reliability assessment and the determination of the importance factors are carried out using a method from the AK-RM family. Given that the numerical model of the blade support case study is computationally demanding, the probabilistic approach coupled with AK-IS is completed with LMT's numerical methods so that the time required to perform the structural reliability analysis is reduced. The global methodology is proven to enable prompt failure probability assessment. An important conclusion drawn from the application of the methodology to the case studies is that structural reliability is essentially influenced by the load modelling and the $S-N$ curve model.

Future work

Following the conclusion on the application of the probabilistic approach to the particular case studies, further investigations should be conducted in the modellings of the in-service loads and $S-N$ curves to enhance reliability assessment. Given that the fatigue behaviour of materials is relatively well known in comparison with the loads applied to structures, attention should first be drawn to the stochastic modelling of the load with other approaches such as stationary Gaussian processes [Pitoiset, 2001; Benasciutti and Tovo, 2005] or Markovian processes [Mattrand and Bourinet, 2011; Mattrand, 2011].

In this research work, sensitivities are examined using importance factors. Global sensitivity analysis such as Sobol' indices is a step forward to a better understanding of random structural response. These indices aim at determining the contribution of each random variable to the variance of the structural response. They are commonly estimated by means of Monte Carlo Simulation and consequently difficult to calculate with time-demanding model evaluations. A Kriging metamodel can be used to estimate them in a more efficient way, and, as proposed by Marrel *et al.* [2009], the full probabilistic information held in the Kriging prediction can be considered to provide confidence intervals on these indices. Other sensitivity measures such as Borgonovo's [2007] may also be calculated.

Safety factors are convenient to use, since they denote multiplicative coefficients to apply to the load and resistance variables in the hope of obtaining a satisfactory design. In comparison, the algorithmic procedure of probabilistic approaches seems disproportionate. However, structural reliability analyses can be used to improve the concept of safety factors. In fact, reliability-based calibration procedures [Gayton *et al.*, 2004] may be employed to set partial factors, which, when added to the design rule, confer the design a given reliability objective. These factors are specific to the structures concerned and consequently carry more meaning than traditional safety factors. They represent a relevant direction to consider in order to settle probabilistic approaches in design offices.

The research as presented in this document is concerned with the problem of reliability assessment, but uncertainties can also be considered in the design optimization process with the purpose of devising robust and cost-effective structures. Such an advanced process is commonly referred to as reliability-based design optimization. Finding the optimal set of design parameters that minimizes some cost function while satisfying a reliability objective is a problem of obvious interest in mechanical engineering. Nevertheless, it represents a significant computational effort, given that a reliability problem needs to be solved for each set of the design parameters. Following the recent advances in this field involving Kriging [Bichon *et al.*, 2009; Dubourg, 2011; Dubourg *et al.*, 2011], the AK-RM family may be adapted to tackle such analyses.

Bibliography

AFCEN. Règles de Conception et de Construction des Matériels des Ilots Nucléaires, (RCC-M), 2000.

AFNOR. A03-405, Metal products - Fatigue testing - Data statistical processing, 1991.

AFNOR. A03-406, Metal products - Fatigue under variable amplitude loading - The Rainflow method of cycle counting, 1993.

H. Akaike. A new look at the statistical model identification. *IEEE Transactions on Automatic Control*, 19(6):716–723, 1974.

C. Amzallag, J. P. Gerey, J.-L. Robert, and J. Bahuaud. Standardization of the rainflow counting method for fatigue analysis. *International Journal of Fatigue*, 16(4):287–293, 1994.

S.-K. Au and J. L. Beck. Estimation of small failure probabilities in high dimensions by Subset Simulation. *Probabilistic Engineering Mechanics*, 16(4):263–277, 2001.

F. Bastenaire. *Etude statistique et physique de la dispersion des résistances et des endurances à la fatigue*. PhD thesis, Faculté des Sciences de l'université de Paris, 1960.

J. Bect, D. Ginsbourger, L. Li, V. Picheny, and E. Vazquez. Sequential design of computer experiments for the estimation of a probability of failure. *Statistics and Computing*, 22: 773–793, 2011.

D. Benasciutti and R. Tovo. Spectral methods for lifetime prediction under wide-band stationary random processes. *International Journal of Fatigue*, 27(8):867–877, 2005.

P. Bernard and M. Fogli. Une méthode de Monte Carlo performante pour le calcul de la probabilité de ruine. *Construction Métallique*, 4:23–29, 1987.

B. J. Bichon, M. S. Eldred, L. P. Swiler, S. Mahadevan, and J. M. McFarland. Efficient Global Reliability Analysis for nonlinear implicit performance functions. *AIAA Journal*, 46:2459–2468, 2008.

B. J. Bichon, S. Mahadevan, and M. Eldred. Reliability-based design optimization using efficient global reliability analysis. In *50th AIAA/ASME/ASCE/ AHS/ASC Structures, Structural Dynamics, and Materials Conference*, Palm Springs, California, USA, May 2009.

B. J. Bichon, J. M. McFarland, and S. Mahadevan. Efficient surrogate models for reliability analysis of systems with multiple failure modes. *Reliability Engineering & System Safety*, 96(10):1386–1395, 2011.

A. Bignonnet and H.-P. Lieurade. Reliability application in the industry of the reliability approach in fatigue design: a CETIM multipartner project. In *2nd Fatigue Design*, Senlis, France, November 2007. CETIM.

A. Bignonnet and J.-J. Thomas. Approche fiabiliste en conception automobile. In *SF2M - Journées de Printemps*, Paris, France, May 2004.

A. Bignonnet, H.-P. Lieurade, I. Hunter, F. Lefebvre, A. Carcan, E. Babaud, and Marquand D. Escoffier, J.-C. The reliability approach in fatigue design: DEFFI project. In *3rd Fatigue Design*, Senlis, France, November 2009. CETIM.

G. Blatman and B. Sudret. An adaptive algorithm to build up sparse polynomial chaos expansions for stochastic finite element analysis. *Probabilistic Engineering Mechanics*, 25(2):183–197, 2010.

B. Boniface. *Modélisation thermo-mécanique et fiabilité des échangeurs réacteurs en carbure de silicium*. PhD thesis, Université de Toulouse, 2010.

J. D. Booker, M. Raines, and K. G. Swift. *Designing Capable and Reliable Products*, chapter Stress Strength Interference (SSI) analysis, pages 176–191. Butterworth-Heinemann, 2001.

E. Borgonovo. A new uncertainty importance measure. *Reliability Engineering & System Safety*, 92(6):771–784, 2007.

P.-A. Boucard and L. Champaney. A suitable computational strategy for the parametric analysis of problems with multiple contact. *International Journal for Numerical Methods in Engineering*, 57(9):1259–1281, 2003.

J.-M. Bourinet, F. Deheeger, and M. Lemaire. Assessing small failure probabilities by combined Subset Simulation and Support Vector Machines. *Structural Safety*, 33(6): 343–353, 2011.

C. G. Bucher and U. Bourgund. A fast and efficient response surface approach for structural reliability problems. *Structural Safety*, 7(1):57–66, 1990.

J.-L. Chaboche. Constitutive equations for cyclic plasticity and cyclic viscoplasticity. *International Journal of Plasticity*, 5(3):247–302, 1989. ISSN 0749-6419.

D. D. Cox and S. John. SDO: A Statistical Method for Global Optimization. In M. N. Alexandrov and M. Y. Hussaini, editors, *Multidisciplinary Design Optimization: State-of-the-Art*, pages 315–329. Siam, Philadelphia, 1997.

R. B. D'Agostino and M. A. Stephens. *Goodness-Of-Fit Techniques*. 1986.

P. K. Das and Y. Zheng. Cumulative formation of response surface and its use in reliability analysis. *Probabilistic Engineering Mechanics*, 15(4):309–315, 2000.

E. De Rocquigny. Structural reliability under monotony: Properties of FORM, simulation or response surface methods and a new class of Monotonous Reliability Methods (MRM). *Structural Safety*, 31(5):363–374, 2009.

G. Defaux, E. Meister, and M. Pendola. Mécanique probabiliste et intégrité des cuves des réacteurs nucléaires. In *6th Journées nationales de la fiabilité*, Toulouse, France, March 2010.

A. Der Kiureghian and T. Dakessian. Multiple design points in first and second-order reliability. *Structural Safety*, 20(1):37–49, 1998.

A. Der Kiureghian and P. L. Liu. Structural reliability under incomplete probability information. *Journal of Engineering Mechanics*, 112(1):85–104, 1986.

O. Ditlevsen and H. O. Madsen. *Structural Reliability Methods*. John Wiley & Sons, 1996.

O. Ditlevsen, P. Bjerager, R. Olesen, and A. M. Hasofer. Directional Simulation in Gaussian processes. *Probabilistic Engineering Mechanics*, 3(4):207–217, 1988.

S. D. Downing and D. F. Socie. Simple rainflow counting algorithms. *International Journal of Fatigue*, 4(1):31–40, 1982.

V. Dubourg. *Adaptive surrogate models for reliability analysis and reliability-based design optimization*. PhD thesis, Université Blaise Pascal – Clermont II, 2011.

V. Dubourg, B. Sudret, and J.-M. Bourinet. Reliability-based design optimization using Kriging surrogates and subset simulation. *Structural and Multidisciplinary Optimization*, 44(5):673–690, 2011.

A. Dumas, B. Echard, N. Gayton, and O. Rochat. AK-ILS: an Active learning method based on Kriging for the Inspection of Large Surfaces. In *3rd International Conference on Surface Metrology*, Annecy, France, March 2012.

A. Dumas, B. Echard, N. Gayton, O. Rochat, J.-Y. Dantan, and S. Van Der Veen. AK-ILS: an Active learning method based on Kriging for the Inspection of Large Surfaces. *Precision Engineering*, 37(1):1–9, 2013.

B. Echard, N. Gayton, and M. Lemaire. Reliability assessment of structures subjected to fatigue failure using Kriging methods. In *3rd Fatigue Design*, Senlis, France, November 2009. CETIM.

B. Echard, N. Gayton, and M. Lemaire. Structural reliability assessment using Kriging metamodel and Monte Carlo Simulation. In D. Straub, L. Esteva, and M. Faber, editors, *Reliability and Optimization of Structural Systems, Proceedings of the 15th IFIP WG 7.5 Working Conference*, pages 61–68. CRC Press, Munich, Germany, 2010a.

B. Echard, N. Gayton, and M. Lemaire. Kriging based Monte Carlo Simulation to compute the probability of failure efficiently: AK-MCS method. In *6th Journées nationales de la fiabilité*, Toulouse, France, March 2010b.

B. Echard, N. Gayton, and M. Lemaire. AK-MCS: An Active learning reliability method combining Kriging and Monte Carlo Simulation. *Structural Safety*, 33(2):145–154, 2011a.

B. Echard, N. Gayton, and M. Lemaire. A Kriging improvement of the Monte Carlo Simulation: AK-MCS method. In M. Faber, J. Köhler, and K. Nishijima, editors, *Applications of Statistics and Probability in Civil Engineering, Proceedings of the 11th International Conference on Applications of Statistics and Probability in Civil Engineering*, pages 679–686. CRC Press, Zurich, Switzerland, August 2011b.

B. Echard, N. Gayton, M. Lemaire, M. Afzali, A. Bignonnet, P.-A. Boucard, G. Defaux, J.-L. Dulong, A. Ghouali, F. Lefebvre, and A. Pyre. Reliability assessment of an aerospace component subjected to fatigue loadings: APPRoFi project. In *4th Fatigue Design*, Senlis, France, November 2011c. CETIM.

B. Echard, N. Gayton, M. Lemaire, and N. Relun. A combined Importance Sampling and Kriging reliability method for small failure probabilities with time-demanding numerical models. *Reliability Engineering & System Safety*, in press, 2012.

FEM. 1.001 - Règles de calcul des appareils de levage, 1998.

M. Ferlin, A. Pyre, F. Lefebvre, S. Oriol, and A. Bignonnet. DEFFI project for a new concept of fatigue design in the aerospace domain. In *50th AIAA/ASME/ASCE/ AHS/ASC Structures, Structural Dynamics, and Materials Conference*, Palm Springs, California, USA, May 2009.

D. E. Finkel. *DIRECT Optimization Algorithm User Guide*. Center for Research in Scientific Computation, North Carolina State University, March 2003.

R. A. Fisher. *Statistical methods for research workers*. Oliver & Boyd, Edinburgh, 1950.

J. M. Gablonsky. *Modifications of the DIRECT algorithm*. PhD thesis, North Carolina State University, 2001.

N. Gayton and B. Echard. AK-RM : une nouvelle famille de méthodes de simulation basée sur le krigeage. In *7th Journées nationales de la fiabilité*, Chambéry, France, June 2012.

N. Gayton, J.-M. Bourinet, and M. Lemaire. CQ2RS: a new statistical approach to the response surface method for reliability analysis. *Structural Safety*, 25(1):99–121, 2003.

N. Gayton, A. Mohamed, J. D. Sorensen, M. Pendola, and M. Lemaire. Calibration methods for reliability-based design codes. *Structural Safety*, 26(1):91–121, 2004.

N. Gayton, M. Afzali, A. Bignonnet, P.-A. Boucard, G. Defaux, J.-L. Dulong, B. Echard, A. Ghouali, F. Lefebvre, M. Lemaire, M. Masmoudi, A. Notin, D. Néron, A. Ostmane, A. Pyre, and N. Relun. APPRoFi Project: A new approach for the reliability assessment of structures subjected to fatigue. In *4th Fatigue Design*, Senlis, France, November 2011. CETIM.

G. Genet. *A statistical approach to multi-input equivalent fatigue loads for the durability of automotive structures*. PhD thesis, Chalmers, Göteborg University, 2006.

R. G. Ghanem and P. D. Spanos. *Stochastic Finite Elements: A Spectral Approach*. Springer, Berlin, 1991.

C. J. Gil Bellosta. *Package 'ADGofTest': Anderson-Darling GoF test with p-value calculation based on Marsaglia's 2004 paper 'Evaluating the Anderson-Darling Distribution'*, 2011. URL `http://cran.r-project.org/web/packages/ADGofTest/ADGofTest.pdf`.

Z. Guédé. *Approche probabiliste de la durée de vie des structures soumises à la fatigue thermique*. PhD thesis, Université Blaise Pascal – Clermont II, 2005.

Z. Guédé, B. Sudret, and M. Lemaire. Life-time reliability based assessment of structures submitted to thermal fatigue. *International Journal of Fatigue*, 29(7):1359–1373, 2007.

S. Hanaki, M. Yamashita, H. Uchida, and M. Zako. On stochastic evaluation of S-N data based on fatigue strength distribution. *International Journal of Fatigue*, 32(3):605–609, 2010.

A. M. Hasofer and N. C. Lind. Exact and invariant second moment code format. *Journal of Engineering Mechanics*, 100:111–121, 1974.

W. K. Hastings. Monte Carlo sampling methods using Markov chains and their applications. *Biometrika*, 57(1):97–109, 1970.

J. E. Hurtado. An examination of methods for approximating implicit limit state functions from the viewpoint of statistical learning theory. *Structural Safety*, 26(3):271–293, 2004.

D. R. Jones, C. D. Perttunen, and B. E. Stuckman. Lipschitzian optimization without the Lipschitz constant. *Journal of Optimization Theory and Applications*, 79(1):157–181, 1993.

D. R. Jones, M. Schonlau, and W. J. Welch. Efficient Global Optimization of expensive black-box functions. *Journal of Global Optimization*, 13(4):455–492, 1998.

D. Karaboga. An idea based on honey bee swarm for numerical optimization. Technical Report TECHNICAL REPORT-TR06, Erciyes University, Engineering Faculty, Computer Engineering Department, 2005. URL `http://mf.erciyes.edu.tr/abc/publ.htm`.

D. Karaboga and B. Basturk. A powerful and efficient algorithm for numerical function optimization: artificial bee colony (ABC) algorithm. *Journal of Global Optimization*, 39:459–471, 2007.

I. Kaymaz. Application of Kriging method to structural reliability problems. *Structural Safety*, 27(2):133–151, 2005.

M. C. Kennedy, C. W. Anderson, S. Conti, and A. O'Hagan. Case studies in Gaussian process modelling of computer codes. *Reliability Engineering & System Safety*, 91(10-11):1301–1309, 2006. The Fourth International Conference on Sensitivity Analysis of Model Output (SAMO 2004).

D. Krige. A statistical approach to some basic mine valuation problems on the Witwatersrand. *Journal of the Chemical, Metallurgical and Mining Society of South Africa*, 52 (6):119–139, 1951.

H. J. Kushner. A new method of locating the maximum of an arbitrary multipeak curve in the presence of noise. *Journal of Basic Engineering*, 86:97–106, 1964.

P. Ladevèze. *Nonlinear Computational Structural Methods: New Approaches and Non-Incremental Methods of Calculation*. Mechanical Engineering Series. Springer-Verlag, 1999.

C. Lalanne. *Mechanical Vibration and Shock: Fatigue Damage*, volume 4. Hermes Penton Ltd, 2002.

R. Lebrun and A. Dutfoy. An innovating analysis of the Nataf transformation from the copula viewpoint. *Probabilistic Engineering Mechanics*, 24(3):312–320, 2009.

F. Lefebvre, M. Ferlin, A. Pyre, A. Ghouali, S. Oriol, J. El Maghnouji, and A. Bignonnet. Reliability approach in fatigue design for aerospace industry. In *3rd Fatigue Design*, Senlis, France, November 2009. CETIM.

M. Lemaire. *Structural reliability*. ISTE, 2009.

J. Lemaitre, J.-L. Chaboche, A. Benallal, and R. Desmorat. *Mécanique des matériaux solides*. 3rd edition, 2009.

L. Li, J. Bect, and E. Vazquez. A numerical comparison of kriging-based sequential strategies for estimating a probability of failure. In M. Faber, J. Köhler, and K. Nishijima, editors, *Applications of Statistics and Probability in Civil Engineering, Proceedings of the 11th International Conference on Applications of Statistics and Probability in Civil Engineering*. CRC Press, Zurich, Switzerland, August 2011.

S. N. Lophaven, H. B. Nielsen, and J. Sondergaard. DACE, a Matlab Kriging Toolbox, Version 2.0. Technical Report IMM-TR-2002-12, Technical University of Denmark, 2002a. URL `http://www2.imm.dtu.dk/~hbn/dace/`.

S. N. Lophaven, H. B. Nielsen, and J. Sondergaard. Aspects of the Matlab Toolbox DACE. Technical Report IMM-REP-2002-13, Technical University of Denmark, 2002b. URL `http://www2.imm.dtu.dk/~hbn/dace/`.

X. Luo, X. Li, J. Zhou, and T. Cheng. A Kriging-based hybrid optimization algorithm for slope reliability analysis. *Structural Safety*, 34(1):401–406, 2012.

A. Marrel, B. Iooss, B. Laurent, and O. Roustant. Calculations of Sobol' indices for the Gaussian process metamodel. *Reliability Engineering & System Safety*, 94(3):742–751, 2009.

G. Marsaglia and J. Marsaglia. Evaluating the Anderson-Darling distribution. *Journal of Statistical Software*, 9(2):1–5, 2004. URL `http://www.jstatsoft.org/v09/i02`.

G. Matheron. The intrinsic random functions and their applications. *Advances in Applied Probability*, 5(3):439–468, 1973.

M. Matsuishi and T. Endo. Fatigue of metals subjected to varying stress. In *Japan Society of Mechanical Engineering*, Jukvoka, Japan, 1968.

C. Mattrand. *Approche probabiliste de la tolérance aux dommages - Application au domaine aéronautique*. PhD thesis, Université Blaise Pascal – Clermont II, 2011.

C. Mattrand and J.-M. Bourinet. Random load sequences and stochastic crack growth based on measured load data. *Engineering Fracture Mechanics*, 78(17):3030 – 3048, 2011.

M. McKay, R. Beckman, and W. Conover. A comparison of three methods for selecting values of input variables in the analysis of output from a computer code. *Technometrics*, 21(2):239–245, 1979.

R.E. Melchers. Radial importance sampling for structural reliability. *Journal of Engineering Mechanics*, 116(1):189–203, 1990.

N. Metropolis, A. W. Rosenbluth, M. N. Rosenbluth, A. H. Teller, and E. Teller. Equation of state calculations by fast computing machines. *The Journal of Chemical Physics*, 21 (6):1087–1092, 1953.

M. A. Miner. Cumulative damage in fatigue. *Journal of Applied Mechanics*, 12:159–164, 1945.

F. Morel, J. Mercier, G. Catherin, A. Bignonnet, J. Petit, and N. Ranganathan. Analyse du comportement en fatigue de composants mécaniques par l'approche du chargement équivalent. In *Journées de printemps: Sollicitations de service et comportement en fatigue*, Paris, France, May 1993. SF2M.

M. Nagode. *rebmix: An R Package for continuous and discrete finite mixture models*, 2012. URL `http://cran.r-project.org/web/packages/rebmix/index.html`.

M. Nagode and M. Fajdiga. A general multi-modal probability density function suitable for the Rainflow ranges of stationary random processes. *International Journal of Fatigue*, 20(3):211–223, 1998.

M. Nagode and M. Fajdiga. An improved algorithm for parameter estimation suitable for mixed Weibull distributions. *International Journal of Fatigue*, 22:75–80, 2000.

M. Nagode and M. Fajdiga. An alternative perspective on the mixture estimation problem. *Reliability Engineering & System Safety*, 91:388–397, 2006.

M. Nagode and M. Fajdiga. The REBMIX algorithm for the multivariate finite mixture estimation. *Communications in Statistics - Theory and Methods*, 40(11):2022–2034, 2011a.

M. Nagode and M. Fajdiga. The REBMIX algorithm for the univariate finite mixture estimation. *Communications in Statistics - Theory and Methods*, 40(5):876–892, 2011b.

M. Nagode, J. Klemenc, and M. Fajdiga. Parametric modelling and scatter prediction of rainflow matrices. *International Journal of Fatigue*, 23(6):525–532, 2001.

A. Nataf. Détermination des distributions dont les marges sont données. *Comptes Rendus Académie des Sciences*, 225:42–43, 1962.

NIST/SEMATECH. e-Handbook of Statistical Methods: Anderson-Darling Test. URL `http://www.itl.nist.gov/div898/handbook/eda/section3/eda35e.htm`.

A. O'Hagan. Bayesian analysis of computer code outputs: a tutorial. *Reliability Engineering & System Safety*, 91(10-11):1290–1300, 2006. The Fourth International Conference on Sensitivity Analysis of Model Output (SAMO 2004).

F. Perrin. *Prise en compte des données expérimentales dans les modèles probabilistes pour la prévision de la durée de vie des structures.* PhD thesis, Université Blaise Pascal – Clermont II, 2008.

V. Picheny, D. Ginsbourger, O. Roustant, R. T. Haftka, and N.-H. Kim. Adaptive designs of experiments for accurate approximation of a target region. *Journal of Mechanical Design*, 132(7):071008, 2010.

X. Pitoiset. *Méthodes spectrales pour une analyse en fatigue des structures métalliques sous chargements aléatoires multiaxiaux.* PhD thesis, Université Libre de Bruxelles, 2001.

R. Rackwitz. Reliability analysis - a review and some perspectives. *Structural Safety*, 23 (4):365–395, 2001.

R. Rackwitz and B. Fiessler. Structural reliability under combined random load sequences. *Computers & Structures*, 9(5):489–494, 1978.

M. R. Rajashekhar and B. R. Ellingwood. A new look at the response surface approach for reliability analysis. *Structural Safety*, 12(3):205–220, 1993.

P. Ranjan, D. Bingham, and G. Michailidis. Sequential experiment design for contour estimation from complex computer codes. *Technometrics*, 50(4):527–541, 2008.

N. Relun. *Stratégie multiparamétrique pour la conception robuste en fatigue.* PhD thesis, Ecole Normale Supérieure de Cachan, 2011.

J.-L. Robert. Dimensionnement en fatigue des pièces mécaniques. Lectures notes in Master Ingénierie Mécanique et Civile, Université Blaise Pascal – Clermont II, 2009.

V. J. Romero, L. P. Swiler, and A. A. Giunta. Construction of response surfaces based on progressive-lattice-sampling experimental designs with application to uncertainty propagation. *Structural Safety*, 26(2):201–219, 2004.

J. Sacks, S. B. Schiller, and W. J. Welch. Design for computer experiment. *Technometrics*, 31(1):41–47, 1989.

T. J. Santner, B. J. Williams, and W. I. Notz. *The Design and Analysis of Computer Experiments.* New York, 2003.

G. Saporta. *Probabilités, analyse des données et statistique*. Editions Technip, 2nd edition, 2006.

L. Schueremans and D. Van Gemert. Benefit of splines and neural networks in simulation based structural reliability analysis. *Structural Safety*, 27(3):246–261, 2005.

G. Schwarz. Estimating the dimension of a model. *The Annals of Statistics*, 6(2):461–464, 1978.

K. N. Smith, P. Watson, and T. H. Topper. A stress-strain function for the fatigue of metals. *Journal of Materials*, 5(4):767–778, 1970.

B. Sudret. *Fatigue of materials and structures*, chapter 5: Probabilistic design of structures submitted to fatigue, pages 223–263. Wiley & Sons, 2011.

B. Sudret and A. Der Kiureghian. Comparison of finite element reliability methods. *Probabilistic Engineering Mechanics*, 17(4):337–348, 2002.

S. Suresh. *Fatigue of materials*. Cambridge University Press, 2nd edition, 1998.

T. Svensson. Prediction uncertainties at variable amplitude fatigue. *International Journal of Fatigue*, 19(93):295–302, 1997.

J.-J. Thomas, G. Perroud, A. Bignonnet, and D. Monnet. Fatigue design and reliability in the automotive industry. In G. Marquis and J. Solin, editors, *Fatigue Design and Reliability*, volume 23 of *European Structural Integrity Society*, pages 1–11. Elsevier, 1999.

A. Törn and A. Zilinskas. Global optimization. *Lecture Notes in Computer Science*, 350, 1989.

R. Tovo. On the fatigue reliability evaluation of structural components under service loading. *International Journal of Fatigue*, 23(7):587–598, 2001.

D. Veldkamp. *Chances in wind energy - a probabilistic approach to wind turbine fatigue design*. PhD thesis, Delft University of Technology: TU Delft, 2006.

P. H. Waarts. *Structural reliability using finite element methods: an appraisal of DARS (Directional Adaptive Response Surface Sampling)*. PhD thesis, TU Delft, 2000.

Y. Zhang and A. Der Kiureghian. Two improved algorithms for reliability analysis. In R. Rackwitz, G. Augusti, and A. Bori, editors, *Reliability and optimization of structural systems, Proceedings of the 6th IFIP WG7.5 Working Conference on reliability and optimization of structural systems*, Assisi, Italy, 1995. Chapman & Hall.

A List of abbreviations

AIC	Akaike information criterion
AK-ILS	Active learning and Kriging-based method for inspection of large surfaces
AK-IS	Active learning and Kriging-based importance sampling
AK-MCS	Active learning and Kriging-based Monte Carlo simulation
AK-MCSm	Active learning and Kriging-based Monte Carlo simulation under monotony
AK-RM	Active learning and Kriging-based reliability methods
AK-SS	Active learning and Kriging-based subset simulation
ANR	Agence nationale de la recherche
APPRoFi	Approche mécano-probabiliste pour la conception robuste en fatigue
BIC	Bayesian information criterion
BLUP	Best linear unbiased predictor
CA	Constant amplitude
CDF	Cumulative distribution function
DEFFI	Démarche fiabiliste de conception en fatigue pour l'industrie
DOE	Design of numerical experiments
EF	Equivalent fatigue
EFF	Expected feasibility function
EGRA	Efficient global reliability analysis
FORM	First order reliability method
GOF	Goodness-Of-Fit
HLRF	Hasofer-Lind-Rackwitz-Fiessler algorithm
IS	Importance sampling
MCS	Monte Carlo simulation
MCSm	Monte Carlo simulation under monotony
ML	Maximum likelihood
MPFP	Most probable failure point
PDF	Probability density function
SS	Subset simulation
SSI	Stress-strength interference
SWT	Smith-Watson-Topper
VA	Variable amplitude

B List of notations

B.1 General notations

$\mathbf{V}$	Column vector
$\mathbf{V}^t$	Line vector
V_i	ith component of $\mathbf{V}$
$\mathbb{M}$	Matrix
$\hat{.}$	Estimation
$\tilde{.}$	Approximation
Prob	Probability

B.2 Deterministic mechanical values

R_m	Tensile strength
N	Number of cycles to failure
b	Basquin's slope, Eqn.(1.3)
B	Fatigue strength coefficient in Basquin's relation, Eqn.(1.3)
$\sigma(t)$, $F(t)$	Stress, force history
σ_m, F_m	Mean value of a cycle
σ_a, F_a	Amplitude value of a cycle
$\sigma_{\min}$, $F_{\min}$	Minimum value of a cycle
$\sigma_{\max}$, $F_{\max}$	Maximum value of a cycle
$\Delta\sigma$, ΔF	Range of a cycle
σ'_a, F'_a	Symmetric alternating amplitude of a cycle
$\mathcal{R}$	Stress or load ratio
σ_{eq}, F_{eq}	Amplitude of the equivalent fatigue (EF) cycle (often fully reversed)
N_{eq}	Number of times an equivalent fatigue (EF) cycle is repeated

B.3 Random values

B.3.1 Scalar and statistical values

X or $X(\omega)$	Random variable
x	Realization of the random variable X
μ_X	Mean of the random variable X
σ_X	Standard deviation of the random variable X
δ_X	Coefficient of variation of the random variable X
$\mathcal{N}(\mu_X, \sigma_X^2)$	Gaussian distribution with mean μ_X and variance σ_X^2
f_X	Probability density function (PDF) of the random variable X
F_X	Cumulative distribution function (CDF) of the random variable X
ϕ	Standard Gaussian probability density function (PDF)
Φ	Standard Gaussian cumulative distribution function (CDF)
m_X	Empirical mean of the random variable X
s_X^*	Unbiased standard deviation estimate of the random variable X

B.3.2 Vectorial values

$\mathbf{X}$	Random vector
$\mathbf{x}$	Realization of the random vector $\mathbf{X}$
$\mathbf{U}$	Random vector of standard Gaussian variables
$\mathbf{u}$	Realization of the standard Gaussian vector $\mathbf{U}$
$\mathbb{P}$	Population of points
$f_{\mathbf{X}}$	Joint probability density function (PDF) of the random vector $\mathbf{X}$
ϕ_n	n-dimensional standard Gaussian probability density function (PDF)

B.3.3 Space notation and random functions

$\mathcal{X}^n$	n-dimensional physical space
$\mathcal{U}^n$	n-dimensional standard space
O	Origin of the standard space
$\mathcal{S}$	Safe domain
$\mathcal{F}$	Failure domain
$G(\mathbf{X})$	Performance function of the random vector $\mathbf{X}$
$H(\mathbf{U})$	Performance function in standard space $\mathcal{U}^n$

B.3.4 Random mechanical values

S	Stress distribution
R	StRength distribution at N_{eq} cycles
U_f	Random isoprobability $S-N$ curve
$\mathbf{X}_l$	Random load parameters
$\mathbf{X}_g$	Random geometry parameters
$\mathbf{X}_m$	Random material parameters

B.3.5 Kriging values

$\mu_{\tilde{H}}(\mathbf{u})$	Kriging mean at a point $\mathbf{u}$
$\sigma^2_{\tilde{H}}(\mathbf{u})$	Kriging variance at a point $\mathbf{u}$
$U(\mathbf{u})$	Learning function at a point $\mathbf{u}$
$\mathbf{u}^\circ$	Point leading to the smallest value of the learning function U
N_E	Number of numerical model (or performance function) evaluations

B.3.6 Reliability analysis products

P_f	Failure probability
$\hat{P}_f$	Failure probability estimator or estimate, depending on the context
$\tilde{P}_f$	Failure probability estimate obtained with a metamodel
P_f°	Reliability objective, *i.e.* targeted failure probability
δ	Coefficient of variation of the failure probability estimator
$P^\star$	Most probable failure point (MPFP)
β	Hasofer-Lind reliability index
α_i	Direction cosines of the ith random variable
E_{p_i}	Elasticities of the Hasofer-Lind reliability index with respect to the parameter p of the ith random variable

C Parametric modelling of the load for the blade support case study

In Section 3.3.3.2, the load applied to the blade support case study is modelled with the symmetric alternating amplitude d' and a random severity coefficient C_S. An alternative approach inspired by the parametric modelling method outlined in Section 1.3.4.2 and developed after the APPRoFi project is proposed in this appendix.

Selection of the symmetric alternating displacement amplitude's CDF

The proposed approach aims at modelling the CDF of the symmetric alternating displacement amplitude for which only 9 vectors $\{\mathbf{d'}^{(i)},\ i = 1, \ldots, 9\}$ are observed (see Figure 3.12). The 'rebmix' package for R [Nagode and Fajdiga, 2011a,b] is used to determine whether multiple component distributions are required to model each vector $\mathbf{d'}^{(i)}$. Mixtures of Weibull or lognormal distributions are assumed, and BIC is used to determine the most adequate number z of components for each vector. The number of component distributions is reported in Table C.1. A single Weibull distribution is found to be appropriate for eight vectors. Only the first vector is better modelled with a mixture of two Weibull distributions. For lognormal models, a single distribution is seen as relatively sufficient. Following these results, it seems acceptable to consider that a vector $\mathbf{d'}^{(i)}$ is adequately modelled with a single distribution.

Given that z is now set to 1, the most satisfactory distribution between Weibull and lognormal must be selected. For that, Table C.2 and Table C.3 report AIC, BIC and the p-values of Kolmogorov-Smirnov tests. According to AIC and BIC (the lower, the better), the Weibull distribution is the most appropriate. Its p-values are also considerably higher than those of the lognormal distribution. The Weibull hypothesis is not rejected at a 5% significance level for five vectors ($\#2, 6, 7, 8, 9$), and the p-values of the four other vectors remain relatively high ($\approx 1\%$) despite the large data set of cycles extracted in each history. The Weibull model is thus selected as the distribution of the symmetric alternating displacement amplitude.

Modelling of the scatter observed in the CDF's parameters

The nine Weibull distributions fitting the vectors $\{\mathbf{d}'^{(i)},\ i = 1,\dots,9\}$ provide nine observations of the random scale $\lambda(\omega)$ and shape $\kappa(\omega)$ parameters. Statistical models are inferred by ML estimation for $\lambda(\omega)$ and $\kappa(\omega)$. Table C.4 shows that Gaussian, lognormal and Weibull models have very similar AIC, BIC and p-values. In this study, $\lambda(\omega)$ is considered as a Weibull variable, since the AIC and BIC values are the lowest. Given that the support of the Weibull distribution is $\mathbb{R}_+$, no truncation at 0 is required for $\lambda(\omega)$.

Concerning the shape parameter $\kappa(\omega)$, it is assumed that its realizations cannot be below 1 which represents the bound between two drastically different Weibull PDF shapes (remember that a Weibull distribution with $\kappa = 1$ corresponds to the exponential PDF). Table C.5 shows that the Gaussian, lognormal and Weibull models have close AIC, BIC and p-values. $\kappa(\omega)$ is defined as a Weibull random variable for its slightly better AIC and BIC values.

For a given realization $\{\kappa, \lambda\}$ of the Weibull distribution's parameters, the Weibull CDF of the symmetric alternating displacement amplitude is built, and a virtual life is obtained by discretizing the CDF into N_f regularly-distributed probability levels. The amplitudes associated with the different probability levels are calculated using the inverse Weibull CDF that reads:

$$F^{-1}(l) = \lambda \left(-\ln(1-l)\right)^{\frac{1}{\kappa}} \tag{C.1}$$

This function is not defined at the probability level $l = 1$. Therefore, a third random variable is necessary to define the highest symmetric alternating displacement amplitude observed in the virtual life. This random variable is denoted by $D_{\max}$ and assumed to be Weibull distributed, as Table C.6 shows that it is the model that best fits the nine maximum amplitudes observed in the vectors $\{\mathbf{d}'^{(i)},\ i = 1,\dots,9\}$.

Comparison with the severity coefficient-based model

A virtual life, *i.e.* a vector $\mathbf{d}'(\kappa, \lambda, d_{\max})$, is generated by selecting a realization $\{\kappa, \lambda, d_{\max}\}$. Using the Basquin's slope b of the $S-N$ curve, the life is summarized into an EF cycle repeated N_{eq} times and characterized by its amplitude $d_{eq}(\kappa, \lambda, d_{\max}, b, N_{eq})$. Figure C.1(a) depicts an empirical distribution of the EF amplitude obtained with the parametric model presented in this appendix. Figure C.1(b) illustrates an empirical distribution which is derived from the severity coefficient-based model exposed in Section 3.3.3.2. The EF amplitude is seen to be less scattered with the parametric method. Using this model in a structural reliability analysis would then lead to a smaller failure probability.

Vector #	z Weibull	z lognormal
1	2	1
2	1	2
3	1	2
4	1	2
5	1	2
6	1	1
7	1	1
8	1	1
9	1	1

Table C.1: Determination using BIC of the number z of component distributions (Weibull or lognormal) required to model each vector $\mathbf{d}'^{(i)}$.

Vector #	Weibull		
	AIC	BIC	p-value
1	−7573	−7562	0.013
2	−8622	−8611	0.621
3	−8863	−8852	0.010
4	−8664	−8653	0.018
5	−9157	−9146	0.009
6	−7831	−7820	0.346
7	−8083	−8073	0.281
8	−7638	−7627	0.768
9	−8381	−8370	0.352

Table C.2: Measures of the relative goodness of fit of the Weibull distribution to the nine vectors $\{\mathbf{d}'^{(i)},\ i = 1, \ldots, 9\}$.

Vector #	Lognormal		
	AIC	BIC	p-value
1	−7396	−7385	0.004
2	−8193	−8182	10^{-11}
3	−8226	−8215	10^{-22}
4	−8040	−8029	10^{-21}
5	−8421	−8410	10^{-25}
6	−7481	−7470	10^{-7}
7	−7629	−7618	10^{-11}
8	−7233	−7222	10^{-7}
9	−7873	−7862	10^{-8}

Table C.3: Measures of the relative goodness of fit of the lognormal distribution to the nine vectors $\{\mathbf{d}'^{(i)},\ i = 1, \ldots, 9\}$.

Distribution	AIC	BIC	p-value
Truncated Gaussian	−64.18	−63.79	0.89
Lognormal	−63.96	−63.56	0.91
Weibull	−64.35	−63.96	0.89

Table C.4: Comparison of Gaussian, lognormal and Weibull models for the random scale parameter $\lambda(\omega)$. Given that the support of $\lambda(\omega)$ is $\mathbb{R}_+^*$, the Gaussian distribution is truncated at 0.

Distribution	AIC	BIC	p-value
Truncated Gaussian	−9.44	−9.05	0.88
Shifted lognormal	−9.72	−9.32	0.96
Shifted Weibull	−9.92	−9.53	0.89

Table C.5: Comparison of Gaussian, lognormal and Weibull models for the random shape parameter $\kappa(\omega)$. The support of $\kappa(\omega)$ is assumed to be $]1; +\infty[$, therefore, the Gaussian distribution is truncated at 1 and the lognormal and Weibull distributions are shifted by +1.

Distribution	AIC	BIC	p-value
Truncated Gaussian	−30.49	30.09	0.91
Lognormal	−28.81	−28.41	0.74
Weibull	−31.22	−30.83	0.93

Table C.6: Comparison of Gaussian, lognormal and Weibull models for the random highest amplitude $D_{\max}$. Given that the support of $D_{\max}$ is $\mathbb{R}_+^*$, the Gaussian distribution is truncated at 0.

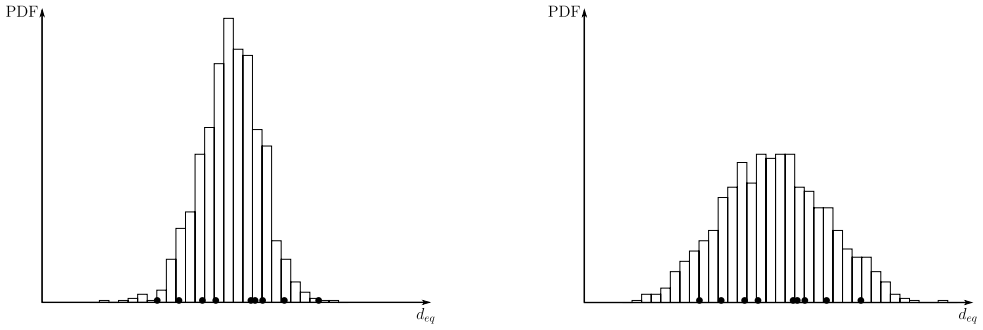

(a) Parametric model.

(b) Severity coefficient-based model.

Figure C.1: Empirical distributions of 1,000 EF amplitudes d_{eq} at N_{eq} cycles. The black dots represent the EF amplitudes summarizing the nine observations $\{\mathbf{d}'^{(i)},\ i = 1, \ldots, 9\}$. The same scale is used for both figures.